

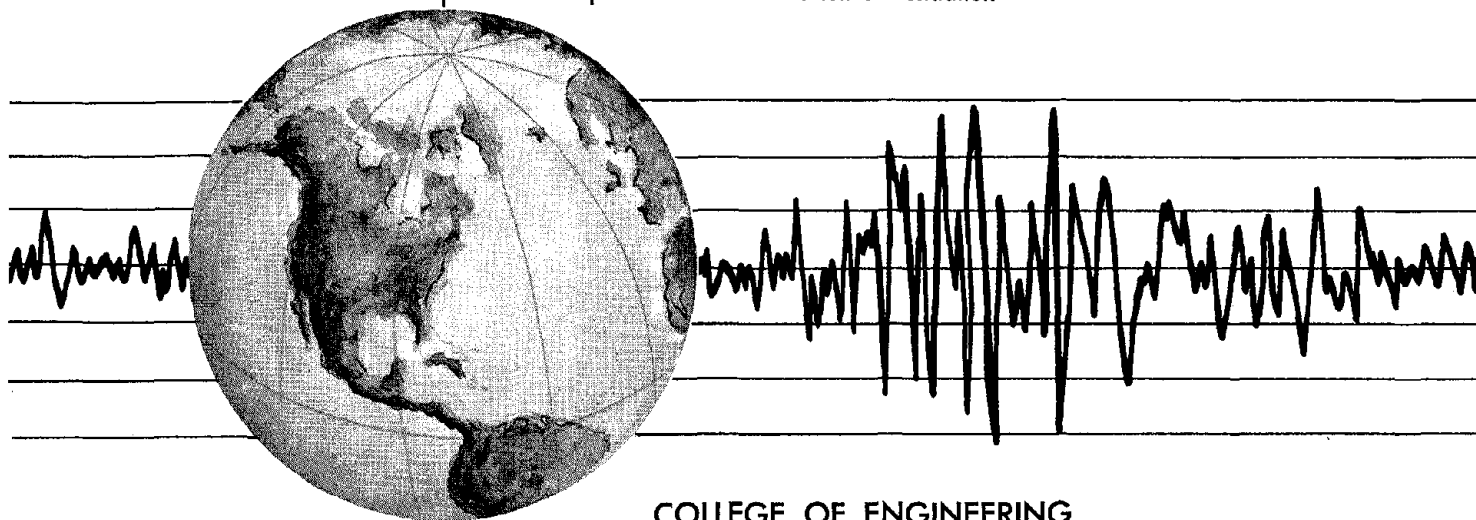
REPORT NO.
UCB/EERC-84/12
JULY 1984

EARTHQUAKE ENGINEERING RESEARCH CENTER

A REFINED PHYSICAL THEORY MODEL FOR PREDICTING THE SEISMIC BEHAVIOR OF BRACED STEEL FRAMES

by
KIYOHIRO IKEDA
STEPHEN A. MAHIN

Report to the National Science Foundation



COLLEGE OF ENGINEERING

UNIVERSITY OF CALIFORNIA • Berkeley, California

REPRODUCED BY
NATIONAL TECHNICAL
INFORMATION SERVICE
U.S. DEPARTMENT OF COMMERCE
SPRINGFIELD, VA. 22161

For sale by the National Technical Information Service, U.S. Department of Commerce, Springfield, Virginia 22161.

See back report for up to date listings of EERC reports.

DISCLAIMER

Any opinions, findings and conclusions or recommendations expressed in this publication are those of the authors and do not necessarily reflect the views of the National Science Foundation or the Earthquake Engineering Research Center, University of California, Berkeley.

**A REFINED PHYSICAL THEORY MODEL FOR
PREDICTING THE SEISMIC BEHAVIOR OF
BRACED STEEL FRAMES**

by

Kiyohiro Ikeda

and

Stephen A. Mahin

A Report to Sponsor
National Science Foundation

Report No. UCB/EERC-84/12
Earthquake Engineering Research Center
College of Engineering
University of California
Berkeley, California
July, 1984

ABSTRACT

This research report presents a state-of-the-art model for inelastic response analysis of braced steel structures. This model achieves realism and efficiency by combining analytical formulations describing plastic hinge behavior with empirical formulae developed based on a study of experimental data. As such it is suitable for studying the inelastic cyclic behavior of individual elements as well as the dynamic response of relatively large structural systems.

The brace is idealized as a pin-ended member with a plastic hinge located at its midspan. The plastic state of the plastic hinge is defined by a specified interaction curve relating axial force and plastic hinge moment. The plastic axial and rotational deformations at the plastic hinge are defined based on the flow rule. Based on these assumptions, analytical expressions for the axial force versus axial deformation behavior of the brace are derived as a solution of the basic beam-column equation. While these expressions form the basis of the new model, several empirical behavioral characteristics are implemented in this modeling in order to achieve better representation of observed cyclic inelastic behavior. These empirical characteristics include: (1) the variation of the tangent modulus of elasticity during cycles, (2) the gradual plastification process of the plastic hinge, and (3) the residual displacement due to material nonlinearities in the nominal elastic range. These characteristics have been identified from an investigation of experimental data.

Verification of the new model is performed on the basis of quasi-static analyses of individual struts and dynamic response analyses of a three-story X-braced steel frame, representative of offshore platforms. The inclusion of the empirical characteristics has achieved a refined representation of hysteresis loops for braces. Furthermore, it has become clear that the new model is able to accurately simulate the cyclic inelastic behavior of steel braces and is efficiently applicable to dynamic analyses of braced frame structures.

The model is applied to the study of the design of a real sized six-story K-braced steel building frame. From this study, it has become clear that the braces' slenderness ratio, buckling strength, and material properties have a great influence on the performance of the braced

frame. The brace model permits the influence of these parameters on structural behavior to be easily assessed.

Conclusions are offered regarding the inelastic behavior of braces. Furthermore, the reliability and practicability of the above analytical approach to modeling the brace behavior are discussed. Topics for further research are identified.

ACKNOWLEDGEMENT

This research program was supported by National Science Foundation. This support is sincerely appreciated. The findings and recommendations in this report, however, are those of the authors and not necessarily those of the sponsor.

The authors are grateful to Professor Egor P. Popov who offered several invaluable contributions to this research. The authors would like to thank Professor Tosio Kato for his encouragement and serving on Mr. Ikeda's dissertation committee. Kazuhiko Kasai was always willing to discuss this research and was very helpful. Joanne Fordham's efforts in proof reading the manuscript and Gail Feazeal's efforts in preparing the figures are greatly appreciated.

Table of Contents

ABSTRACT	i
ACKNOWLEDGEMENT	iii
TABLES OF CONTENTS	iv
LIST OF SYMBOLS	ix
1. INTRODUCTION	1
1.0 General	1
1.1 Available Physical Theory Brace Models	2
1.1.1 Available Information	2
1.1.2 Gugerli model	5
1.1.3 Zayas Model	9
1.2 Limitations of Previous Physical Theory Brace Models	11
1.3 Objectives	12
1.4 Scope	13
2. STUDY OF SOME EXPERIMENTAL RESULTS	15
2.0 Introduction	15
2.1 Plastic Hinge	16
2.2 Zone Definition	16
2.3 Axial Force - Plastic Hinge Moment Curves	18
2.4 Axial Force - Plastic Hinge Rotation Curves	20
2.4.1 Calculation of Axial Force - Plastic Hinge Rotation Curve	20

2.4.2 Study of Behavioral Characteristics of Axial Force - Plastic Hinge	
Rotation Curves	22
2.4.3 Degradation of Plastic Hinge Rotation	22
2.5 Hysteretic Behavior of Tangent Modulus of Elasticity	23
2.6 Residual Displacement due to Material Nonlinearities in the Nominal Elastic	
Range	24
2.7 Summary	25
3. REFINED PHYSICAL THEORY BRACE MODEL	27
3.0 Introduction	27
3.1 Assumptions	28
3.2 Basic Equations	29
3.2.0 General	29
3.2.1 Axial Elastic Displacement	29
3.2.2 Geometric Shortening	29
3.2.3 Plastic Hinge Displacement	30
3.2.4 Tensile Yield Displacement	31
3.2.5 Residual Displacement due to Material Nonlinearities in the Nominal	
Elastic Range	31
3.3 Buckling Behavior	31
3.3.1 Elastic Buckling	32
3.3.2 Plastic Buckling	32
3.4 Empirical Formulas Employed in the Model	33
3.4.0 General	33
3.4.1 Axial Force - Plastic Hinge Moment Interaction Curve	33

3.4.2	Tangent Modulus of Elasticity	34
3.4.3	Axial Force - Plastic Hinge Rotation Curves	36
3.5	Method for Computing Transition Points	36
3.6	Solution Methods for Nonlinear Equations	38
3.7	Computation of Tangent Stiffness for a Strut	38
3.8	Summary	39
4.	QUASI-STATIC ANALYSES OF INDIVIDUAL STRUTS	40
4.0	Introduction	40
4.1	Input Data for Analyses	40
4.2	Comparison of Analytical Results with Experimental Results	41
4.2.1	Axial Force - Axial Displacement Curves	41
4.2.2	Axial Force - Plastic Hinge Moment Curves	42
4.2.3	Axial Force - Plastic Hinge Rotation Curves	42
4.2.4	Buckling Loads and Maximum Tensile Loads	43
4.3	Comparison with Other Analytical Models	43
4.4	Sensitivities of Analytical Results to Empirical Parameters	45
4.5	Relative Contributions of Axial Displacement Components	46
4.6	Effect of Boundary conditions	47
4.7	Concluding Remarks	47
5.	DYNAMIC ANALYSES ON A THREE STORY X-BRACED FRAME	49
5.0	Introduction	49
5.1	Analytical Modeling of the Frame	50
5.2	Capabilities of the Refined Model for Earthquake Type Excitations	51
5.3	Parametric Studies	53

5.3.0 General	53
5.3.1 Effects of Numerical Techniques	53
5.3.2 Effects of Sectional and Material Properties	56
5.3.3 Effects of Earthquake Ground Accelerations	57
5.4 Concluding Remarks	57
6. EFFECTS OF BRACE DESIGN ON THE PERFORMANCE OF K-BRACED FRAME	59
6.0 Introduction	59
6.1 Analytical Modeling of the Frame	59
6.1.1 Structural Model	59
6.1.2 Gravity Loads	61
6.1.3 Dynamic Properties	61
6.2 Analysis of the Standard Case	62
6.3 Influence of Brace Design on the Performance of the Frame	64
6.3.0 General Information	64
6.3.1 Influence of Effective Slenderness Ratios of Braces	64
6.3.2 Influence of Buckling Capacities of Braces	67
6.3.3 Influence of Section Properties of Braces	67
6.4 Nondeterministic Nature of the Dynamic Response of the Frame	68
6.4.0 General	68
6.4.1 Influence of Variations in Material Properties of Braces	69
6.4.2 Influence of Variations in Earthquake Ground Accelerations	69
6.5 Concluding Remarks	70
7. SUMMARY AND CONCLUSIONS	72

7.1 Summary	72
7.2 Conclusions	74
REFERENCES	77
TABLES	81
FIGURES	87
APPENDIX	168
A. DRAIN-2D2 PROGRAM	168
B. INPUT DATA FOR THE REFINED PHYSICAL THEORY BRACE MODEL	169
B.1 Control Information	170
B.2 Stiffness Types	171
B.3 Element Generation Data	172
B.4 Note	173

LIST OF SYMBOLS

a_2	Constant defining theoretical interaction curve
A	Cross-sectional area
b_1, b_2	Constants defining theoretical interaction curve
B	Elastic force - deformation matrix
c_1, c_2	Constants defining theoretical interaction curve
C	Constant defining effective lateral displacement
e_1, e_2, e_3, e_4	Constants defining tangent modulus of elasticity
E	Initial modulus of elasticity
E_t	Tangent modulus of elasticity
E_t^+	Tangent modulus value just after a displacement history reversal
E_t^-	Tangent modulus value just before a displacement history reversal
f	Function for nonlinearity of deflected shape as function of x
g, g_1	Functions for geometric nonlinearity of relation between plastic hinge moment and plastic hinge rotation as functions of κ
h_1	Function for nonlinearity of geometric shortening as function of κ
I	Cross-sectional moment of inertia
k	Effective length factor
kL	Effective member length
kL/r	Effective slenderness ratio
L	Member length of a strut
L_p	Plastic hinge deformation (used in the Zayas model)

x	
m	Normalized plastic hinge moment
M	Plastic hinge moment
\bar{M}	Bending moment at x
\underline{M}	Function for theoretical interaction curve as function of axial force
\underline{M}^*	Function for empirical interaction curve as function of axial force
M_p	Plastic moment of cross section
M_y	Yield moment of cross section
p	Normalized applied axial force
p_{12}	Constant defining theoretical interaction curve
P	Applied axial force
P_{cr}	Euler buckling load
P_y	Tensile yield load
P_0	Axial force at which plastic hinge initially became plastic
r	Radius of gyration
R	Strain hardening ratio as a proportion to E
S	Arc length
T	Time period of a structure
x, y	Coordinates
y_n	Location of instantaneous neutral axis
α_t, α_c	Magnification factors for interaction curve on tension side and that in compression side
β	Parameter defining plastic hinge rotation degradation in Zone EL2
Δ	Lateral deflection at midspan

$\bar{\Delta}$	Lateral deflection along strut as function of x
Δ_{eff}	Effective lateral deflection
Δt	Analysis Time Step
δ	Axial displacement of strut
δ_e	Elastic axial displacement
δ_g	Geometric shortening
δ_m	Residual displacement due to material nonlinearities in the nominal elastic range
δ_{mo}	Cumulative value of residual displacement due to material nonlinearities
δ_p	Plastic hinge displacement
δ_{po}	Cumulative value of plastic hinge displacement
δ_{ty}	Tensile yield displacement
δ_y	Axial displacement at the yield load
ϵ	Axial strain
ϵ_y	Axial yield strain
θ	Plastic hinge rotation
Θ	Rotation angle of beam segment as function of S
κ	Parameter for geometric nonlinearity
λ	Plastic deformation scalar
ϕ	Member end rotation
ϕ_e	Elastic member end rotation
ϕ_p	Plastic member end rotation
Φ	Formula for interaction curve as function of both P and M

$\Phi_{,P}, \Phi_{,M}$	Derivatives of Φ regarding P and regarding M
σ	Axial stress
σ_y	Axial yield stress

1. INTRODUCTION

1.0 General Information

In seismically active sites, it is generally not economically feasible to design conventional structures to be capable of remaining elastic during severe earthquake ground motions. Fortunately, this may not be necessary, if it is possible to take advantage of the inherent ability of many types of structures to absorb and dissipate energy by means of inelastic deformations. Steel moment-resisting frames are widely recognized as being highly efficient in absorbing such earthquake energy demands. However, in high rise buildings such frames tend to develop large interstory drifts. Consequently, concentrically braced steel frames are frequently used in order to increase the structure's strength and stiffness. Such frames generally rely on inelastic deformations in the braces as the main source of earthquake energy dissipation. However, the cyclic inelastic behavior of such braces is quite complex. As can be seen in Fig. 1.1, this cyclic behavior involves several complex physical phenomena [1], including buckling by compressive loads, yielding by tensile loads, post-buckling deterioration of compressive load capacity, and so on. Because of the complexity of this hysteretic behavior, it is difficult to predict the seismic response of braced frame structures and to assess their reliability without the aid of nonlinear computer analyses.

Several analytical models have been developed to represent the cyclic buckling behavior of steel braces. As indicated in an earlier report [2], these models can be divided into three different general types: the finite element, the phenomenological, and the physical theory brace models (examples of these models are shown in Fig. 1.2).

Finite element models generally subdivide a brace longitudinally into a series of segments which are further subdivided into a number of fibers. While providing the most realistic representation of a brace's behavior, finite element models usually demand computations too costly to be applied to practical analyses of large-scale braced structures.

Phenomenological models are based on simplified hysteretic rules which only mimic the observed axial force - axial displacement curves of a brace. Currently, phenomenological

modeling is the most common approach to the analyses of large-scale braced structures. However, users of such models need to specify numerous empirical input parameters for each strut analyzed. It is difficult to select these parameters properly without access either to appropriate experimental results or, alternatively, to the analytical results obtained using other more refined models. For these reasons, phenomenological models are often costly to use and restrictive in their applicability.

Physical theory brace models incorporate simplified theoretical formulations based on the physical considerations that permit the cyclic inelastic behavior to be computed. Unlike the prior empirical information on cyclic inelastic behavior required for phenomenological models, the input parameters for physical theory models are based on material properties and common geometric or derived engineering properties of a member (e.g., the cross-sectional area, cross-sectional moment of inertia, effective member length, plastic section modulus, etc). However, the geometric representation of a brace is considerably simpler than used for a finite element model (Fig. 1.2). Thus, physical theory models attempt to combine the realism of finite element approaches with the computational simplicity of phenomenological modeling. It appears that physical theory brace models provide a promising method for representing the cyclic inelastic behavior of braces in large structures. When fully developed and verified, such physical theory brace models could be valuable in selecting input parameters for phenomenological models as well as in analyzing large-scale structures.

1.1 Available Physical Theory Brace Models

1.1.1 Available Information

Several physical theory models have been developed to simulate the inelastic buckling behavior of steel braces [2 to 20]. Geometrically these bracing members usually have a plastic hinge at midspan which connects two elastic beam segments (see Fig. 1.3). The boundary conditions considered in general are of two types: pinned-pinned [2 to 14] and fixed-fixed [15 to 20]. The axial component of the plastic hinge deformation was neglected in early physical

theory brace models [3 to 5] in favor of the rotational component; however, both components were included in later models [2 and 6 to 20].

Most of these models [2 to 10, and 15 to 20] employed the following set of assumptions:

- (1) Material properties of the plastic hinge, as well as brace segments, are of the elasto-perfectly plastic type.
- (2) The plastic state of the hinge is described by a interaction curve relating the fully plastic moment and axial force at the plastic hinge.
- (3) The beam segments permit elastic axial and flexural deformation components.

A different set of assumptions has been employed by Wakabayashi *et al* [11 to 14] in the development of an elasto-plastic hinge model:

- (1) The center hinge exhibits an arbitrary plastic hinge moment - plastic hinge rotation relation.
- (2) The beam segments are flexurally rigid and permit only an axial deformation.

One of the first physical theory brace models was developed by Higginbotham [3] (see Fig. 1.4). Since only concentrated flexural deformations were permitted at the plastic hinge, this model was only appropriate for slender braces (effective slenderness ratio > 100). The plastic hinge moment was modified according to a specified interaction curve between the plastic hinge moment and axial force. Higginbotham used a basic equation,

$$EI \frac{d\Theta(S)}{dS} = P \quad (1.1)$$

where

E = modulus of elasticity;

I = moment of inertia of cross section;

S = arc length;

Θ = rotation angle of the beam segment as a function of S ;

P = axial force.

He derived an analytical solution for this equation to express the post-buckling force -

deformation behavior of braces. Since the solution to this equation includes elliptic integrals, it entails costly computation.

Nirforoushan [4] formulated a quite similar (but somewhat simpler) model and used it to arrive at parameters for his phenomenological model. Singh [5] also developed a model having assumptions similar to Higginbotham's. However, he used the energy method in formulating basic equations and assumed sine curves for the deflected shapes of the two beam segments under compression. Since a sine curve satisfies the beam-column equation [21] for a compressed beam, his formulation can also be said to be based on this equation.

Nonaka [6,7] and Gugerli [8] developed models close to Singh's model (see Fig. 1.5). Their models, however, included axial and rotational deformation components at the plastic hinge. They solved the beam-column equation directly, obtaining sine curves for the deflected shape of the beam segments under compression and hyperbolic sine curves for beam segments under tension. The resultant basic equations contained trigonometric functions for compressive axial forces and hyperbolic functions for tensile forces.

Fujiwara [9,10] formulated a similar model employing the same assumptions about the plastic hinge and beam segments. He employed the slope deflection method in formulating basic equations, which were similar to Nonaka's and Gugerli's.

Wakabayashi *et al* developed a more general plastic hinge model [11 to 14]. The brace model consisted of two flexurally rigid and axially elastic truss bars and an inelastic hinge at the center (Fig. 1.6). This hinge exhibited arbitrarily specified inelastic cyclic deformation relationships which included the Baushinger effect. Furthermore, since the truss bars were flexurally rigid, complex functions were not needed to specify their deflected shape thereby greatly simplifying the computations.

The formulations of the above models [3 to 14] obtain axial displacement as a function of an axial force. Such models are categorized into the force method. All of these models necessitate iterations in evaluating the value of axial force for the given displacement. Moreover, these formulations are inconsistent with typical finite element analysis procedures used to

analyze the dynamic response of structures. These typically employ the displacement method.

Zayas, Shing, Mahin and Popov [2] formulated a physical theory brace model using the displacement method. Their model included lateral midspan deflection as a second degree of freedom which is removed by elastic condensation during the formulation of the element axial stiffness. The deflected shape of the beam segments was represented by cubic Hermitian polynomials. Based on this idealization, the tangent stiffness matrix could be easily formulated. Moreover, their basic equations were formulated in an incremental form so that their model was compatible with conventional nonlinear analysis programs. Elastic buckling was taken into account by the use of the tangent modulus approach.

Wakabayashi *et al* [15,16,17], Prathuangsit [18], Mitani [19], and Toma [20] developed models for a member whose rotations were constrained at both ends. To replicate the constraints at the ends, References 15,16,18 and 19 used springs at both ends (see Fig. 1.7 [16]) and References 17 and 20 assumed fixed-fixed end conditions.

To give a better understanding of the various approaches used to formulate physical theory models, two models will be discussed in more detail.

1.1.2 Gugerli Model

(a) General

This subsection introduces the basic theoretical formulations and equations employed in the Gugerli model [8]. To be compatible with subsequent derivation in this report, Gugerli's derivation have been modified somewhat, but the basic principles of his formulation were left unchanged.

(b) Assumptions

The Gugerli model consists of a pin-ended brace with a plastic hinge located at its midspan as shown in Fig. 1.3. The formulation of this model is based on the following set of assumptions:

- (1) Every cross section along the axis retains its shape.
- (2) The effects of shearing stresses and strains are neglected.
- (3) The axial strains are distributed linearly over the cross section (plane sections remain plane).
- (4) Only cross sections with one axis of symmetry are considered.
- (5) The lateral deflections and the corresponding slopes are small.
- (6) The material is of the elasto-perfectly plastic type.
- (7) Partial plastification within the hinge as well as along the member axis is disregarded.

(c) **Basic Equations**

For simplicity, equations will be developed for only one half of the brace. The deflected shape of the left half of a brace shown in Fig. 1.3 is obtained by solving the basic beam-column equation.

$$\bar{\Delta}(x) = \frac{\theta L}{2} f(x) \quad (1.2)$$

where

$$f(x) = \begin{cases} \frac{\sin \frac{\kappa x}{L}}{\kappa \cos \frac{\kappa}{2}} & \text{if } P < 0 \\ \frac{\sinh \frac{\kappa x}{L}}{\kappa \cosh \frac{\kappa}{2}} & \text{if } P > 0 \end{cases} \quad (1.3)$$

$$\kappa^2 = \frac{|P|L^2}{EI};$$

x = coordinate;

$\bar{\Delta}(x)$ = lateral deflection at x ;

θ = plastic hinge rotation;

L = member length.

The sign convention adopted here and throughout the remainder of this report is that tensile forces and elongation are positive. When Eq. 1.2 is applied to the plastic hinge location, the plastic hinge moment M is related to the plastic hinge rotation angle θ by,

$$M = g(\kappa) \frac{EI}{L} \theta \quad (1.4)$$

where

$$g(\kappa) = \begin{cases} -\frac{\kappa}{2} \tan \frac{\kappa}{2} & \text{if } P < 0 \\ \frac{\kappa}{2} \tanh \frac{\kappa}{2} & \text{if } P > 0 \end{cases} \quad (1.5)$$

The axial displacement δ of the brace consists of five components,

$$\delta = \delta_e + \delta_g + \delta_p + \delta_{po} + \delta_{ty} \quad (1.6)$$

where

δ_e = elastic axial displacement;

δ_g = geometric shortening;

δ_p = plastic hinge displacement;

δ_{po} = accumulated plastic hinge displacement;

δ_{ty} = tensile yield displacement.

The elastic axial displacement δ_e is expressed as

$$\delta_e = \frac{PL}{AE} \quad (1.7)$$

where A is the cross-sectional area.

The expression for δ_g is:

$$\delta_g = -h_1(\kappa) \theta^2 L \quad (1.8)$$

where

$$h_1(\kappa) = \begin{cases} \frac{\sin\kappa + 1}{\kappa} & \text{if } P < 0 \\ \frac{16\cos^2\frac{\kappa}{2}}{\kappa} & \\ \frac{\sinh\kappa + 1}{\kappa} & \text{if } P > 0 \\ \frac{16\cosh^2\frac{\kappa}{2}}{\kappa} & \end{cases} \quad (1.9)$$

The axial displacement, δ_p , associated with plastic hinge deformations occurring during a plastic excursion of the hinge takes the form:

$$\delta_p = \int_{P_0}^P \frac{d\delta_p(P^*)}{dP^*} dP^* \quad (1.10)$$

where P_0 is the axial force value at which the plastic hinge initially became plastic. This term includes the effects of plastic axial and rotational deformations on the brace length.

The plastic flow rule based on Drucker's postulate [22] was used to arrive at an expression for the incremental axial plastic hinge deformation $d\delta_p$:

$$d\delta_p = -y_n d\theta \quad (1.11)$$

where y_n denotes the location of instantaneous neutral axis (see Fig. 1.8). The plastic hinge rotation θ can be determined by the use of Eq. 1.4.

(d) Zone Definition of Gugerli Model

Five different zones shown in Fig. 1.5 are used in formulating cyclic buckling behavior based on the above equations. The Gugerli model distinguishes between elastic and plastic states of the plastic hinge and makes special considerations when the brace is straight in tension.

1.1.3 Zayas Model

(a) General

This subsection introduces the basic formulations used in the Zayas model (see Fig. 1.9). As mentioned previously, this model follows an approach based on the displacement method of analysis. While this approach is not followed in this research report, the model incorporates several important features which are used and provides an alternative implementation strategy that should be further evaluated. The model adheres to the same basic assumptions discussed for the Gugerli model.

(b) Basic equations

In the analytical formulation, the brace is treated as a two-degree-of-freedom system. The incremental forces at the plastic hinge, dP and dM , are related to the total incremental end deformations through the tangent stiffness matrix K_t .

$$\begin{bmatrix} dP \\ dM \end{bmatrix} = K_t \begin{bmatrix} d\delta \\ d\phi \end{bmatrix} \quad (1.12)$$

The deformation terms δ and ϕ correspond to the member end axial deformation and rotation, respectively, as shown in Fig. 1.9. Before use in an analysis the element is reduced to a single-degree-of-freedom system by static condensation. The rest of this subsection derives the basic expression for the tangent stiffness matrix K_t .

The total incremental strut end deformations are assumed to be the sum of the elastic and plastic parts.

$$\begin{bmatrix} d\delta \\ d\phi \end{bmatrix} = \begin{bmatrix} d\delta_e \\ d\phi_e \end{bmatrix} + \begin{bmatrix} d\delta_p \\ d\phi_p \end{bmatrix} \quad (1.13)$$

where the subscripts e and p represent the elastic and plastic contributions, respectively.

Zayas developed the following incremental equation, where the incremental axial force dP and moment dM at the plastic hinge are related to the elastic strut end deformations by means of the elastic force - deformation matrix B .

$$\begin{bmatrix} dP \\ dM \end{bmatrix} = B \begin{bmatrix} d\delta_e \\ d\phi_e \end{bmatrix} \quad (1.14)$$

The plastic end deformations are related to the plastic hinge deformations by means of the geometric transformation matrix.

$$\begin{bmatrix} d\delta_p \\ d\phi_p \end{bmatrix} = \begin{bmatrix} \cos\phi & L\sin\phi \\ 0 & 1 \end{bmatrix} \begin{bmatrix} dL_p \\ d\phi_p \end{bmatrix} \quad (1.15)$$

where L_p is the axial plastic hinge deformation. Let us note that Zayas distinguishes in this formulation the difference between axial plastic hinge deformation L_p and end displacement due to plastic hinge deformation δ_p . Gugerli assumed the lateral deflection of the brace was small ($\phi \approx 0$) and ignored this difference.

The outward normal flow rule [22] can be applied to the plastic hinge deformations.

$$\begin{bmatrix} dL_p \\ d\phi_p \end{bmatrix} = \begin{bmatrix} \Phi_{,P} \\ \Phi_{,M} \end{bmatrix} \lambda \quad (1.16)$$

where

λ = plastic deformation scalar;

Φ = formula for interaction curve;

$\Phi_{,P}$ = derivative of Φ with respect to P ;

$\Phi_{,M}$ = derivative of Φ with respect to M .

Combining Eqs. 1.15 and 1.16, the flow rule for the strut end deformations can be written as follows:

$$\begin{bmatrix} d\delta_p \\ d\phi_p \end{bmatrix} = J\lambda \quad (1.17)$$

where

$$J = \begin{bmatrix} \cos\phi & \Phi_{,P} + L\sin\phi & \Phi_{,M} \\ & \Phi_{,M} & \end{bmatrix} \quad (1.18)$$

Employing the condition that the interaction function Φ remains constant, one can arrive at the following equations:

$$\begin{bmatrix} dP \\ dM \end{bmatrix} = B \begin{bmatrix} d\delta \\ d\phi \end{bmatrix} - J\lambda \quad (1.19)$$

$$\lambda = G \begin{bmatrix} d\delta \\ d\phi \end{bmatrix} \quad (1.20)$$

where

$$G = [\Phi_{,s}^T B J]^{-1} [\Phi_{,s}^T B] \quad (1.21)$$

$$\Phi_{,s} = \begin{bmatrix} \Phi_{,P} \\ \Phi_{,M} \end{bmatrix} \quad (1.22)$$

Finally, Eqs. 1.19 and 1.20 can be combined and solved for the tangent stiffness matrix K_t .

$$K_t = (B - B J G) \quad (1.23)$$

1.2 Limitations of Previous Physical Theory Brace Models

While capable of capturing the basic aspects of brace hysteretic behavior, available physical theory brace models (including the Wakabayashi, the Gugerli, the Nonaka, and the Zayas models) have significant limitations. These will be discussed in this section

All of these models assume elasto-perfectly plastic material properties for both the plastic hinge and the beam segments. In these models, the transition from an elastic state to a plastic state at the plastic hinge and in the beam segments takes place instantaneously. In reality, such an instantaneous transition does not happen. As Okamura [23] suggested, plastification progresses gradually and continuously, in association with the loss of stiffness of infinitesimal elements in the material even before the overall yield condition is satisfied. Yielding will occur gradually and spread over finite length of the member.

The assumption of elasto-perfectly plastic material properties by these physical theory brace models therefore results in inaccurate analytical predictions of member behavior. One

consequence of this is that transitions occur more suddenly with the models than in reality. For example, the analytical hysteresis loops shown in Figs. 1.4 (Pt. F), 1.5 (Pt. G), and 1.7 (Pts. A and B) have kinks at the transition points when a plastic hinge goes from an elastic to a plastic state under tensile loading. Such kinks have not been observed in experimental data (see Fig. 1.1), resulting in discrepancies between experimental and analytical hysteresis loops.

All of the models assume that the values of the modulus of elasticity do not vary during cyclic buckling processes, and the initial value of the modulus is used in analyses. However, it is generally accepted that, in evaluating buckling loads, the tangent modulus or the secant modulus of elasticity provides better results than the initial modulus of elasticity. Cyclic inelastic behavior will be similarly better expressed by the tangent or the secant modulus. Moreover, these moduli directly account for the influence of material nonlinearities, which is expected to be particularly important for stocky braces and for cyclic loading. Thus, the models using the initial modulus of elasticity cannot account for the deterioration of buckling load with inelastic cycling.

Many physical theory brace models express axial displacement as a function of axial force. Thus, these models require iterations to estimate the value of the axial force for a given displacement in the analyses by the matrix displacement method. While Zayas formulated the basic equations suitable for the matrix displacement method, he retained the other limitations. None of the models discussed have been implemented in programs capable of performing non-linear dynamic analyses of complete structures. Verification of these types of models and evaluation of their computational abilities would appear to be a logical progression of research in this area.

1.3 Objectives

This research is undertaken in order to formulate a refined physical theory brace model able to provide a good representation of brace hysteresis loops and to overcome some of the limitations of the previous physical theory brace models. While improved modeling of cyclic

inelastic behavior is the focus of this investigation, constraints are imposed to insure that the element could be used in the dynamic analyses of large structures. Thus, much of the effort is to find suitable analytical and theoretical simplifications to permit efficient computation of brace behavior.

It has been common to use experimental hysteresis loops and $P-M$ interaction curves in the development of the available physical theory brace models. In this study, experimental axial force - plastic hinge moment curves and experimental axial force - plastic hinge rotations curves are also examined. Based on these observations, empirical modifications of the previous models are introduced. Special attention is paid to monitor the gradual plastification of the braces. To implement the gradual progress in our analytical model, the following features are incorporated: (1) the gradual increase of plastic hinge rotation prior to satisfying the yield condition and (2) the variation of tangent modulus of elasticity. In addition, mathematical formulations for solving the basic equations are expressed in an efficient manner.

This investigation also attempts to assess the model's suitability and applicability to the dynamic response analyses of braced frames and to the study of the design of such frames. The refined model as developed herein is suitable for the study of cyclic behavior of individual elements, for the determination of input parameters for phenomenological models, and, above all, for general purpose dynamic analyses based on the tangent stiffness method.

1.4 Scope

To achieve the aforementioned objectives, the following studies are performed. Chapter 2 examines the cyclic buckling behavior of steel braces based on test data for six struts taken from Reference 1. The struts consist of five wide flanges and one tube. The effective slenderness ratios are either 40, 80, or 120; the boundary conditions are of two types, fixed-pinned and pinned-pinned. The emphasis in this chapter is placed on identifying the behavioral characteristics to be implemented in the analytical model.

Chapter 3 introduces the formulation for a refined physical theory model. This model is a refinement of the approach taken by Gugerli. The refined model includes the behavioral characteristics noted in Chapter 2. These include empirical models for: interaction curves, axial force - plastic hinge rotation curves, and the history of tangent moduli of elasticity.

Chapter 4 applies the refined model to quasi-static analyses of individual steel braces so as to assess the adequacy of the assumptions used in this model. Analytical results are compared with test results based on various standpoints: hysteresis loops, axial force - plastic hinge moment curves, axial force - plastic hinge rotation curves, buckling loads, maximum tensile loads, etc. In addition, the analytical results are compared with those obtained using a refined phenomenological model (DRAIN-2D2 ELEMENT TYPE 4) [24] and the Gugerli model [8].

Chapter 5 presents parametric studies using the refined model based on the simple dynamic analyses of a three story X-braced frame. An emphasis is placed on identifying the input parameters having a large influence on dynamic response of the structure and/or the brace. This chapter and the previous chapter fully demonstrate numerical features of the refined model.

Chapter 6 applies the refined model to the study of a steel braced frame's design. Brace parameters having large influence on the performance of the frame are identified. In addition, the nondeterministic nature of the dynamic response of braced frames is discussed.

Chapter 7 offers conclusions regarding the reliability and practicability of the refined physical theory brace model. Behavioral characteristics which must be accounted for in modeling are identified. Needs for further research and development are discussed.

Appendix A presents a brief explanation of the DRAIN-2D2 program [25], in which the refined model has been implemented. Appendix B constitutes a user's guide for the computer implementation of the refined physical theory model.

2. STUDY OF SOME EXPERIMENTAL DATA

2.0 Introduction

Prior to the formulation of an analytical model for the cyclic buckling behavior of braces, it is important to refer to experimental data so as to identify the important aspects which must be incorporated in the model. Strut data from the experiments by Black, Wenger, and Popov [1] have been used to examine the cyclic buckling behavior of braces in this chapter and in comparing with analytical results subsequently. These authors reported test data for 24 struts, subjected to quasi-statically applied, cyclic axial loads simulating earthquake loading effects. These data are particularly useful because they included an axial force - axial displacement curve as well as an axial force - lateral displacement curve for each of the struts (see Fig. 1.1 for an example). It also contained complete cyclic stress - strain curves for two coupons, cut from W6×20 and TS4×4×½ sections (see Fig. 2.1), in addition to tables of conventionally measured material properties.

These data are herein further processed to arrive at additional information about the cyclic inelastic behavior of steel braces. Among the 24 struts, six representative struts, five wide flanges (Struts 1, 3, 7, 19, and 23) and a tube (Strut 18), are selected for detailed study. All of the wide flange members buckled about their weak axis in the experiments. Table 2.1 contains the member and material properties for these struts. Members with effective slenderness ratios of 40, 80, or 120 were considered so that the influence of this parameter could be observed. Four of the struts are simply supported and the remaining two are fixed at one end and pinned at the other end. The data for simply supported struts will be subsequently compared with analytical results obtained using a refined physical theory brace model developed for the simply supported boundary conditions. The data for the two fixed-pinned struts will be employed to assess whether the concept of effective member length (relating a strut with pinned ends to a strut with arbitrary boundary conditions) is applicable to this model.

2.1 Plastic Hinge

The basic geometric representation of the strut considered in this report is the same as that used by Gugerli [8] and others [2 to 10]. It is assumed that the strut is pin ended and consists of two beam segments attached at the midspan by a plastic hinge, as shown in Fig. 1.3. The adequacy of this model and its relationship to the behavior of actual struts are examined below. During cyclic load tests, a plastic hinging region can usually be detected near the midspan of a strut as it buckles laterally. Figure 2.2 (a) [26] shows the cumulative history of axial strain distributions in a strut and Fig. 2.2 (b) the corresponding hysteresis loop. A band of concentrated axial strains, which grew from cycle to cycle, is observed near the midspan. Inelastic axial and rotational deformations tend to form in such plastic hinge regions. The plastic hinge, however, can be seen to have a finite length. Many physical theory brace models assume the plastic hinge to be a point. According to these models, the hinge has elasto-perfectly plastic mechanical properties and, thus, forms instantaneously when the cross section at the potential plastic hinge location becomes fully plastic, (in other words, when the axial force - plastic hinge moment curve arrives at the interaction curve). This method of defining the plastic state of the plastic hinge disregards the gradual plastification across a section or along a region of a strut. In this report, a gradual transition from an elastic state to a plastic one is incorporated in the model to better reflect observed behavior.

2.2 Zone Definition

In studying the cyclic buckling behavior of steel braces, it is common to divide a cycle into a set of zones corresponding to different behavioral characteristics. The definition of these zones is closely related to the interpretation of the cyclic inelastic behavior. A new way to define the zones, shown in Fig. 2.3 (a) through (d), is proposed for a better interpretation of cyclic behavior. Firstly, a cycle of member behavior can be roughly divided into four general categories: elastic zones, plastic zones, the yield zone, and the elastic buckling zone. Note that the terms "elastic" and "plastic" correspond to the state of the plastic hinge, while the term

"yield" is associated with the state of the beam segments. The beam segments are assumed elastic except in the yield zone, where they are yielded by axial forces exceeding the tensile capacity of the strut. Secondly, the elastic zone is subdivided into the elastic shortening zone and the elastic lengthening zone. Differences between these two elastic zones are:

- (1) In the elastic shortening zone, both member lengths and axial loads decrease (note that tension is positive).
- (2) In the elastic lengthening zone, both member lengths and axial loads increase.

This distinction between the two elastic zones significantly contributes to progress in the subsequent analytical model.

Finally, the elastic shortening, the elastic lengthening, and the plastic zones are each further subdivided into the zones in tension and those in compression. For simplicity in the following discussion, this zone definition is abbreviated as follows:

- ES1 : elastic shortening zone in compression;
- ES2 : elastic shortening zone in tension;
- EL1 : elastic lengthening zone in compression;
- EL2 : elastic lengthening zone in tension;
- BU : buckling zone;
- P1 : plastic zone in compression;
- P2 : plastic zone in tension;
- PY : yielding zone.

where "E" corresponds to elastic, "P" to plastic, "BU" to buckling, and "Y" to yielding. "S" represents shortening, "L" represents lengthening. "1" indicates compression, "2" indicates tension. The eight zones defined in this manner will be used in discussing member behavior. Note that the basic behavior of a strut associated with each zone is shown in Fig. 2.3 (b), while an empirical rule of zone transition is summarized in Table 2.2.

The zone definition also applies to axial force - plastic hinge moment curves and to axial force - plastic hinge rotation curves, as shown in Figs. 2.3 (c) and (d) respectively. In order to

achieve deeper insight into member behavior, some of these curves will be examined zone by zone in the following two sections.

Many physical theory brace models recognize the fact that plastic zones are irreversible and that they exit to elastic zones upon displacement history reversals. However, these models generally disregard the fact that elastic zones are also irreversible. For example, the elastic lengthening zone exits to the elastic shortening zone and vice versa upon load history reversals. The irreversibility of elastic zones arises from the following features: (1) the discontinuity of tangent modulus values at load history reversals and (2) a difference of the plastic hinge rotation characteristics in the elastic lengthening zone and in the elastic shortening zone. These features will also be deduced from test data in the subsequent sections.

2.3 Axial Force - Plastic Hinge Moment Curves

Axial force - plastic hinge moment ($P-M$) curves play a dominant role in understanding plastic hinge behavior. In order to increase the data available concerning this behavior, these relations were computed for the aforementioned six struts.

For simply supported struts, bending moments are computed from the static equilibrium equation shown below:

$$\bar{M}(x) = P \cdot \bar{\Delta}(x) \quad (2.1)$$

where $\bar{M}(x)$ is the bending moment at x and $\bar{\Delta}(x)$ is the lateral displacement at x .

This is not applicable to struts with other boundary conditions, since the bending moments must vanish at the inflection points of the buckled shape rather than at the ends of the member. This feature can be accounted for by employing the concept of effective lateral displacement, explained by the use of Fig. 2.4 [1]. Based on this concept, the effective moment at the potential plastic hinge location can be expressed by the following formula:

$$M = P \cdot \Delta_{eff} \quad (2.2)$$

where Δ_{eff} is the effective lateral displacement. Based on the method suggested in Reference

21, the following formulas relating the effective lateral displacement to the measured lateral displacement are presented.

$$\Delta_{eff} = \Delta \cdot C \quad (2.3.a)$$

$$C = \begin{cases} 1.0 & \text{pinned-pinned} \\ 1.398 & \text{fixed-pinned} \end{cases} \quad (2.3.b)$$

Using Eqs. 2.2 and 2.3, $P-M$ curves shown in Figs. 2.5 to 2.7 were computed from experimental $P-\Delta$ curves taken from Reference 1. The theoretical fully plastic $P-M$ interaction curve (usually called interaction curve), as well as the first yield $P-M$ interaction curve for each strut, are also shown in these figures. The formulas for the fully plastic interaction curve are summarized in Table 2.3 [8], whereas those for the first yield interaction curve are illustrated in the figures. All of these formulas are based on measured yield stress and assume rigid-perfectly plastic material properties. They neglect wall thickness considerations. The plastic hinge should theoretically remain elastic until the experimental $P-M$ curve reaches the first yield interaction curve; partial plastification of the hinge progresses in the area between the first yield interaction curve and the fully plastic interaction curve; deformation hardening occurs outside of this curve.

A comparison of the fully plastic interaction curves and the enveloping surface of the experimental $P-M$ curves shows the following features:

- (1) Struts 1,3, and 23 developed significant strain hardening as represented by shifts in the experimental $P-M$ curves during the later cycles. Correspondingly, struts 7 and 19 showed signs of softening in the compression side during the later cycles.
- (2) For struts 1 and 18, the experimental interaction curves on the compression side had from 20 to 40 percent smaller plastic hinge moment capacities than the fully plastic interaction curves. Strut 18 had a very high yield strength, so that the aforementioned assumptions might have been violated. The effective slenderness ratio of Strut 1 equaled 120 so that the elastic buckling prevailed. For this strut, the yield moment M_y , which

corresponds to the onset of yielding in the strut, will be more important than the fully plastic moment M_p .

The following characteristics of $P-M$ curves can be identified through the observation of these test data:

- (1) The $P-M$ curves are almost linear in Zones ES2 and EL1, as unloading takes place at the plastic hinge.
- (2) Small nonlinearities exist in the Zones ES1 and EL2 apparently due to the deterioration of the tangent modulus.
- (3) In the plastic zones (Zones P1 and P2), the $P-M$ curves tend to follow the theoretical fully plastic interaction curve.
- (4) There is no significant influence of effective slenderness ratio values on the shape of the $P-M$ curves.

2.4 Axial Force - Plastic Hinge Rotation Curves

2.4.1 Calculation of Axial Force - Plastic Hinge Rotation Curves

There is little experimental data concerning the plastic hinge rotation under inelastic cycling because it is both difficult and laborious to measure. This section attempts to increase information about the plastic hinge behavior by computing axial force - plastic hinge rotation ($P-\theta$) curves. The computation is carried out as explained below.

Applying Eq. 1.2 for the case where $x=L/2$, we obtain

$$\theta = \frac{4\Delta}{Lg_1(\kappa)} \quad (2.4)$$

where

$$g_1(\kappa) = \begin{cases} \frac{2}{\kappa} \tan \frac{\kappa}{2} & \text{if } P < 0 \\ \frac{2}{\kappa} \tanh \frac{\kappa}{2} & \text{if } P > 0 \end{cases} \quad (2.5)$$

In computing these $P-\theta$ curves from the $P-\Delta$ curves, the following assumptions were made:

- (1) The computations associated with Eq. 2.4 utilize the point hinge model employed in the aforementioned physical theory models.
- (2) For the struts having boundary conditions different from simple supports, the effective member length kL is used instead of the member length L , and the effective lateral displacement Δ_{eff} is used in place of the lateral displacement Δ .
- (3) The value of the modulus of elasticity is assumed to be constant ($E = 29000$ ksi (200000 MPa)).

Using experimental $P-\Delta$ curves from Reference 1 in Eqs. 2.3 and 2.4, the $P-\theta$ curves shown in Figs. 2.8 to 2.10 were obtained. The theoretical (fully plastic) interaction curves between P and θ are also shown in these figures to illustrate the influence of plastic action. These interaction curves are computed by eliminating M from Eq. 1.4 by using the theoretical formulas for interaction curve between P and M listed in Table 2.3.

Prior to using these $P-\theta$ curves in subsequent discussions, it is important to assess the adequacy of Assumptions (1) to (3) employed in computing these curves. Assumption (1), based on the point hinge model, seems to be relatively accurate and consistent with subsequent developments of the physical theory model.

Assumption (2) was used in computing the $P-\theta$ curve for Struts 19 and 23, both with fixed-pinned end conditions. However, this assumption was not used in computing the curves for the remaining struts, which were simply supported. It was observed that there was not a drastic difference between the shape of the $P-\theta$ curves for struts with fixed-pinned end conditions and those for the remaining simply supported struts. Therefore, Assumption (2) does not appear to create a large amount of error in the $P-\theta$ curves computed.

Assumption (3) is employed to simplify the evaluation of the modulus of elasticity; however, in reality, the modulus of elasticity varies from one cycle to the next. In order to observe

the error created by Assumption (3), two $P-\theta$ curves are computed for Strut 3 using two significantly different values of the modulus of elasticity: $E = E_0 = 29000$ ksi (20000 MPa) and $E = E_0/2 = 14500$ ksi (100000 MPa). A comparison of these curves, shown in Fig. 2.11, indicates that the value of the modulus of elasticity does not have a large influence. It appears that Assumption (3) does not cause significant error.

Based on this discussion, it can be concluded that the $P-\theta$ curves computed above are sufficiently accurate to be employed in discussing their behavioral characteristics and in comparing with analytical results.

2.4.2 Study of Behavioral Characteristics of Axial Force - Plastic Hinge Rotation Curves

The characteristics of the axial force - plastic hinge rotation ($P-\theta$) curves shown in Figs. 2.8 to 2.10 were studied zone by zone. These results are summarized in Table 2.4. The dominant influence of the effective slenderness ratio on the shape of $P-\theta$ curves is observed in these figures; the struts with smaller effective slenderness ratios exhibit the fuller curves.

Comparison of these empirical $P-\theta$ curves with a typical analytical $P-\theta$ curve representative of previous physical theory brace models shown in Fig. 2.12 is useful. This comparison indicates that the analytical curve does not account for the degradation of the hinge rotation in Zone EL2 and fails to represent the gradual transition from Zone ES1 to P1.

2.4.3 Degradation of Plastic Hinge Rotation

Degradation of the plastic hinge rotation θ in Zone EL2, an "elastic" zone, may seem paradoxical. It is usually assumed that plastic hinge rotation can occur only in the plastic zones. This is a consequence of the elasto-perfectly plastic nature of the idealized plastic hinge. However, in this context the term "elastic" does not necessarily mean that the plastic hinge is fully elastic, but rather indicates that the section is not fully plastic. Even in an "elastic" zone, some inelastic action can occur, resulting in a degradation of the plastic hinge rotation in Zone EL2. This is associated with two cases. First, materials are no longer elasto-perfectly plastic due to the Baushinger effect under reversed loading. Second, cycling produces complex distribution of residual stresses which would be expected to significantly lower the nominal yield moment,

thereby producing partial plastification of the hinge region in the "elastic" range.

2.5 Hysteretic Behavior of Tangent Modulus of Elasticity

The tangent modulus of elasticity deteriorates significantly during inelastic cycling. This deterioration is illustrated by observing the tangent modulus histories for two coupons. One coupon was cut from the W6×20 section, used for Struts 3 and 19, and another coupon was cut from the TS4×4×½ section, used for Strut 18. The stress - strain diagrams enable one to compute tangent modulus versus axial stress curves by the use of the following equation:

$$E_t = \frac{d\sigma}{d\epsilon} \quad (2.6)$$

where

E_t = tangent modulus of elasticity;

σ = axial stress;

ϵ = axial strain.

The shape of the tangent modulus versus axial stress curve, which plays an important role in the subsequent idealization of tangent modulus histories, can be seen in the example shown in Fig. 2.13 (a) and (b). Figure 2.13 (a) illustrates a cycle of a σ - ϵ relation and Fig. 2.13 (b) indicates the corresponding tangent modulus versus axial stress relation. Tangent modulus values are almost constant from Point A to Point B in this figure, i.e., until the first load history reversal. They increase discontinuously from Point B to Point B' when load history reverses at Point B-B'. They monotonically decrease during the unloading from Point B' to Point C.

Likewise, tangent modulus versus stress relations for the two coupons are computed (see Fig. 2.14). The tangent moduli are normalized by $E = 29000$ ksi (200000 MPa) and axial forces by the measured yield load for each strut. Since there are discontinuities in the tangent of the stress - strain curves at load history reversals, the tangent moduli are also discontinuous at these points. These figures show that the values of the tangent modulus:

- (1) are almost constant until the first load history reversal point.
- (2) increase discontinuously at load history reversals and decrease continuously after them until the next reversal.
- (3) degrade from one cycle to the next.

Based on these considerations, linear idealization curves for the six struts were developed, as shown in Fig. 2.14. The coupon test results for the W6×20 section (Struts 3 and 19) were also used in defining curves for Struts 1, 7, and 23 because there was no data for these wide flanges. In determining the linear idealization curve for each strut, the difference in loading conditions between the coupons and the struts was taken into account. The coupons were cyclically loaded below the yield stress in the first few cycles. They experienced complete yielding both in tension and compression in later cycles. Since Struts 7, 19 and 23 had similar loading conditions to these coupons, the linear idealization curves for these struts were chosen so that the curves could accurately simulate both the earlier and later cycles of the E_t-P curve of the corresponding coupon. On the other hand, Struts 1, 3, and 18 were loaded below the tensile yield stress even in later cycles. Hence the linear idealization curves for these struts were chosen so as to simulate the first few cycles of the E_t-P curve.

2.6 Residual Displacement due to Material Nonlinearities in the Nominal Elastic Range

This section discusses possible sources of the residual axial displacement of a strut. For the ideal elasto-perfectly plastic materials assumed, there are only two sources of the residual axial displacement for a strut: (1) concentrated plastic deformations at the plastic hinge and (2) axially distributed deformations due to yielding by tensile forces. For this reason, only these two sources were considered in the previous physical theory brace models which assume elasto-perfectly plastic material properties. It appears that these previous models fail to account completely for material nonlinearities of steel, which are not of an ideal elasto-perfectly plastic type, as can be seen from a stress - strain diagram of steel (see Fig. 2.15). In order to account for the influence of such material nonlinearities, "the residual displacement due to material

nonlinearities occurring in the nominal elastic range" is introduced as one more source of residual displacement. The existence of this residual displacement is assessed as below.

Let us observe the stress - strain diagram of a strut shown in Fig. 2.15. It indicates that axial strains increase from Point O to Point A and they decrease from Point A to B. During this process, the values of axial stress remain below the yield stress. Due to material nonlinearities, the average tangent of Curve A-B is larger than that of O-A. Such an increase of tangent moduli causes a residual strain O-B, defined as the residual displacement due to material nonlinearities. This residual displacement is implemented in our modeling for better simulation of cyclic buckling behavior.

2.7 Summary

Empirical studies undertaken in this chapter are summarized as follows. A set of zones was defined so as to facilitate interpretation of a cycle of member behavior. This zone definition was applied to hysteresis loops, axial force - plastic hinge moment curves, and axial force - plastic hinge rotation curves. This zone definition will also be used in developing the refined physical theory brace model.

The empirical axial force - plastic hinge moment ($P-M$) curves showed that the theoretical interaction curves were able to express overall behavior of the $P-M$ curves but failed to express such detailed aspects as strain hardening and strain softening. An empirical method for resolving these discrepancies will be discussed in the subsequent chapter. In the elastic zones, $P-M$ curves were almost linear although small nonlinearities were observed in the section of transition to a plastic zone. In the plastic zones, $P-M$ curves tended to follow the theoretical interaction curve. The characteristics of $P-M$ curves observed in this manner will be compared with the analytical results obtained using the refined physical theory brace model in Chapter 4.

Empirical axial force - plastic hinge rotation curves were computed from test data by the use of Eq. 2.4, derived for a "point hinge model" by Gugerli. Based on these curves, basic

behavior in each zone was studied and compared with a typical analytical $P-\theta$ curves used in current physical theory brace models. This comparison indicated that these models fail to include the degradation of plastic hinge rotations in Zone EL2. Several causes of this degradation were advanced.

A study of tangent modulus histories for two coupons indicated that tangent modulus values increase discontinuously at load history reversals, decrease after a reversal until the next reversal, and deteriorate from one cycle to the next. In addition, the existence of the residual displacements due to material nonlinearities was assessed from a qualitative observation of test data.

3. REFINED PHYSICAL THEORY BRACE MODEL

3.0 Introduction

This chapter introduces a refined physical theory brace model. This model is derived from the basic approach taken by Gugerli [8]. As introduced previously, he derived analytical expressions for the axial force - deformation behavior for a pin-ended bracing member with a plastic hinge at midspan (see Fig. 1.3). While these expressions are incorporated in the formulation of the refined model, the empirical behavioral characteristics noted in Chapter 2 are implemented in the new model. The behavioral characteristics implemented include: (1) the variation of the tangent modulus of elasticity during cycles, (2) the deterioration of the plastic hinge rotation in Zone EL2, and (3) the residual displacements due to material nonlinearities occurring in the nominal "elastic" range. These provide an improved representation of cyclic inelastic behavior. However, the model still does not completely account for the following features: (1) the Baushinger effect including the progressive degradation of tangent moduli during cycles, (2) local buckling, and (3) the gradual spread of plastification along the length of the brace.

In addition to discussing the analytical model used to represent the inelastic buckling behavior, numerical techniques used in this model are also examined in this chapter. Some of these techniques are related to the DRAIN-2D2 program [25] (see Appendix A), in which the refined model has been implemented as an inelastic-truss element. Dynamic analyses of complex braced structures can be performed with the aid of the DRAIN-2D2 program, which contains a series of planar elements in its library.

A user's guide for the computer analysis program for the refined model can be found in Appendix B. The complete information on the input data for the program is presented in this appendix.

3.1 Assumptions

The geometric representation adopted for the element is shown in Fig. 1.3. The following assumptions were made in formulating the refined physical theory brace model presented herein:

- (1) Every cross section along the axis retains its shape.
- (2) The effects of shearing stresses and strains are disregarded.
- (3) Plane sections remain plane.
- (4) Only cross sections with one axis of symmetry are considered.
- (5) The lateral deflections and the corresponding slopes are relatively small.
- (6) The tangent modulus of elasticity is employed in place of the initial modulus of elasticity so as to express material nonlinearities.
- (7) The degradation of the tangent modulus of elasticity from cycle to cycle is disregarded.
- (8) The beam segments become plastic at the tensile yield load. The effect of strain hardening is considered for axial loads exceeding the yield load.
- (9) The plastic deformations at the plastic hinge are determined based on the flow rule [22].
- (10) The zone definition introduced in Fig. 2.3 (a) to (d) is used. In addition, the rule of zone transition listed in Table 2.2 is employed.
- (11) The effective member length kL is used in place of the member length L for determining buckling characteristics.

While Assumptions (1) through (5) are identical to those used in the Gugerli model. Assumptions (6) through (11) are implemented in the new model so as to achieve a refined representation of cyclic inelastic behavior.

3.2 Basic Equations

3.2.0 General

The axial displacement, δ , of the brace consists of seven components,

$$\delta = \delta_e + \delta_g + \delta_p + \delta_{po} + \delta_{ly} + \delta_m + \delta_{mo} \quad (3.1)$$

where the first five terms are the same as in Eq. 1.6, δ_m denotes the residual displacement due to material nonlinearities in the nominal elastic range, and δ_{mo} is the cumulative value of δ_m .

The first five terms in Eq. 3.1 had already been employed by Gugerli. Nonaka used δ_e , δ_g , δ_p , and δ_{ly} to express δ . However, since δ_{po} was included in δ_p in Nonaka's formulation, it is basically identical to Gugerli's. By contrast, the last two terms in Eq. 3.1, δ_m and δ_{mo} , have been introduced in this research report. The definition of the term δ_m has already been discussed in detail in Section 2.6.

The formulas for δ_e , δ_g , and δ_p presented by Gugerli are almost taken directly into the refined model. The changes made to the Gugerli's formulation are to replace the initial modulus of elasticity E by the tangent modulus of elasticity E_t so as to better replicate material nonlinearities and to utilize the effective member length kL in determining the geometric shortening δ_g in order to represent arbitrary boundary conditions (see Fig. 2.4).

3.2.1 Axial Elastic Displacement

Due to the incremental nature of the tangent modulus, the formula of δ_e is expressed in an integral form:

$$\delta_e = \frac{L}{A} \int_0^P \frac{dP^*}{E_t(P^*)} \quad (3.2)$$

3.2.2 Geometric Shortening

The geometric shortening δ_g is evaluated from Eq. 1.8.

3.2.3 Plastic Hinge Displacement

Gugerli presented Eq. 1.10 for the plastic hinge displacement δ_p ; however, he did not explicitly specify a method for the evaluation of the integral in the right hand side of this equation. The method explained below is proposed for its evaluation.

The outward normal plastic flow rule resulting from Drucker's Postulate [22] states that the incremental deformation vector must be tangent to the interaction curve. In other words, the incremental deformation vector must be parallel to the normal vector of the interaction curve Φ , i.e.,

$$\begin{bmatrix} d\delta_p \\ d\theta \end{bmatrix} = \lambda \begin{bmatrix} \Phi_{,P} \\ \Phi_{,M} \end{bmatrix} \quad (3.3)$$

Let us assume that the the interaction curve is expressed as follows:

$$\Phi(M, P) = M - \underline{M}(P) = 0 \quad (3.4)$$

in which $\underline{M}(P)$ is the theoretical P - M interaction curve as a function of P .

By eliminating the constant λ from Eq. 3.3 (dividing the first line by the second line) and using Eq. 3.4 to compute $\Phi_{,P}$ and $\Phi_{,M}$, one can arrive at the following expression for $d\delta_p$:

$$d\delta_p = -d\theta \frac{dM}{dP} \quad (3.5)$$

Substitution of this equation into Eq. 1.10 yields the formula for δ_p .

$$\delta_p = - \int_{P_0}^P \frac{dM(P^*)}{dP^*} \frac{d\theta}{dP^*} dP^* \quad (3.6)$$

Since formulas for the interaction curve $\underline{M}(P)$ are in many cases simple, it is easy to calculate the derivatives for $\underline{M}(P)$. By contrast, it is usually difficult to calculate the derivatives for θ (see Eq. 1.4 for the expression of θ). In order to avoid such a difficulty, Eq. 3.6 is rewritten by integrating by parts.

$$\delta_p = - \left(\frac{dM(P^*)}{dP^*} \theta \right) \Big|_{P_0}^P + \int_{P_0}^P \frac{d^2M(P^*)}{dP^{*2}} \theta(P^*) dP^* \quad (3.7)$$

It is suggested that this equation, which does not include the derivative of θ , be used in computing δ_p . The plastic hinge rotation θ used in this equation can be determined by the use of Eq. 1.4.

3.2.4 Tensile Yield Displacement

In Zone PY, tangent stiffness values are assumed to be a constant, $R \times E$ (see Fig. 3.1), where R denotes the strain hardening ratio as a proportion to the initial value of modulus of elasticity, E . For this reason, the tensile yield displacement δ_{ly} is not a function of axial force P , but of the given axial displacement $\underline{\delta}$, that is,

$$\delta_{ly} = \underline{\delta} - (\delta_e + \delta_g + \delta_p + \delta_{po} + \delta_m + \delta_{mo}) \Big|_{P = P_y} \quad (3.8)$$

3.2.5 Residual Displacement due to Material Nonlinearities in the Nominal Elastic Range

A discontinuity in the values of E_t at a load history reversal point results in a discontinuity in the values of δ_e and δ_g . The elastic residual displacement due to material nonlinearities δ_m is defined as the sum of the gaps of these variable values at the load history reversal,

$$\delta_m = (\delta_e + \delta_g) \Big|_{E_t = E_t^+} - (\delta_e + \delta_g) \Big|_{E_t = E_t^-} \quad (3.9)$$

where

E_t^+ = value of the tangent modulus of elasticity just after the load history reversal;

E_t^- = value of the tangent modulus of elasticity just before the load history reversal.

3.3 Buckling Behavior

When an element shortens while on Zone ES1, it may buckle. For convenience buckling will be categorized into two behavioral modes: (1) elastic buckling and (2) plastic buckling. These two types of buckling, implemented in the new model, are explained below.

3.3.1 Elastic Buckling

Elastic buckling takes place in the following two cases (see Fig. 3.2 (a)):

- (1) The plastic hinge rotation is non-zero ($\theta \neq 0$) due to plastic deformations on previous cycles. In this case the member is not initially straight.
- (2) The plastic hinge rotation does not exist ($\theta = 0$) and at the same time the magnitude of the Euler buckling load P_{cr} is less than that of the compressive yield load $-P_y$.

$$|P_{cr}| < |P_y| \quad (3.10)$$

where P_{cr} is defined as follows:

$$P_{cr} = -\frac{\pi^2 E_t I}{(kL)^2} \quad (3.11)$$

Note that the Euler buckling load P_{cr} is a function of E_t so that its value varies as the value of E_t varies.

In Case (1), the δ_g value becomes minus infinity at $P = P_{cr}$ as can be seen from Eqs. 1.8 and 1.9. Because of this singularity, axial compressive strengths cannot reach the Euler buckling load P_{cr} and slopes of the P - δ curve asymptotically approach to zero as the axial force P approaches P_{cr} . When a plastic hinge is formed at Point C in Figure 3.2, the decrease of compressive strength is initiated. The axial force at Point C is the maximum compressive strength reached and is defined as the buckling load.

In Case (2), the compressive strength increases until the buckling load P_{cr} is reached. When the axial force reaches P_{cr} , the strut buckles elastically at Point A. Next, a plastic hinge is formed at Point B, from which the compressive strength decrease is initiated. In this case, the buckling load equals the Euler buckling load.

3.3.2 Plastic Buckling

Plastic buckling takes place when both of the following two equations are satisfied (see Fig. 3.2 (b)):

$$\theta = 0 \quad (3.12.a)$$

$$|P_{cr}| > |P_y| \quad (3.12.b)$$

A plastic hinge is then formed when the axial force reaches the compressive yield load $-P_y$. After the plastic hinge has been formed, compressive strengths decrease following the interaction curve. Hence the load $-P_y$ can be defined as the nominal buckling load.

3.4 Empirical Formulas Employed in the Model

3.4.0 General

This section presents empirical formulas for the interaction curve, for the axial force - plastic hinge rotation curve, and for the tangent modulus of elasticity based on the experimental cyclic inelastic behavior of the aforementioned six struts.

3.4.1 Axial Force - Plastic Hinge Moment Interaction curve

As previously mentioned, there are discrepancies between the experimental $P-M$ interaction curves and the theoretical ones. In order to reduce these discrepancies, the following empirical formulas for the $P-M$ interaction curve is introduced (see Fig.3.3):

$$M = \underline{M}^*(P) \quad (3.13)$$

$$\underline{M}^*(P) = \underline{M}(P) \cdot \alpha_i \quad i = t \text{ or } c \quad (3.14)$$

where

\underline{M}^* = function for empirical $P-M$ interaction curve as a function of P ;

α_t = magnification factor for the $P-M$ interaction curve on the tension side;

α_c = magnification factor for the $P-M$ interaction curve on the compression side.

Two different magnification factors, α_t and α_c , are employed so as to express the unsymmetric nature of the interaction curves observed in the experiments.

In order to simplify the element, the theoretical interaction curve is simulated by two parabolic curves and a horizontal line (see Fig. 3.4):

$$m = 1 + b_1 p + c_1 p^2 \quad 0 \leq p \leq p_{12}$$

$$\begin{aligned}
 m &= a_2 + b_2 p + c_2 p^2 & p_{12} \leq p \leq 1 \\
 a_2 + b_2 + c_2 &\leq m \leq 1 & p = 1
 \end{aligned}
 \tag{3.15}$$

where

m = normalized plastic hinge moment, M/M_p ;

p = normalized axial force, P/P_y .

Note that the users of the element need to define the normalized interaction curve only in the first quadrant.

It is possible to omit the horizontal cutoff at the yield load, $|p|=1$, by choosing $a_2 + b_2 + c_2 = 1$, as shown in Fig. 3.5. However, in this case, Eq. 1.4 yields a zero θ value for the yield load, which corresponds to the state where the strut is perfectly straight. In reality, such a state cannot be realized after cycles of buckling and yielding of the strut. By contrast, the interaction curve having the straight line part at the yield load is able to provide non-zero m and θ values for the yield load, thus expressing a crookedness of the strut. The use of a $P-M$ interaction curve having the horizontal cutoff is preferable for the case where the yield load is repeatedly reached.

3.4.2 Tangent Modulus of Elasticity

A piecewise linear axial stress - axial strain curve is often used to account for material nonlinearities (see Fig. 3.6 [27] for an example). This curve enables one to easily compute tangent moduli of elasticity, equal to the slope of this curve. However, such curves are not suited for modeling for the tangent modulus in this case because tangent moduli computed using this curve are very sensitive to the assumed shape of the curve. Moreover, abrupt changes in moduli occur as one progresses from one segment to another. Continuous curves are overly complex to implement and require differentiability.

In order to increase the accuracy of tangent modulus values, while retaining the desired simplicity, an empirical model has been formulated for the tangent modulus as a function of the normalized axial force P/P_y . Figure 3.7 (a) illustrates the tangent modulus model and Fig.

3.7 (b) illustrates the corresponding axial force - axial displacement curve. As can be seen from this figure, the history of the tangent modulus is defined zone by zone. The model is based on the following assumptions:

- (1) The tangent modulus is a function of the axial force P and the load history.
- (2) The deterioration of the tangent modulus from one cycle the next is omitted (i.e., the curves are assumed stable).
- (3) Tangent moduli are constant until the strut buckles or yields for the first time (this behavior corresponds to the state between Points A and B in Fig. 3.7).
- (4) Tangent moduli increase discontinuously at the buckling points and maximum load points. (Points C-C' and D-D')
- (5) Tangent moduli decrease monotonically as axial forces decrease continuously. (C' to D)
- (6) Tangent moduli decrease monotonically as axial forces increase continuously. (D' to H)

Assumptions (1) and (2) are employed so as to simplify the model; Assumptions (3) through (6) are derived from the discussion in Section 2.5 with regards to the E_t-P relations for the two coupons. Let us note that Assumption (3) is also used to identify the behavioral difference between the E_t-P history prior to the first buckling or the first yielding and its history afterwards. This assumption reflects the concept presented by Popov and Peterson that there are two states of material: a "virgin state" and a "fully cycled state" [28, 29].

In addition to the basic characteristics of the E_t-P history model as discussed above, the pattern of decrease in tangent moduli needs to be defined. For this purpose, a simple model for the decrease pattern is shown in Fig. 3.8. As can be seen, two linear idealization curves are used to define the decrease pattern. The first curve is used when axial forces decrease continuously, while the second is used when axial forces increase continuously. Through the selection of the values of four parameters e_1 , e_2 , e_3 , and e_4 , users are able to account for available information regarding the tangent modulus of elasticity of the strut analyzed. The model for the tangent modulus history presented in this manner will contribute to better analytical

representation of cyclic inelastic behavior.

3.4.3 Axial Force - Plastic Hinge Rotation Curves

Current physical theory brace models yield an analytical axial force - plastic hinge rotation ($P-\theta$) curve as shown in Fig. 2.12. This $P-\theta$ curve shows that the values of plastic hinge rotation are constant in the elastic zones, increase in Zone P1 and decrease in Zone P2. As previously mentioned, these models fail to implement several observed empirical features, including: (1) a degradation of plastic hinge rotation in Zone EL2 and (2) a gradual transition from Zone ES1 to P1. In order to resolve these problems, the $P-\theta$ relation model shown in Fig. 3.9 is proposed.

The model incorporates the degradation of θ in Zone EL2 by the use of the following assumptions. In Zone EL2, θ decreases following the straight line, where this line is defined by the following two points: the zero crossing point of Zone EL1 and the point having the coordinate $(0,\beta)$. Let us note that β must be greater than 1.0, which corresponds to the normalized yield load. The selection of β less than or equal to 1.0 would result in such erroneous analytical behavior that the plastic hinge would remain elastic even for large tensile forces.

The gradual transition from Zone ES1 to P1 is automatically implemented in the refined model due to the addition of a flat transition part, Zone BU (see Fig. 3.9). In this zone, plastic hinge rotations increase until the plastic hinge becomes fully plastic, while axial loads are constant. The capability of the analytical axial force - plastic hinge rotation curve model as developed herein will be assessed in Chapter 4 based on quasi-static analyses of individual struts.

3.5 Method for Computing Transition Points

In analysis, the transition Points A to G shown in Fig. 3.10 must be computed. A method for computing these points is listed below:

- (1) Buckling Start Point (Pt. A)

$$\begin{cases} \delta = \delta_e \Big|_{P = P_{cr}} + \delta_{po} + \delta_{mo} \\ P = P_{cr} \end{cases} \quad (3.16)$$

- (2) Buckling End Point (Pt. B)

$$\begin{cases} \delta = (\delta_e + \delta_g) \Big|_{P = P_{cr}} + \delta_{po} + \delta_{mo} \\ P = P_{cr} \end{cases} \quad (3.17)$$

- (3) Buckling Point (Pt. C)

P is the solution of the simultaneous equations 1.4 and 3.13.

δ can be evaluated from Eq. 3.1.

- (4) Displacement History Reversal Points (Pts. D and G)

δ is given by the displacement history;

The corresponding P is computed from Eq. 3.1.

- (5) Plastic Point (Pt. E)

P is the solution of the simultaneous equations 1.4 and 3.13;

δ can be evaluated from Eq. 3.1.

- (6) Yield Point (Pt. F)

$$\begin{cases} \delta = \underline{\delta} \\ P = (\delta - \delta_y) \cdot \frac{AE}{L} \cdot R \end{cases} \quad (3.18)$$

where δ_y is the displacement at the yield load (see Fig. 3.1).

At the load history reversals (Points B, C, and G), the values of the cumulative deformations, δ_{po} and δ_{mo} , must be updated. Updating rules are as follows:

$$\delta_{po} \Big|_{NEW} = \delta_{po} \Big|_{OLD} + \delta_p \Big|_{pt. B, C, \text{ or } G} \quad (3.19)$$

$$\delta_{mo} \Big|_{NEW} = \delta_{mo} \Big|_{OLD} + \delta_m \Big|_{pt. B, C, \text{ or } G} \quad (3.20)$$

3.6 Solution Methods for Nonlinear Equations

The refined physical theory brace model formulates axial displacement δ as a function of axial force P , as do many physical theory brace models. Such a formulation, however, is inappropriate for the analysis of structures by the matrix displacement method, which defines force as a function of displacement. This necessitates iteration in evaluating P for a specified δ value. Also, the determination of the buckling point and the plastic point (Points C and E in Fig. 3.10) necessitates iteration.

In the refined model, the regula falsi (false position) method has been employed for these iterations. This method has only the first order convergence, while both the secant and the Newton methods have second order convergence. However, the regula falsi method has a guarantee of convergence, unlike the secant and the Newton methods. Since the primary concern of this research is on the modeling of cyclic buckling behavior, it is for the time being sufficient to use the regula-falsi method.

3.7 Computation of Tangent Stiffness for a Strut

In defining the member stiffness of a simply supported strut, it is common to define its value as the tangent of the axial force - axial displacement ($P-\delta$) curve. In our element, however, the $P-\delta$ curve is modeled by a set of curved lines so that even a very small change in the value of δ will result in the change of the tangent of the curve. In the DRAIN-2D2 program, in which the element is being implemented, the tangent stiffness matrix of the entire structure being analyzed is constructed by assembling the tangent stiffness matrices for each member. Reassembly and re-trianglerization of the structural stiffness matrix is required whenever member stiffness changes. For this reason, the direct use of the tangent of the $P-\delta$ curve as member tangent stiffness would necessitate the reassembly of the structure stiffness matrix at each solution step. This would result in excessive computational effort. In order to avoid such a problem, each zone is divided into a finite number of sections and member tangent stiffness is assumed to be constant during each section (see Fig. 3.11). The number of divisions is an

input parameter specified by the users. Note that the number of divisions for Zone P1 is twice that used for the remaining zones because Zone P1 has a much larger curvature. The use of this simplified computation of tangent stiffness, however, causes discretizing errors in tangent stiffnesses and unbalanced forces. In order to reduce these errors, a sufficiently large number of divisions must be specified.

3.8 Summary

In this chapter, the formulation of the refined physical theory model was introduced. The basic equations used in modeling were derived on the basis of a series of assumptions also presented herein. In addition, a number of empirical formulas were implemented in the model so as to incorporate the behavioral characteristics of braces noted in Chapter 2. The validity of this model will be assessed in the following chapters.

4. QUASI-STATIC ANALYSES OF INDIVIDUAL STRUTS

4.0 Introduction

The performance of the refined model developed in the previous chapter and implemented as an element for the DRAIN-2D2 program depends mainly on the following two features: (1) the ability of the model to simulate a brace's axial force - axial displacement curve and (2) the capability of the numerical techniques used in the program. This chapter treats the first feature; the second will be studied in the following chapter.

Quasi-static analyses are performed on each of the six struts introduced in Chapter 2. Experimental data for these struts is used to assess the validity of the analytical results. Since the DRAIN-2D2 program is not suitable for these quasi-static analyses, a simple main program was developed to exercise the element through a specified displacement history in order to obtain the desired analytical results.

In discussing analytical cyclic buckling behavior, it has been common to inspect axial force - axial displacement curves and $P-M$ interaction curves. As mentioned in the introduction, the refined model attempts to simulate other aspects of the behavior, including axial force - plastic hinge moment curves, axial force - plastic hinge rotation curves, and so on. The experimental and analytical results are compared from these standpoints as well. Drawbacks of the model are identified and discussed in detail so that the model may be improved in the future.

4.1 Input Data for Analyses

This section introduces a series of input data for each strut analyzed. Figure 4.1 contains displacement histories for each strut analyzed. These were the same as imposed in the experiments. Table 2.1 contains the values of the effective member length and the yield stress. Note that the concept of effective member length is utilized to apply the refined model to the strut which is not simply supported.

Table 4.1 presents the values of the parameters used for defining the empirical formulas presented in Section 3.4. As shown in this table, the β values, defining the analytical axial force - plastic hinge rotation curve, were chosen as 1.2 for all the struts. This selection of β values was done based on the observation of empirical $P-\theta$ curves shown in Figs. 2.8 through 2.10. The parameters, p_{12} , b_1 , c_1 , a_2 , b_2 , and c_2 , used in defining the theoretical $P-M$ interaction curve were chosen based on the theoretical formulas for the interaction curve listed in Table 2.3. The magnification factors, α_t and α_c , used in defining the empirical $P-M$ interaction curve were selected so that this curve, defined by Eq. 3.13, is able to simulate the envelope of the experimental axial force - plastic hinge moment curves, shown in Figs. 2.5 through 2.7. The linear idealization curves shown in Figs. 2.14, based on the coupon test results (see Fig. 2.1), were suggested for use in defining the decrease pattern of tangent moduli of elasticity. Later in this chapter studies will be shown to indicate the sensitivity of analytical results to uncertainties in these input parameters.

4.2 Comparison of Analytical Results with Experimental Results

4.2.1 Axial Force - Axial Displacement Curves

Figures 4.2 to 4.7 compare analytical axial force - axial displacement ($P-\delta$) curves with experimental curves. As can be seen from these figures, the refined model is able to simulate the overall cyclic buckling behavior very well. However, the model fails to express the following detailed characteristics:

- (1) For slender struts with a kL/r value of 120 (Struts 1 and 23), the analytical results in Zones EL2 and P2 underestimate the slopes of $P-\delta$ curves and the tensile axial strengths. As can be observed from the experimental axial force - plastic hinge moment curves, these struts experienced strain hardening during the later cycles (see Figs. 2.5 and 2.7). A better implementation of the Baushinger effect in modeling would account for the effects of strain hardening and softening, thus resolving this underestimation.

- (2) Experimental $P-\delta$ curves, in many cases, show smooth transitions from Zone ES1 to Zone P1. However, analytical curves have a kink at the transition point (buckling point). This is due to an instantaneous transition from an elastic to plastic state at the plastic hinge location assumed in the refined model. In order to avoid such a kink, one must consider the effect of the gradual spread of plastification across a section and/or length of the brace.

4.2.2 Axial Force - Plastic Hinge Moment Curves

Analytical axial force - plastic hinge moment ($P-M$) curves, shown in Figs. 4.8 to 4.10, generally correspond well with the experimental data, except for the following minor problems. Firstly, the analytical $P-M$ curves have discontinuities at load history reversal points. Such physically infeasible behavior results from discontinuities in tangent modulus values at the reversals. Secondly, the model fails to represent the strain hardening in the later cycles of Struts 1, 3, and 23, and the strain softening in the later cycles of Struts 7 and 19.

4.2.3 Axial Force - Plastic Hinge Rotation Curves

Figures 4.11 and 4.12 compare the analytical axial force - plastic hinge rotation ($P-\theta$) curves with corresponding data derived from test results. These figures demonstrate the following features:

- (1) The first cycle of the $P-\theta$ curve has different behavioral characteristics from the remaining cycles. Such behavior results from the assumption that tangent moduli equal a constant until the strut experiences buckling or yielding for the first time.
- (2) For Struts 1, 3, 7, and 18, tensile axial forces are slightly overestimated when θ is large.
- (3) The refined model assigns straight line segments to the elastic zones; however, test data shows that actual elastic zones have significant curvatures.

In spite of these minor problems, the refined model is able to simulate the overall cyclic behavior of $P-\theta$ curves very well.

4.2.4 Buckling Loads and Maximum Tensile Loads

Many analytical models have attempted to represent the deterioration of the buckling load; however, it still remains an active subject for research. Reference 1 reported that there are two main causes of this deterioration: (1) material nonlinearities and (2) the crookedness of a strut. Previous physical theory brace models are able to account for the effect of the crookedness by including the plastic hinge rotation as a degree of freedom. However, these models fail to implement the effect of material nonlinearities. The refined model, however, is able to implement this effect by varying the tangent modulus of elasticity.

Figure 4.13 compares analytical buckling loads with experimental ones. The interrelation between them is relatively good except for Struts 7 and 19, for which buckling loads are overestimated. As can be seen from experimental $P-M$ curves, these two struts had exhibited significant strain softening during later cycles (see Figs. 2.6 and 2.7). This strain softening apparently resulted in the degradation of tangent moduli, which then resulted in the reduction of buckling loads. A better implementation of the Baushinger effect would enable the refined model to represent strain softening.

The maximum tensile load is an important feature to be simulated by the analytical model. Figure 4.14 compares analytical maximum tensile loads with experimental ones. These analytical results correlate well with experimental results except in the cases of Struts 1 and 23. As previously mentioned, it seems that these two struts were influenced by the Baushinger effect, not completely accounted for in the refined model.

4.3 Comparison with Other Analytical Models

In order to observe the capability of the refined model, this model is compared with a refined phenomenological model [24] and the Gugerli physical theory brace model [8]. Figure 4.15 shows the analytical $P-\delta$ curves obtained using these three models and corresponding experimental data. The analytical result for the Gugerli model was obtained with a special computer program developed following his algorithm. The analytical results obtained using this

program should be very similar to those of Gugerli's original model.

This comparison indicates that the $P-\delta$ curve obtained using the refined model correlates best with test data. The inclusion of 'the variation of the tangent modulus of elasticity' and 'the degradation of plastic hinge rotation in Zone EL2' has resulted in more accurate simulation of $P-\delta$ curves especially in the elastic zones. Because of the constant modulus of elasticity assumed in the Gugerli model, it fails to simulate the dramatic deterioration in the buckling load with cycling. This would appear to be a major limitation with that formulation.

Figure 4.16 compares $P-M$ curves obtained using the refined model and using the Gugerli model. The first result has discontinuities at load history reversals. The Gugerli model does not. However, the refined model shows much better overall simulation of the test data regarding the following features:

- (1) nonlinearities in the $P-M$ curves in Zones ES1 and EL2;
- (2) smooth transitions from an elastic zone to a plastic zone;
- (3) gradual increase of maximum plastic hinge moments from one cycle to the next.

The comparison of the $P-\theta$ curves, shown in Fig. 4.17, demonstrates that the refined model is superior to the Gugerli model. In the refined model, the $P-\theta$ curve has been improved by the assumption that plastic hinge rotations degrade in Zone EL2.

The phenomenological model, a one-dimensional model, appears to achieve very realistic results as shown in Fig. 4.15. This is somewhat misleading in that the numerous parameters needed to be specified for this model were derived on the basis of the experimental results. If a different loading history were specified or if the strut section or the effective slenderness ratio were altered, comparable results would not be expected. The reliance of these models on experimental and analytical results is a serious limitation.

The above comparisons of analytical results for these models have demonstrated that the refined model is superior to other models regarding the representation of cyclic behavior, at least for the quasi-static analyses of individual struts. Although the refined model requires a

little more empirical information than the Gugerli model, it appears worthwhile to prepare the information so as to improve analytical results.

4.4 Sensitivities of Analytical Results to Empirical Parameters

The users of the refined model need to select several empirical parameters, including α_t , α_c , β , and $E_t(P)$. In the foregoing analyses, the values of these parameters were chosen based on corresponding test data. These parameters will be subject to significant uncertainty in practice due to several factors, including material variability. In the design process, empirical parameters may have to be selected without supporting test data (since it is usually too costly to prepare test data for each strut of the structure to be analyzed). It is therefore desirable that analytical results not be too sensitive to the values of these empirical parameters.

In this section, the sensitivity of analytical results to these empirical parameters is examined by comparing analytical P - δ curves computed for different values of an empirical parameter. Also, the influence of each parameter on analytical results is identified.

The parameters α_t and α_c are used in defining an empirical P - M interaction curve. Figure 4.18 illustrates the influence of α_t values on P - δ curves, while Fig. 4.19 shows the influence of α_c values. The results seem to be relatively insensitive to these parameters. An increase in α_t , that is, an increase in the plastic hinge moment capacity in the tension side, reduces buckling capacities. On the other hand, an increase in α_c enlarges buckling loads.

The parameter β is used in defining the analytical axial force - plastic hinge rotation curve. Figure 4.20 compares hysteretic P - δ curves computed for three β values, 1.0, 1.2, and 1.4. Note that β value of 1.0 violates the aforementioned rule which requires it be greater than 1.0. For this case, Zone PI does not exist, even for very large tensile loads. Moreover, the analytically computed P - δ curve greatly overestimates both maximum tensile and buckling capacities. There are no significant differences between the results for $\beta=1.2$ and for 1.4. It appears that analytical results are insensitive to β as long as its values are not too close to 1.0. It is suggested that the β value be chosen to be equal to or larger than 1.2.

Figure 4.21 illustrates the influence of the idealized tangent modulus of elasticity on the $P-\delta$ curves. Each of the three curves shown is computed using one of three tangent modulus models Types 1, 2, and 3: Type 1 gives the smallest tangent moduli; Type 2, a larger moduli; and Type 3, the largest. As can be seen, tangent moduli are directly proportional to buckling load capacities and to maximum tensile loads. This tendency is more significant for larger tangent moduli.

From discussions in this section, it can be concluded that analytical $P-\delta$ curves, in general, are not very sensitive to the value of empirical parameters except for β values close to 1.0 and for large tangent moduli. Hence, uncertainties in the selection of the values for these parameters do not entail many practical problems.

4.5 Relative Contributions of Axial Displacement Components

The axial displacement δ is made up of seven components, as indicated in Eq. 3.1. This section studies the relative contributions of three major components: axial elastic displacement δ_e ; geometric shortening δ_g ; and plastic hinge displacement δ_p . Figure 4.22 shows the relative contributions of these components for three different effective slenderness ratios, 40, 80, and 120. This figure demonstrates the following features:

- (1) The larger the effective slenderness ratio, the larger the influence of δ_g . For large magnitudes of axial shortening, δ_g is by far the largest among these three components.
- (2) The relative contribution of δ_e in the δ value is amplified for large axial forces due to the reduction of the tangent modulus of elasticity and the reduced contribution of δ_g .
- (3) The relative contribution of δ_p is inversely proportional to effective slenderness ratios. The contribution is large for a kL/r value of 40 but almost negligible for kL/r of 120.

4.6 Effect of Boundary Conditions

Two types of boundary conditions, fixed-pinned and pinned-pinned, were used in the foregoing analyses. The concept of effective member length was employed in applying the refined model to the fixed-pinned boundary conditions. It has been observed that analytical results for the fixed-pinned case are as good as those for the pinned-pinned case. It can be concluded that the refined model is at least applicable to the fixed-pinned boundary conditions where this concept is used. Furthermore, it is expected that the concept of effective member length enables one to analyze struts with general boundary conditions. This concept will be applied to the fixed-fixed case in the dynamic response analysis of braced frames in the following chapters.

4.7 Concluding Remarks

In this chapter, quasi-static analyses of individual struts were undertaken for the verification of the refined physical theory brace model. The studies presented in this chapter demonstrate that the refined physical theory brace model is able to represent cyclic buckling behavior very well. Major results obtained in this chapter are summarized below.

The refined model is capable of accurately simulating $P-\delta$ curves, $P-M$ curves, $P-\theta$ curves, buckling loads, and maximum tensile loads. In addition, this model is superior to both state-of-the-art models: the Gugerli physical theory model and the refined phenomenological model. The refined physical theory model performed well due to the inclusion of new features: (1) the variation of tangent modulus of elasticity, (2) the degradation of plastic hinge rotations in Zone EL2, (3) the residual displacement due to material nonlinearities in the nominal elastic range, and so on. Moreover, it is expected that the performance of the model would be further improved by a better implementation of the Baushinger effect. The sensitivity of analytical results to empirical parameters (α_r , α_c , β , and E_t) is generally low except for (1) β values close to 1.0 and (2) large E_t values.

A study on the relative contributions of three major axial displacement components indicated the following points. The geometric shortening is the largest component for large amplitudes of axial shortening, while the contribution of the axial elastic displacement is enlarged for large amplitudes of axial forces. The contribution of the plastic hinge displacement is very small for struts with large kL/r and relatively large for struts with small kL/r . As the study of the effect of boundary conditions indicates, the refined model is applicable to arbitrary boundary conditions when the concept of effective member length is used.

5. DYNAMIC ANALYSES ON A THREE STORY X-BRACED FRAME

5.0 Introduction

The previous chapter demonstrated the capabilities of the refined physical theory brace model to simulate the shape of the axial force - axial displacement curve of an individual brace. The main objective of this chapter is to evaluate the reliability and practicability of the refined model when used to compute the dynamic response of braced frames under earthquake type excitations.

Extensive research has been performed on dynamic response analyses of braced frames [30-33]. The computational effort involved has led to the use of phenomenological type models in nearly all of these analyses. Because of the limited experience with physical theory models in application to dynamic analyses and the apparent increase in computational effort, a systematic study has been made herein on a simple braced frame. The model offshore structure shown in Fig. 5.1 has been extensively analyzed in recent years. Gilani and Mahin [33] analyzed this frame, utilizing the DRAIN-2D2 program in their analysis, employing the refined phenomenological model [24] to express the inelastic buckling behavior of steel braces, and using experimental data from Reference 31 for verification of the analytical results. In this chapter, the same frame is analyzed for verification of the refined physical theory model. While the DRAIN-2D2 program was also used for the analysis, the refined model was employed in modeling the braces. The validity of the analysis obtained using this model is assessed by comparison with corresponding experimental data and with Gilani and Mahin's previous analytical results.

The analytical dynamic responses of a structure obtained using the refined model are influenced by various factors, including: (1) the numerical techniques of the DRAIN-2D2 program, (2) the sectional, material, and other properties specified for the brace, and (3) the input earthquake ground accelerations. All of these factors need to be specified as input parameters for the program. It is crucial to the successful application of the refined model that these input parameters be properly prepared. A series of parametric studies are presented so as to provide

comprehensive information on the influence of these factors on the dynamic response of the braces and the structure analyzed.

As reported in Reference 31, the X-braced frame considered had relatively strong girders (horizontal braces) and columns (jacket legs) which permitted inelastic deformations to occur only in the diagonal bracing members. Hence, all the analytical results presented in this chapter are characterized by inelastic deformations concentrated in the diagonal bracing members. Cases in which plastic hinges form in girders and columns will be studied in the following chapter.

5.1 Analytical Modeling of the Frame

The frame selected for this analysis is a three story, X-braced, tubular steel frame, 17 ft 9 1/8 in. (5.4 m) and 75 in. (1.9 m) wide, representative of offshore platforms. This frame is a 5/48 scale model of a Southern California Example Platform. It has been tested by several researchers, including Ghanaat and Clough [30], Shing and Mahin [31], and so on. Also, several analyses have been undertaken on the frame [30,31,33]. Table 5.1 lists the section sizes of the bracing members, while member identification numbers are shown in Fig. 5.1.

The analytical modeling of the X-braced frame used in this study (Fig. 5.2) was taken from the report by Gilani and Mahin [33]. The only change made to their modeling of the frame was the replacement of the phenomenological model with the refined model. Those who are interested in more detailed aspects of this modeling may refer to Reference 33.

The X-braced frame was modeled using three types of one-dimensional elements implemented in the DRAIN-2D2 program, as illustrated in Fig. 5.2. The three elements consisted of (1) the bilinear truss element, (2) the beam-column element and (3) the refined physical theory brace element. Figure 5.3 illustrates the typical force - deformation model used in each element. The columns and the deck of the frame were represented by the beam-column element, able to represent the potential formation of the plastic hinge at member ends. Braces 2 and 4 had buckled during the experiments [32], but the remaining braces had not. Therefore,

Braces 2 and 4 were modeled using the refined model, while other braces were assumed not to buckle and were represented by the bilinear truss element. The mass of the frame was assumed to be concentrated at the deck level and to be equal to a value of $0.105 \text{ kip}\cdot\text{sec}^2/\text{in.}$ (18.3 m.t.), accounting for 99 percent of the total mass of the frame. As a viscous damping value, 1.5 percent tangent stiffness proportional damping was used. The measured initial period of the frame was 0.418 second.

The input data for the refined model were prepared following the procedure indicated in the previous chapter and referring to the user's guide for the refined model in Appendix B. Table 5.2 contains the input data used for this analysis. An effective length factor (k) of 0.5 was employed so as to account for the influence of fixed-fixed boundaries of the braces observed in the tests. The validity of the use of the effective length factor has already been studied based on simple analyses in Section 4.6.

5.2 Capabilities of the Refined Model for Earthquake Type Excitations

This section demonstrates the capabilities of the refined model under earthquake type excitations. A dynamic analysis was run on the X-braced frame using a record obtained during a shaking table test in which significant inelastic deformations were observed in Braces 2 and 4. This record is based on the 1952 Taft (S69E) record and is designated the 1952 Taft (S69E). It has a peak ground acceleration of 0.58g and a duration of 15 seconds. A constant time step, $\Delta t = 0.01$ second, was used for the step-by-step integration. The "event-to-event" solution strategy was employed. In other words, the tangent stiffness matrix for the entire structure was modified whenever any of the braces modeled by the refined model encountered an event, i.e., a stiffness transition. This analysis for the frame indicated that there was no yielding in the columns, horizontal braces, and lower panel braces. This agreed with the experimental results given in Reference 31, as well as previous analytical research [33].

Figures 5.4 and 5.5 illustrate the axial force - axial displacement ($P-\delta$) curves of Braces 2 and 4, respectively. Each of these figures also includes the corresponding experimental data

and the analytical results for the refined phenomenological model. Figure 5.6 shows the time history of the tip deflection computed, which represents the global behavior of the entire frame. As can be seen from these figures, the analytical time histories and $P-\delta$ curves obtained using the refined model correlated well with the experiment, especially in the first stage of the analysis. The refined model appears to accurately represent the shape of the $P-\delta$ curves. However, the amplitude of the tip deflection was overestimated after seven seconds. Moreover, both buckling loads and maximum tensile loads were overestimated after the first few cycles. It is very likely that these discrepancies are associated with local buckling observed during the experiment [32] (see Fig. 5.7). In general, the local buckling reduces buckling and tensile capacities. The refined model, which omits the effects of local buckling, fails to represent this reduction. Local buckling appears to be an important feature to be implemented in future modeling so as to represent cyclic buckling behaviors of braces with large plastic deformations.

As can be seen from Table 5.3, comparing relative CPU time for different models and numerical techniques, the refined model required approximately 50 percent more CPU time than the phenomenological model. Furthermore, as shown in Figs. 5.4 to 5.6, the phenomenological model is superior to the refined model regarding the simulation of buckling loads and maximum tensile loads in the later cycles. Again, such a characteristic resulted from the omission of the influence of local buckling in the refined model. The input parameters used for the phenomenological model were selected following the experiment to capture this aspect of the response. For the refined model, no special modeling was done. In addition, this element is able to exhibit smoother and more realistic $P-\delta$ curves. In other words, the refined model is able to represent a continuous degradation of tangent stiffness values in each zone, while the phenomenological model disregards this important characteristic.

The phenomenological model appears to be as capable as the refined model in the representation of the shape of $P-\delta$ curve. However, as mentioned in Chapter 1, the phenomenological model necessitates large amounts of information regarding the $P-\delta$ curve of the brace analyzed in specifying input parameters. This limits the usefulness of this model, as

it is usually too costly to prepare this information for hundreds of braces. Furthermore, it is very likely that the phenomenological model necessitates a series of trial runs prior to the final analysis in order to optimize input parameters. By contrast, the refined model requires relatively small amounts of information and does not necessitate any trial runs. The refined model can be more practical than the phenomenological model, especially in the case where there is no experimental data regarding the cyclic inelastic behavior of braces.

5.3 Parametric Studies

5.3.0 General

As demonstrated in the previous section, the refined model can accurately represent the dynamic response of the X-braced frame with the aid of the DRAIN-2D2 program. However, it is crucial in successful application of this model that input parameters be properly specified. This section offers a series of parametric studies in order to inspect the influence of input parameters on the dynamic response of the frame.

In these parametric studies, the analytical results presented in the previous section were taken as the standard case (see Figs. 5.4. to 5.6). By varying the value of each parameter investigated and comparing the analytical results obtained with those for the standard case, the sensitivity of the response to input data can be assessed. These comparisons are made for each of the $P-\delta$ curves of Braces 2 and 4 and the time history of the tip deflection.

5.3.1 Effects of Numerical Techniques

The DRAIN-2D2 program is a general purpose dynamic analysis program and as such incorporates various numerical techniques, including: the step-by-step integration scheme, the event-to-event solution strategy, and so on. It is vital to the successful application of the program that these techniques be properly used. This subsection demonstrates the influence of numerical techniques on analytical results. Furthermore, a suggestion is made for the proper use of these techniques.

(a) Time Step

The influence of time step (Δt) used in the step-by-step integration scheme on analytical results is studied below. The time step affects the cost of an analysis by controlling the number of computations performed. In addition, the results should improve by the use of smaller time steps due to the characteristics of the numerical methods and the improved representation of the hysteretic behavior of the members. A series of dynamic response analyses were performed on the X-braced frame using four different values of Δt : 0.01, 0.03, 0.05, and 0.07 second, with the use of the event-to-event method. These time intervals were selected so that Δt values of 0.01, 0.03, and 0.05 second satisfy the recommended maximum values for the constant average acceleration method used in the program:

$$\Delta t \leq \frac{T}{2\pi} \approx 0.067 \text{ (sec.)} \quad (5.1)$$

where T indicates the structure's period of vibration. This condition is derived assuming elastic structural response and the maximum value $T/2\pi$ is computed for the linear acceleration method. The Δt of 0.07 second violates this recommendation. The step-by-step integration scheme is unconditionally stable, but this limit is still often used to insure accuracy.

Figures 5.8 and 5.9 show P - δ curves for Braces 2 and 4 respectively, while Figure 5.10 contains the time histories of the tip deflection. For Δt of 0.07 second, which violates the previous recommendation, the analytical P - δ curves did not exhibit numerical instabilities. Nonetheless, the P - δ curves showed a significant underestimation of both positive and negative axial deformations. Moreover, the tip deflection history was greatly influenced with substantial reductions of peak deflections. Above all, Δt of 0.07 second was too large to obtain a smooth time history.

For Δt of 0.05 second, approximately 80 percent of the recommended limit, the time history was improved. However, the P - δ curves were still inaccurate. For Δt of both 0.01 second, (approximately 15 percent of the recommended limit), and 0.03 second (50 percent), the P - δ curves and the time history were each greatly improved.

These analytical results tended to demonstrate that the finer the time intervals, the better the analytical results. In practice, the use of Δt values ranging from 10 to 50 percent of the recommended limit is suggested. This is necessary to insure adequate tracking of the hysteresis loops in the dynamic response analyses of the structure.

(b) Event-to-Event Solution Strategy

Since the structure is assumed to remain linear during a step, equilibrium errors can occur at the end of a step if any change in element stiffness occurs. The DRAIN-2D2 program imposes unbalanced forces on the nodes of the structure analyzed so as to minimize cumulative effects of such errors within a previous step. These unbalanced forces, however, can become so large that they cause spurious results. The user can reduce the time step duration in such cases. Alternatively, the automatic event-to-event solution strategy implemented in the DRAIN-2D2 program greatly reduces unbalanced forces, thus reducing numerical errors.

The event-to-event method sometimes causes a flip-flop type instability at certain events (transitions between zones). This instability tends to occur when tangent stiffnesses change greatly between two neighboring zones. Figure 5.11 shows an example of the flip-flop type instability occurring when Zone ES1 exits to Zone P1. Since this problem is apparently associated with the DRAIN-2D2 program framework, no attempt has been made to devise a solution in this report. Users should use the step-by-step method when such flip-flop types of instability is observed.

In order to investigate the influence of the use of the event-to-event method on analytical results, two analyses were undertaken. The first analysis used the event-to-event method, while the second had used the step-by-step method. In both cases, a time step of 0.01 second was used. The first analysis resulted in approximately a 23 percent increase in CPU time (see Table 5.3 for a comparison of relative CPU time required for different numerical techniques). In the second analysis, the quality of the $P-\delta$ curves significantly deteriorated as can be seen from the $P-\delta$ curves for these two cases, shown in Figs. 5.12 and 5.13. The $P-\delta$ curves computed in the second analysis exhibited numerical instabilities, expressed by sharp kinks (see

Points A and B in Fig. 5.13). In addition, appreciable errors were caused by using the step-by-step method, as can be seen from Fig. 5.14, which compares the time histories for these two cases. It is worthwhile to use the event-to-event method in order to achieve more reliable analyses, despite the apparent expense of additional computations. However, it is important to note that the analytical results obtained using the step-by-step method with Δt of 0.01 second were very similar to those obtained using the event-to-event method with Δt of 0.03 second (see Figs. 5.8 through 5.10). For this reason, it can be stated that the step-by-step method necessitated three times smaller time steps in order to achieve comparable accuracy with the event-to-event method. A comparison of CPU times for these two cases (see Table 5.3) indicates that the use of the event-to-event method achieves an approximately 50 percent reduction in computational effort to attain the desired level of accuracy. To fully utilize this feature, however, additional research is needed to alleviate the flip-flop type of instabilities occasionally observed with this method.

5.3.2 Effects of Sectional and Material Properties

This subsection investigates the influence of the sectional and material properties of a single brace on the dynamic response of the frame. The sectional and material properties studied herein include the cross-sectional area (A), the cross-sectional moment of inertia (I), the interaction curve ($\underline{M}^*(P)$), and the tangent modulus of elasticity (E_t).

A series of analyses were carried out by varying the value of each of these parameters for Brace 2 by approximately ± 25 percent. Properties of all other braces were held constant. Figures 5.15 through 5.18 illustrate the effects of the sectional and material properties of Brace 2 on the dynamic response of the brace. As can be seen from these figures, these variations had relatively little effect on the brace behavior. Also, the global behavior of the frame, represented by the time histories of the tip deflection (see Figs. 5.19 to 5.22), was not greatly influenced by the variations. Thus, the dynamic response analysis of this X-braced frame, for which inelastic deformations are concentrated in the diagonal bracing members, is relatively stable with regards to the sectional and material properties of individual braces. Of course,

systematic changes in the properties of all braces might be expected to have a greater influence on the overall behavior.

5.3.3 Effects of Earthquake Ground Accelerations

This subsection discusses the effects of earthquake ground accelerations on the dynamic response of the frame. For this purpose, the following three ground acceleration records were used: (1) 1952 TAFT (S69E), (2) 1940 El Centro (N-S), and (3) 1949 Olympia (E-W). All of these acceleration records had their peak ground acceleration amplitudes scaled to 0.35g. Comparisons of analytical results are shown in Figs. 5.23 and 5.24. As can be seen, the response of both the brace and the frame is totally dependent on the earthquake ground motion used. Thus, the greatest source of uncertainty in the analysis is the characteristics of the ground motion to be used. This will be examined in more detail in the next chapter. It is, however, clear that several different ground motions should be considered in the design and analysis of a structure.

5.4 Concluding Remarks

As illustrated in the foregoing analyses, the refined physical theory brace model can accurately simulate the dynamic response of braced structures. Furthermore, the refined model is superior to the phenomenological model in that the refined model does not necessitate the extensive empirical information on the shape of $P-\delta$ curves of the brace analyzed. The refined model seems to be very useful, especially when such information is unavailable. The importance of local buckling, as a feature to be implemented in future modeling, was demonstrated.

Parametric studies monitored the effects of input parameter values on analytical results. The results of these studies showed that numerical techniques used in the DRAIN-2D2 program can cause appreciable errors, if used improperly. As suggested, it is advisable to use Δt values ranging from 10 to 50 percent of the recommended maximum value (Eq. 5.1) and to employ the event-to-event solution strategy if there is no flip-flop type instability. Whenever such instability is observed, the user should use the step-by-step method with a reduced time

step.

As discussed in the previous chapter, analytical results seem to be relatively insensitive to changes in input parameters. This is especially true in the case considered in this chapter where inelastic deformations were limited to a few braces. Larger errors may be associated with the user's selection of parameters which control the numerical techniques employed in the program. These must be carefully selected and results be thoroughly examined so as to detect the various types of instabilities that may occur. The largest source of uncertainty is associated with the choice of excitation used in the analysis. This selection must be carefully considered, and the use of an ensemble of ground motions is recommended.

6. EFFECTS OF BRACE DESIGN ON THE PERFORMANCE OF K-BRACED FRAME

6.0 Introduction

As the development of the high speed computer progresses, it is expected that it will become more common to carry out nonlinear structural analyses for the purpose of design. However, at present, the design of braced structures relies primarily on elastic analyses, despite the expected buckling and yielding of braces during earthquakes. Currently, a lack of computer programs conveniently applicable to the inelastic analyses of braced structures is limiting the progress of their design. The previous chapters demonstrated that the refined model can accurately represent not only the nonlinear behavior of braces but also the dynamic response of braced structures. There naturally arises a question of the model's suitability for use in the design of braced structures. This chapter applies the refined model to a limited study of the effect of brace design on the performance of the structure and an investigation of the nondeterministic nature of inelastic dynamic response of braced frames.

A series of analyses have been undertaken on a hypothetical full sized K-braced building frame. In these analyses, the intensity of the input earthquake ground accelerations were specified as strong enough as to cause not only buckling of braces but also plastic hinging in columns and girders. While the previous chapter presents the case where inelastic deformations in the frame occurred solely in braces, this chapter presents the case in which inelastic deformations are spread over braces, columns, and girders.

6.1 Analytical Modeling of the Frame

6.1.1 Structural Model

The braced frame studied in this chapter is derived from a part of a full-scale, six-story, steel structure built and tested in the Large Scale Structure Laboratory of the Building Research Institute (BRI), Ministry of Construction, Tsukuba, Japan. This building is 42.21 ft (15 m) square in plan and 73.43 ft (22.38 m) tall. A series of analytical and experimental works have been conducted on this building by members of the U.S.-Japan Cooperative Earthquake

Research Program [34 and 35]. The intent of the analyses reported herein is to assess the practicability of the brace model and to study the behavior of braced frames in general. Consequently, the modeling of the structure does not entirely represent the actual structure. Because of these simplifying assumptions, the analytical results presented herein would not be expected to match experimental data.

The general plan view of the building is illustrated in Fig. 6.1. This building is made up of six frames; Frames A, B, C, 1, 2, and 3. Frames A, B, and C are parallel to the direction of loading, shown by the use of the arrow in the figure, while Frames 1, 2, and 3 are perpendicular to this direction. The elevation view of Frame B is shown in Figure 6.2. The left half of this frame, which has K-bracing in every story, forms the basis of the analyses presented in this chapter. Table 6.1 lists the section sizes and material properties for the frame members, while Table 6.2 contains those for bracing members. Figure 6.3 indicates the member identification numbers adopted herein. The design of the frame analyzed herein has been taken almost directly from Reference 34. However, two minor changes were made to the design of the braces in order to realize more uniform distribution of inelastic deformations throughout the frame. A $5 \times 5 \times \frac{1}{4}$ section was used in place of the $6 \times 6 \times \frac{1}{4}$ section for Braces 7 and 8. In addition, the yield stresses of the braces were changed. The measured yield stresses are listed in Table 6.2 along with the values assumed in the analysis (indicated by the use of parentheses).

The K-braced frame was modeled using two one-dimensional elements: (1) the beam-column element and (2) the refined physical theory brace element. The former was used for the representation of columns and girders and the latter for braces.

The girders and columns were assumed to have moment-resisting connections and account for the potential formation of plastic hinges. Figure 6.4 shows the normalized interaction curve used for girders and columns. This interaction curve is based on the AISC specifications [36] for a strong axis bending for wide flanges. The yield loads and plastic moments of the cross section, used for defining interaction curves, were computed from the material properties of girders and columns listed in Tables 6.1. The strain hardening ratios

were assumed to be three percent. The effect of geometric nonlinearities was included for columns but disregarded for girders. For simplicity, the influence of both shear deformations and end eccentricities was omitted.

The braces in the model were pinned at their ends; however, an effective member length factor (k) of 0.5 was used to account for the influence of the boundary conditions associated with the construction details used. Euler buckling loads for these braces are much greater than their yield loads, as shown in Table 6.2. Therefore, plastic buckling is expected to prevail. The input data for the braces are listed in Table 6.3.

6.1.2 Gravity Loads

In the analyses in this chapter, the gravity load of the K-braced frame was assumed to be equal to dead loads, consisting of 75 psf (0.0036 MPa) for the roof and 90 psf (0.0043 MPa) for the floors. Based on the framing system used for the floor, it was assumed that 3/8 of the total area of the floor contributed to the gravity load applied to the K-braced frame. Figure 6.5 illustrates the contributing area, which is further divided into three areas, a^* , b^* , and c^* . Area a^* contributes to the concentrated load at the left end of the frame (Pt. D), Area b^* the right end (Pt. E), while Area c^* accounts for the distributed loads applied to the frame. Figure 6.6 illustrates the equivalent nodal gravity loads computed based on this assumption. These loads were applied to the frame as static nodal loads. Consistent with the experimental setup, live loading effects were disregarded in the analyses.

6.1.3 Dynamic Properties

The mass of the K-braced frame is lumped at each node of the frame, as shown in Fig. 6.7. The rotational mass of nodal points was disregarded. The total horizontal mass resisted by the braced frame is assumed to be equal to half of the mass of the building. This assumption reflects the Japanese building design codes and achieves a more desirable intensity of inelastic deformations. The mass of the building is computed by accounting for dead loads of floors.

It is not common to include vertical mass effects when only horizontal components of excitations are considered. However, it was observed in preliminary analyses that the central

nodes connecting K-braces to the girders often oscillate with very high frequencies when plastic hinges were formed at these nodes. In order to avoid such oscillations, the vertical mass for the nodes was included by taking into account the mass of one foot square section of the floor. Accurate and stable results were obtained as long as a reasonable tributary area was assumed for computing these masses.

One percent initial stiffness proportional damping was used as a viscous damping value. A period of 0.619 second, corresponding to the period for the first mode of Frame B computed by Midorikawa *et al* [35], was used in computing the damping coefficient. The validity of this assumption will be discussed in the following section based on analytical results.

6.2 Analysis of the Standard Case

In order to establish a standard case for subsequent comparisons, an analysis was performed on the K-braced six-story frame using the Taft (S69E) record with a peak ground acceleration of 0.60g. A constant time step, Δt of 0.007 second, was used for the step-by-step integration. The event-to-event method was not used to avoid the flip-flop type instability problem discussed in Chapter 5 (see Fig. 5.11).

Figure 6.8 shows the time history of the roof deflection of the frame. As can be seen, slightly more than four inches (101.6 mm) of maximum roof displacement occurred and approximately two inches (50.8 mm) of residual lateral roof deflection remained following the excitation. Figure 6.9 shows, in an elevation view, the inelastic deformations in the frame. In this figure, a curved line indicates buckling of a brace; a straight, dotted line denotes yielding; a curved, dotted line indicates that a brace had experienced both buckling and yielding. A dot denotes a plastic hinge formed in either a girder or column, while a number in this figure indicates the value of maximum plastic hinge rotation angle. These notations will be used throughout this chapter. As can be seen, there were large inelastic deformations in the columns and girders in the fifth and sixth floors, while the buckling and yielding of the braces were severe in the third and fourth floors. The bottom two stories remained elastic. Figure

6.10 illustrates the progress of inelastic deformations in the frame for five different times corresponding to Pts. A to E in Fig. 6.8. As can be seen, most of the inelastic deformations occurred in a very short time, from Pt. B to Pt. D. The plastic deformations which developed between these two points remained as residual plastic deformations.

Figure 6.11 describes the story lateral displacements at different times. Story displacement patterns were very close to the first mode shape until the frame was severely damaged at Point C. After this point, the patterns were greatly changed due to large interfloor drifts between the fifth and sixth floors. A soft story mechanism developed between the fifth and sixth floors associated with the yielding and buckling of the braces and the formation of plastic hinges in the columns (see Fig. 6.9 for the magnitudes of plastic hinge rotations).

In computing the damping of the frame, the period of the frame was determined based on the elastic first mode. However, there is a significant lengthening of the apparent natural period of the structure associated with the damping effects of the inelastic deformations (see Fig. 6.8). Also, the deflected shape of the frame was assumed to be equal to that of the elastic first mode. As can be seen from Fig. 6.11, this assumption held well until Point C, but it did not hold well after this point. Thus, the effective modal characteristics of the structure are changing significantly. Hence, the modeling of viscous damping effects, once the structure yields, is only an approximation at best. Fortunately, it is expected that hysteretic energy dissipation should dominate the response and that these uncertainties are acceptable.

It is also interesting to inspect the vertical vibration of Nodes 2, 5, 8, and 11, connecting the K-braces to the girders. Figure 6.12 shows the time histories of the vertical displacements for these nodes. As can be seen, changes in the amplitudes of these vibrations remained relatively small except for a time interval, $3.822 \leq t \leq 3.892$ second, in which most of the frame's damage occurred. Residual vertical displacements remained at these nodes after this time interval. Nodes 5 and 8, where plastic hinges formed in the adjacent beams, exhibited large vertical displacements. Nodes 2 and 11, where girders remained elastic, exhibited small vertical displacements. Negligible vertical displacements occurred at Nodes 14 and 17 where beams and

braces remained elastic. Major portion of the vertical displacement at these nodes appear to be contributed by yielding of girders due to the differences between the tensile and compressive capacities of braces framing into them. It is important to design a girder having sufficient strength to avoid excessive girder deformations which can result in severe floor diaphragm damages.

Figures 6.13 and 6.14 illustrate the axial force - axial displacement curves for Braces 1 through 8. It appears that the refined model was able to accurately simulate the shape of axial force - axial displacement curves expected for these braces. In addition, the braces were capable of dissipating seismic energy under cycling, except for Braces 2 and 4, which remained elastic.

6.3 Influence of Brace Design on the Performance of the Frame

6.3.0 General

It is important to appropriately design bracing members so as to optimize the design of a braced frame. This section examines the influence of brace design on the performance of the K-braced frame. Parametric studies were undertaken with respect to the effective slenderness ratio of braces and their buckling capacities. In addition, the sensitivity of the frame's dynamic response to the section properties of a brace was investigated.

6.3.1 Influence of Effective Slenderness Ratios of Braces

The slenderness ratio of braces, the most important parameter influencing their buckling behavior, is expected to have a dominant influence on the overall performance of braced building frames as well. This section investigates the influence of the effective slenderness ratio of braces on the performance of the frame. Investigation of this influence is undertaken for six different kL/r ratios. The standard case presented previously has braces with kL/r ratios of approximately 50 ($42.7 \leq kL/r \leq 63.7$), while the other five cases have braces with kL/r ratios of 40, 60, 70, 80, and 90 respectively. Let us note that the section properties of a brace, represented by the section area (A), and moment of inertia (I), cannot be uniquely determined

by simply specifying a kL/r value. In order to determine these properties uniquely, the buckling loads for braces were kept constant for each different value of kL/r . This restriction reflects current design approach for braced building frames. Figure 6.15 contains the simplified buckling stress versus kL/r relationship used for defining buckling loads. As can be seen, plastic buckling prevailed for the cases with $kL/r \leq 60$ and elastic buckling prevailed for $kL/r \geq 80$. For kL/r of 70, elastic buckling prevailed for Braces 3 and 4, while plastic buckling prevailed for the remaining braces. Table 6.4 contains section properties of the braces as computed based on this relationship. Real sections were not selected but effective section properties were specified. The values of the plastic moment of cross sections M_p listed in this table were computed based on the assumption that M_p is proportional to \sqrt{AI} , i.e.,

$$M_p \propto \sqrt{AI} \quad (6.1)$$

For the plastic buckling cases, larger kL/r values resulted in smaller moments of inertia, while cross-sectional areas were constant. An exception exists for Braces 3 and 4 for $kL/r=70$, for which cross-sectional areas slightly increased from the standard case. For elastic buckling cases, larger kL/r values resulted in larger cross-sectional areas, while moments of inertia were constant.

Figure 6.16 compares the compressive sides of the $P-\delta$ envelope curves of Brace 7 for different kL/r ratios. The cases with kL/r of 80 and 90, for which elastic buckling prevailed, showed larger initial tangent stiffnesses than those of the remaining cases due to their larger areas. While the buckling capacities of braces were kept constant, the kL/r ratios were inversely proportional to their post-buckling capacities. Thus, braces with smaller kL/r ratios showed a fuller and more ductile post-buckling behavior. It can be stated that braces with kL/r of 80 and 90 have better (stiffer) pre-buckling behavior and braces with smaller kL/r have better (more ductile) post-buckling behavior.

Dynamic analyses were performed for these six cases with different kL/r ratios, while all other assumptions were the same. These analyses are discussed below. Figure 6.17 shows the time histories of the roof deflection computed for the six cases. Figure 6.18 shows the

maximum and residual roof deflections as a function of kL/r . The residual roof deflections were computed by averaging the amplitudes of the roof deflection from 10 to 15 seconds. For $kL/r \leq 70$, better responses (represented by smaller maximum and residual roof deflections) were observed for cases which had smaller kL/r ratios. These differences were influenced primarily by the plastic deformations occurring in one cycle at about 3.8 sec. For $kL/r \geq 80$, deflections decreased with increasing kL/r . Figure 6.19 compares the inelastic deformations in the frame for the six cases. The cases with $kL/r \leq 70$ exhibited both buckling of braces and yielding of girders and columns, while the case with kL/r of 80 showed less inelastic deformations, and that with kL/r of 90 showed no inelastic deformations at all. This improved performance of the structure with higher kL/r ratios appears to be a result of the altered dynamic characteristics of the building as a result of the stiffer braces used.

The following conclusions can be drawn based on these investigations. For constant buckling capacities of braces, the use of larger kL/r ratios ($kL/r \geq 80$) will increase the cross-sectional areas of braces. Increased cross-sectional areas improved the frame's dynamic response for the excitation considered by increasing its initial stiffness but, at the same time, boosted construction costs by increasing the requisite amount of steel. In addition, the tensile strength of the braces associated with the increased cross-sectional areas will be somewhat wasted. The possible large differences between tensile and compressive capacities with such braces will tend to result in girder plastification. Such a design, therefore, cannot be recommended.

For $kL/r \leq 70$, smaller kL/r ratios will make a frame more ductile and improve its dynamic performance without boosting the requisite amount of steel. Thus, the use of braces having small kL/r ratios is more desirable for the purpose of design. Of course, braces with small kL/r ratios have a decrease of wall thicknesses and thus tend to develop local buckling. It may be preferable to select kL/r ratios as small as possible in the design of braced frames, as long as the wall thickness ratios of braces satisfy code or other specifications regarding local buckling.

6.3.2 Influence of Buckling Capacities of Braces

In the previous section, the influence of kL/r ratios of braces was studied, while their buckling capacities were kept constant. In this section, the influence of their buckling capacities is studied for a constant kL/r ratio. For this purpose, a series of analyses were performed on the K-braced frame. Only the buckling capacities of Braces 3 and 4 are changed as these had undergone severe inelastic cycling in the analysis for the standard case. These analyses also indicate the sensitivity of the response of braced frames to design alternatives.

The buckling capacities for these braces, for which plastic buckling prevailed, are proportional to their yield stresses. For simplicity the variation in buckling load was accomplished in the program by the use of different yield stresses ranging from 50 to 80 ksi (344.5 to 551.2 MPa). Figure 6.20 illustrates the variation of maximum and residual roof deflections as a function of the buckling capacity of Braces 3 and 4. Although minor nonlinearities were observed, the cases with higher buckling capacities tended to show improved response represented by smaller maximum and residual roof deflections. Of course, such a tendency is dependent on the stiffness distribution in the frame and other factors so that the case may arise in which this tendency is violated. At the least, however, it appears that the buckling capacity of a brace is an important parameter influencing the dynamic response of the frame. An appropriate increase of buckling capacities of the braces can improve the performance of a braced frame. The results also indicate the general sensitivity of the response of this type of system to small changes in design. The refined model can be helpful in the appropriate specification of buckling capacities.

6.3.3 Influence of Section Properties of Braces

It was demonstrated in Subsection 5.3.3 that approximately ± 25 percent changes in the section properties of a single brace did not have a large influence on the dynamic responses of the X-braced frame, for which inelastic deformations solely occurred in bracing members. By contrast, the K-braced frame studied herein had undergone more distributed plastic deformations, occurring not only in braces but also in columns and girders. This section inspects the

sensitivity of the dynamic response of the K-braced frame to the selection of the following section properties of a brace: A and I .

A series of analyses, similar to those performed in Subsection 5.3.3, were undertaken for the K-braced frame by varying the value of each of the A and I values of Brace 3 by ± 25 percent. Properties of all other bracing members were held constant. Figure 6.21 and 6.22 illustrate the influence of the variations of these values on the roof deflection histories. As can be seen, its behavior is significantly affected by the values of I and is greatly influenced by A values. Thus, the dynamic response of the K-braced frame, under large inelastic deformations, was highly sensitive to the section properties of a single brace.

In general, the dynamic response of a concentric braced building frame under severe earthquakes is highly nonlinear and extremely complex. Moreover, the plastification of such a frame occurs progressively. A mere formation of a plastic hinge or buckling of a brace can cause significant redistribution of the frame stiffness, resulting often in further plastic hinge formations and/or brace buckling. Thus, the dynamic response of a concentric braced frame undergoing large inelastic deformations can be extremely sensitive to the section properties of individual braces. By contrast, the response of the X-braced offshore platform frame, which had much stronger framing members, was relatively insensitive to a brace's section properties (see Chapter 5). Hence, it is clear that that framing members also have a great contribution to the dynamic behavior of the frame. Thus, appropriate methods for designing the frame and assessing their contribution to the behavior of the braced frame are subjects requiring further studies.

6.4 Nondeterministic Nature of the Dynamic Response of the Frame

6.4.0 General

One can deterministically compute the inelastic dynamic response of a braced frame for specific input data with the use of the refined model. However, in reality, it is impossible to predict such a response deterministically because of the nondeterministic and uncertain nature

of the some of the input data. The following can be pointed out as examples: the yield stresses of braces, the earthquake ground accelerations, and so on. This section inspects the influence of the variations of some of these on the dynamic response of the K-braced frame.

6.4.1 Influence of Variations in Material Properties of Braces

There exist appreciable variations in the actual yield stresses of the steel used in practice. For example, the measured yield stresses of the braces for the K-braced frame differed by as much as 10 percent from the specified values, as can be seen from Table 6.2. Such variations in steel strength may be a major source of the errors in the dynamic response analyses of braced frames. In order to investigate the influence of these variations, a series of analyses were performed on the K-braced frame by the use of three different yield stresses for Braces 3 and 4: 55, 60, and 65 ksi (379.0, 413.4 and 447.9 MPa). As can be seen from Fig. 6.23, an approximately 18 percent change in the yield stresses for Braces 3 and 4 greatly influenced the dynamic responses of the frame. The influence of yield stresses on the inelastic deformation distribution in the frame is illustrated in Fig. 6.24. As can be seen, the change in yield stresses for Braces 3 and 4 drastically affected the distribution of inelastic deformations. In practice, it is possible that variations in steel strength can cause a significant redistribution of the structure's stiffness, thus resulting in unanticipated and undesirable behavioral modes of the structure. It is very important to consider the effects of material variability in order to prevent such behavior. This consideration, however, requires a probabilistic study of the frame's performance. Since such a study necessitates an extensive series of dynamic inelastic analyses of braced frames, the availability of a versatile and economical computer program for these analyses is crucial to the progress of the probabilistic design of braced frames.

6.4.2 Influence of Variations in Earthquake Ground Accelerations

In an earthquake resistant design of braced frames, it is common to design frames based on a few specific earthquake ground accelerations. In order to assess the influence of the accelerations, a series of analyses were performed on the K-braced frame using four different earthquake ground acceleration histories. These accelerations consisted of the 1952 Taft

(S69E) records with a peak ground acceleration of 0.60g and with a peak of 0.35g, as well as the 1940 El Centro (N-S) record with peaks of 0.60g and 0.35g.

Figure 6.25 illustrates the time histories of the roof deflection computed for these accelerations. As can be seen, input ground accelerations greatly influenced the performance of the frame. For example, the frame oscillated with larger amplitudes for the El Centro records than for the Taft records at the same peak ground accelerations. Figure 6.26 compares inelastic deformations in the frame for these cases. For the 1952 Taft (S69E) record with a peak of 0.60g, inelastic deformations were concentrated in the fourth through sixth floors, while inelastic deformations mainly occurred in the third and fourth floors for the El Centro record with a peak of 0.60g. One can state that the patterns of inelastic deformation distribution are dependent on the characteristics of earthquake ground accelerations. Therefore, there is no guarantee that a frame designed "optimally" for one acceleration will perform well for other accelerations even if peak ground accelerations are similar. It is suggested to consider the effects of the variations of earthquake ground accelerations in the design of braced frames.

6.5 Concluding Remarks

In this chapter, the refined model was applied to the study of the influence of brace design on the performance of a K-braced frame and the investigation of the nondeterministic nature of the dynamic response of the frame. This braced frame showed highly complex behavior, including: the yielding of columns and girders, and the buckling and yielding of braces. Furthermore, the dynamic response of the frame was sensitive to both small changes in brace design and to uncertainties in model input data. Such high sensitivity seems to be associated with redistribution characteristics of system and frame action. Further future study of frame contribution is desired.

Major conclusions drawn from this study are summarized below. Parametric studies were undertaken by changing the effective slenderness ratios (kL/r) of braces and by keeping the buckling capacities of braces constant. The use of braces with kL/r ratios smaller than 70 can

improve the post-buckling behavior of braces and fully utilize the energy dissipation capabilities of braces. Above all, it does not boost construction costs compared to more slender braces with the same buckling capacity. It appears advisable to use braces with smaller kL/r values, though a more thorough study of this is required.

The influence of the buckling capacities of the braces on the dynamic response of the frame was studied. It was observed that appropriately increased buckling capacities could greatly improve the performance of the frame. The refined model can be helpful in the selection of buckling capacities.

It appears that the section properties of a single brace have a large influence on the dynamic response of a braced building frame with large inelastic deformations spreading over braces, girders, and columns. The use of appropriately designed bracing members can greatly increase the ultimate strength of such a frame.

It is impossible to deterministically predict the inelastic dynamic response of a braced frame due to the nondeterministic and uncertain nature of various properties, including the yield stresses of braces and the earthquake ground accelerations. Parametric studies indicated a dominant influence of these properties on the dynamic response of the K-braced frame. It is suggested to consider the influence of variations of such properties in the design of braced frames. The probabilistic prediction of the inelastic dynamic response of a braced frame may be the problem to be settled in the future.

7. SUMMARY AND CONCLUSIONS

7.1 Summary

This research report presents a new physical theory type model for cyclic inelastic buckling analyses for steel braces. The major objectives of this investigation are to formulate this model, verify its validity, and assess its applicability to the seismic design and analysis of braced building frames.

In Chapter 1, previous research works on physical theory models for steel braces were reviewed. To give a better understanding of the different approaches used in formulating these models, the Gugerli and the Zayas models were described in some detail. In addition, limitations of the previous physical theory brace models were identified and discussed.

Various studies of test data were undertaken in Chapter 2 to identify experimental bases for an improved analytical model. Six representative struts were chosen from the 24 struts tested by Black, Wenger, and Popov [1]. These six struts, consisting of five wide flanges and a tube, had two types of boundary conditions, fixed-pinned and pinned-pinned. The effective slenderness ratios were either 40, 80, or 120. Axial force - plastic hinge moment curves and axial force - plastic hinge rotation curves were computed for the six struts. The observation of axial force - plastic hinge rotation curves assessed the existence of the degradation of plastic hinge rotations in Zone EL2. Tangent modulus versus axial stress histories were computed from stress - strain diagrams for two coupons. Qualitative observations of these histories were undertaken for the development of an analytical tangent modulus history model.

In Chapter 3, the formulation of the refined physical theory brace model was introduced. The geometric representation for this model consisted of a simply supported elastic brace member with a plastic hinge at midspan. The model included empirical behavioral characteristics noted in Chapter 2. Basic equations were derived with special attention to the variation of tangent modulus of elasticity during cycles and the effective member length. Two types of buckling, elastic and plastic, were defined. In addition, the method for the computation of transition points and the numerical iteration schemes for solving nonlinear equations were

introduced.

The refined model was applied in Chapter 4 to quasi-static analyses of individual struts. The analytical results obtained using this model were compared with experimental results based on many points of view, including hysteresis loops, axial force - plastic hinge moment curves, axial force - plastic hinge rotation curves, buckling loads, and maximum tensile loads. Also, the refined model was compared with the Gugerli physical theory model [8] and with a refined phenomenological model [24]. In addition, the following aspects were studied: (1) the sensitivities of analytical results to uncertainties in empirical parameters, (2) the effect of boundary conditions, and (3) the relative contributions of major axial displacement components.

In Chapter 5, the refined model was applied to dynamic response analyses of a three-story X-braced frame, a 5/48 scale model of a Southern California Example Offshore Platform. The analytical results presented represent the case where inelastic deformations were concentrated in bracing members. The capabilities of the refined model were assessed by comparing its analytical results with the test data and with the analytical results obtained using the phenomenological model. A series of parametric studies were undertaken regarding (1) numerical techniques, (2) the sectional and material properties of braces, and (3) earthquake ground accelerations. Both the numerical techniques and earthquake ground accelerations had a dominant influence on the frame's dynamic behavior, while the influence of sectional and material properties was relatively small. Suggestions were made for the proper use of the numerical techniques utilized.

The refined model was applied in Chapter 6 to the study of the design of braced frames. For this purpose, analyses were performed on a six-story, K-braced, steel frame; a part of a full-scale, six-story building built and tested in Tsukuba, Japan. The analytical results represent the case where inelastic deformations spread over braces, columns, and girders. Parametric studies were performed in order to identify the parameters for braces having large influence on the performance of the frame. The parameters studied include slenderness ratio, buckling strength, and material properties. In addition, the nondeterministic nature of the dynamic response of braced frame was investigated.

7.2 Conclusions

The major conclusions regarding empirical results, analytical results, and studies related to design decisions attained through this research are set forth as follows.

(a) Empirical Results

The zone definition presented in Fig. 2.3 (a) through (d) helps the explanation of the physical behavior of struts with various effective slenderness ratios ($kL/r = 40, 80, \text{ or } 120$). This zone definition is applicable to axial force - axial displacement curves, axial force - plastic hinge moment curves, and axial force - plastic hinge rotation curves. Both elastic zones and plastic zones (excluding the elastic buckling zone) are irreversible and enter another zone upon displacement history reversals. Nonlinear transitional regions exist in member behavior in the transition from an elastic to a plastic zone. For example, plastic hinge rotations degrade in Zone EL2, an elastic zone. The major causes of this degradation and transition include: material nonlinearities, nonuniform distributions of axial stresses in the cross section at the center hinge, partial yielding of the cross section at the hinge, and the gradual spread of plastification along the length of the brace.

Axial force - plastic hinge moment histories are insensitive to effective slenderness ratios. The ratios have a large influence on hysteresis loops as well as on axial force - plastic hinge rotation curves. Several empirical axial force - plastic hinge moment curves showed strain hardening or softening in later cycles. Such behavior resulted in discrepancies between the theoretical axial force - plastic hinge moment interaction curves and experimental ones. In axial force - plastic hinge rotation curves, the plastic zones are in good accordance with the theoretical axial force - plastic hinge rotation interaction curve.

Tangent moduli of elasticity are almost constant until a strut experiences tensile yielding or buckling for the first time. These values increase discontinuously at load history reversals and decrease after one reversal until the next. Meanwhile the values deteriorate during cycles.

(b) Analytical Results

The refined model is able to simulate the cyclic inelastic buckling behavior of braces very well both in quasi-static and dynamic analyses. Moreover, the refined model is superior to either the Gugerli model or the phenomenological model. The quality of a brace's axial force - axial displacement curve obtained using the refined model has been substantially improved by varying the tangent modulus of elasticity, degrading plastic hinge rotations in Zone EL2, and so on. Currently the model still does not completely account for the following features: (1) the Baushinger effect, including the progressive degradation of the tangent modulus during cycles; (2) local buckling; or (3) the gradual spread of plastification along the length of the brace. The performance of the refined model would be improved by the implementation of these features.

In the quasi-static analyses of individual struts, the analytical cyclic behavior of braces is relatively insensitive to both the required empirical parameters, and the sectional and material properties of braces. In the dynamic responses, the sensitivity of this behavior is highly dependent on the state of the inelastic deformations of the frame. In the case where inelastic deformations solely occurred in bracing members and the frame contributes significantly to the lateral resistance, sensitivity to sectional and material properties is substantially low. In the case where inelastic deformations spread over braces, girders, and columns, and the frame contribution is low, the sensitivity to these properties is very high. By contrast, the sensitivity of results to the earthquake ground motion records used is extremely high for both of these cases.

In dynamic response analyses utilizing the DRAIN-2D2 program, the numerical techniques of the program exert an important influence on analytical results. These techniques must be used properly. It is advisable to use the event-to-event procedure, with analysis time steps ranging from 10 to 50 percent of the recommended limit in Eq. 5.1.

(c) Studies Related to Design Decisions

The use of slender braces ($kL/r \geq 80$) to achieve a specified buckling load capacity can increase the initial stiffness of the frame but wastes tensile strength of braces, thus boosting construction costs. The use of stocky braces ($kL/r \approx 40$) can improve the post-buckling

behavior of braces without boosting these costs. Stocky braces are suggested for use in the design of braced frames provided the geometry of the section is resistant to local buckling.

Both an appropriate increase of the buckling capacities of braces and/or their sectional properties can improve the performance of braced frames. The refined model can be useful in the determination of appropriate specifications for these values.

The inelastic dynamic response of a braced frame has an unavoidable nondeterministic nature associated with variations in the yield stresses of the braces and in earthquake ground accelerations. These variations, which can have a large influence on the dynamic response of braced frames, must be considered in their design. For the time being, it is advisable to consider several different ground motions. However, the problem of combining the deterministic computation by the refined model with probabilistic design strategies remains to be solved.

REFERENCES

- 1 Black, R.G., Wenger, W.A.B. and Popov, E.P., "Inelastic Buckling of Steel Strut under Cyclic Load Reversals," Report No. UCB/EERC-80/40, Earthquake Engineering Research Center, University of California, Berkeley, CA., October 1980.
- 2 Zayas, A.Z., Shing, P.B., Mahin, S.A. and Popov, E.P., "Inelastic Structural Modeling of Braced Offshore Platforms for Seismic Loading," Report No. UCB/EERC-81/04, Earthquake Engineering Research Center, University of California Berkeley, CA., January 1981.
- 3 Higginbotham, A.B., "The Inelastic Cyclic Behavior of Axially-Loaded Steel Members," Dissertation, University of Michigan, Ann Arbor, January 1973.
- 4 Nilforoushan, R., "Seismic Behavior of Multi-Story K-Braced Frame Structures," University of Michigan Research Report UMEE 73R9, Ann Arbor, November 1973.
- 5 Singh, P., "Seismic Behavior of Braces and Braced Steel Frames," Dissertation, University of Michigan, Ann Arbor, July 1977.
- 6 Nonaka, T., "An Elastic-Plastic Analysis of a bar under Repeated Axial Loading," *Int. J. Solids Structures* 9, 560-580 (1973) (Erratum in No. 10, p.569).
- 7 Nonaka, T., "Approximation of Yield Condition for the Hysteretic Behavior of a Bar Under Repeated Axial Loading," *Int. J. Solids Structures*, 1977, Vol. B, pp. 637-643. Paramon Press. Printed in Great Britain.
- 8 Gugerli, H. and Goel, S.C., "Inelastic Cyclic Behavior of Steel Bracing Members," Report No. UMEE 82R1, Department of Civil Engineering, The University of Michigan, Ann Arbor, Michigan, January 1982.
- 9 Fujiwara, T., "Earthquake Response of Framed Structures Having Aseismic Elements Part 1," *Trans. of AIJ*, pp. 101-108, No. 285, November 1979.

- 10 Fujiwara, T., "Seismic Behavior of Inelastic Member of Braced Frame Structure," Proc. of 7th World Conference on Earthquake Engineering, September 1980.
- 11 Wakabayashi, M., Nonaka, T. and Shibata, M., "Studies on the Post Buckling Behavior of Braces, Part 1," Abstracts, Annual Meeting of Kinki Branch of AIJ, pp. 197-200, June 1972 (in Japanese).
- 12 Wakabayashi, M., Nonaka, T., Shibata, M., "Studies on the Post Buckling Behavior of Braces, Part 2," Abstracts, Annual Meeting of Kinki Branch of AIJ, pp. 1317-1318, October 1972 (in Japanese).
- 13 Wakabayashi, M., Nonaka, T., Shibata, M., Masuda, H. and Okada, K. " Studies on the Post Buckling Behavior of Braces, Part 3," Abstracts, Annual Meeting of Kinki Branch of AIJ, pp. 1013-1014, October 1973 (in Japanese).
- 14 Wakabayashi, M. and Shibata, M., "Studies on the Post Buckling Behavior of Braces, Part 4," Abstracts, Annual Meeting of Kinki Branch of AIJ, pp. 201-204, June 1976 (in Japanese).
- 15 Wakabayashi, M., Matsui, C., and Mitani, I., "Cyclic Behavior of a Restrained Brace Under Axial Loading," Proceedings, Sixth World Conference on Earthquake Engineering, Vol. II, New Delhi, India, January 1977, pp. 637-643.
- 16 Wakabayashi, M., Nonaka, T., and Yoshida, N., "Cyclic Behavior of Restrained Steel Brace under Repeated Axial Loading," Abstracts, Annual Meeting of Kinki Branch of AIJ, pp.197-200, June, 1976, (in Japanese).
- 17 Wakabayashi, M., Shibata, M. and Masuda, H., "An Elastic-Plastic Analysis of a Brace Subjected to End Displacement," Annuals, Disaster Prevention Research Institute, Kyoto University, No. 18B, pp. 143~154, April 1974 (in Japanese).
- 18 Prathuangsit, D., Goel, S.C., and Hanson, D., "Axial Hysteresis Behavior with End Restraints," Journal of the Structural Division, Proceeding of ASCE, Vol. 104, No. ST6, June 1978, pp. 883-895.

- 19 Mitani, i., "An Elastic-plastic Analysis of a Restrained Steel Bar under Repeated Eccentric Axial Loading," Transactions AIJ, No. 274, December 1978, pp. 65-73.
- 20 Toma, S. and Chen, W.F., "Cyclic Analysis of Fixed-Ended Steel Beam-Columns," Journal of the Structural Division, Proceeding of ASCE, Vol. 108, No. ST6, June 1982, pp. 1385-1399.
- 21 Timoshenko, S.P. and Gere, J.M., "Theory of Elastic Stability," Second Edition.
- 22 Drucker, D.C., "Plasticity," Structural Mechanics, Pergamon Press, London, 1960, pp. 407-488.
- 23 Okamura, H., Personal Meeting with Prof. Okamura, Prof. in Civil Eng. Dept., University of Tokyo, September 1983.
- 24 Ikeda, K., and Mahin, S.A., and Dermitzakis, S.N., "Phenomenological Modeling of Steel Braces under Cyclic Loading," Report No. UCB/EERC-84/09, Earthquake Engineering Research Center, University of California, Berkeley, CA., May 1984.
- 25 Golafshani, A. and Powell, G.H., "DRAIN-2D2, A Program for Inelastic Seismic Response of Structures," Ph.D. Thesis, Dept. of Civil Engineering, University of California, Berkeley, April 1982.
- 26 Zayas, V.A., Popov, E.P., and Mahin, S.A., "Cyclic Inelastic Buckling of Tubular Steel Braces," EERC Report No. 80-16, Earthquake Engineering Research Center, University of California, Berkeley, June 1980.
- 27 Mosaddad, B. and Powell, G.M., "Computational Models for Cyclic Plasticity, Rate Dependence, and Creep in Finite Element Analysis," EERC Report No. 82-26, Earthquake Engineering Research Center, University of California, Berkeley, November 1982.
- 28 Peterson, H. and Popov E.P., "Constitutive Relations for Generalized Loadings," Journal of Engineering Mechanics Division, ASCE, Vol. 103, No. EM4, Proc. Paper 13144, August 1977, pp. 611-627.

- 29 Popov, E.P. and Peterson, H., "Cyclic Metal Plasticity: Experiments and Theory," Journal of Engineering Mechanics Division, ASCE, Vol. 104, December 1978, pp. 1371-1388.
- 30 Ghanaat, Y. and Clough, R.W., "Shaking Table Test of a Tubular Steel Frame Model," Report No. UCB/EERC-82/02, Earthquake Engineering Research Center, University of California, Berkeley, January 1982.
- 31 Shing, P.B., Javadian, A.S. and Mahin, S.A., "Evaluation of Seismic Behavior of a Braced Tubular Structure by Pseudodynamic Testing," Report to the Offshore Technology Conference, June 1983.
- 32 Shing, P.B. and Mahin, S.A., "Pseudodynamic Test Method for Seismic Performance Evaluation Theory and Implementation," Report No. UCB/EERC-84/01, Earthquake Engineering Research Center, University of California, Berkeley, January 1984.
- 33 Gilani, A.S., and Mahin, S.A., "Earthquake Response of a Tubular Steel Offshore Platform," (in Publication), University of California, Berkeley.
- 34 Foutch, D.A., Yamanouchi, H., Midorikawa, M., and Nishiyama, I., "Construction of Full Scale Six Story Steel Test Structure," Fourth JTCC Meeting, Part of U.S.-Japan Joint Earthquake Research Project Utilizing Large Scale Testing Facilities, June 1983.
- 35 Midorikawa, M., Yamanouchi, H., Yamazaki, T., Sanda, D., and Takada, M., "Preliminary Analysis of The Full-Scale Six-Story Steel Building," Fourth JTCC Meeting, Part of U.S.-Japan Joint Earthquake Research Project Utilizing Large Scale Testing Facilities, June 1983.
- 36 "Manual of Steel Construction," Eighth Edition, Structural Steel Educational Council.


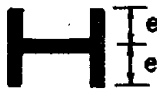
Table 2.1 List of Test Specimens
(1 ft. = 304.8 mm; 1 ksi = 6.89 MPa)

Strut No.	Shape	kL/r	kL(ft.)	Yield Stress (ksi)
struts pinned at both ends				
1	W8×20	120	12.5	40.4
3	W6×20	80	10.07	40.2
7	W6×15.5	40	4.87	50.0
18	TS4×4×½	80	9.07	82.0
struts pinned at one end fixed at the other end				
19	W6×20	40	5.03	40.2
23	W5×16	120	8.40	35.7

Table 2.2 Zone Transition Rules

Current Zones	Possible Next Zones	
	External Deformation Proceeds	External Deformation Reverses
ES1	EB, P1	EL1
EB	P1	EB
P1	none	EL1
EL1	EL2	ES1
EL2	P2, PY	ES2
P2	PY	ES2
PY	none	ES2
ES2	ES1	EL2

Table 2.3 Theoretical P-M Interaction Curves for Different Cross Sections [8]

Sections	Interaction Curve	Limits	M_p
	$\pm m = 1 - \frac{4}{3}p^2$ $\pm m = \frac{4}{3} \pm \frac{4}{3}p$	$ p < \frac{1}{2}$ $ p > \frac{1}{2}$	$\frac{3}{4}\sigma_y A_e$
	$\pm m = 1$ $\pm m = 1 - \left(\frac{\pm pA - A_w}{2A_f} \right)^2$	$ p < \frac{A_w}{A}$ $ p > \frac{A_w}{A}$	$\sigma_y A_f e$

$$A_f = \text{Cross-sectional area of flanges} \quad p = P/P_y$$

$$A_w = \text{Cross-sectional area of web} \quad m = M/M_p$$

Table 2.4 Plastic Hinge Rotation Behavior

Name of Zones	Plastic Hinge Rotation Behavior
ES1	gradually increases, the rate of its decrease is amplified near the buckling point.
EB	increases, while axial loads are almost constant.
P1	increases following the interaction curve.
EL1	slightly decreases when its values are large, whereas θ is almost constant when its values are small.
EL2	decreases as the tensile loads increase. The axial force and θ are almost linearly related.
P2	decreases following the interaction curve.
PY	decreases. The tendencies of the decrease are similar to those in Zone P2.
ES2	remains almost constant.

Table 4.1 Empirical Parameters for Struts 1, 3, 7, 18, 19, and 23

Parameters	Strut No.					
	1	3	7	18	19	23
β	1.2	1.2	1.2	1.2	1.2	1.2
α_t	0.7	1.0	0.7	0.8	1.0	1.0
α_c	0.7	1.0	0.75	0.9	1.0	1.0
p_{12}	.324	.25	.294	.5	.25	.23
b_1	0.0	0.0	0.0	0.0	0.0	0.0
c_1	0.0	0.0	0.0	-1.33	0.0	0.0
a_2	.771	.889	.827	1.33	.889	.911
b_2	1.42	.889	1.18	-1.33	.889	-.766
c_2	-2.19	-1.78	-2.01	0.0	-1.78	-1.69
e_1	0.30	0.30	0.15	0.05	0.15	0.15
e_2	1.0	1.0	0.9	0.9	0.9	0.9
e_3	1.25	1.25	1.20	1.25	1.20	1.20
e_4	0.0	0.0	0.0	-0.25	0.0	0.0

Table 5.1 Member Sizes and Material Properties [31]
(1 ksi = 6.89 MPa; 1 in. = 25.4 mm)

Member No. Description	Tube Dimensions Nominal Diameter (D) x Wall Thickness (t) (in.)	Yield Stress (ksi)	Ultimate Stress (ksi)
1,3	2 ½ × 0.049	30.7	40.2
2,4	2 ½ × 0.049	27.4	37.8
5,6,7,8	3 × 0.083	31.5	51.7
9,10	3 ½ × 0.083	32.0	53.0
11,12,13	2 ½ × 0.049	19.6	41.0
Jacket Legs	8 × 0.188	48.0	62.0

Table 5.2 Input Data for the Refined Model used in API Frame Analysis
(see Appendix B for Format Specification)

5	2	1	Element 5					
1	5	60	.000001	.000001				
2								
.377		24.0	1.201	29000.	0.15	0.90	1.2	0.
6.95		0.	1.	1.	1.25	.005	0.5	
1.0		-0.168	-0.765	1.	-0.168	-0.765		
.377		28.8	1.201	29000.	0.15	0.90	1.2	0.
6.95		0.	1.	1.	1.25	.005	0.5	
1.0		-0.168	-0.765	1.	-0.168	-0.765		
1	6	8	1	4				
2	6	7	2	4				

Table 5.3 Comparison of CPU Times for Different
Models and Numerical Techniques

Model	Phenomenological	Refined Physical Theory		
	Step-by-Step	Event-to-Event		Step-by-Step
Time Step	0.01 s	0.01 s	0.03 s	0.01 s
Relative CPU Time	44%	100%	39%	77%

Table 6.1 Member Sizes and Material Properties for Frame Members
(1 ksi = 6.89 MPa; 1 in. = 25.4 mm)

Member No. Description	Section Types	Yield Stress (ksi) *
1,2	W10 × 30	43.60
3,4	W10 × 60	42.60
5	W12 × 79	40.75
6,11	W12 × 106	39.05
7,8	W12 × 40	40.75
9,10	W12 × 72	41.75
12	W12 × 136	37.06
13,14,15,16	W16 × 31	40.33
17,18,19,20	W18 × 35	43.59
21,22,23,24	W18 × 40	43.03

* : Agrees with measured values [34]

Table 6.2 Member Sizes and Material Properties for Bracing Members
(1 ksi = 6.89 MPa; 1 kip = 4.45 kN)

Member No. Description	Section Types	Yield Stress (ksi)	kL/r	Euler Buckling Loads (kips)	P_y (kips)
1,2	4 × 4 × 1/5.56	55.0 (61.49)	63.7	194.	151.
3,4	5 × 5 × 1/5.56	60.0 (55.1)	50.4	390.	191.
5,6,7,8	5 × 5 × 1/4	50.0 (58.22)	51.9	488.	230.
9,10	6 × 6 × 1/4	55.0 (55.24)	42.7	875.	307.
11,12	6 × 6 × 1/2	55.0 (62.2)	52.4	1459.	572.

() : Measured yield stresses [34]

Table 6.3 Input Data for the Refined Model
used in the K-Braced Frame Analysis
(see Appendix B for Input Format)

5	12	0	Element 5					
1	5	60	.000001	.000001				
5								
2.75		55.0	6.7	29000.	0.15	0.90	1.2	0.
253.6		0.	1.	1.	1.25	.003	0.5	
1.0		0.	-1.3333	1.3333	-1.3333	0.		
3.47		60.0	16.9	29000.	0.15	0.90	1.2	0.
358.5		0.	1.	1.	1.25	.003	0.5	
1.0		0.	-1.3333	1.3333	-1.3333	0.		
4.59		50.0	16.9	29000.	0.15	0.90	1.2	0.
501.1		0.	1.	1.	1.25	.003	0.5	
1.0		0.	-1.3333	1.3333	-1.3333	0.		
5.59		55.0	30.3	29000.	0.15	0.90	1.2	0.
694.8		0.	1.	1.	1.25	.003	0.5	
1.0		0.	-1.3333	1.3333	-1.3333	0.		
10.4		55.0	50.5	29000.	0.15	0.90	1.2	0.
1455.5		0.	1.	1.	1.25	.003	0.5	
1.0		0.	-1.3333	1.3333	-1.3333	0.		
1	2	4	1	4				
2	2	6	1	4				
3	5	7	2	4				
4	5	9	2	4				
5	8	10	3	4				
6	8	12	3	4				
7	11	13	3	4				
8	11	15	3	4				
9	14	16	4	4				
10	14	18	4	4				
11	17	19	5	4				
12	17	20	5	4				

Table 6.4 Section Properties of Braces for
Different Effective Slenderness ratios
(1 kip = 4.45 kN; 1 in. = 25.4 mm)

Section Properties	Brace Number	kL/r					
		40	Standard Case kL/r ≈ 50	60	70	80	90
A (in. ²)	1,2	2.75	2.75	2.75	2.75	3.38	4.28
	3,4	3.47	3.47	3.47	3.57	4.66	5.89
	5,6,7,8	4.59	4.59	4.59	4.59	5.13	6.50
	9,10	5.59	5.59	5.59	5.59	6.88	8.70
	11,12	10.4	10.4	10.4	10.4	12.8	16.2
I (in. ⁴)	1,2	17.0	6.70	7.6	5.6	5.2	5.2
	3,4	21.5	13.5	9.6	7.2	7.2	7.2
	5,6,7,8	28.4	16.9	12.7	9.3	8.0	8.0
	9,10	34.6	30.3	15.4	11.3	10.7	10.7
	11,12	86.2	50.5	38.4	28.2	26.6	26.6
M _p (k·in.)	1,2	404.1	253.6	269.8	231.3	248.9	280.0
	3,4	452.1	358.5	301.8	265.8	303.7	341.7
	5,6,7,8	649.6	501.1	433.7	371.7	363.7	409.1
	9,10	742.3	694.8	495.6	424.8	452.7	514.3
	11,12	1904.1	1455.5	1269.4	1088.1	1170.9	1317.3

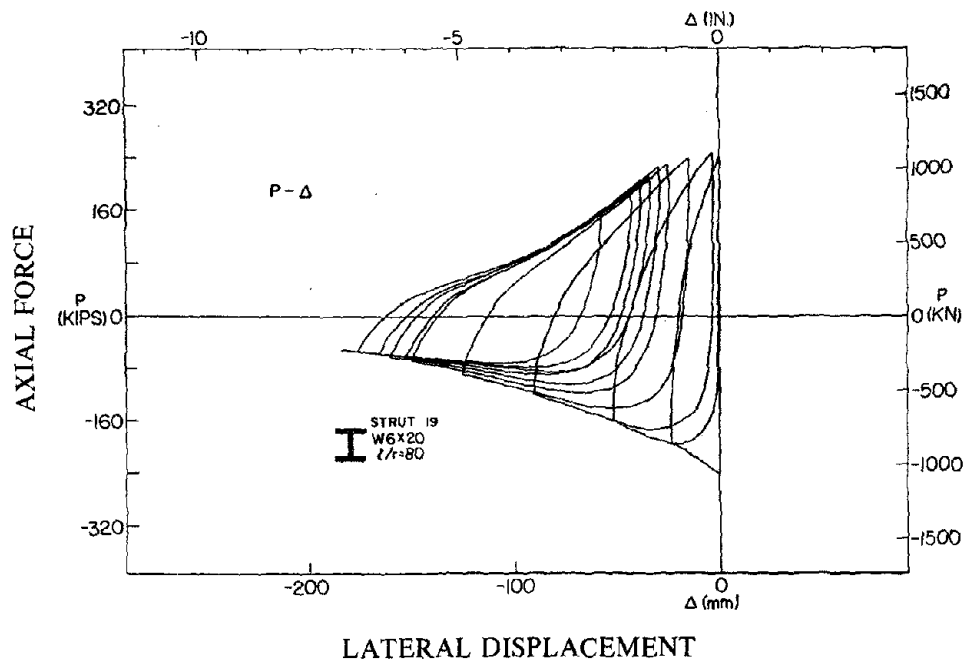
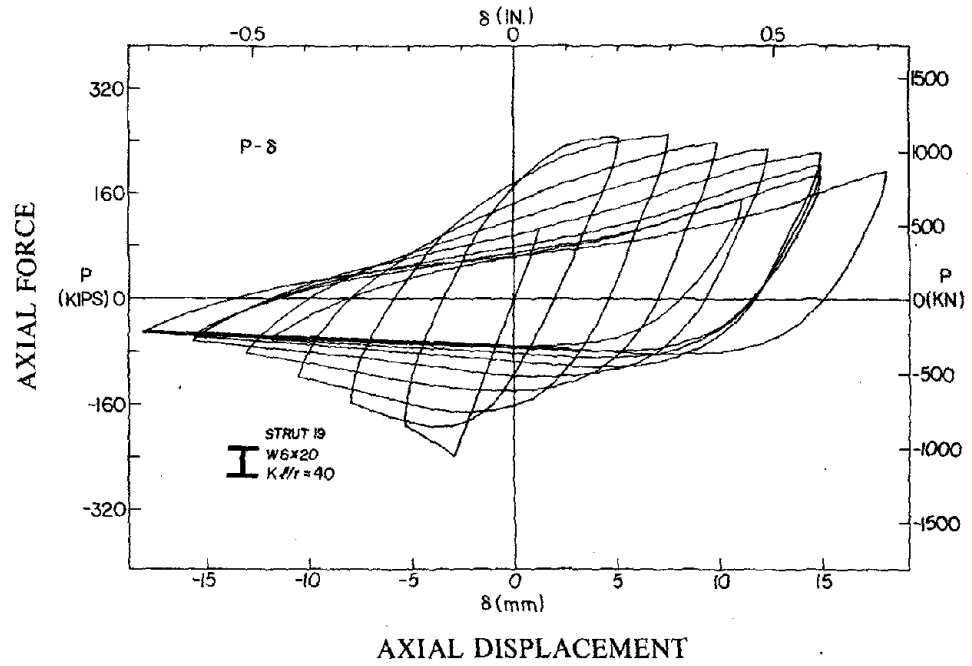
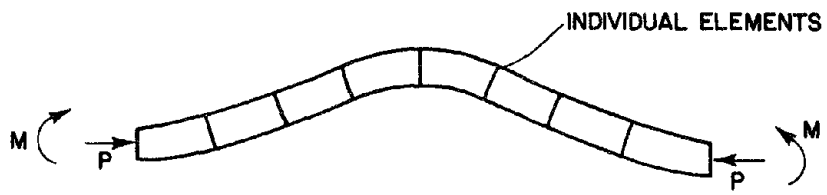
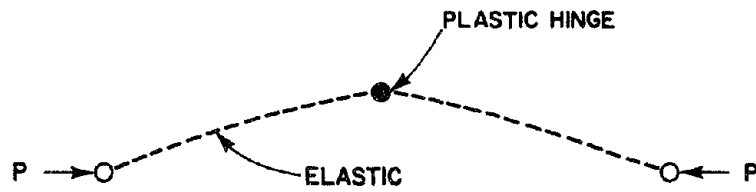


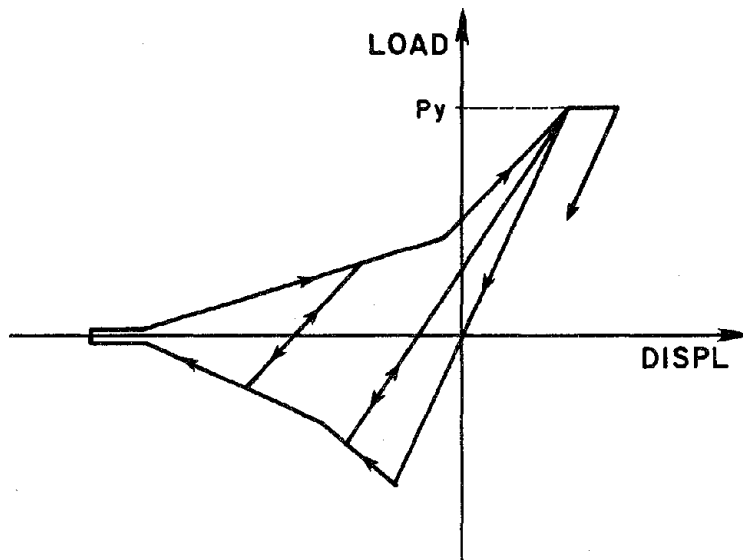
Fig. 1.1 Cyclic Behavior of a Steel Brace [1]



(a) Finite Element Models



(b) Physical Theory Brace Models



(c) Phenomenological Models

Fig. 1.2 Various Models [2]

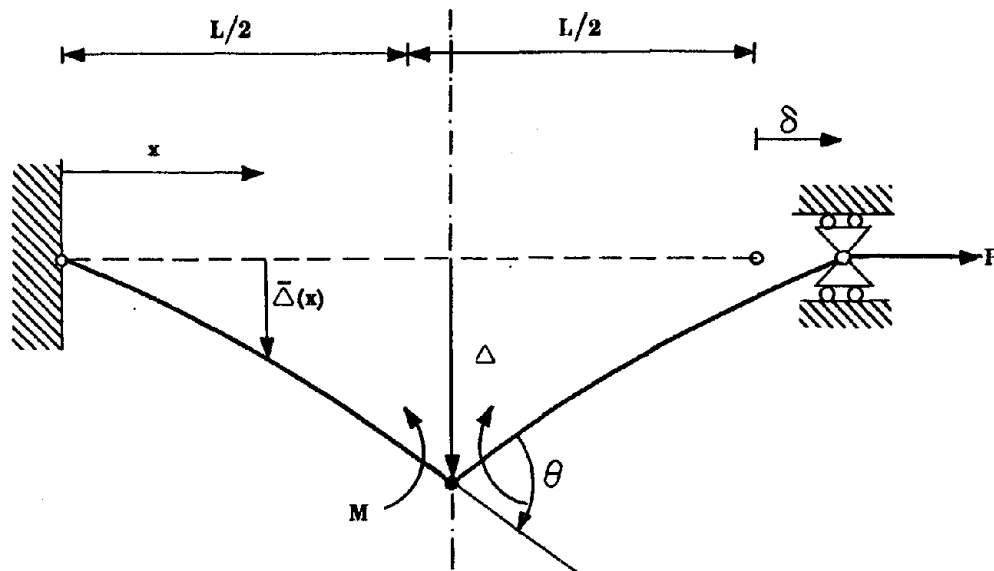


Fig. 1.3 Typical Member Geometry of Point Hinge Model [8]

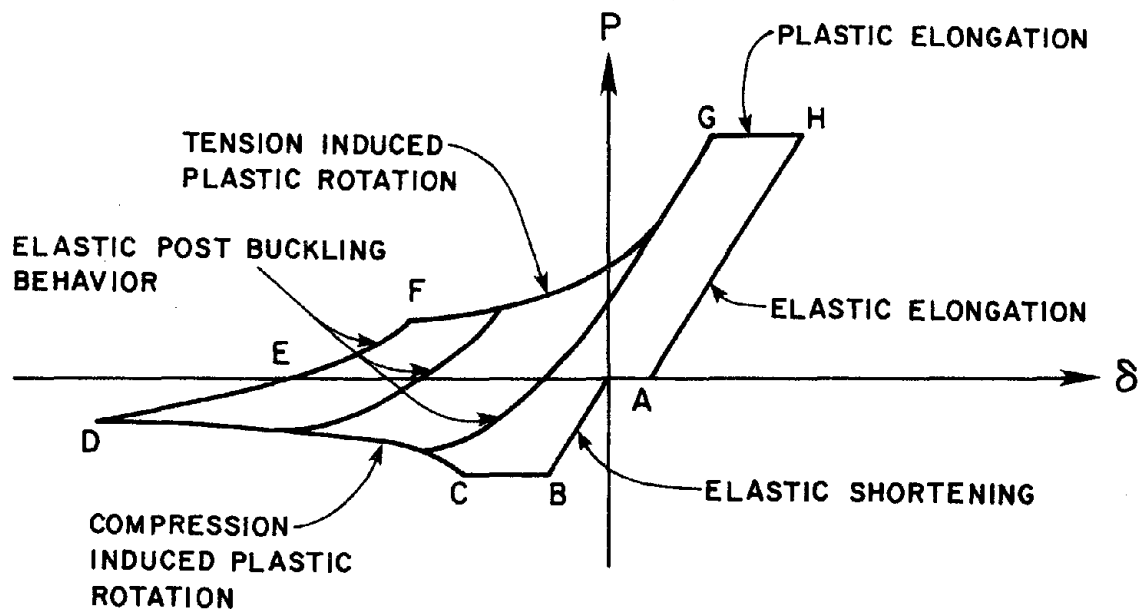


Fig. 1.4 P- δ Curve used in the Higginbotham Model [3]

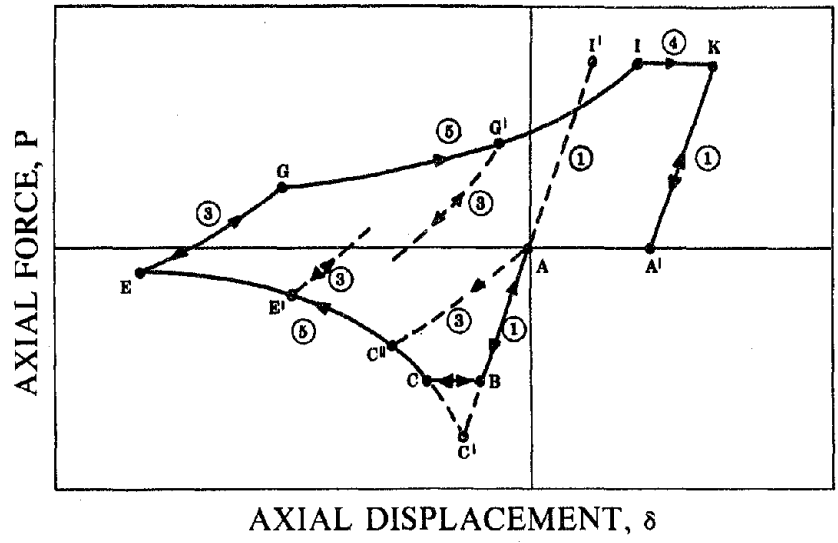
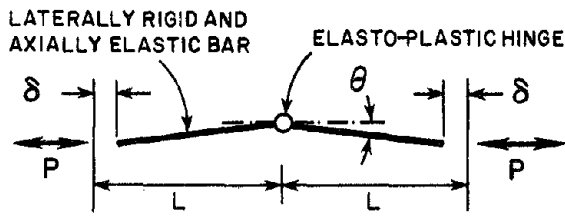
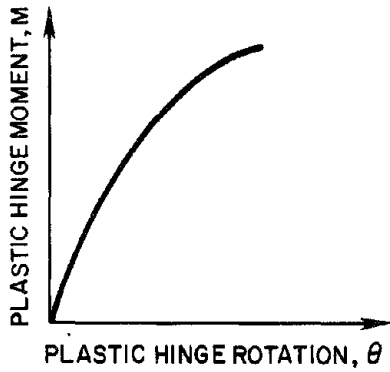
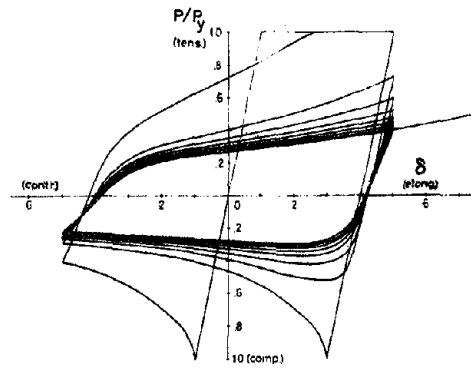


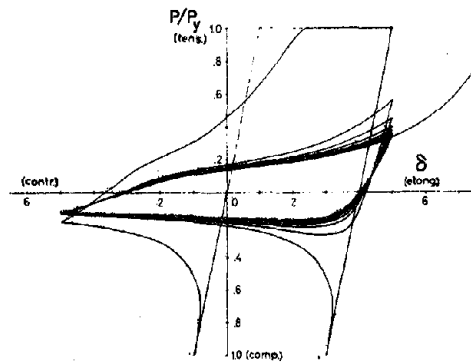
Fig. 1.5 P- δ Curve used in the Gugerli Model [8]



(a) Member Geometry



(b) M- θ Relationship used in the Elasto-Plastic Hinge



(c) P- δ Curves

Fig. 1.6 Elasto-Plastic Hinge Model by Wakabayashi [11 to 14]

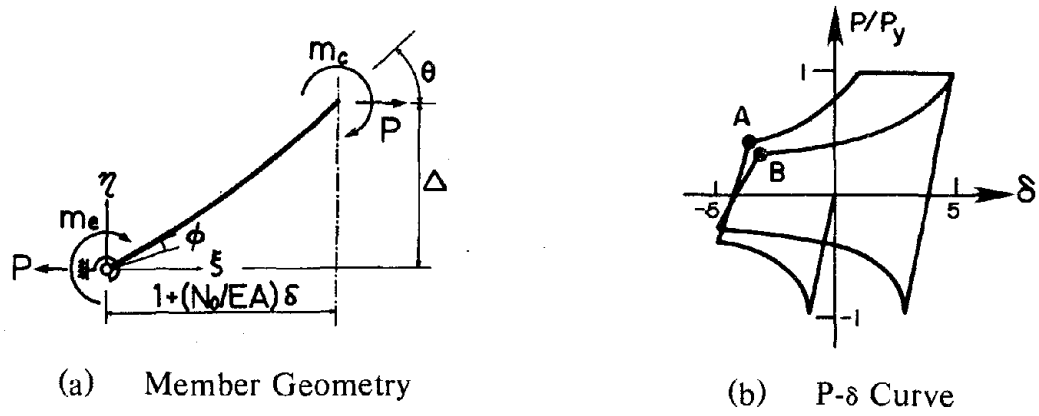


Fig. 1.7 End constrained Member Model by Wakabayashi [16]

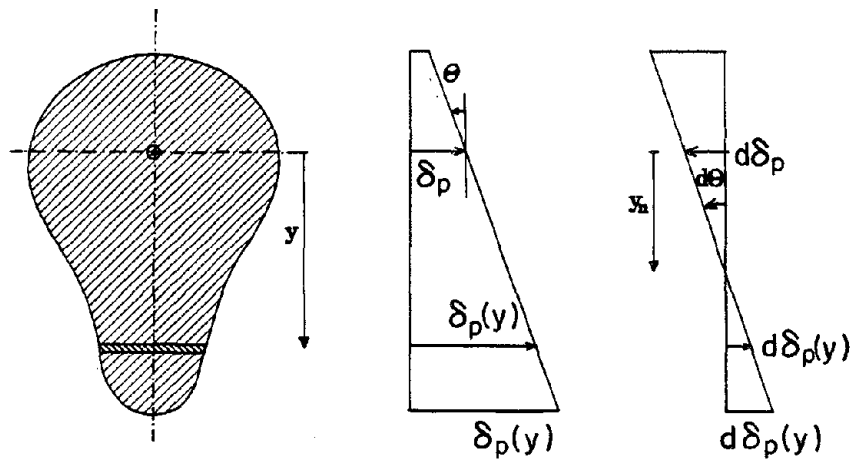


Fig. 1.8 Definition of the Location of Instantaneous Neutral Axis y_n [8]

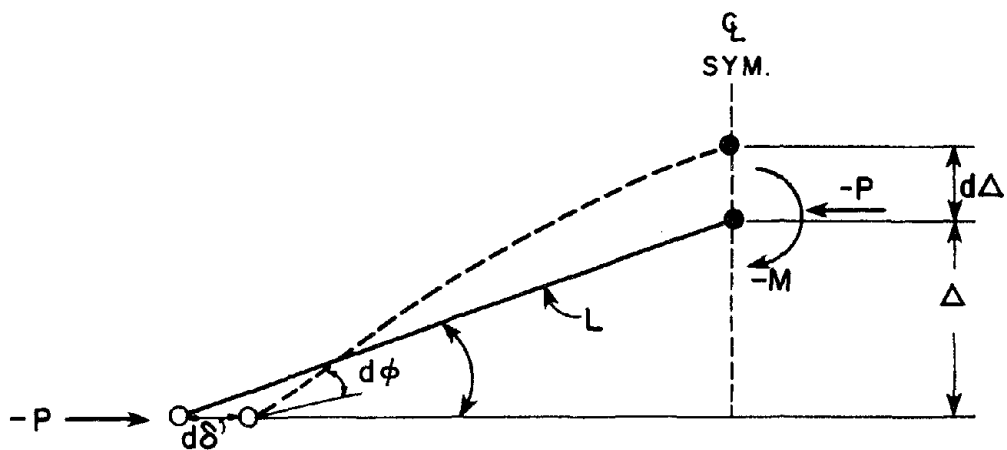


Fig. 1.9 Member Geometry for the Zayas Model [2]

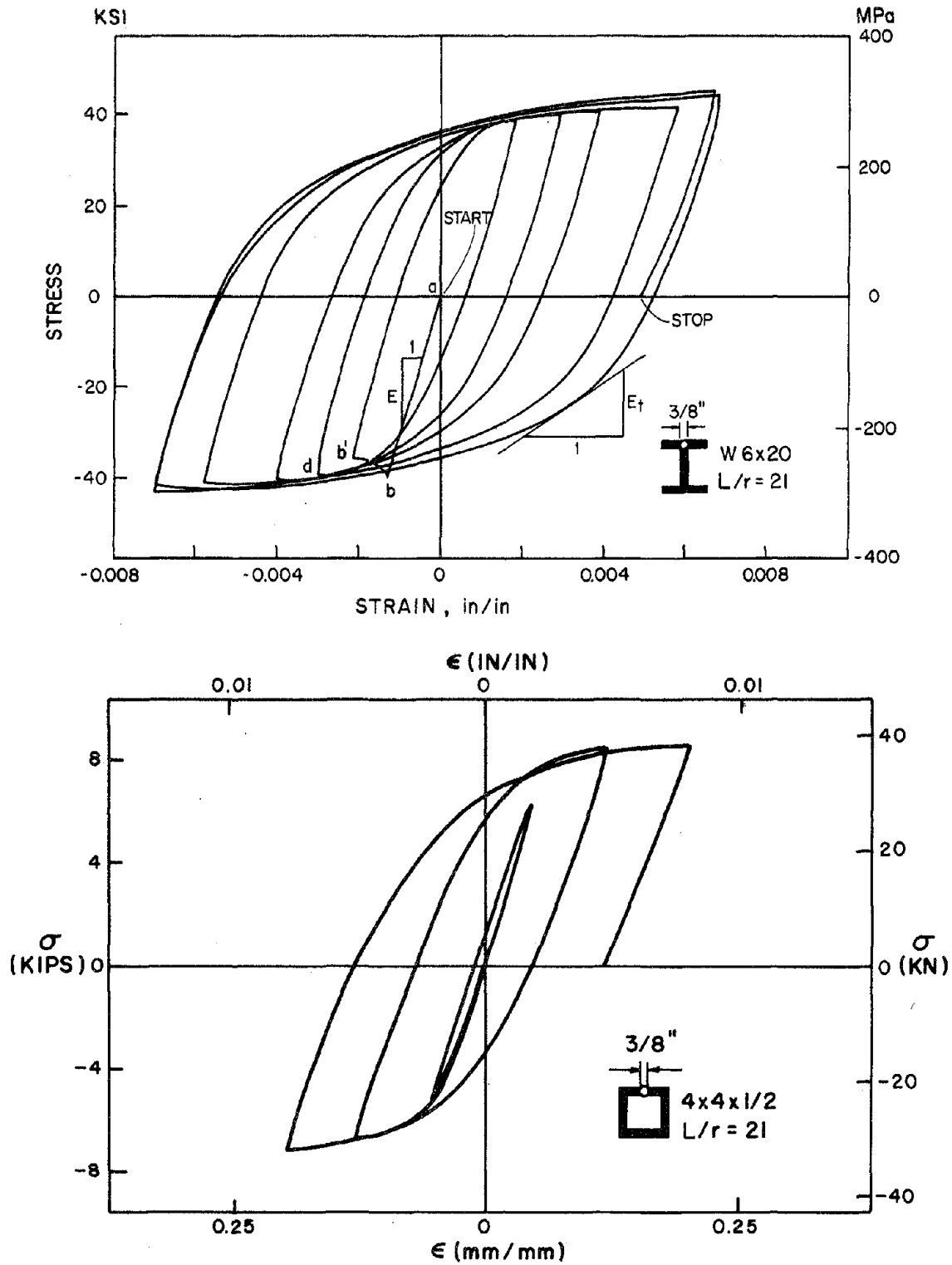
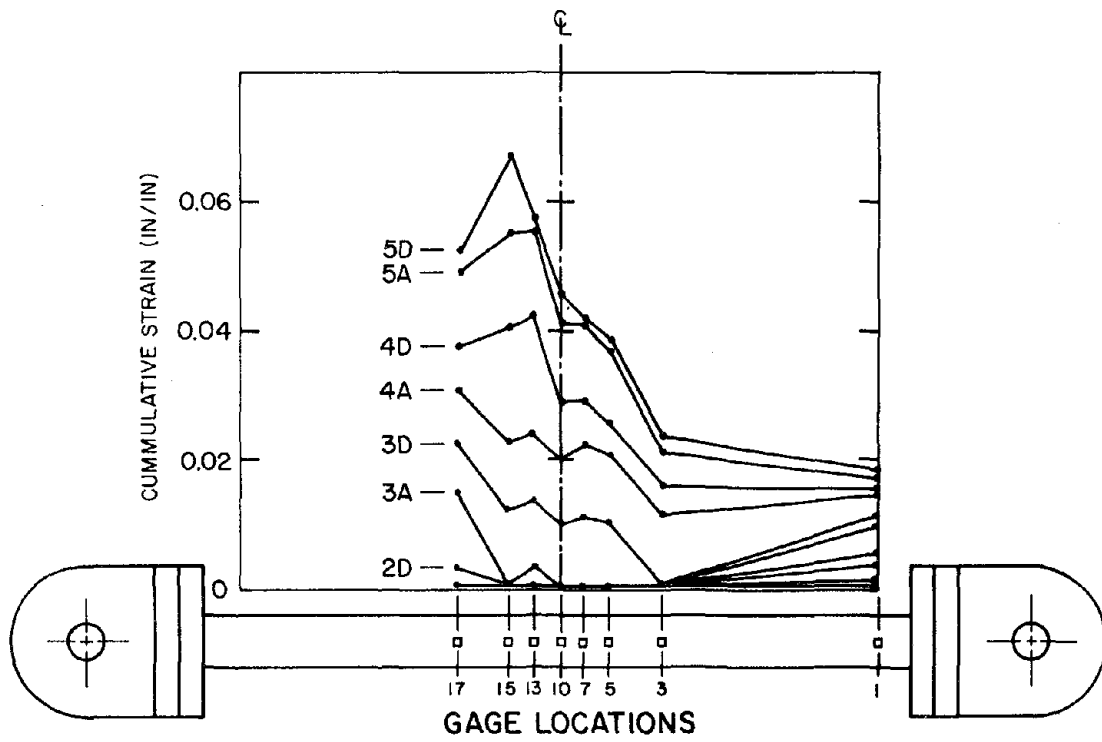


Fig. 2.1 Hysteretic Stress - Strain Curves from Cyclic Coupon Tests [1]



(a) Cumulative Inelastic Axial Strain

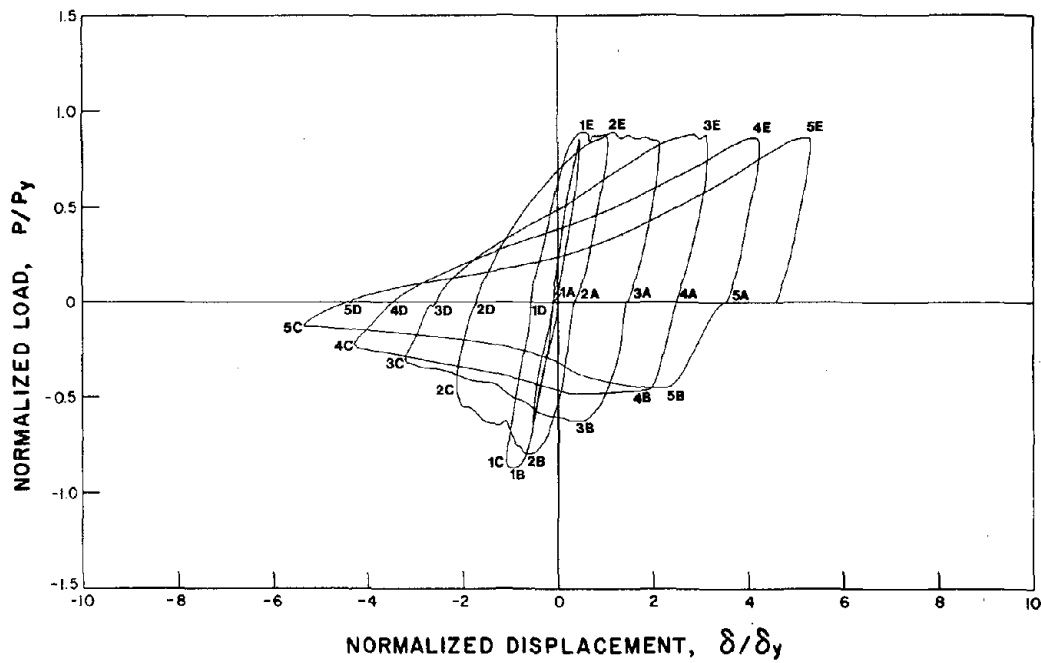
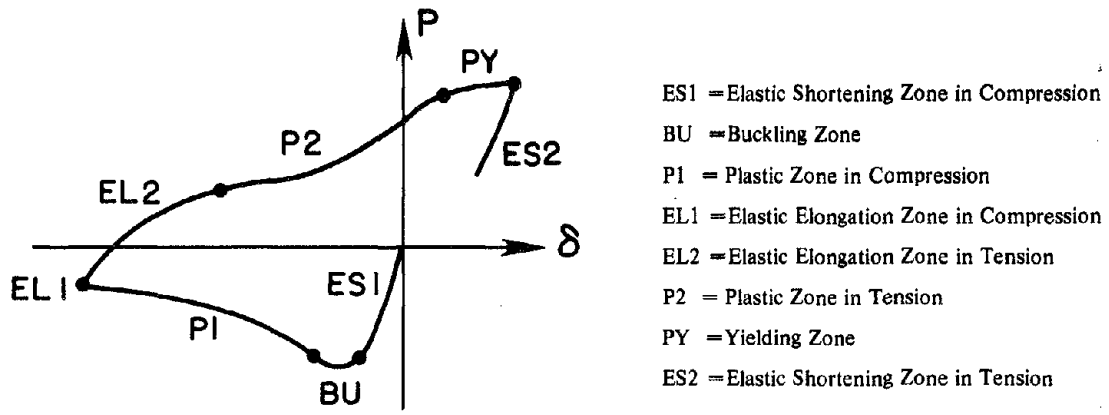
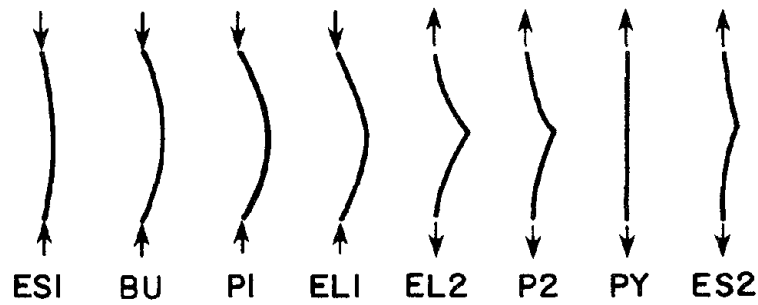
(b) Corresponding P- δ Curve

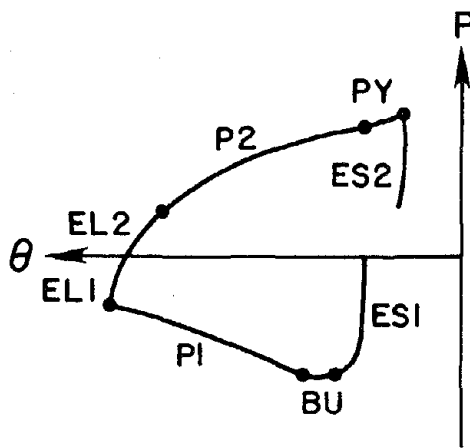
Fig. 2.2 Concentrated Axial Strain at Plastic Hinge Location [26]



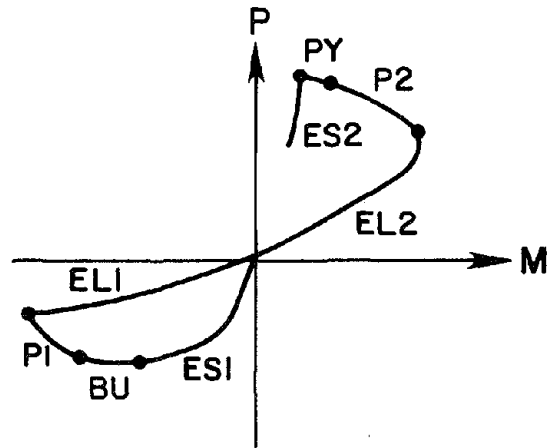
(a) P-δ Curve



(b) Basic Behavior of a Brace associated with each Zone



(c) P-θ Curve



(d) P-M Curve

Fig. 2.3 Definition of Different Zones

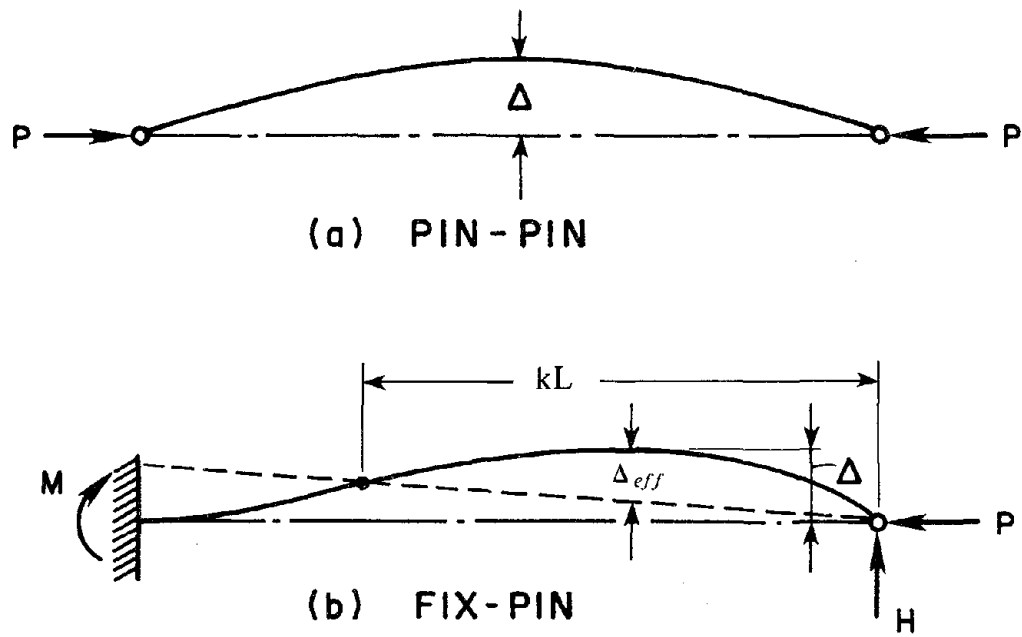


Fig. 2.4 Definition of the Effective Lateral Displacement Δ_{eff} and the Effective Member Length kL [1]

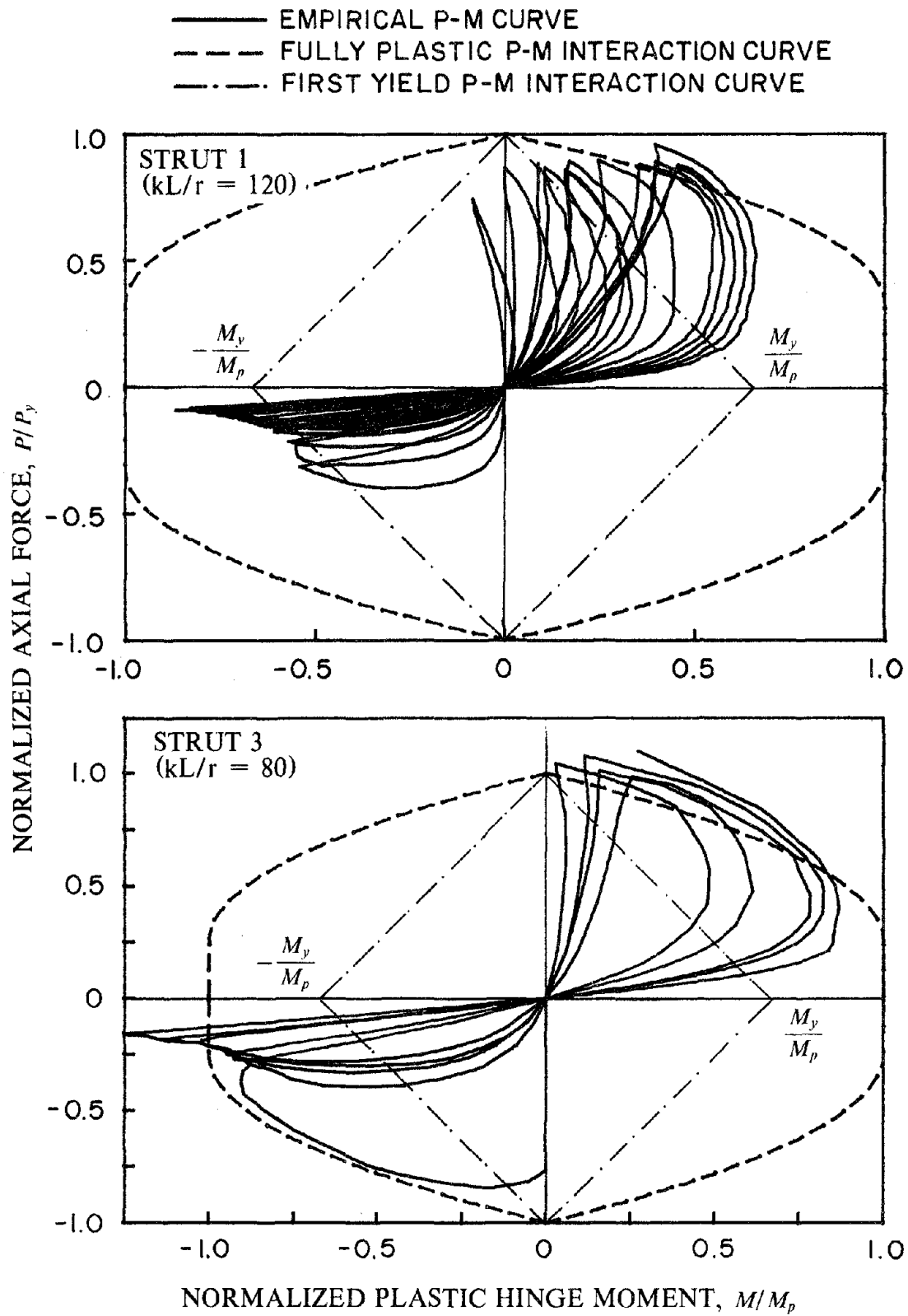


Fig. 2.5 Empirical Axial Force - Plastic Hinge Moment Curves for Struts 1 and 3

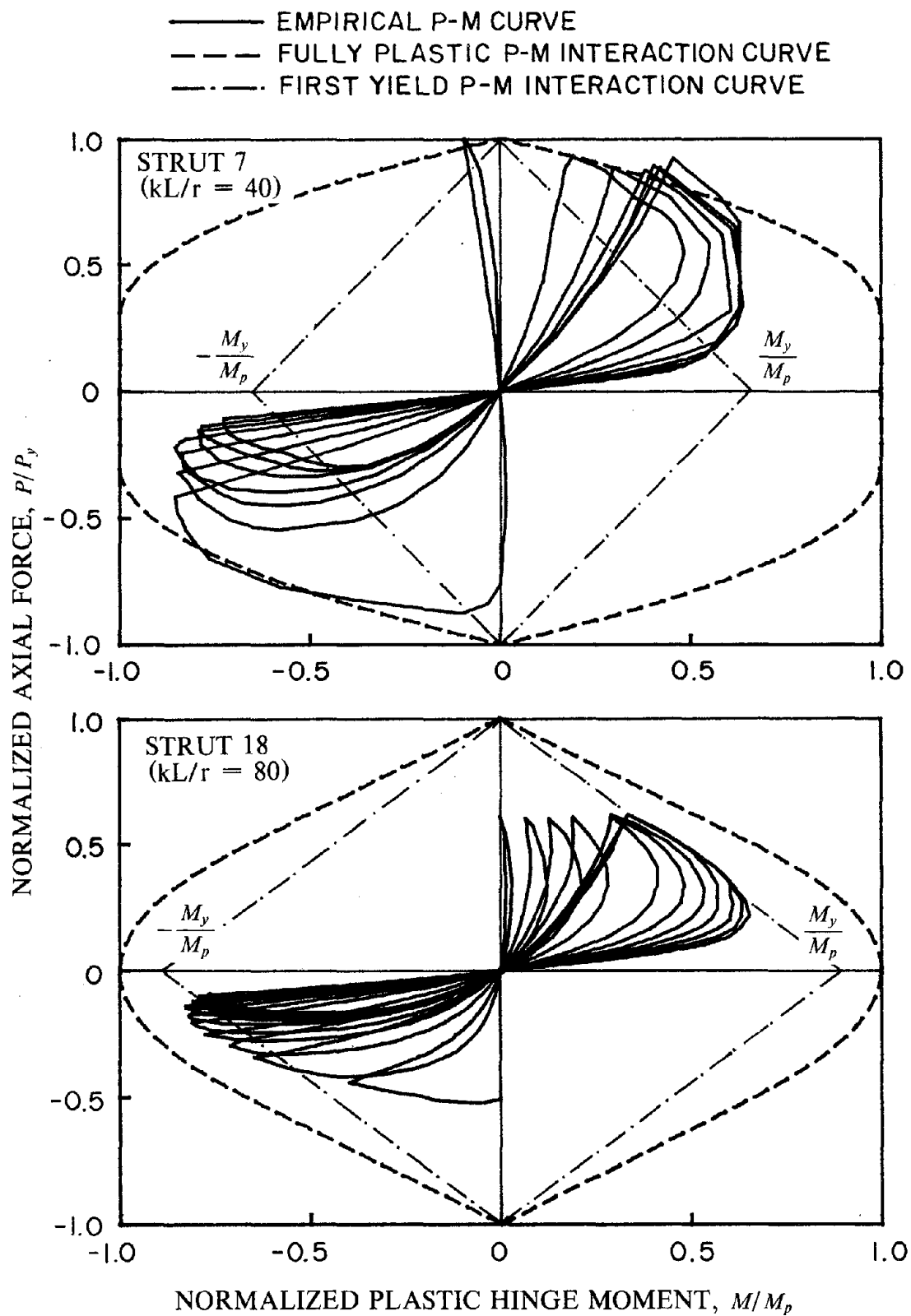


Fig. 2.6 Empirical Axial Force - Plastic Hinge Moment Curves for Struts 7 and 18

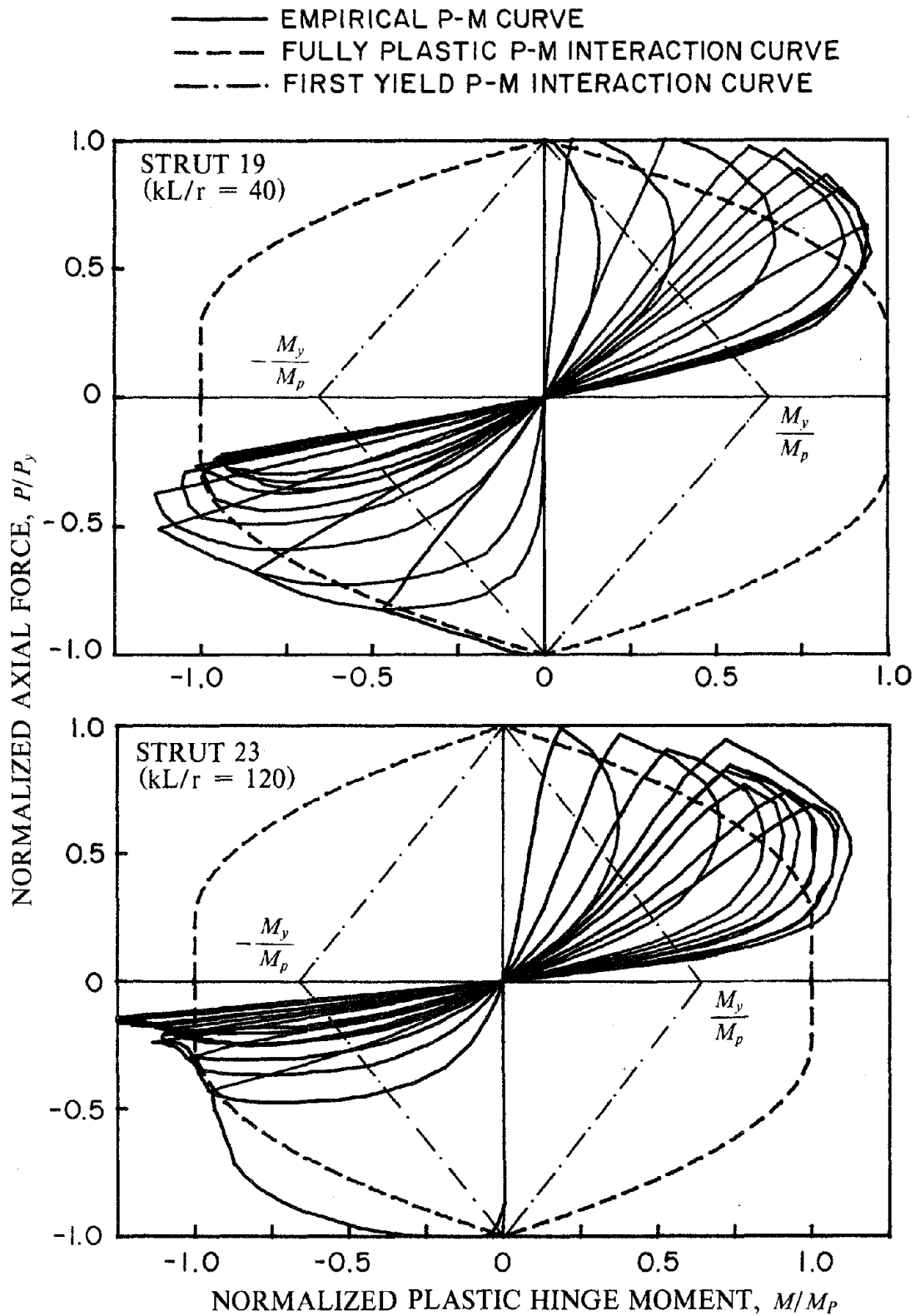


Fig. 2.7 Empirical Axial Force - Plastic Hinge Moment Curves for Struts 19 and 23

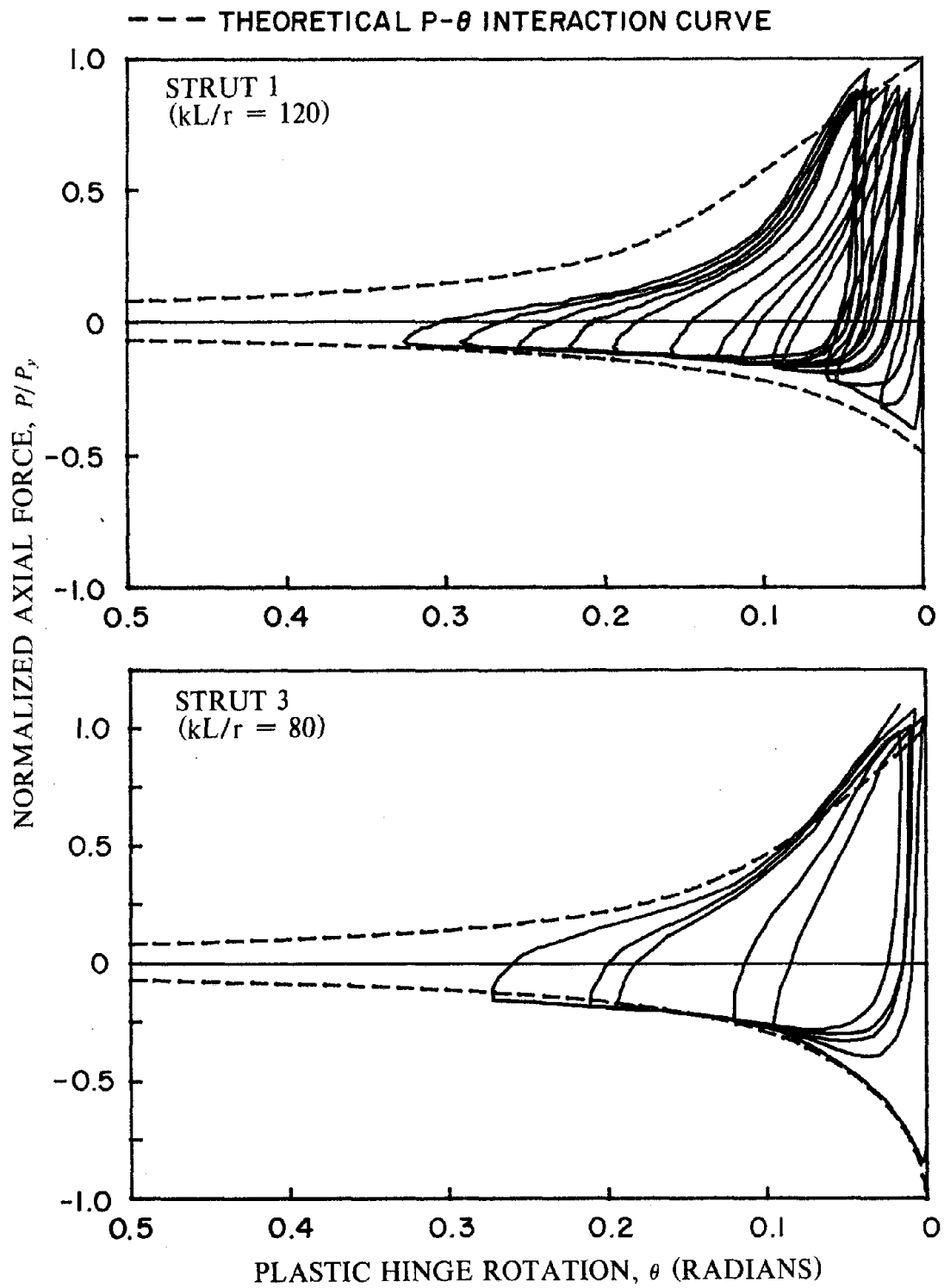


Fig. 2.8 Empirical Axial Force - Plastic Hinge Rotation Curves for Struts 1 and 3

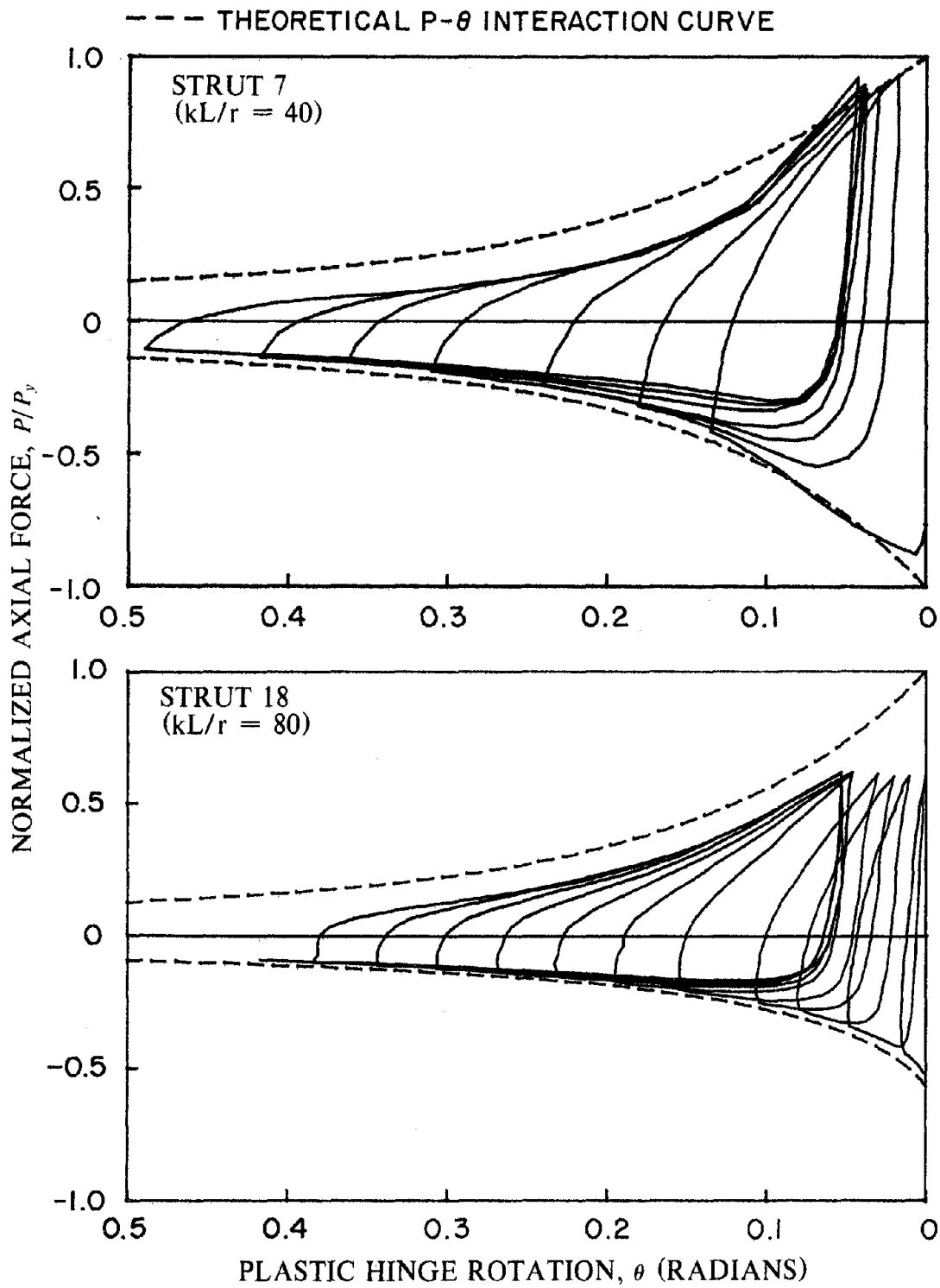


Fig. 2.9 Empirical Axial Force - Plastic Hinge Rotation Curves for Struts 7 and 18

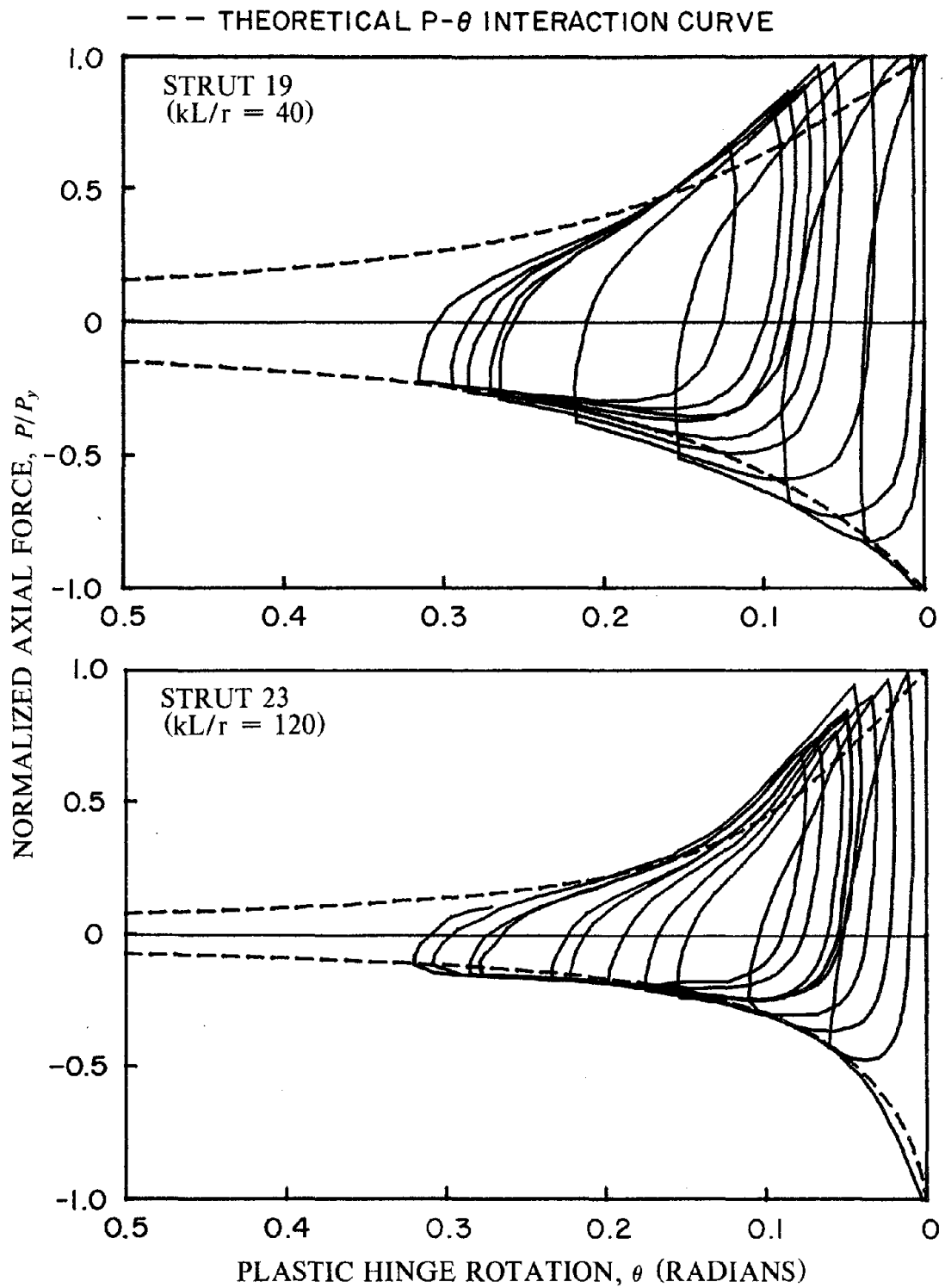


Fig. 2.10 Empirical Axial Force - Plastic Hinge Rotation Curves for Struts 19 and 23

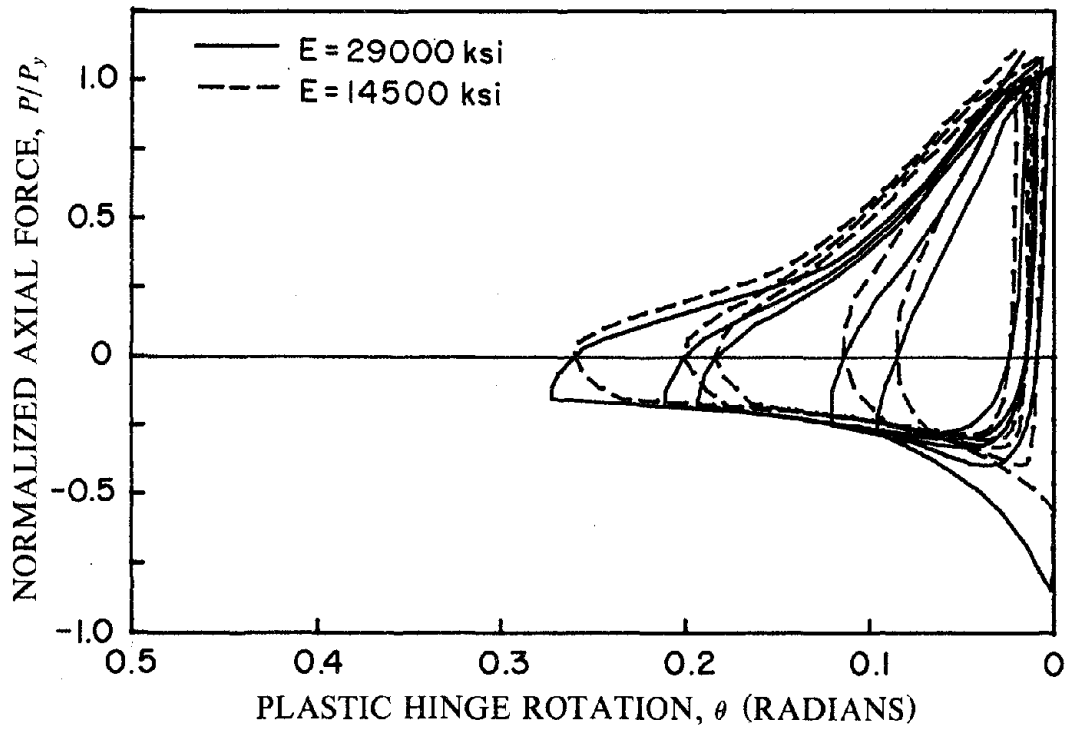


Fig. 2.11 Influence of Initial Moduli of Elasticity on Axial Force - Plastic Hinge Rotation Curves (Strut 3) (1 ksi = 6.89 MPa)

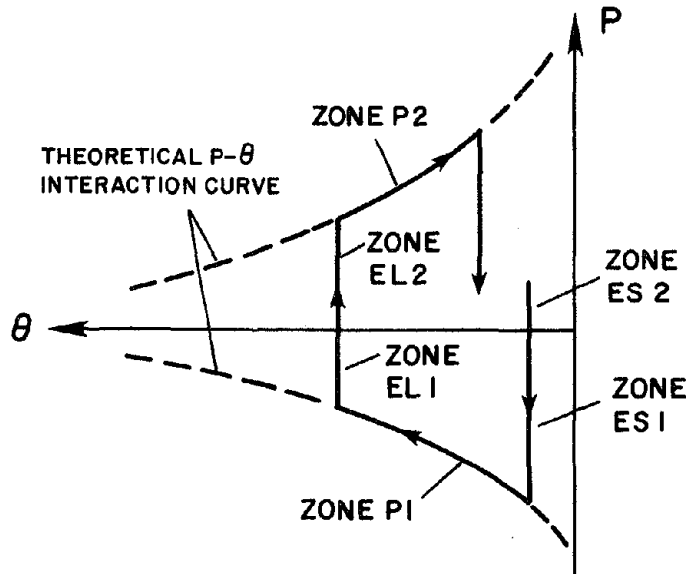


Fig. 2.12 Typical Analytical Axial Force - Plastic Hinge Rotation Curve used in Physical Theory Brace Models

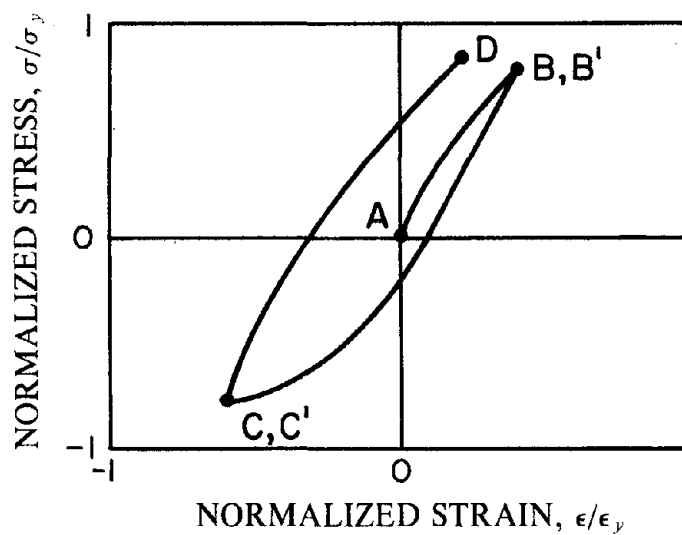
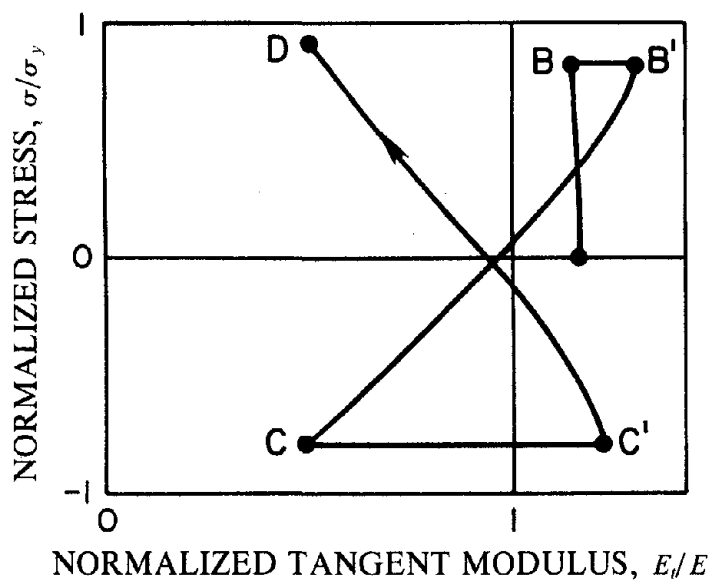
(a) $\sigma/\sigma_y - \epsilon/\epsilon_y$ Curve(b) $\sigma/\sigma_y - E_t/E$ Curve

Fig. 2.13 Explanation of Normalized Tangent Modulus versus Stress Relationship
(1 ksi = 6.89 MPa)

— TANGENT MODULUS OF ELASTICITY HISTORY
 - - - LINEAR IDEALIZATION CURVES WHEN AXIAL FORCES INCREASE
 - · - · LINEAR IDEALIZATION CURVES WHEN AXIAL FORCES DECREASE

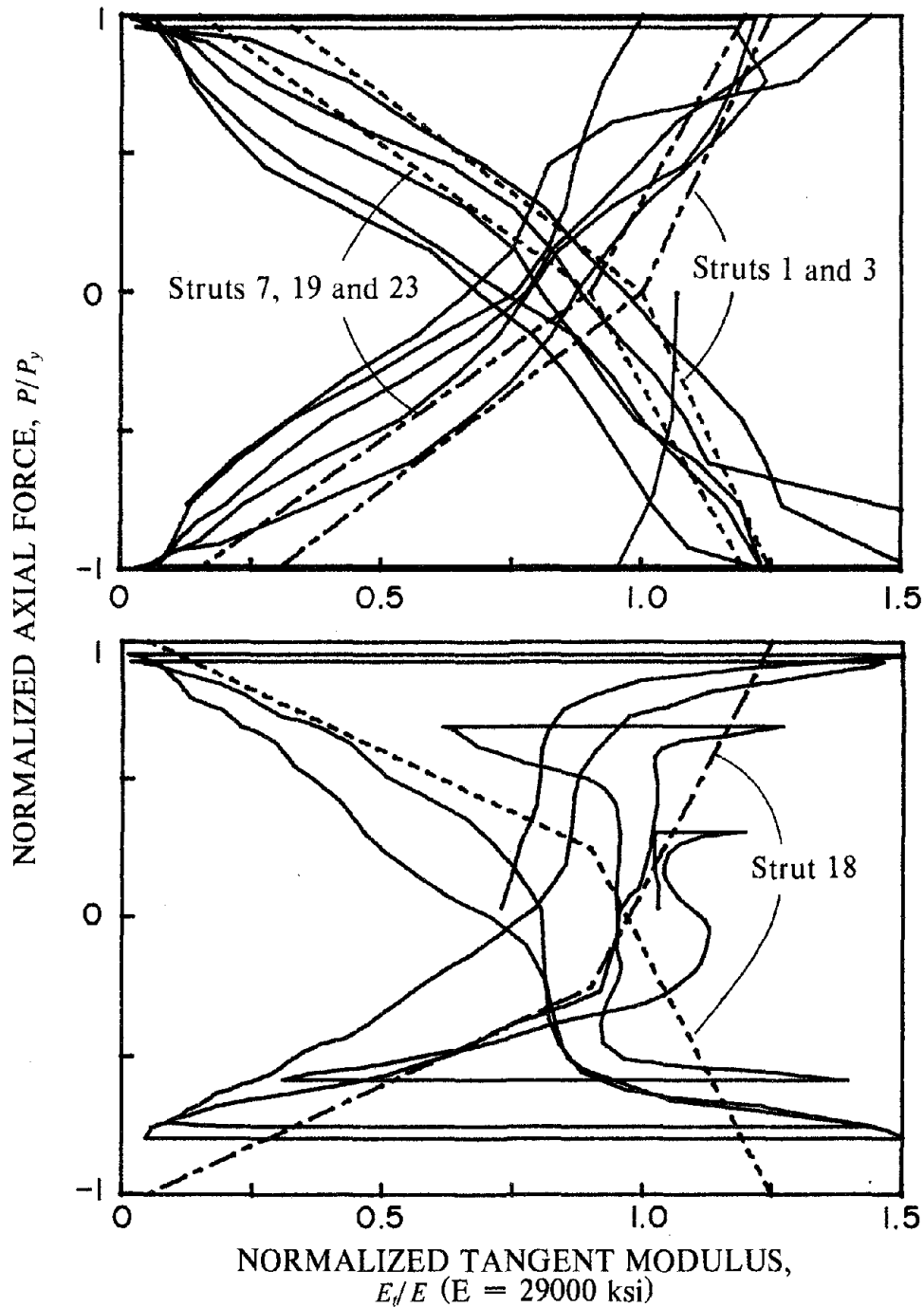
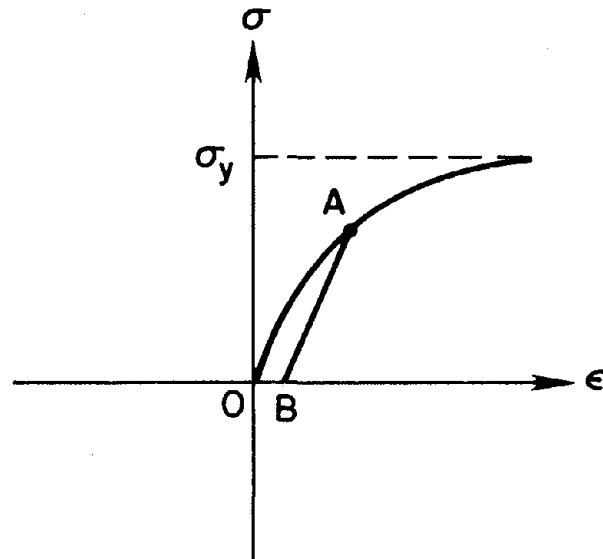


Fig. 2.14 Tangent Modulus Histories for Coupons cut from W6×20 and TS4×4×½ (Strut 18) and Linear Idealization Curves (1 ksi = 6.89 MPa)



\overline{OB} = RESIDUAL STRAIN

$\overline{OB} \cdot L$ = RESIDUAL DISPLACEMENT DUE TO MATERIAL NONLINEARITIES

Fig. 2.15 Definition of Residual Displacement due to Material Nonlinearities occurring in the Nominal "Elastic" Range

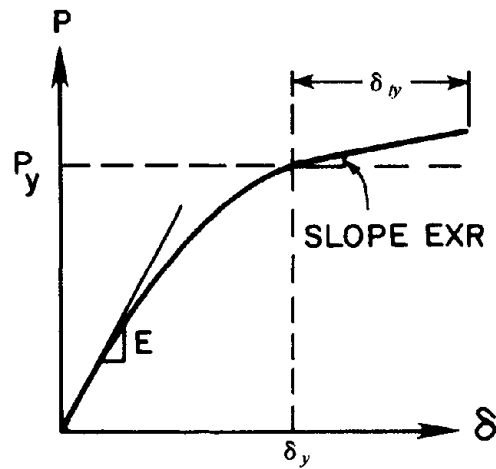
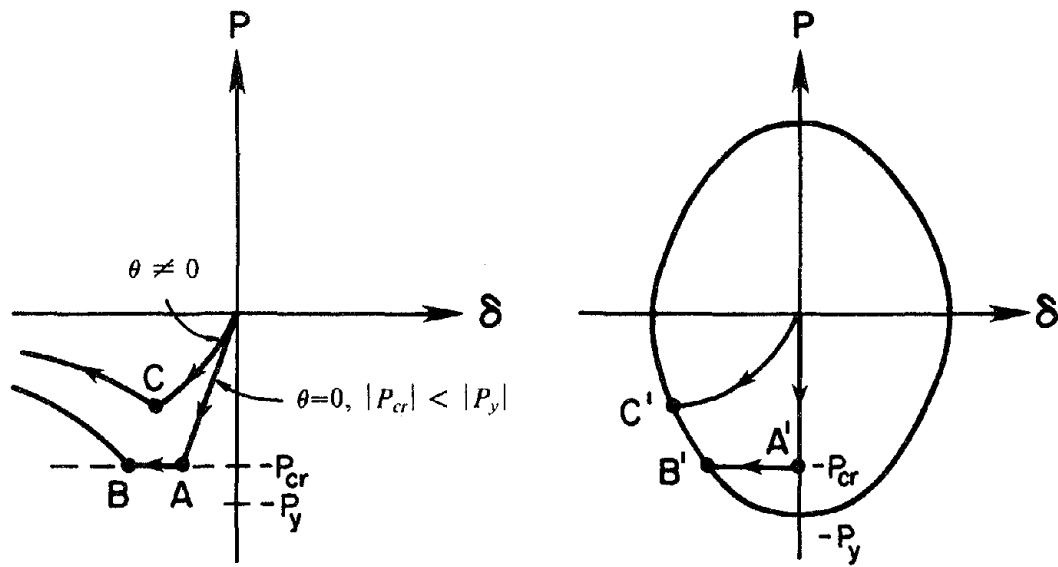
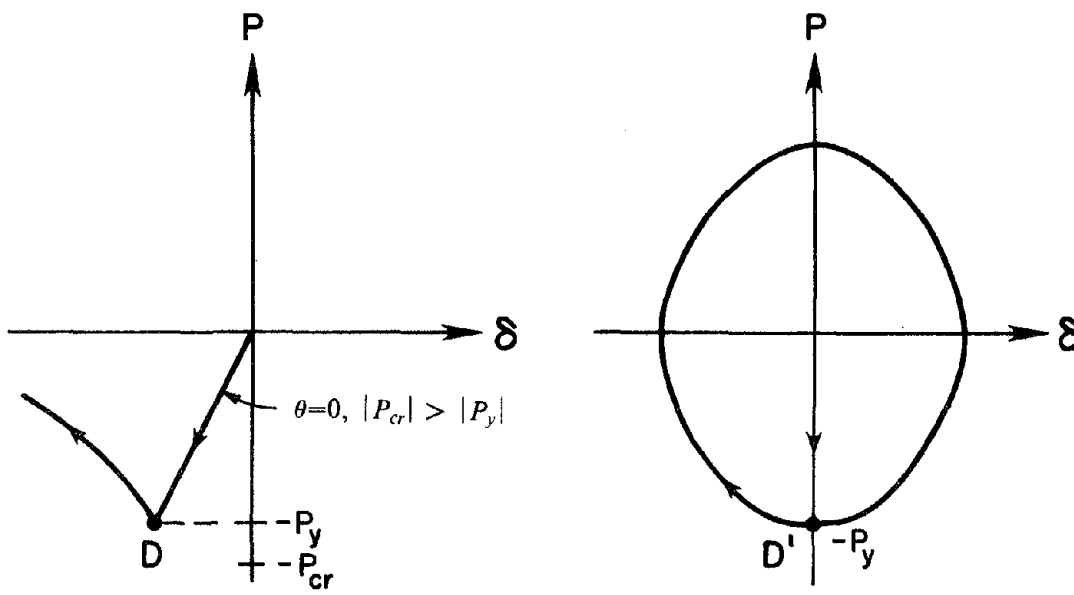


Fig. 3.1 Definition of Strain Hardening



(a) Elastic Buckling



(b) Plastic Buckling

Fig. 3.2 Two Types of Buckling

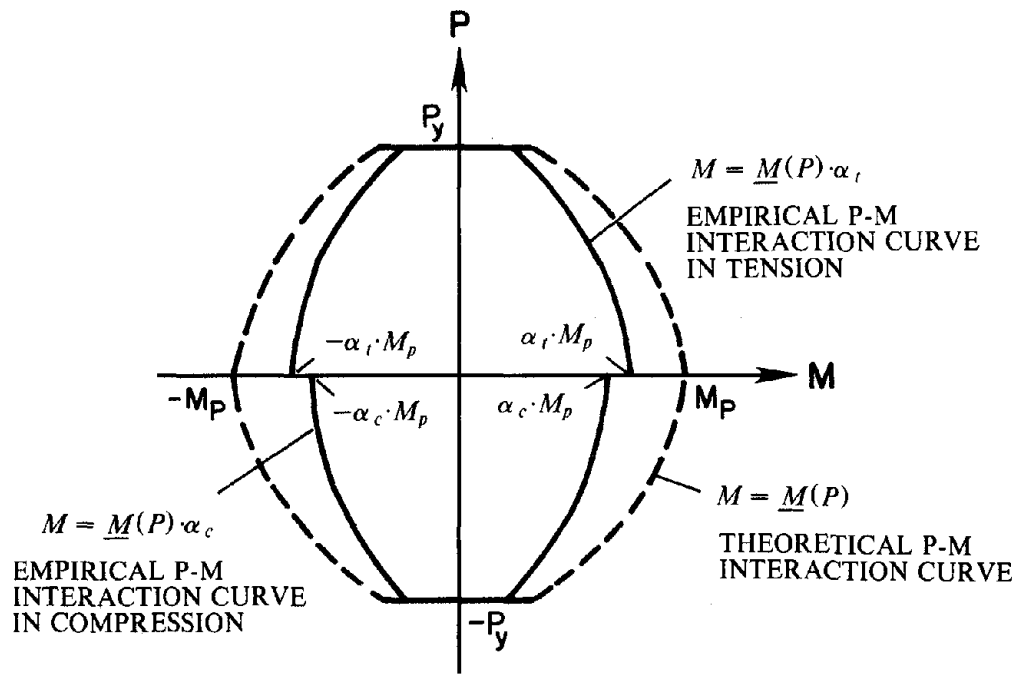


Fig. 3.3 Empirical P-M Interaction Curve

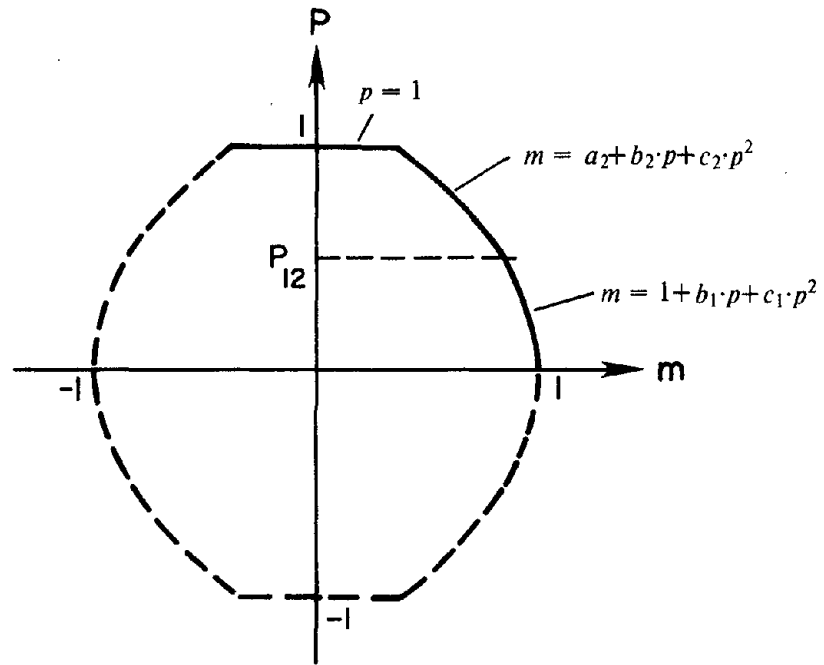


Fig. 3.4 Theoretical P-M Interaction Curve Model

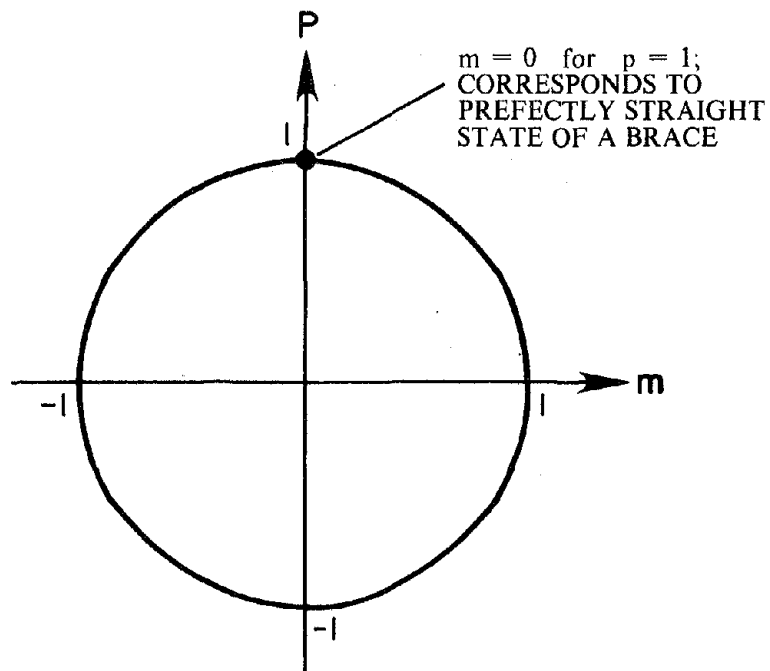


Fig. 3.5 Theoretical P-M Interaction Curve Omitting the Straight Line at the Yield Load, $|p| = 1$

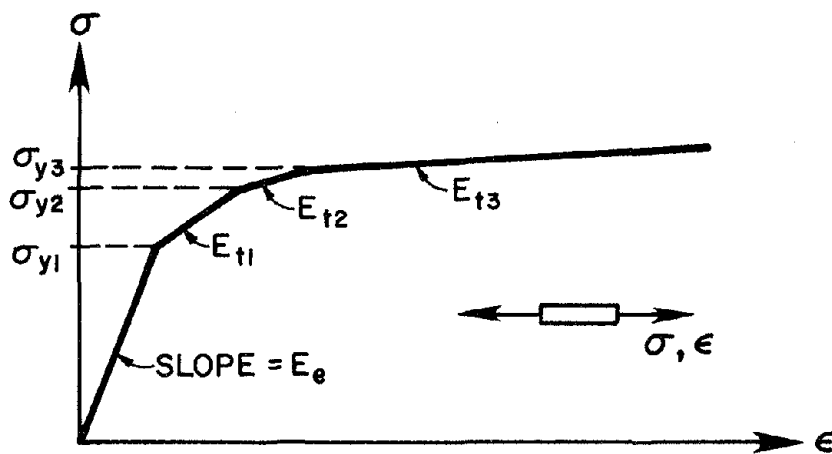
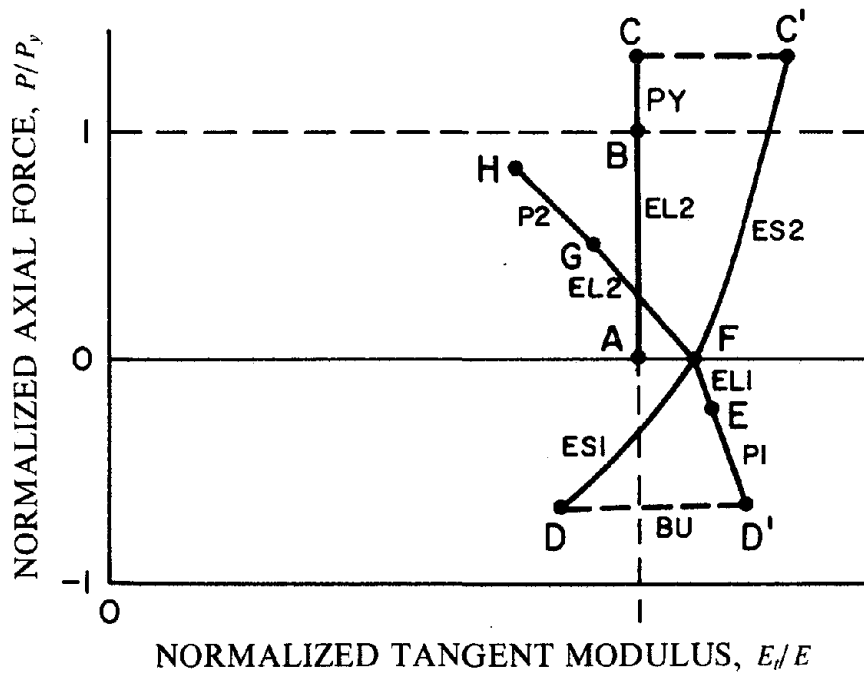


Fig. 3.6 Multilinear-Type Uniaxial Stress-strain Relationship Model [27]



(a) Tangent Modulus-Axial Force Relationship

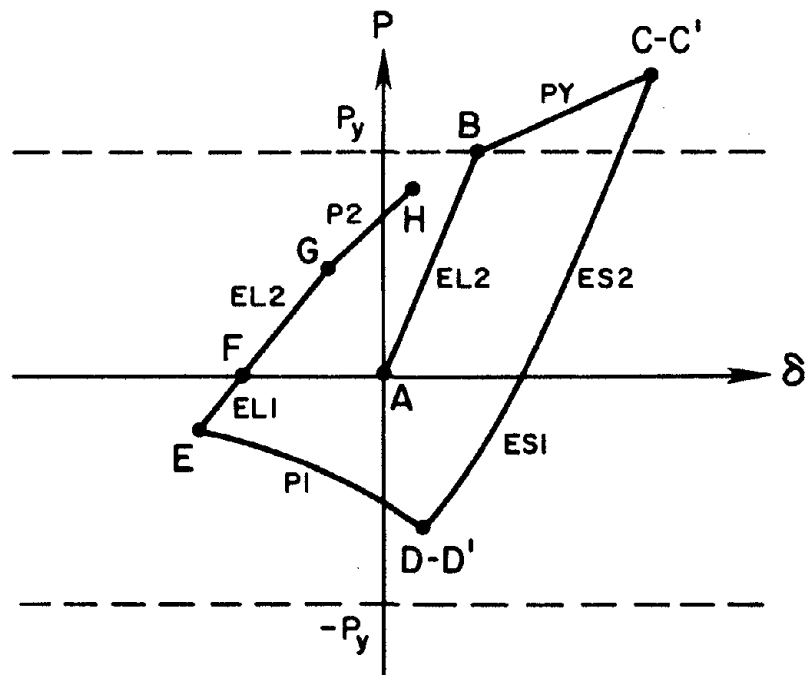
(b) Corresponding P - δ Curve

Fig. 3.7 Empirical Model of Tangent Modulus of Elasticity

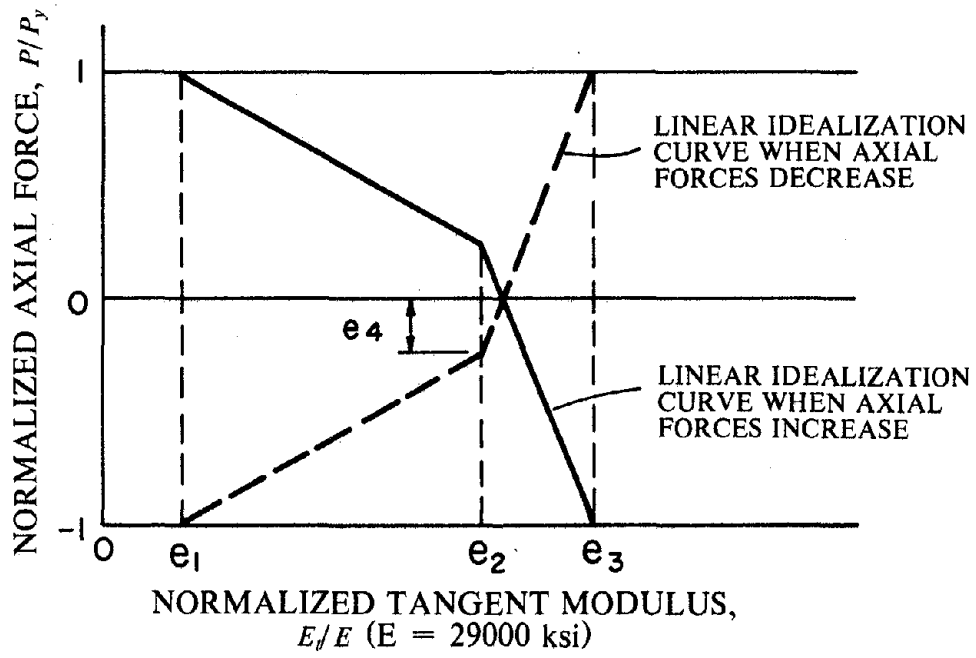


Fig. 3.8 Linear Idealization Curves for Tangent Modulus History

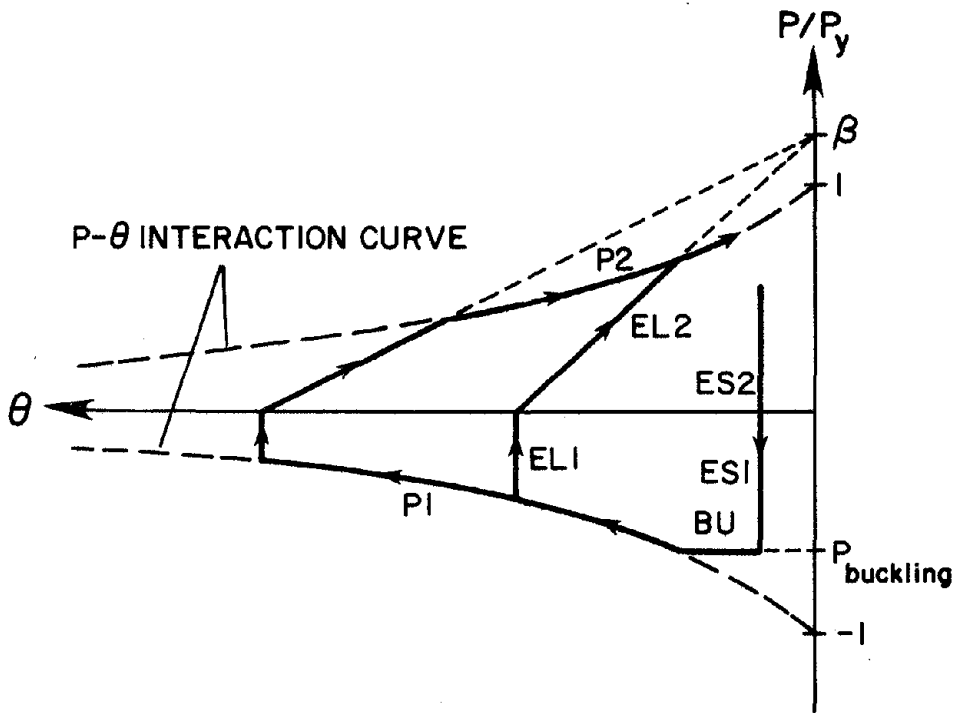


Fig. 3.9 Analytical Axial Force - Plastic Hinge Rotation Curve Model

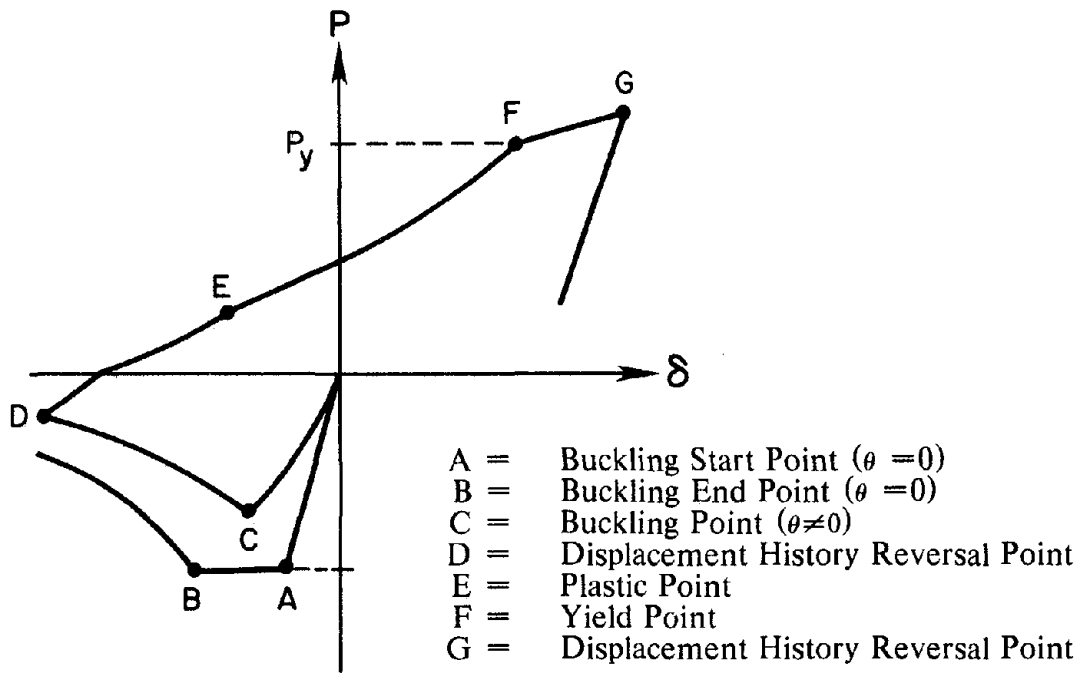


Fig. 3.10 Definition of Transition Points

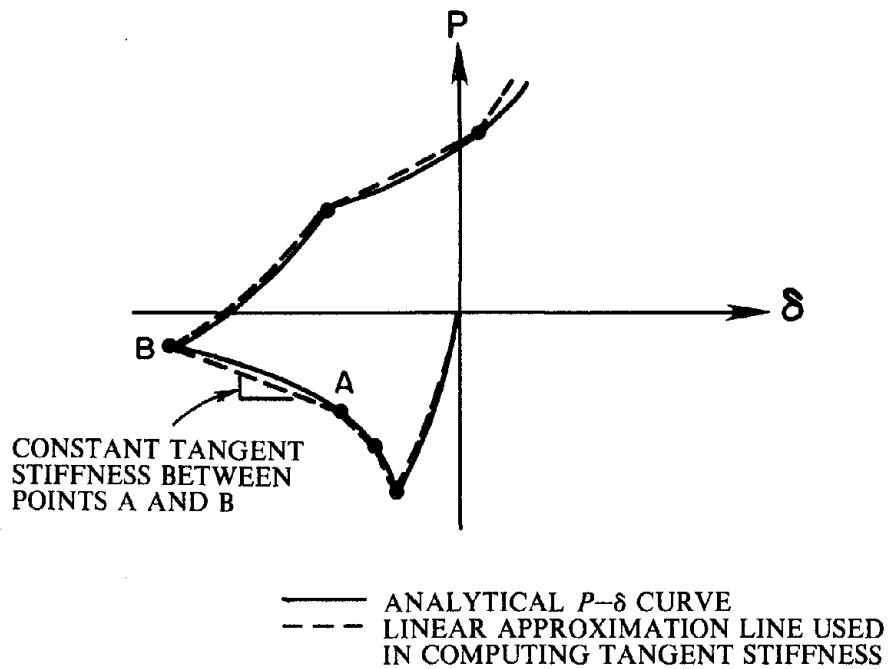


Fig. 3.11 Simplified Computation of Tangent Stiffness of a Brace using Linear Approximation Lines

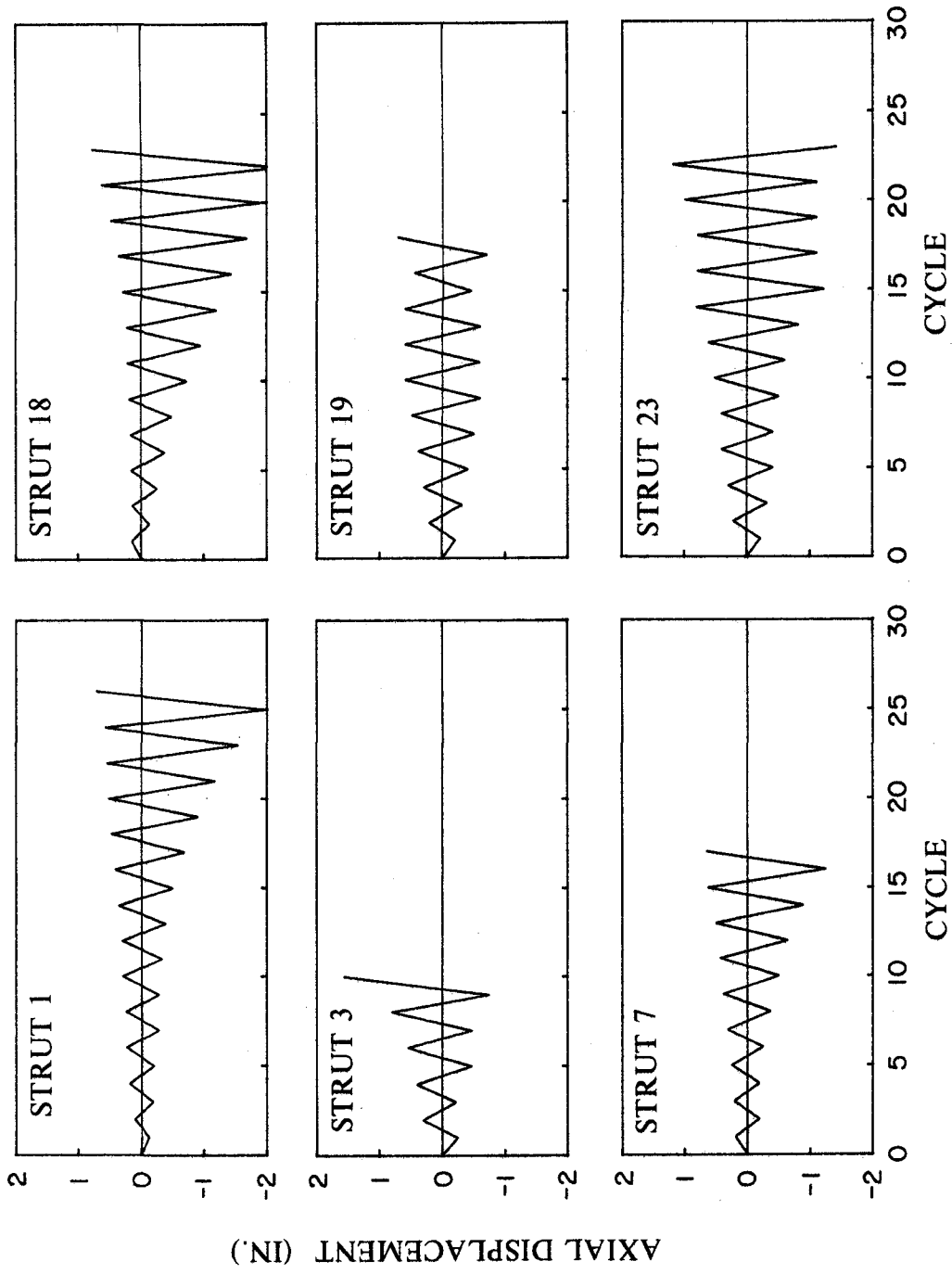


Fig. 4.1 Displacement Histories (1 in. = 25.4 mm)

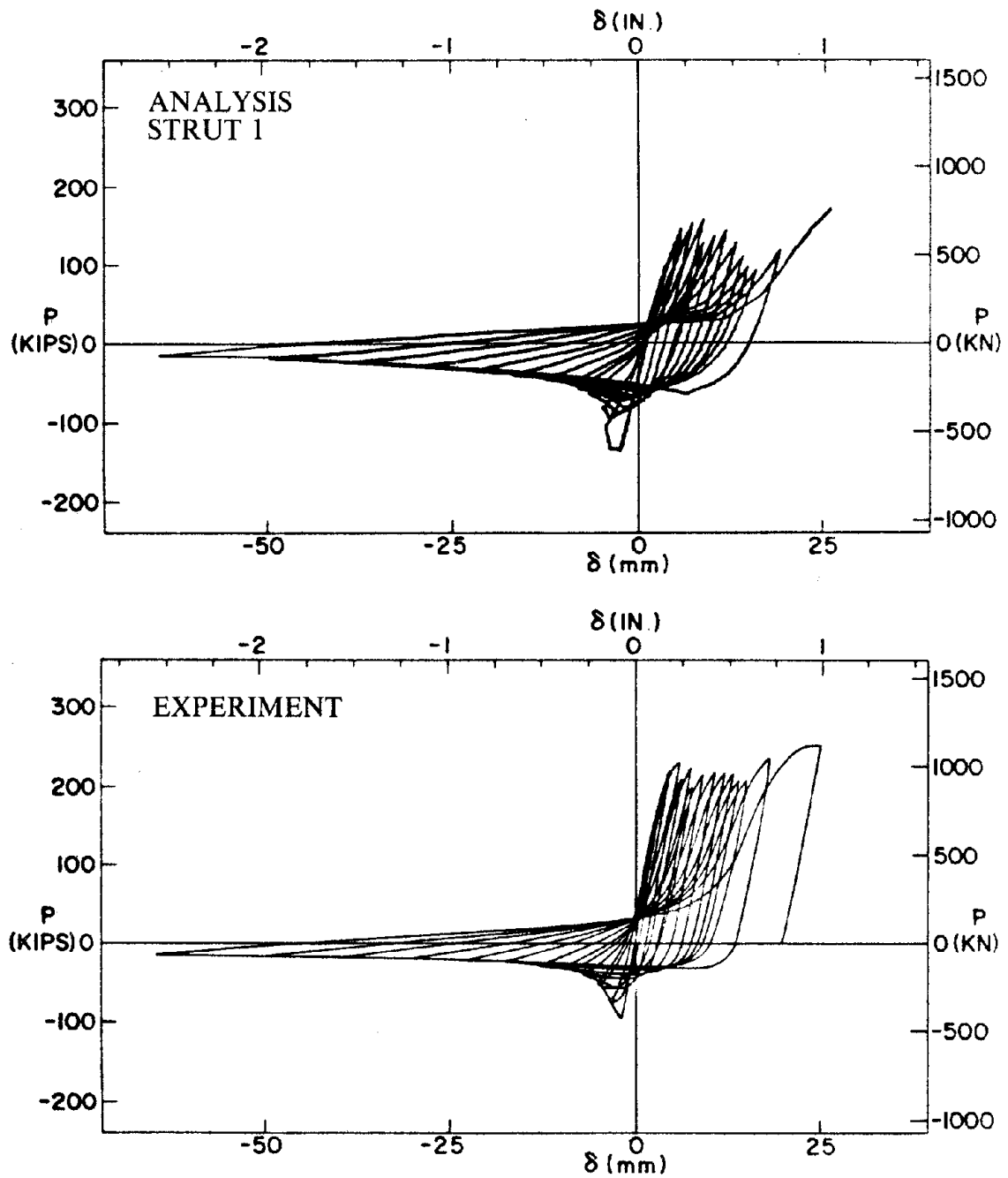


Fig. 4.2 Comparison of Analytical and Experimental Axial Force - Axial Displacement Curves for Strut 1

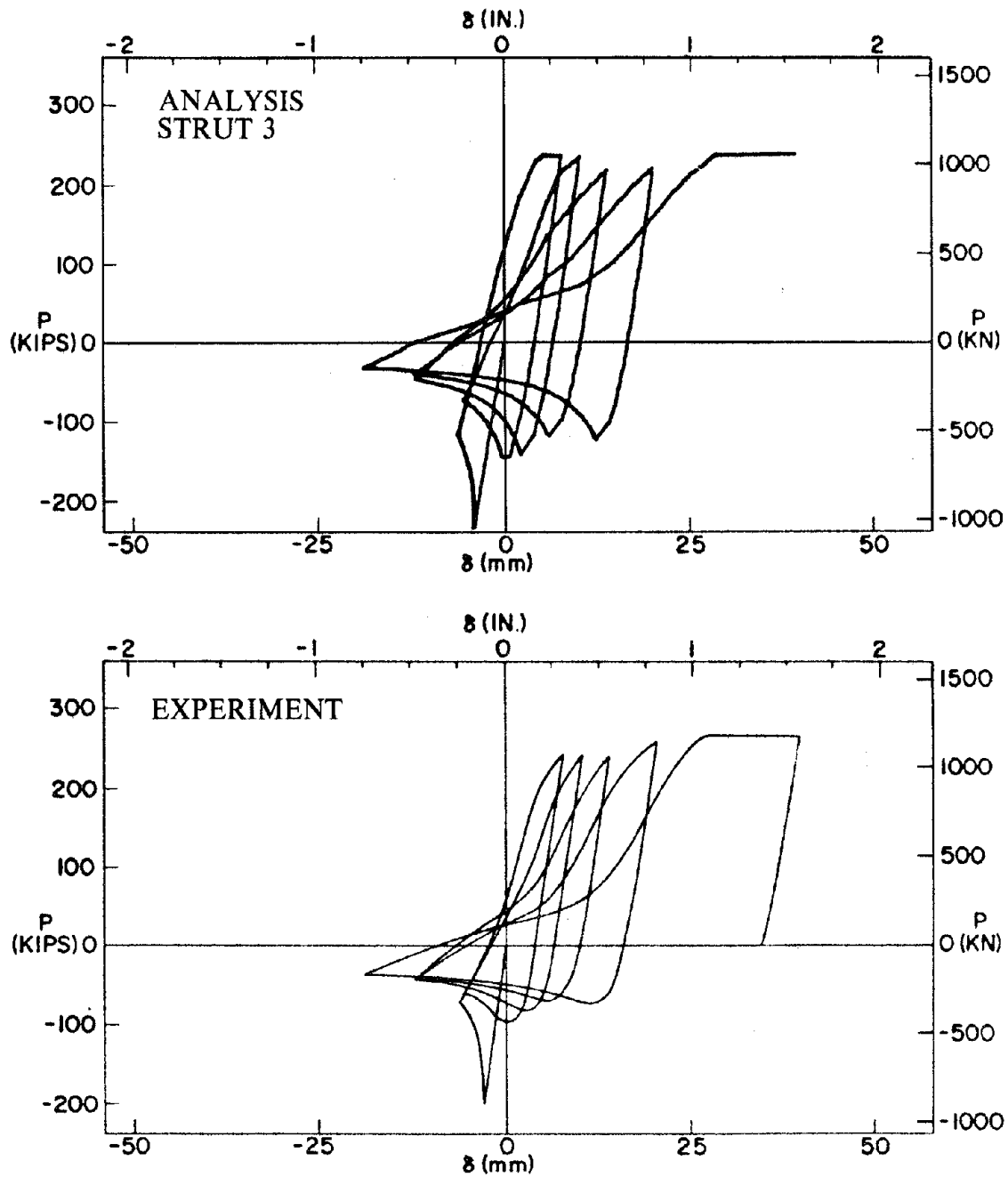


Fig. 4.3 Comparison of Analytical and Experimental Axial Force - Axial Displacement Curves for Strut 3

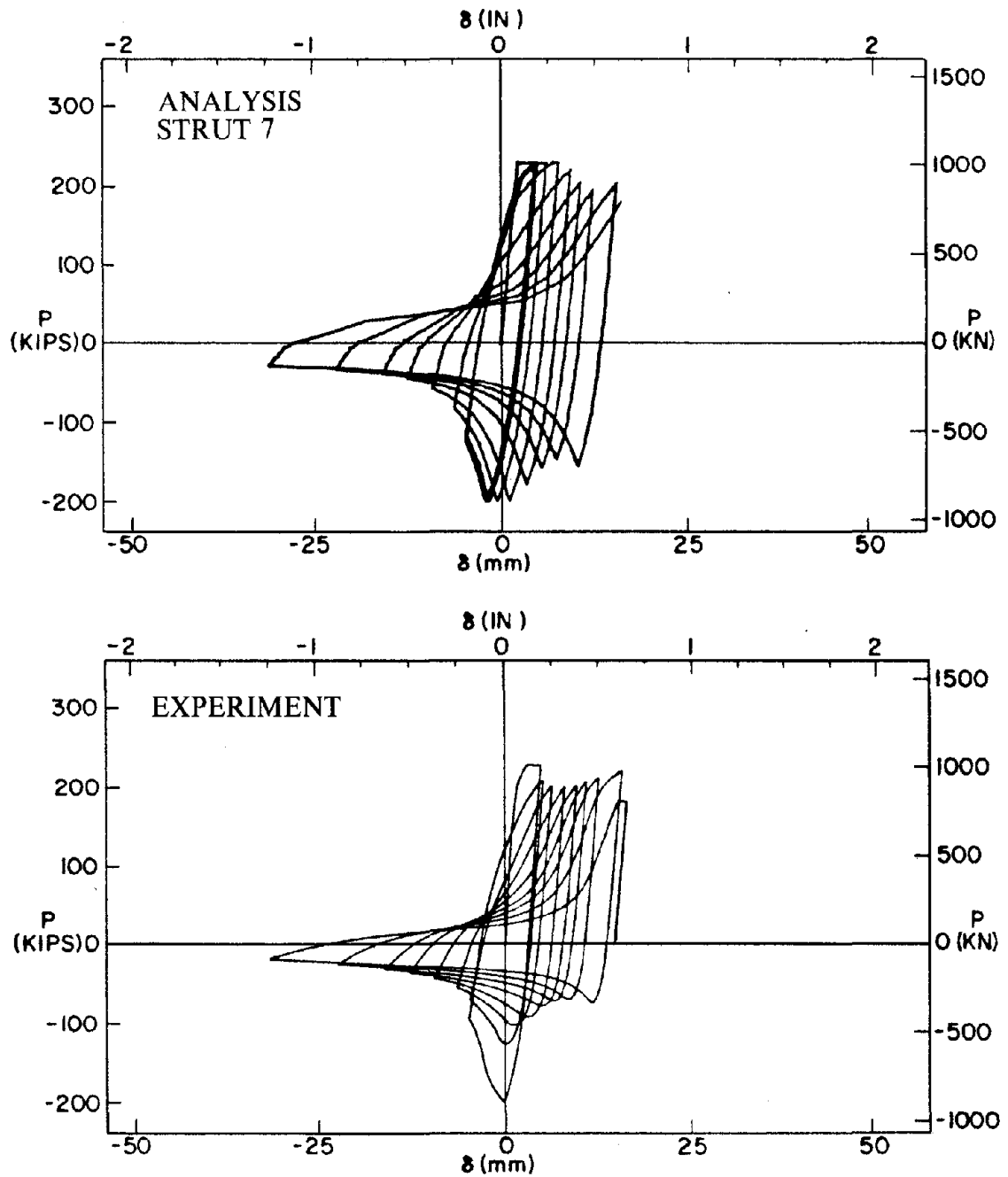


Fig. 4.4 Comparison of Analytical and Experimental Axial Force - Axial Displacement Curves for Strut 7

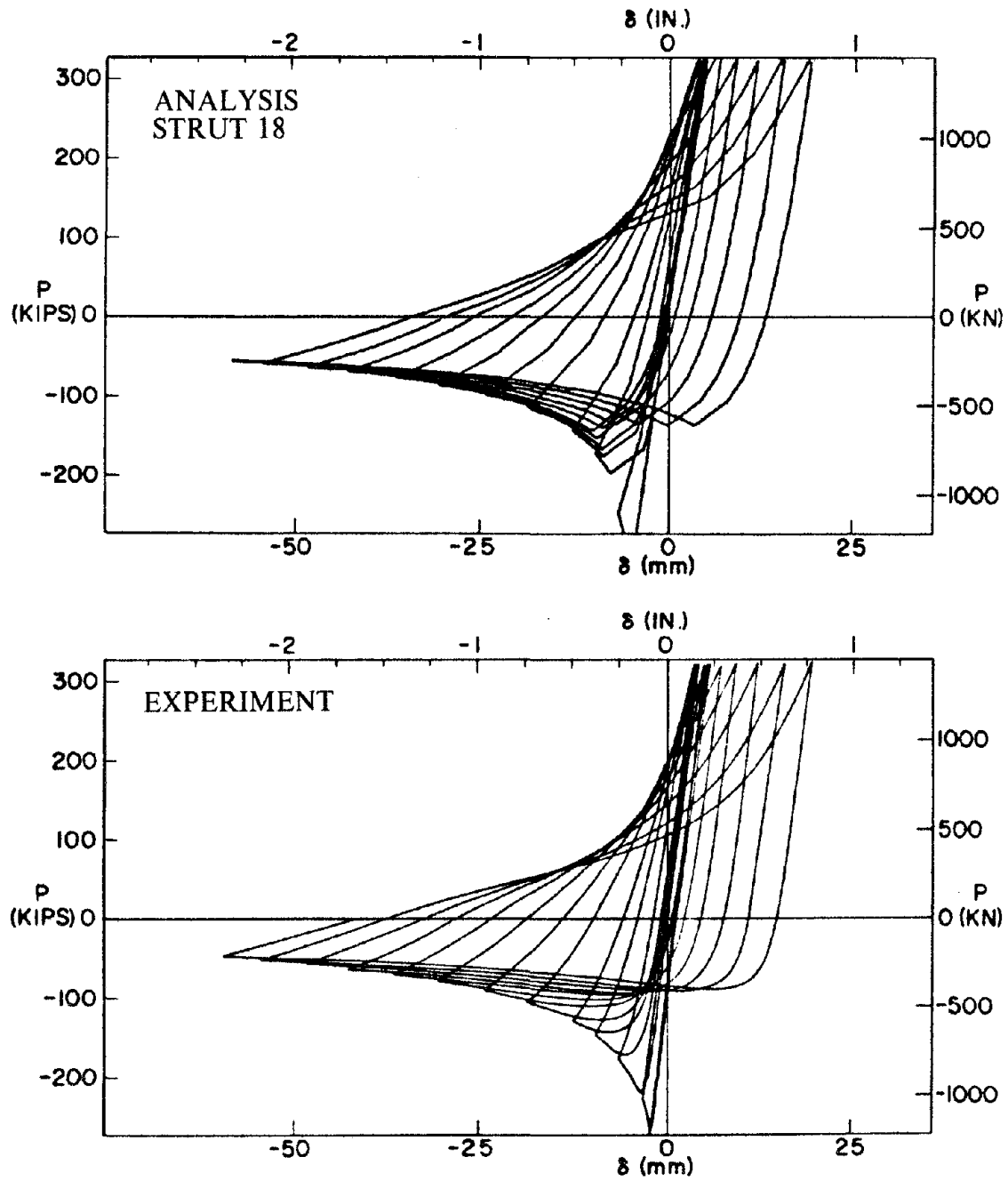


Fig. 4.5 Comparison of Analytical and Experimental Axial Force - Axial Displacement Curves for Strut 18

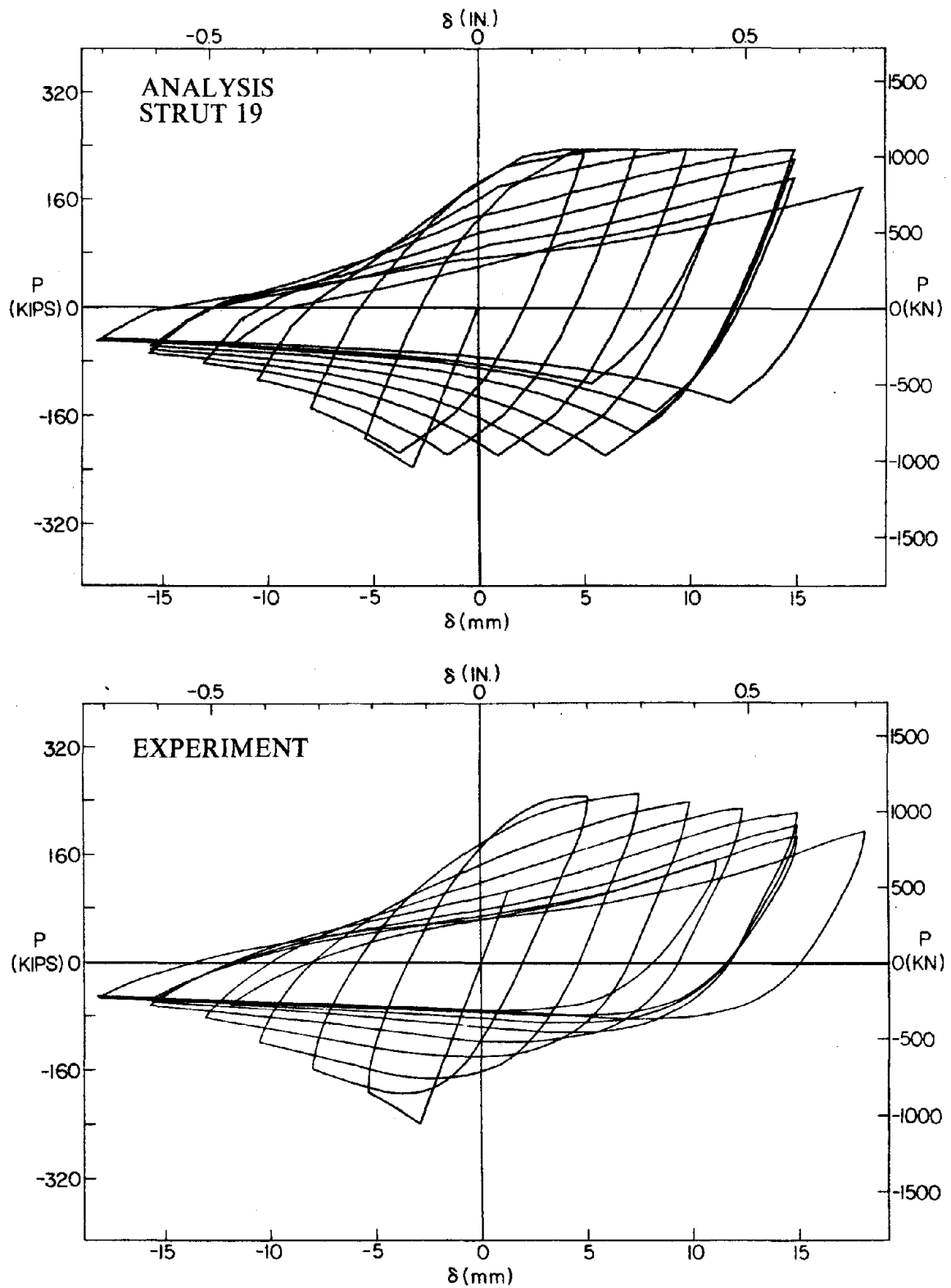


Fig. 4.6 Comparison of Analytical and Experimental Axial Force - Axial Displacement Curves for Strut 19

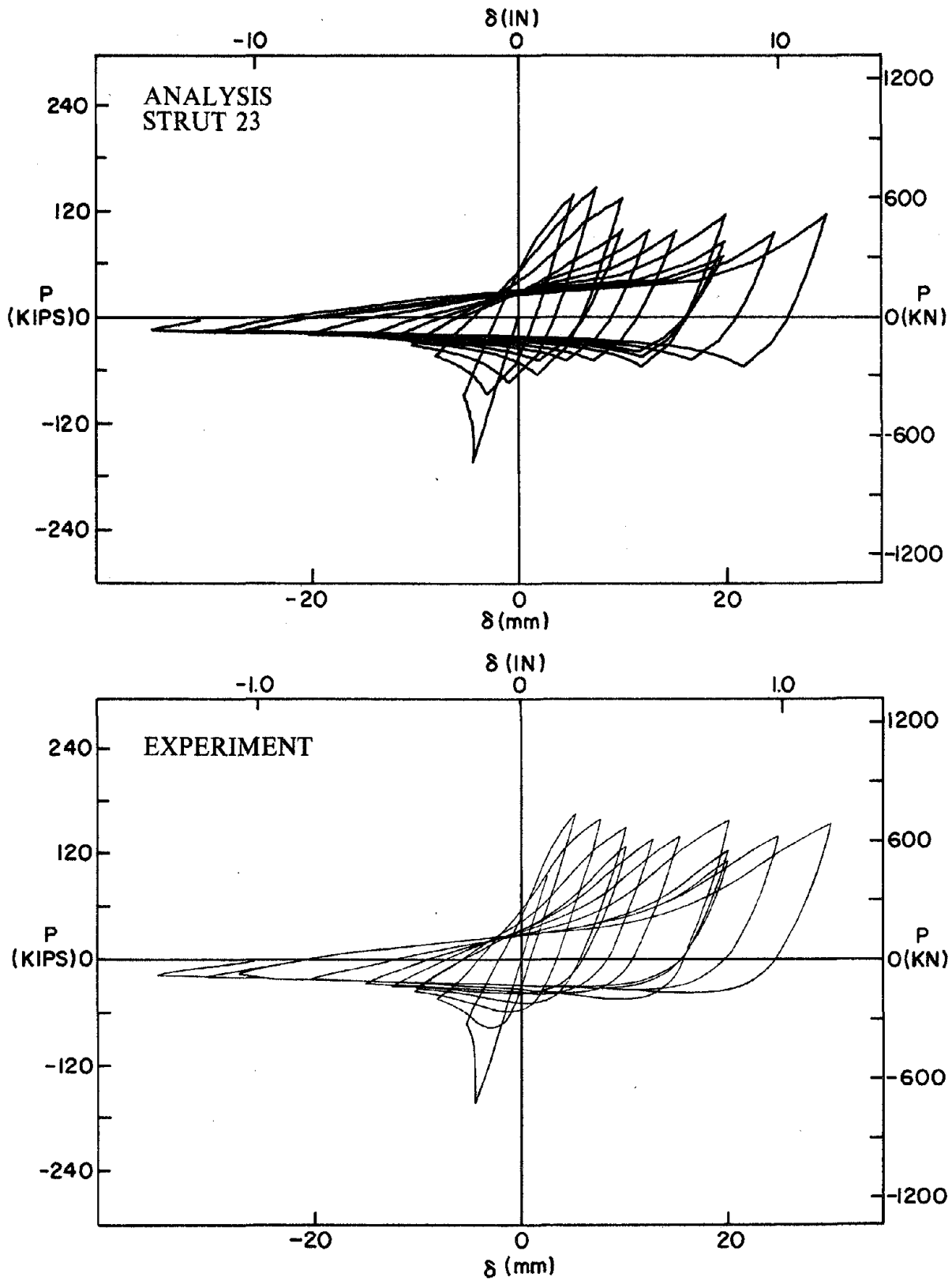


Fig. 4.7 Comparison of Analytical and Experimental Axial Force - Axial Displacement Curves for Strut 23

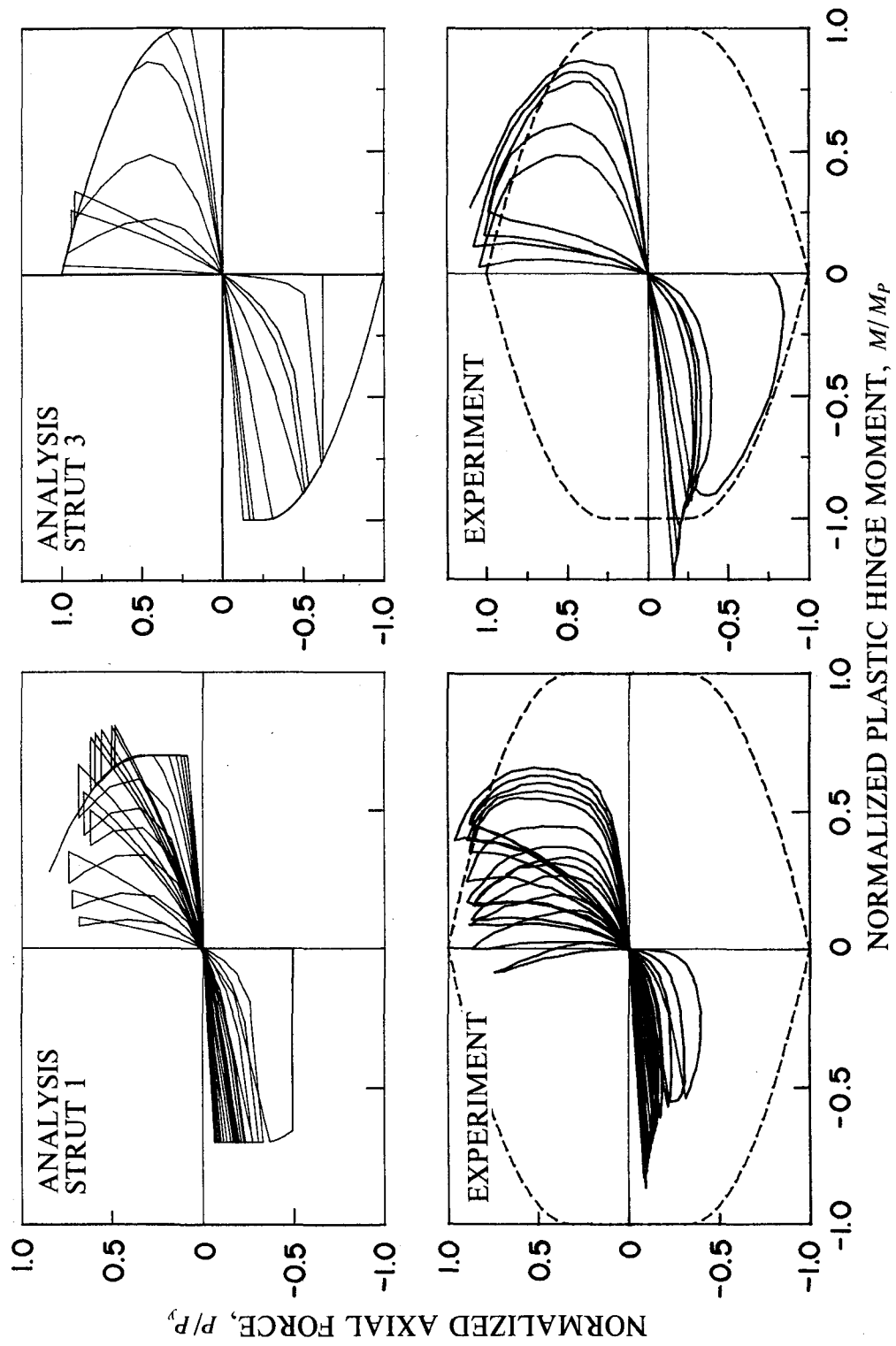


Fig. 4.8 Comparisons of Analytical and Experimental Axial Force - Plastic Hinge Moment Curves for Struts 1 and 3

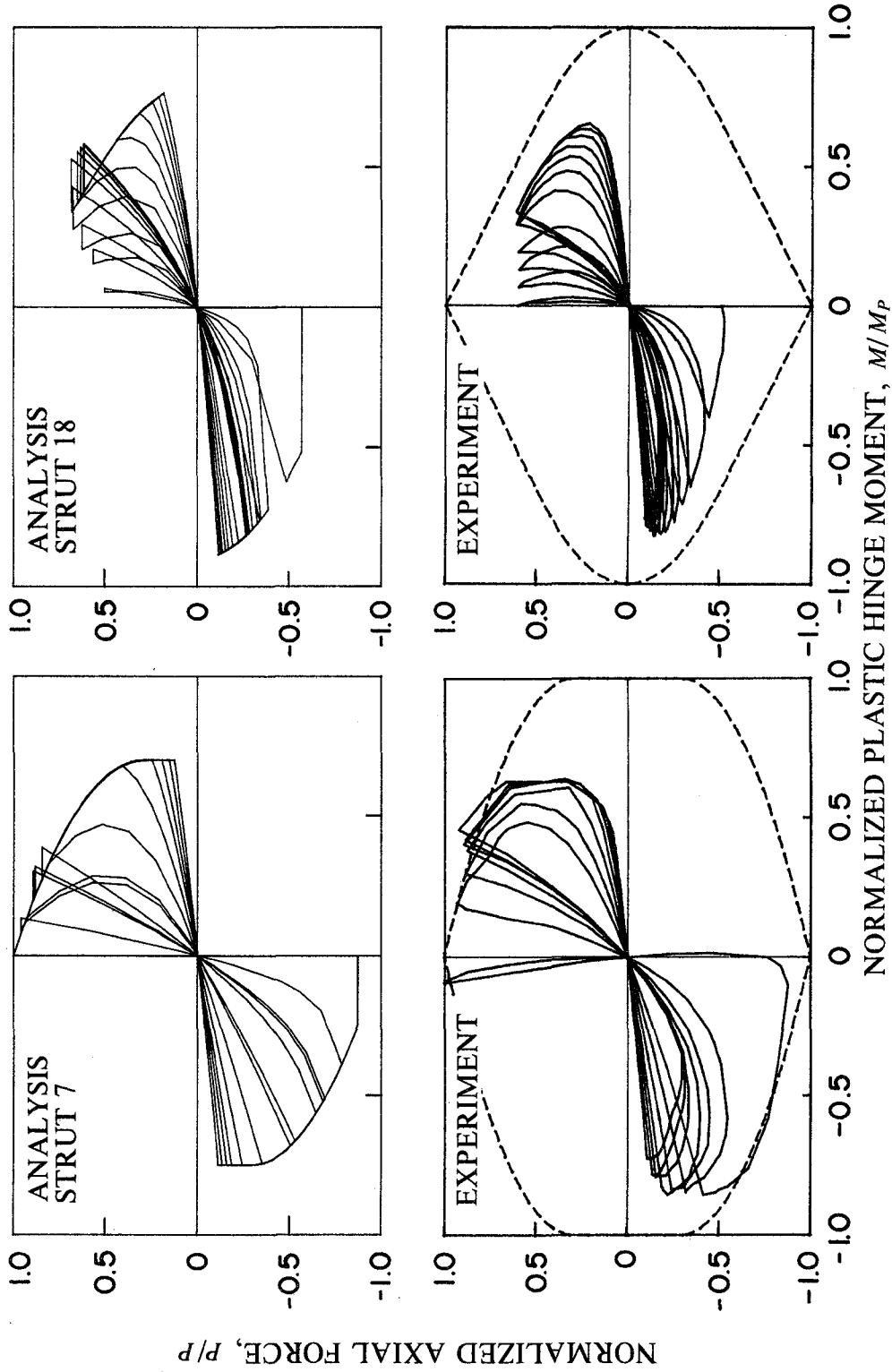


Fig. 4.9 Comparisons of Analytical and Experimental Axial Force - Plastic Hinge Moment Curves for Struts 7 and 18

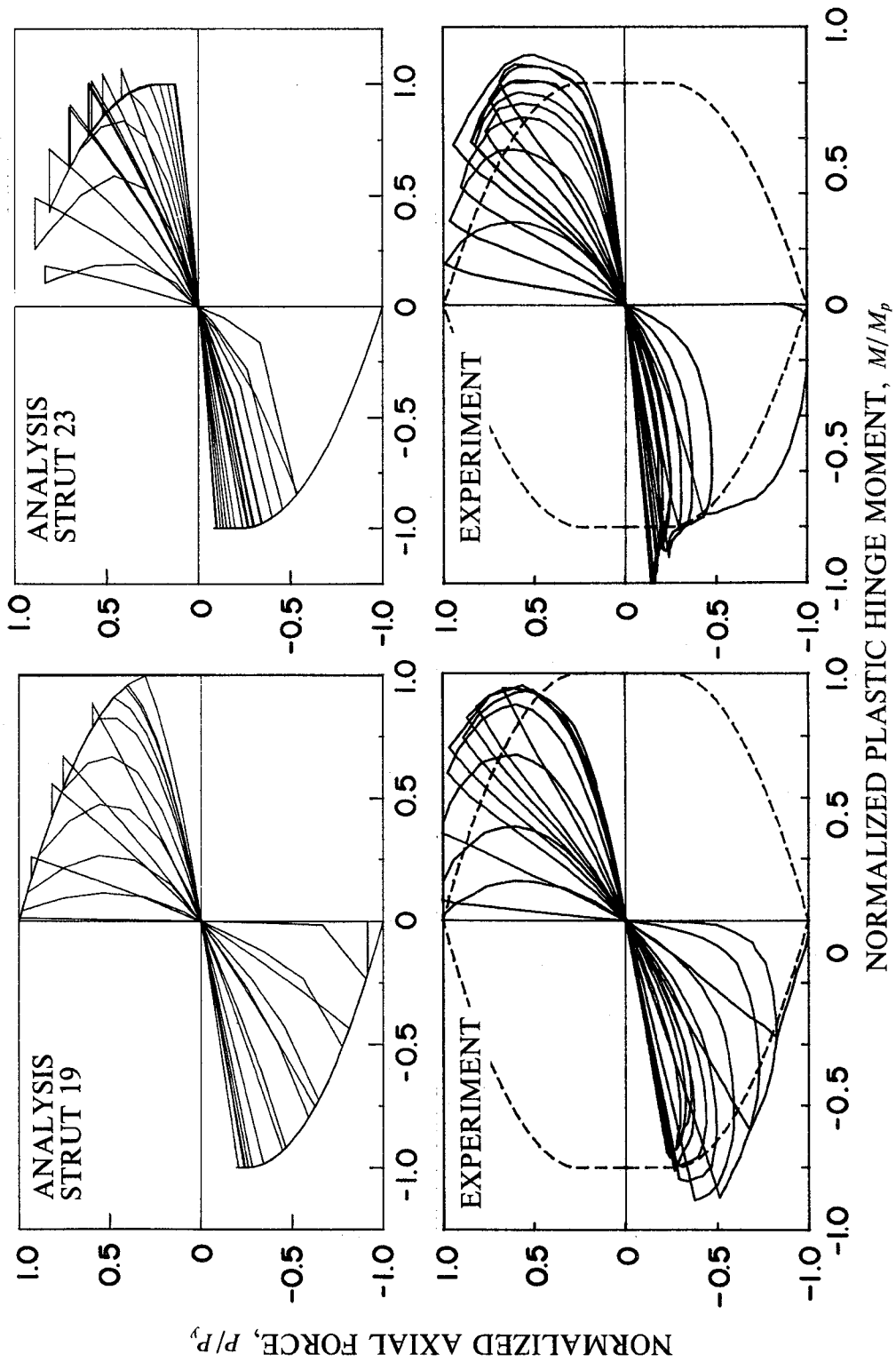


Fig. 4.10 Comparisons of Analytical and Experimental Axial Force - Plastic Hinge Moment Curves for Struts 19 and 23

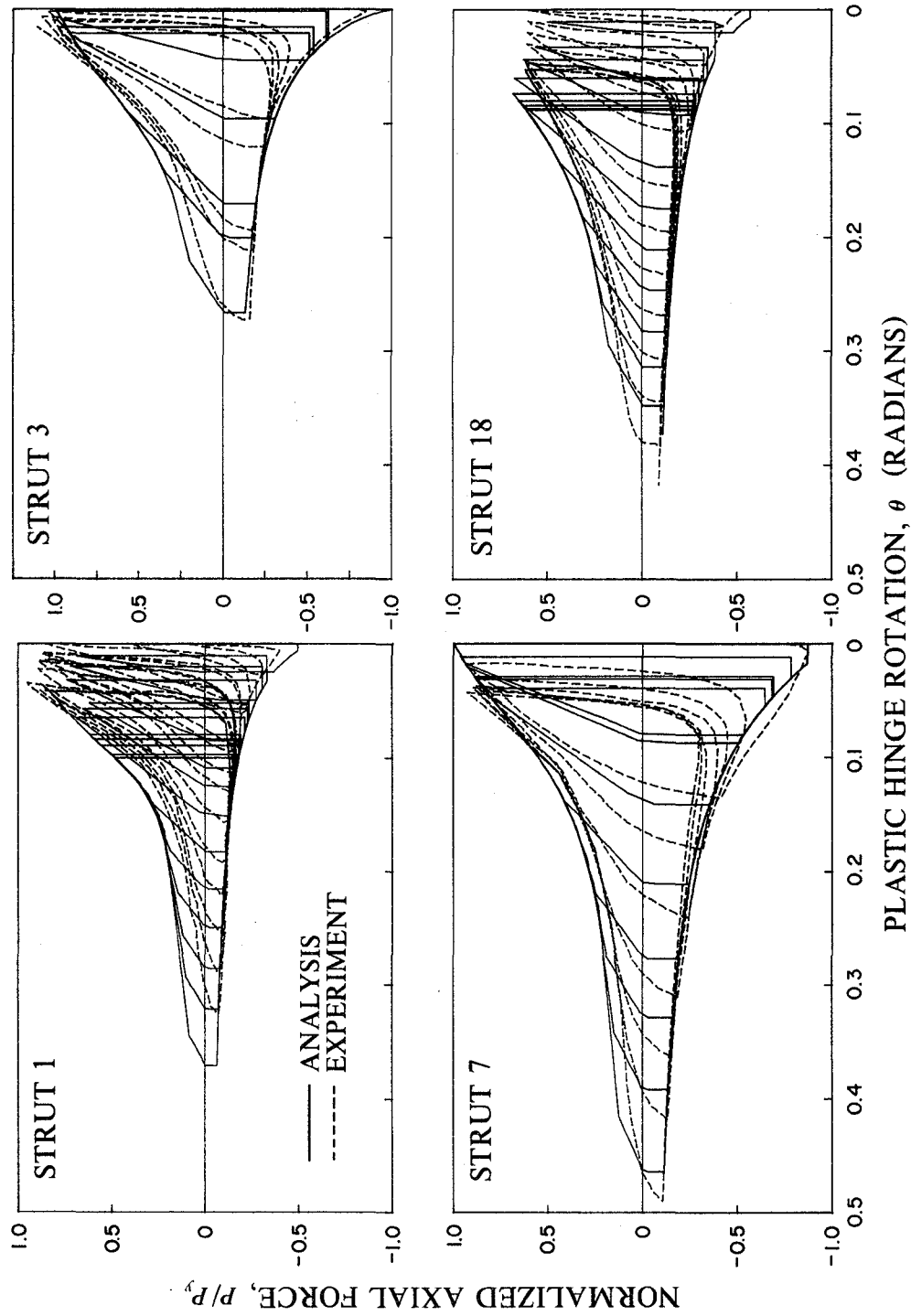


Fig. 4.11 Comparisons of Analytical and Experimental Axial Force - Plastic Hinge Rotation Curves for Struts 1, 3, 7, and 18

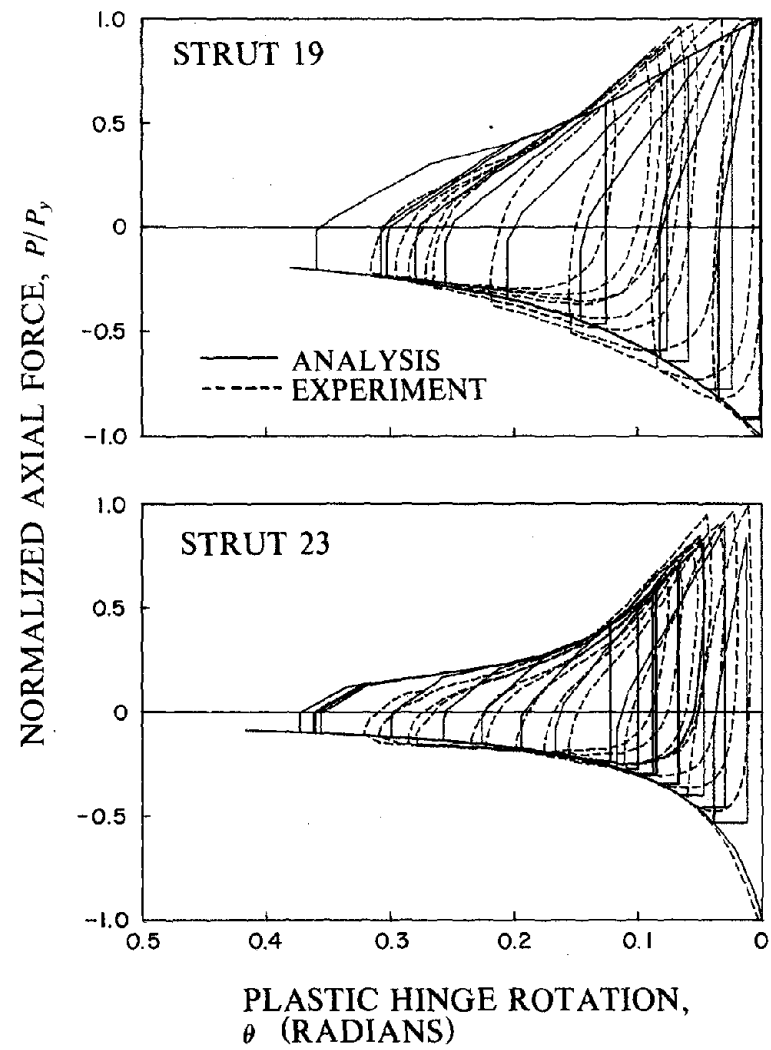


Fig. 4.12 Comparisons of Analytical and Experimental Axial Force - Plastic Hinge Rotation Curves for Struts 19 and 23

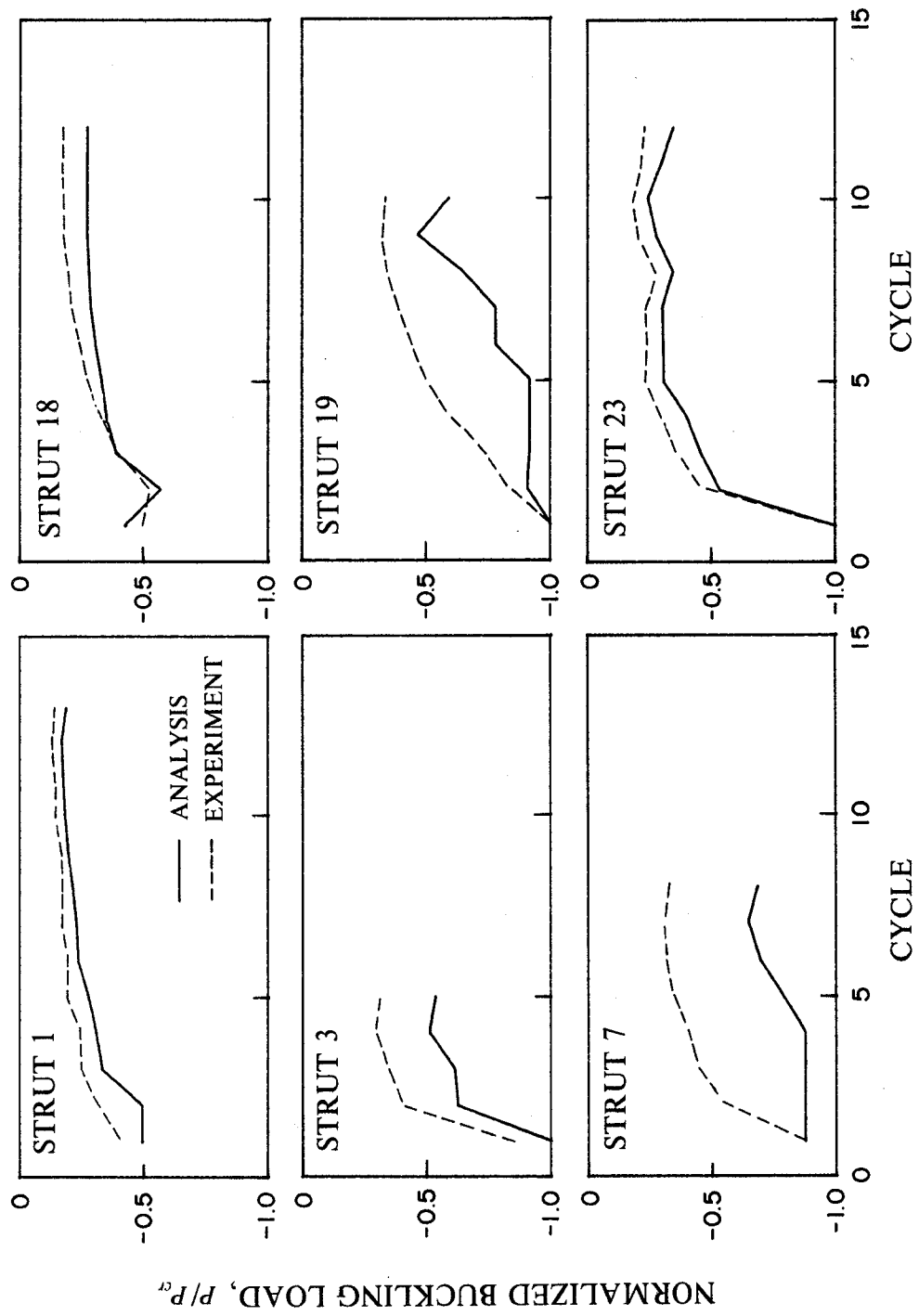


Fig. 4.13 Comparisons of Analytical and Experimental Buckling Loads

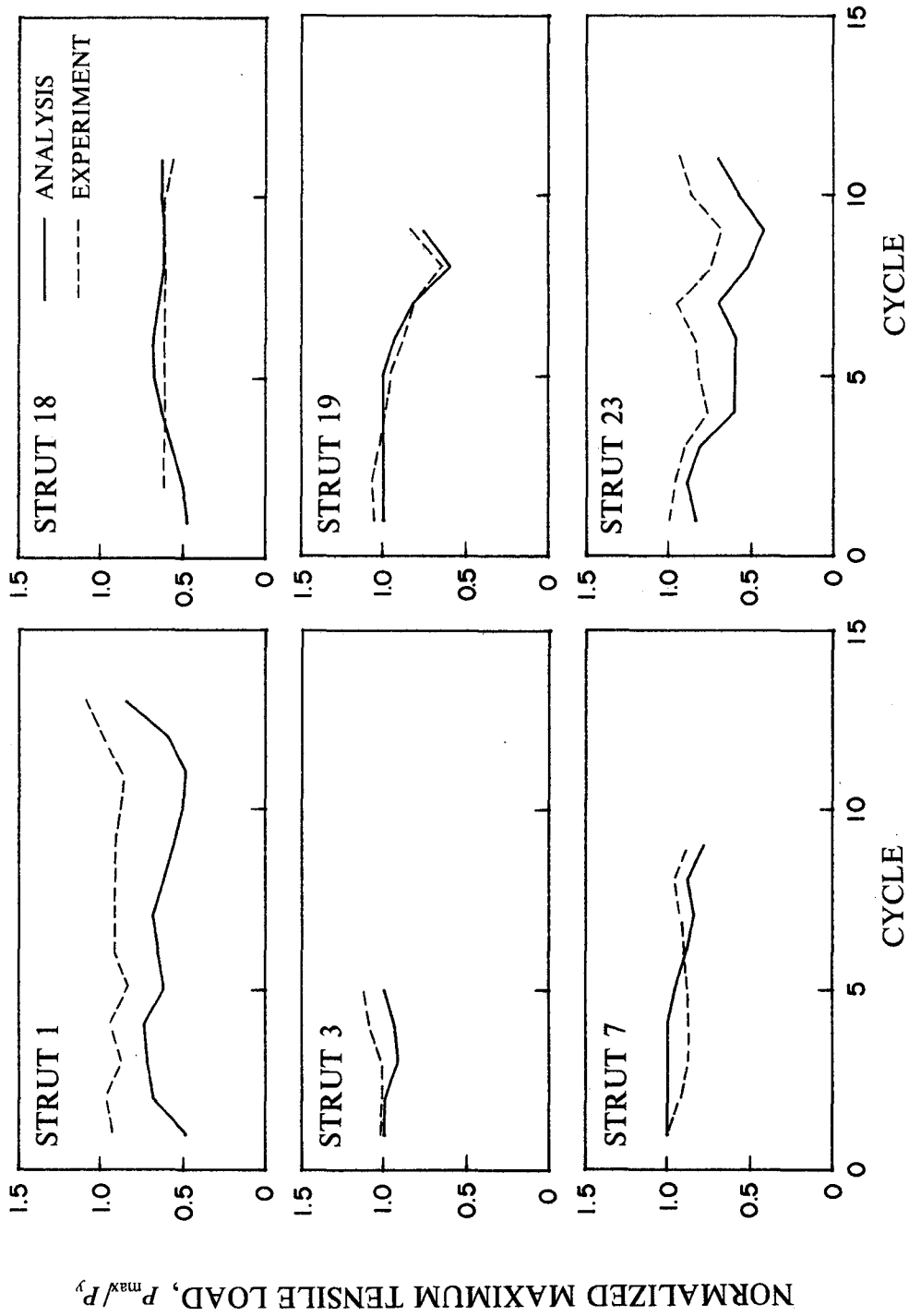


Fig. 4.14 Comparisons of Analytical and Experimental Maximum Tensile Loads

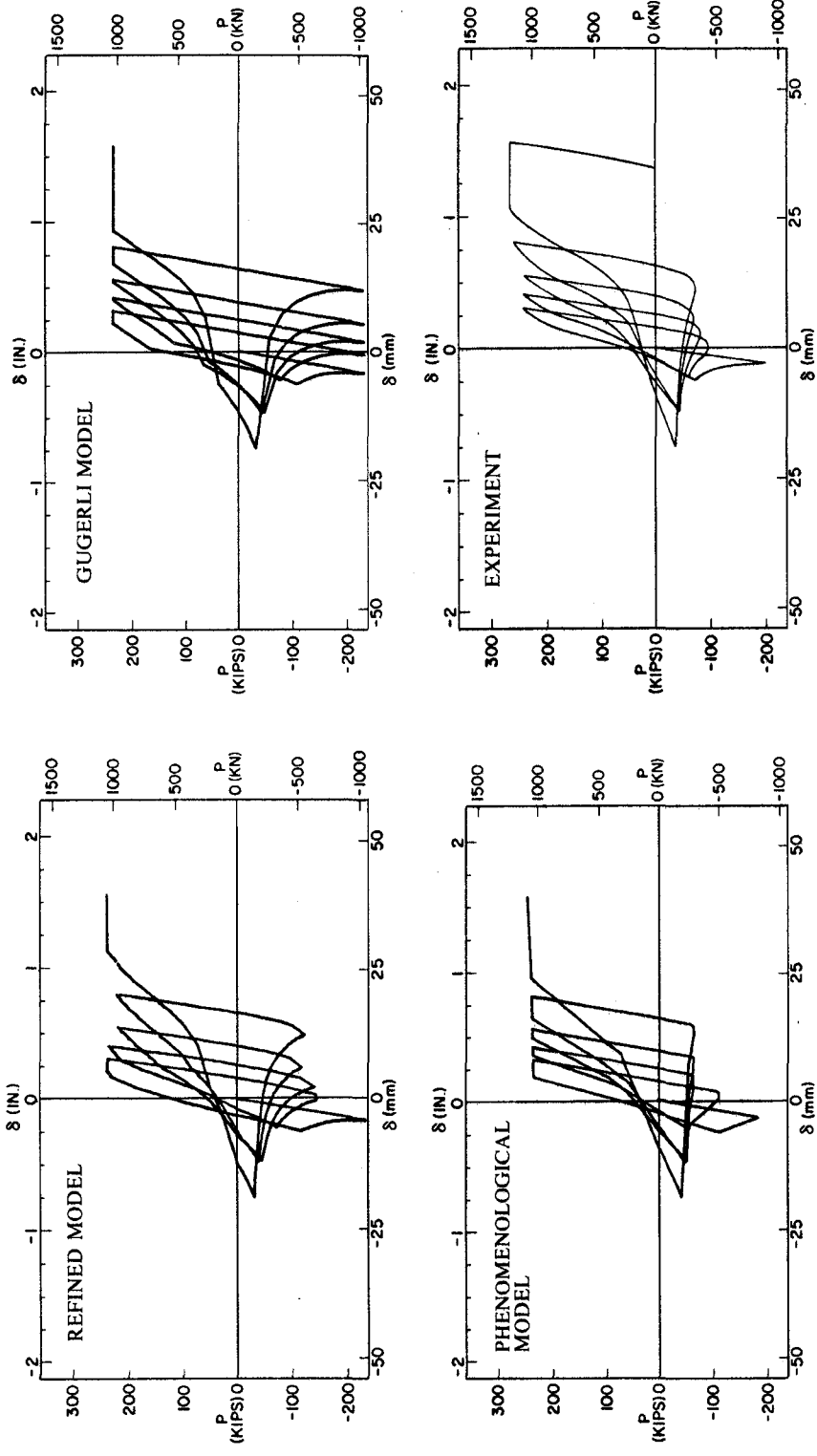


Fig. 4.15 Comparison of Axial Force - Axial Displacement Curves obtained using Different Models with the Corresponding Experimental Data

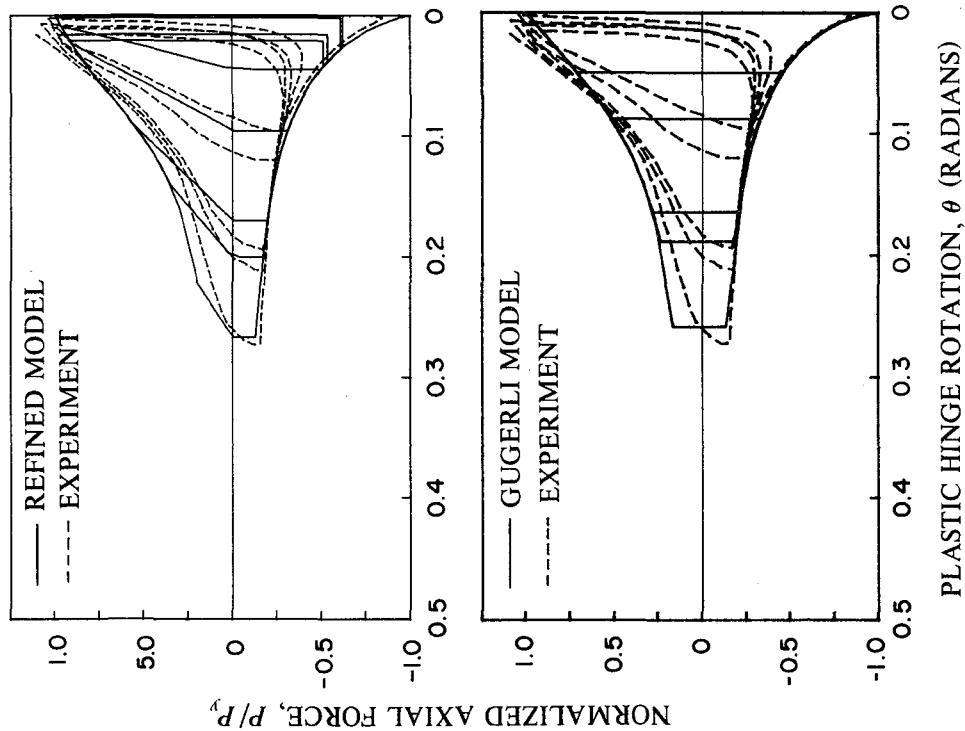


Fig. 4.16 Comparison of the Refined Physical Theory Brace Model and the Gugerli Model with respect to P-M Curves

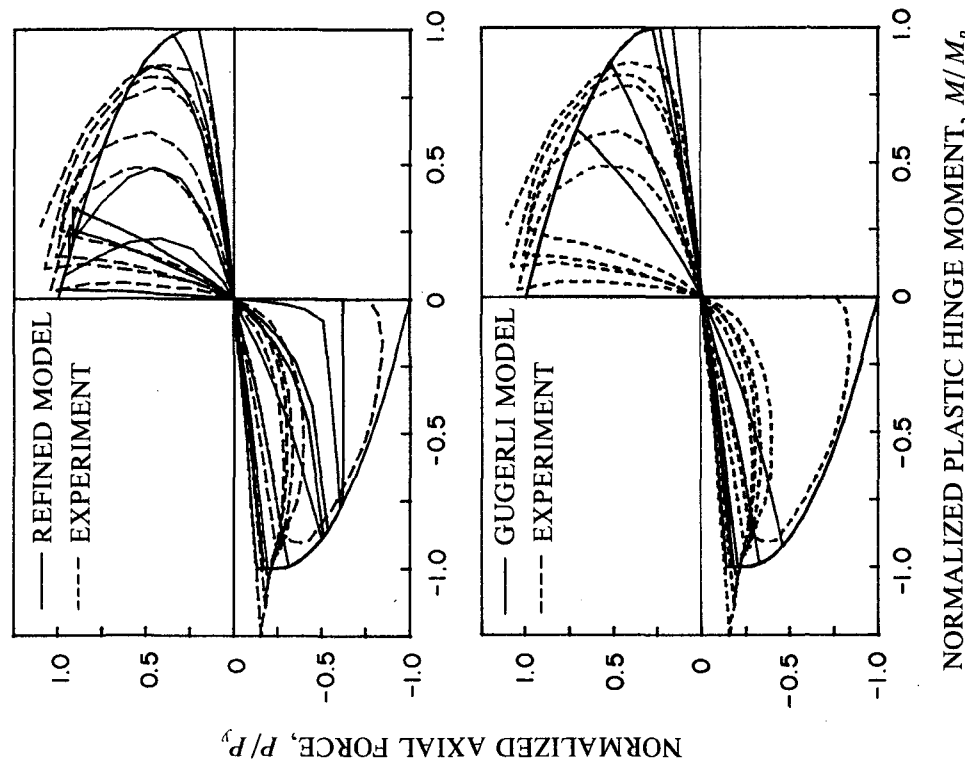


Fig. 4.17 Comparison of the Refined Physical Theory Brace Model and the Gugerli Model with respect to P-θ Curves

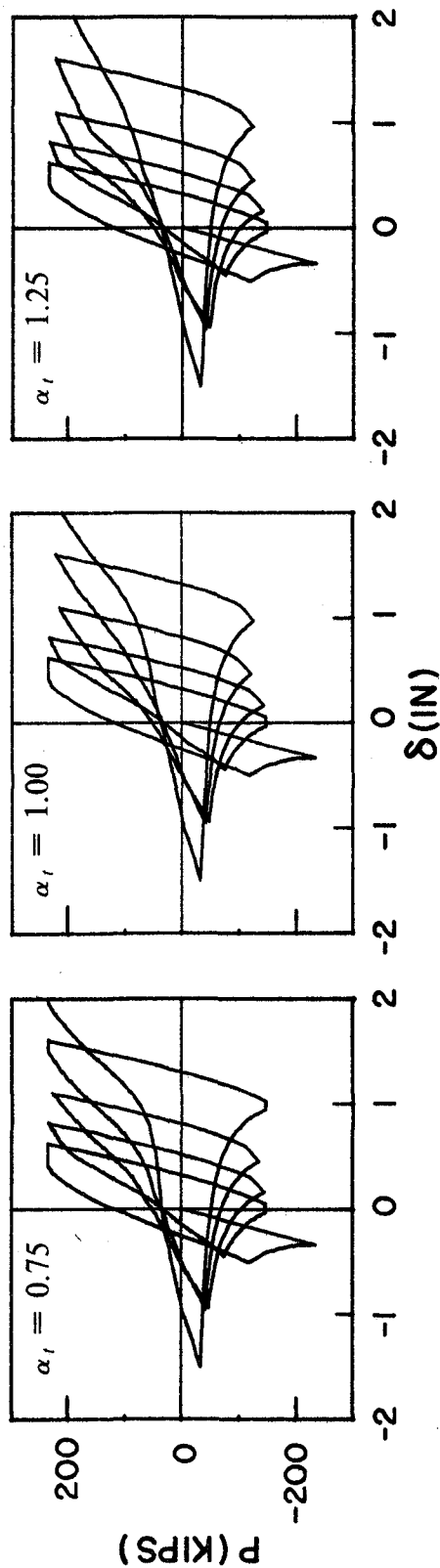


Fig. 4.18 Influence of α_t Values on Axial Force - Axial Displacement Curves
(1 kip = 4.45 kN; 1 in. = 25.4 mm)

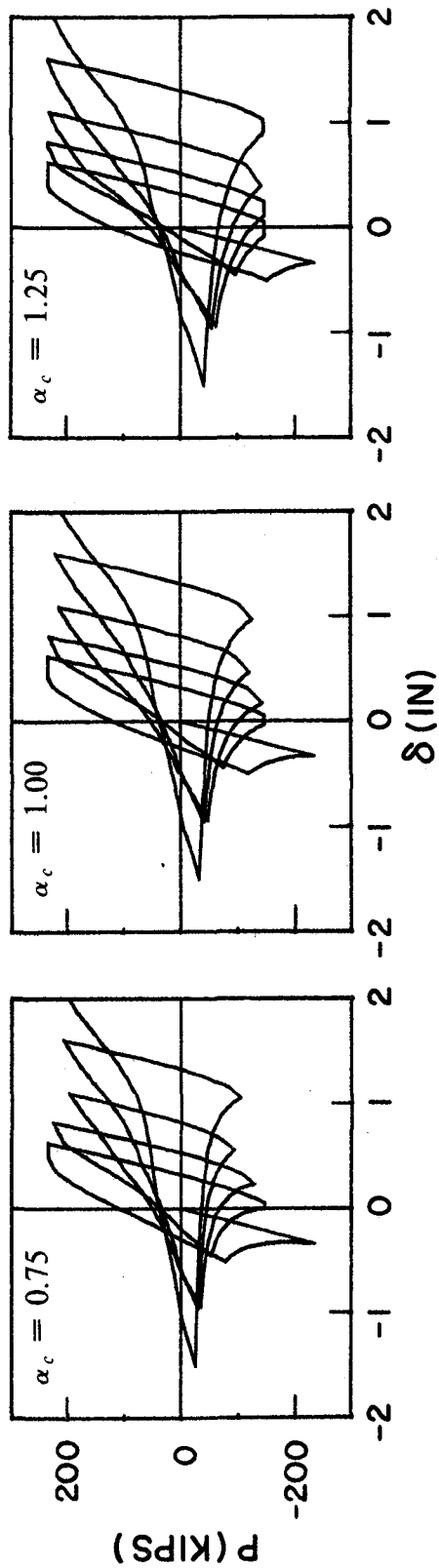


Fig. 4.19 Influence of α_c Values on Axial Force - Axial Displacement Curves
(1 kip = 4.45 kN; 1 in. = 25.4 mm)

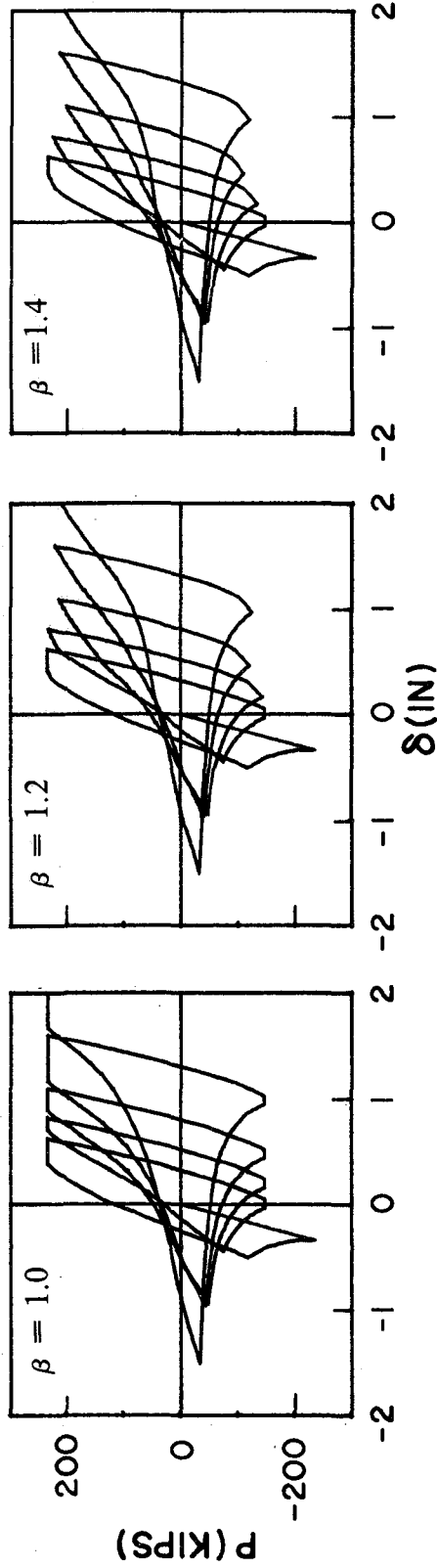


Fig. 4.20 Influence of β Values on Axial Force - Axial Displacement Curves
(1 kip = 4.45 kN; 1 in. = 25.4 mm)

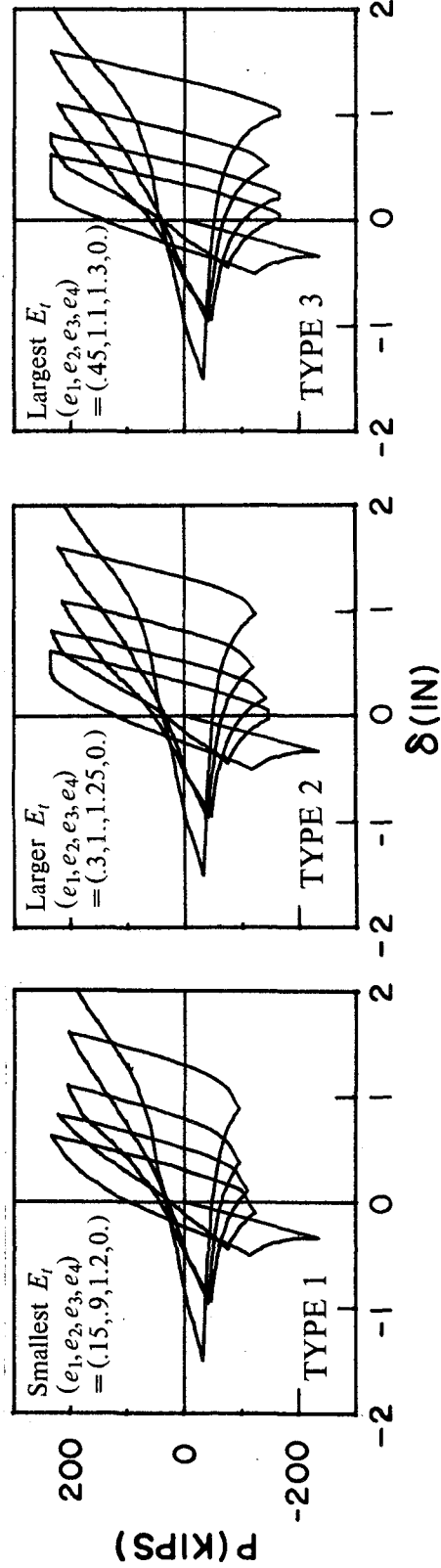


Fig. 4.21 Influence of Tangent Moduli on Axial Force - Axial Displacement Curves (1 kip = 4.45 kN; 1 in. = 25.4 mm)

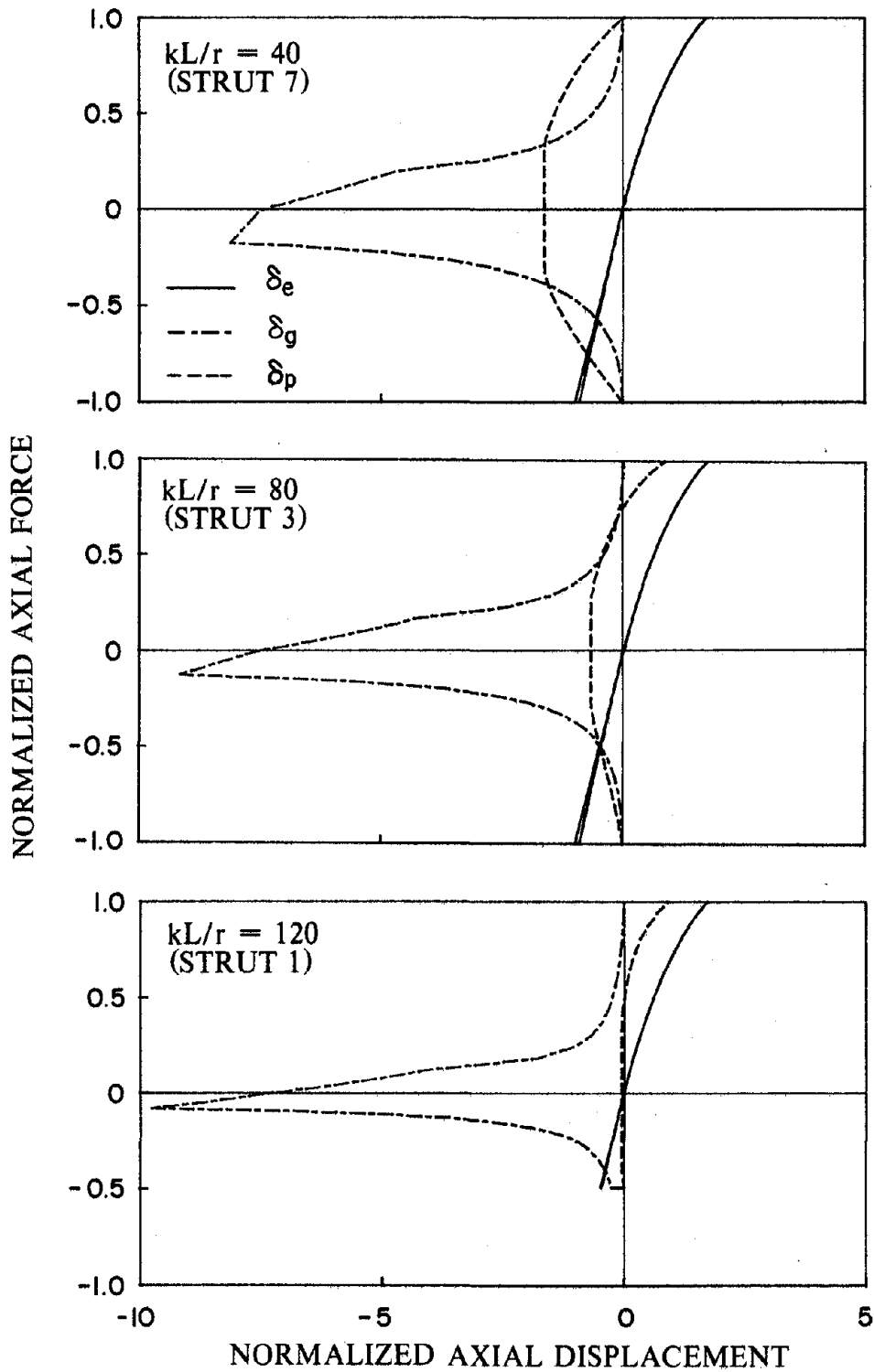


Fig. 4.22 Comparison of Contributions of Three major Axial Displacement Components, δ_e , δ_g , δ_p

- - - BILINEAR TRUSS ELEMENT
 ——— REFINED ELEMENT
 ——— BEAM-COLUMN ELEMENT

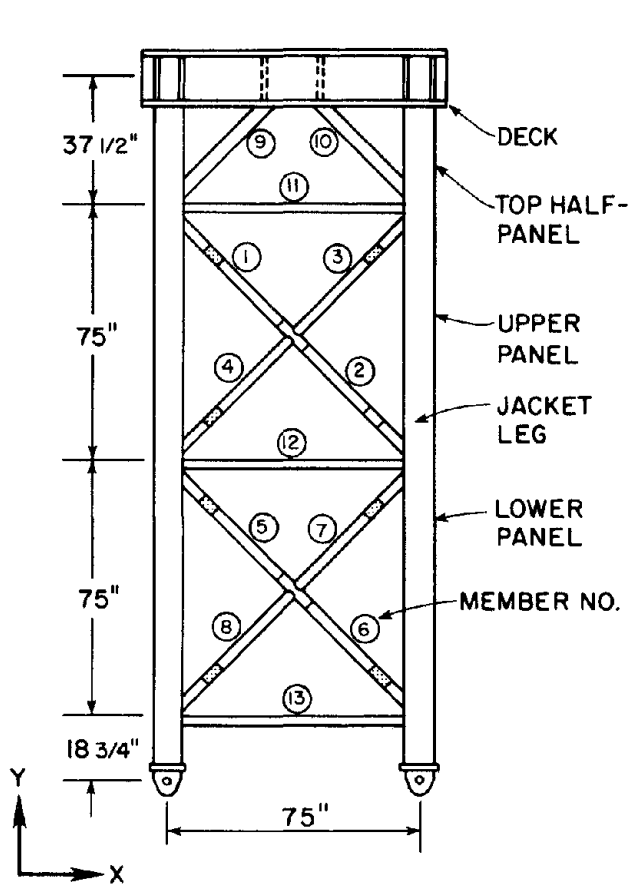


Fig. 5.1 Elevation View of the API Frame [33] (1 in. = 2.54 mm)

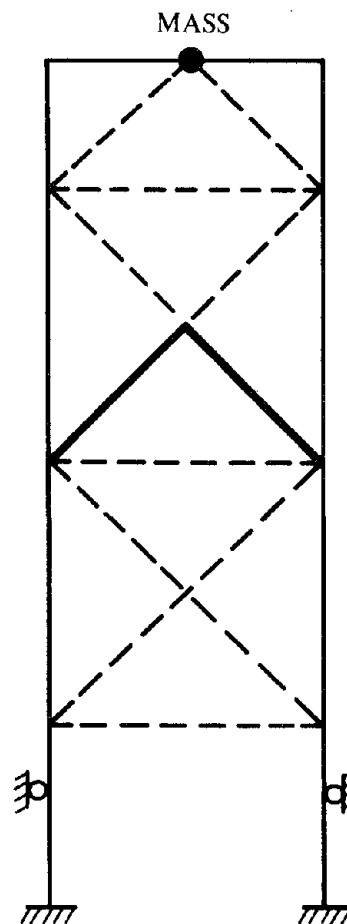


Fig. 5.2 Modeling of the API Frame [33]

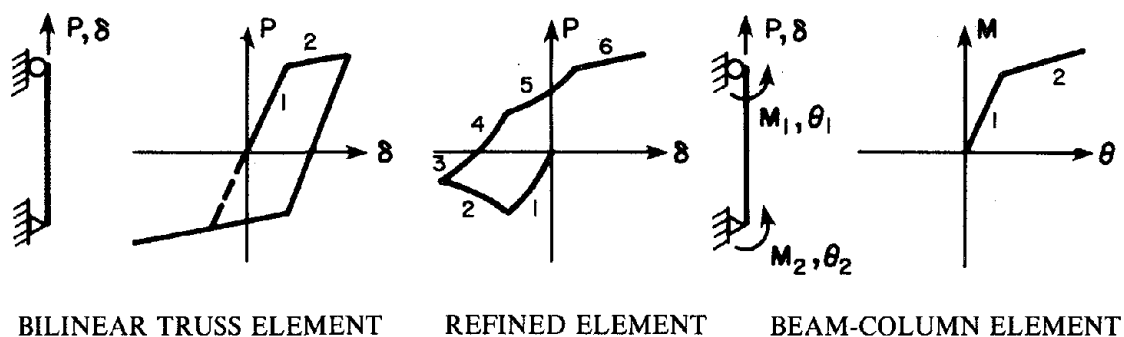


Fig. 5.3 Elements used in Analyses for the API frame [33]

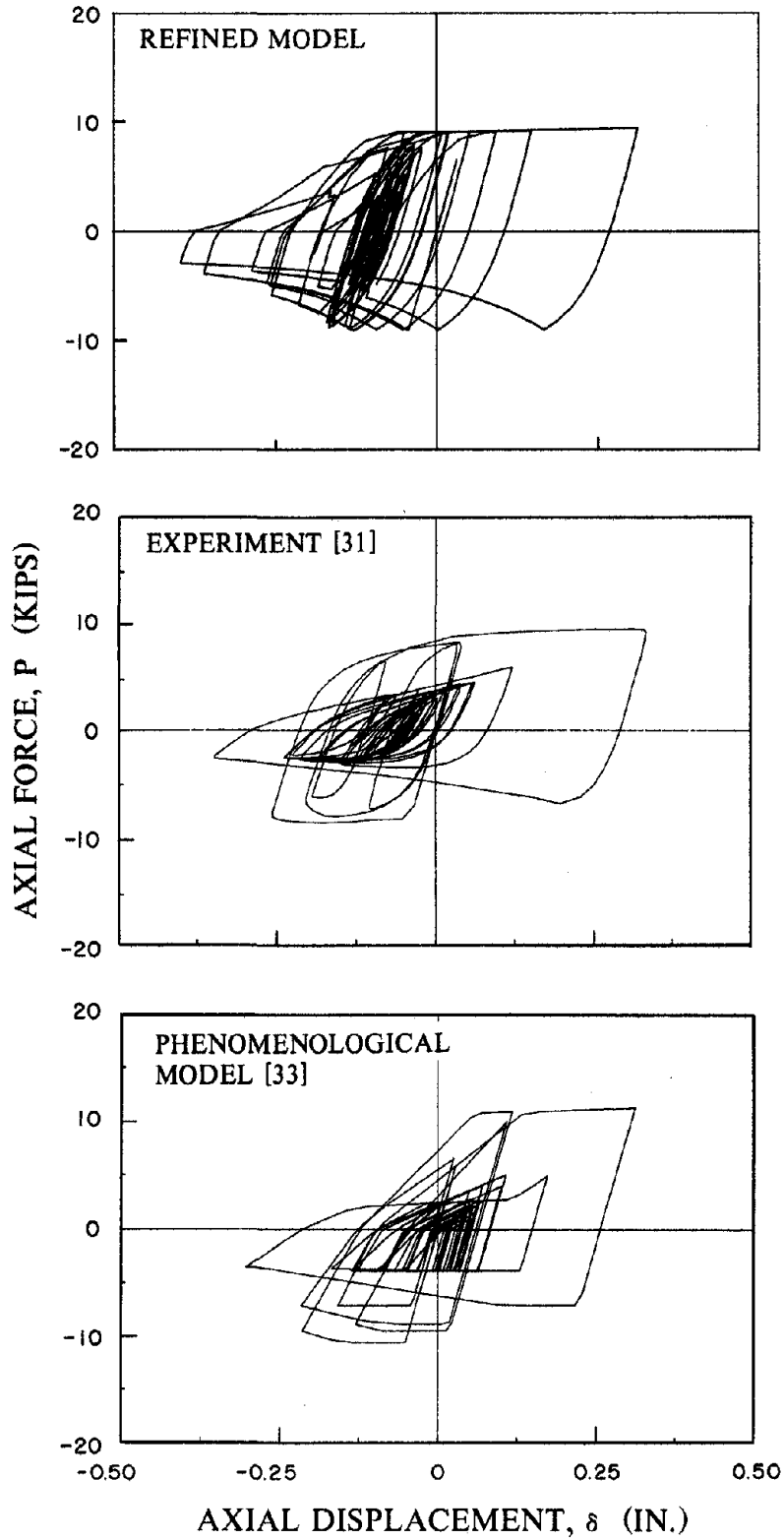


Fig. 5.4 Comparison of Analytical and Experimental Hysteresis Loops for Brace 2 ($\Delta t = 0.01$ sec.) (1 kip = 4.45 kN; 1 in. = 25.4 mm)

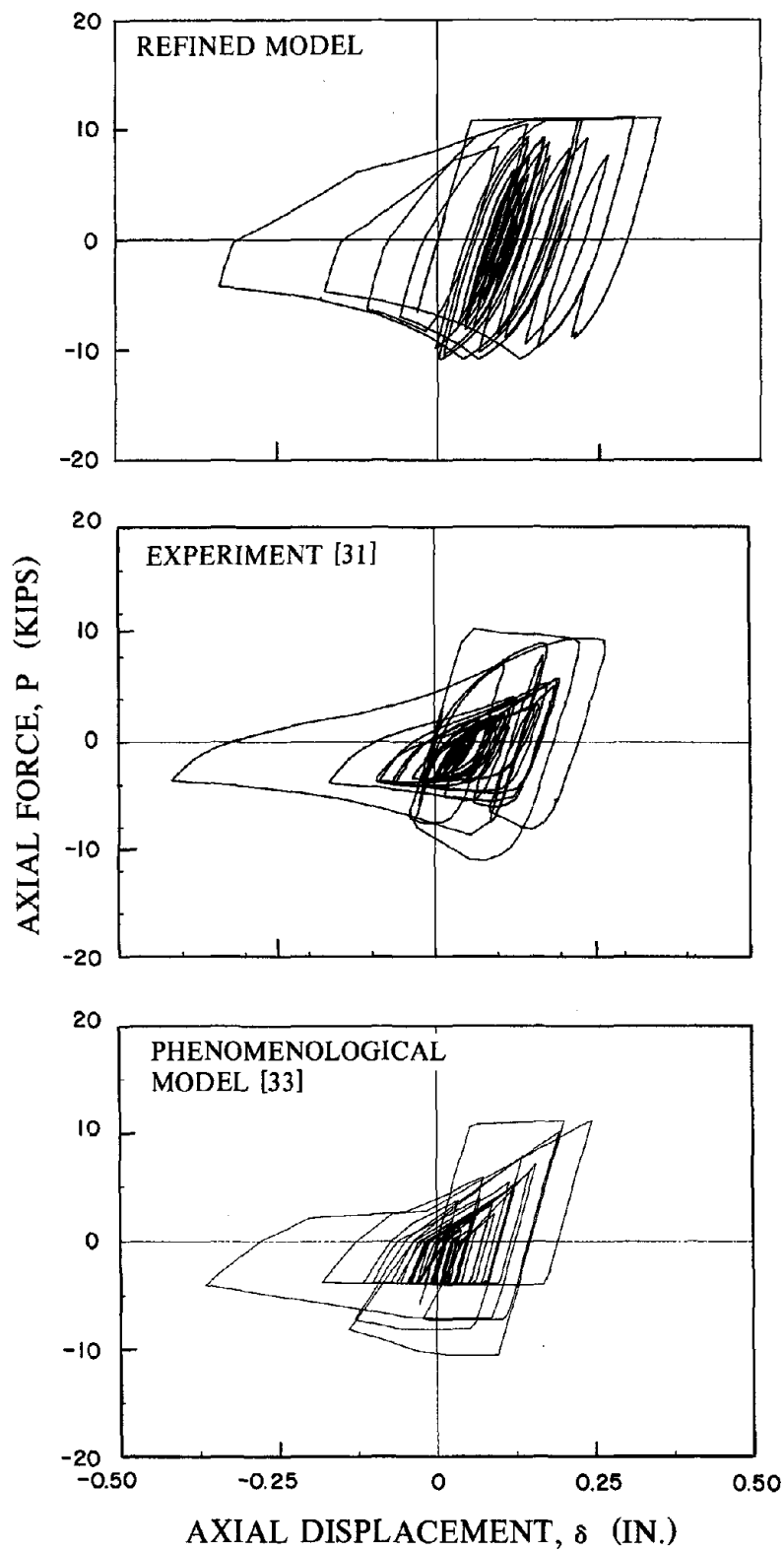


Fig. 5.5 Comparison of Analytical and Experimental Hysteresis Loops for Brace 4 ($\Delta t = 0.01$ sec.) (1 kip = 4.45 kN; 1 in. = 25.4 mm)

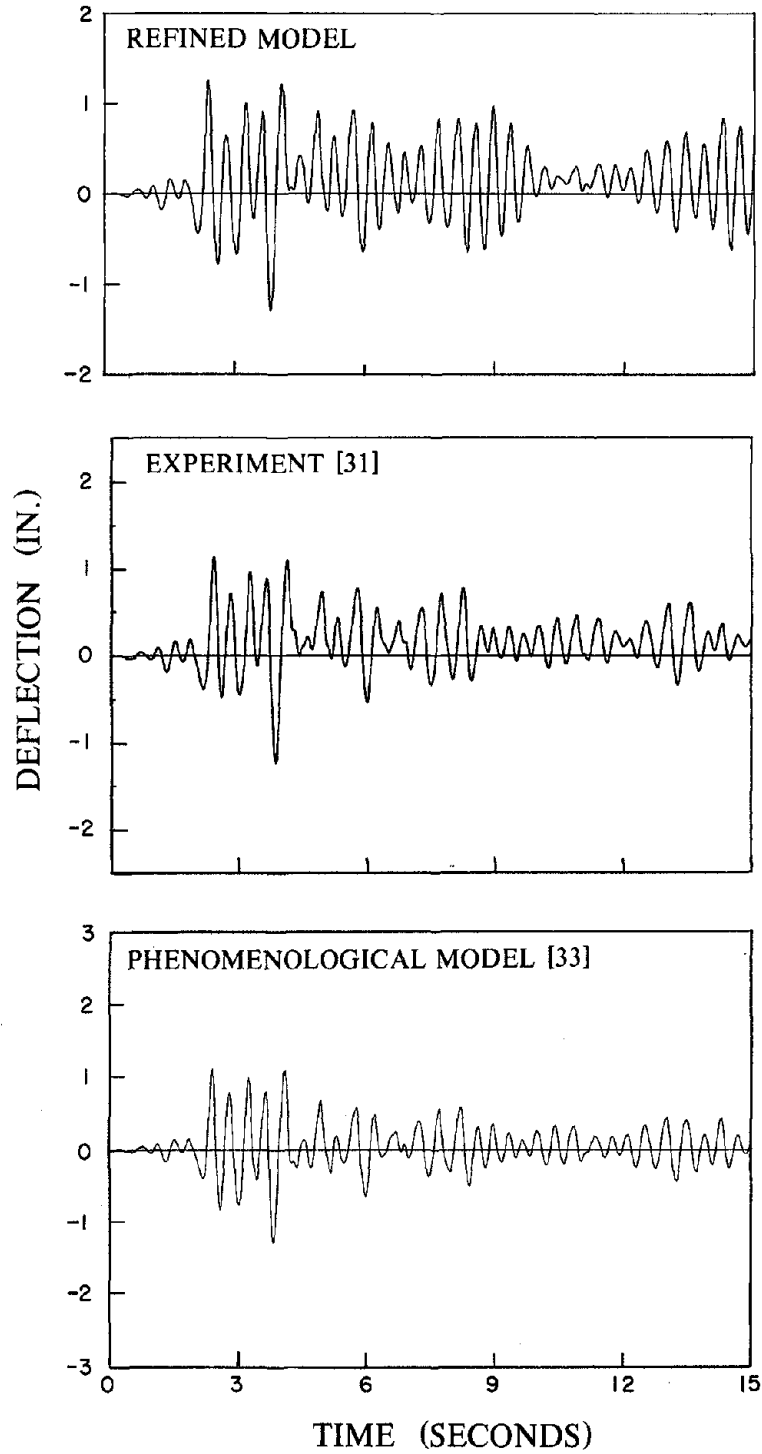


Fig. 5.6 Comparison of Analytical and Experimental Tip Deflection Histories of the Frame ($\Delta t = 0.01$ sec.) (1 in. = 25.4 mm)

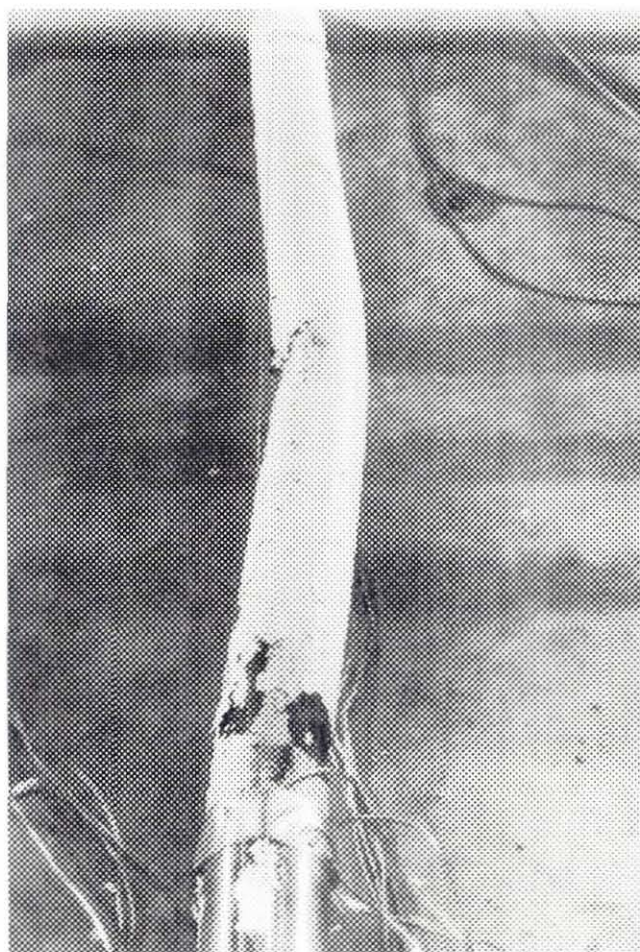


Fig. 5.7 A Photograph of Damages of Brace 2 during the Pseudodynamic Test [32]

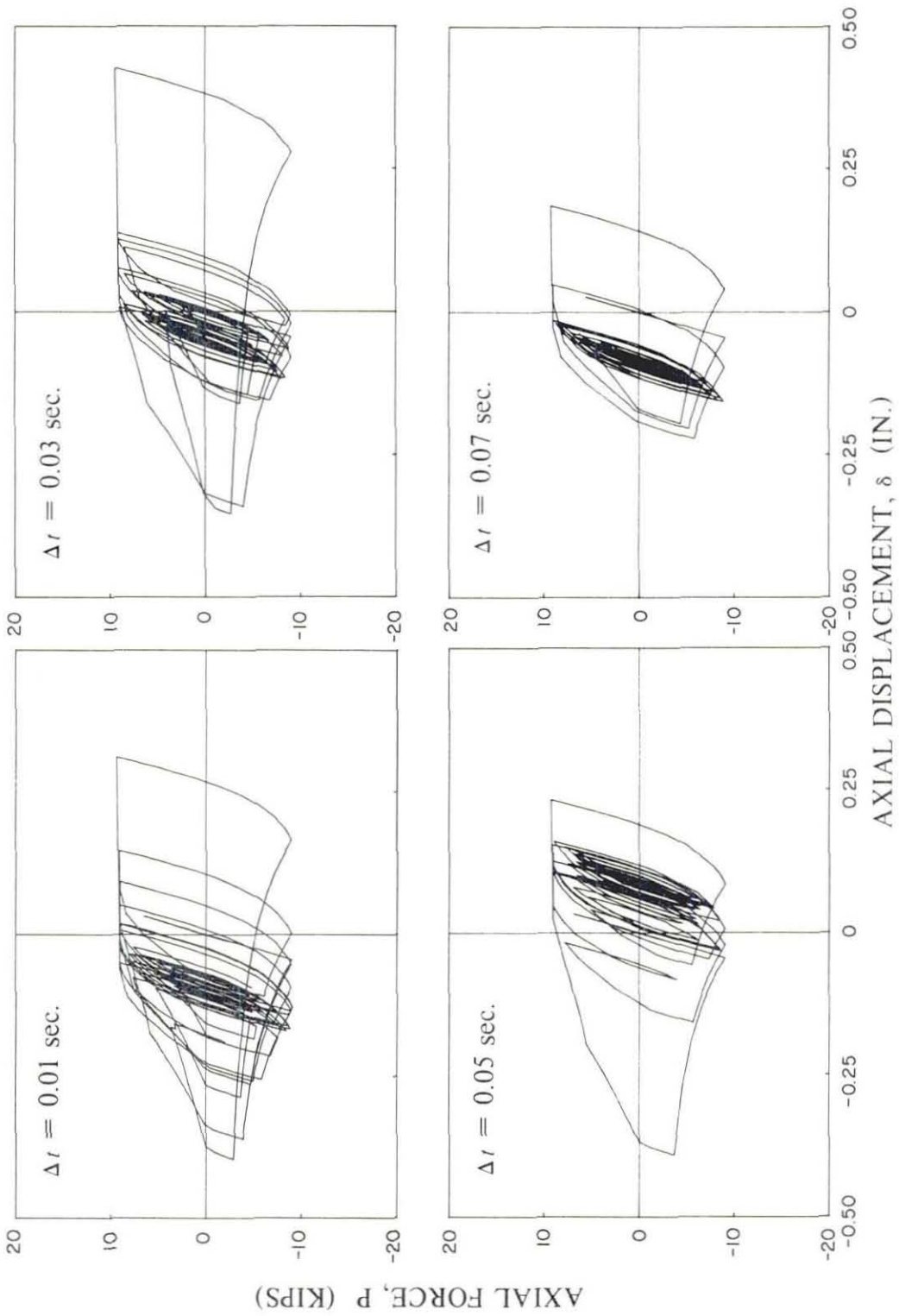


Fig. 5.8 Influence of Analysis Time Steps on Hysteresis Loops of Brace 2 (Event-to-Event Method) (1 kip = 4.45 kN; 1 in. = 25.4 mm)

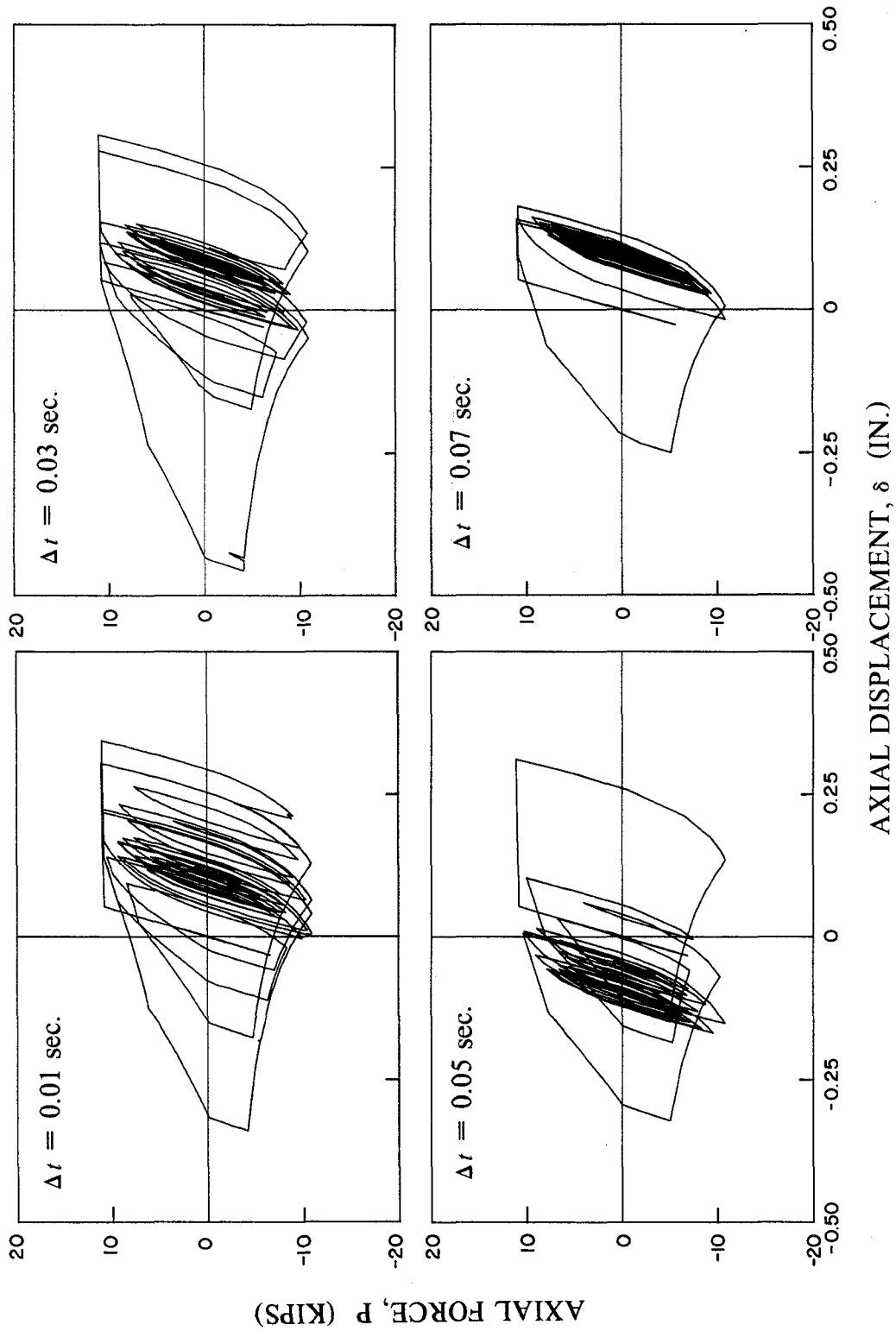


Fig. 5.9 Influence of Analysis Time Steps on Hysteresis Loops of Brace 4 (Event-to-Event Method) (1 kip = 4.45 kN; 1 in. = 25.4 mm)

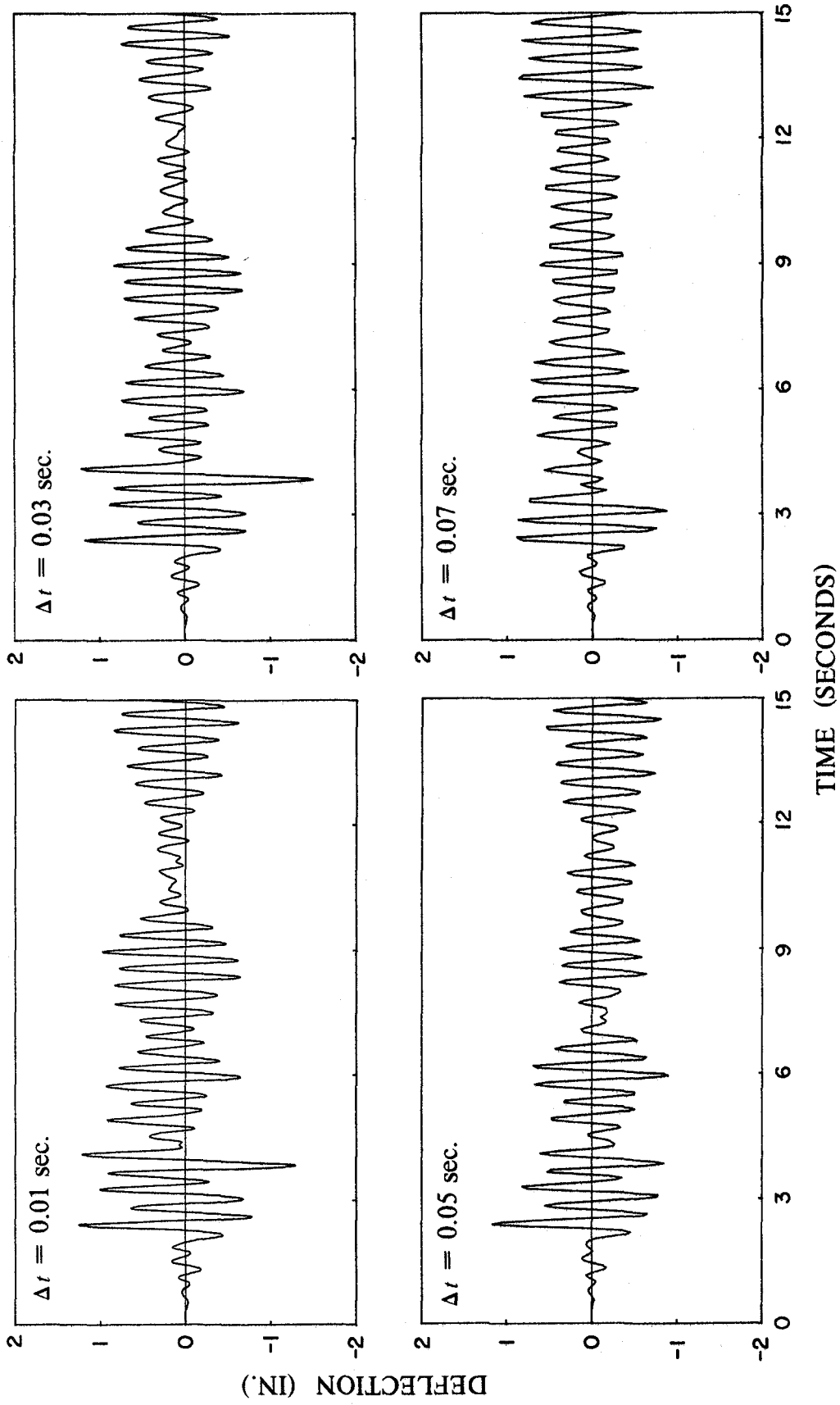


Fig. 5.10 Influence of Analysis Time Steps on Tip Deflection Histories of the Frame (Event-to-Event Method) (1 in. = 25.4 mm)

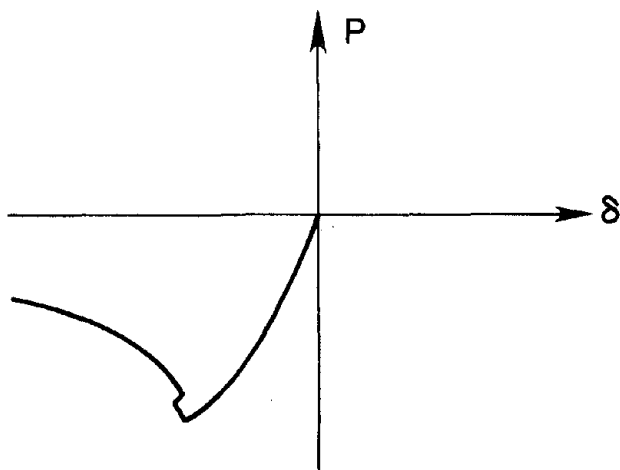


Fig. 5.11 Flip-Flop Type Instability associated with the Event-to-Event Method

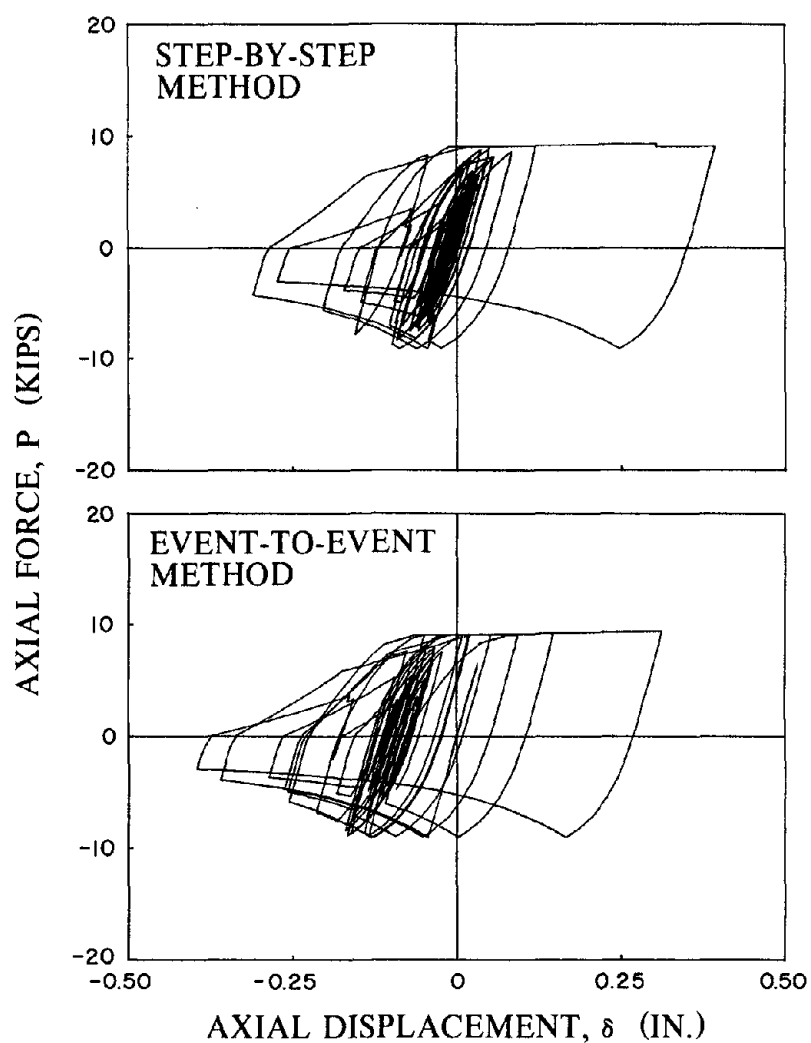


Fig. 5.12 Hysteresis Loops of Brace 2 for Two Numerical Methods ($\Delta t = 0.01$ sec.) (1 kip = 4.45 kN; 1 in. = 25.4 mm)

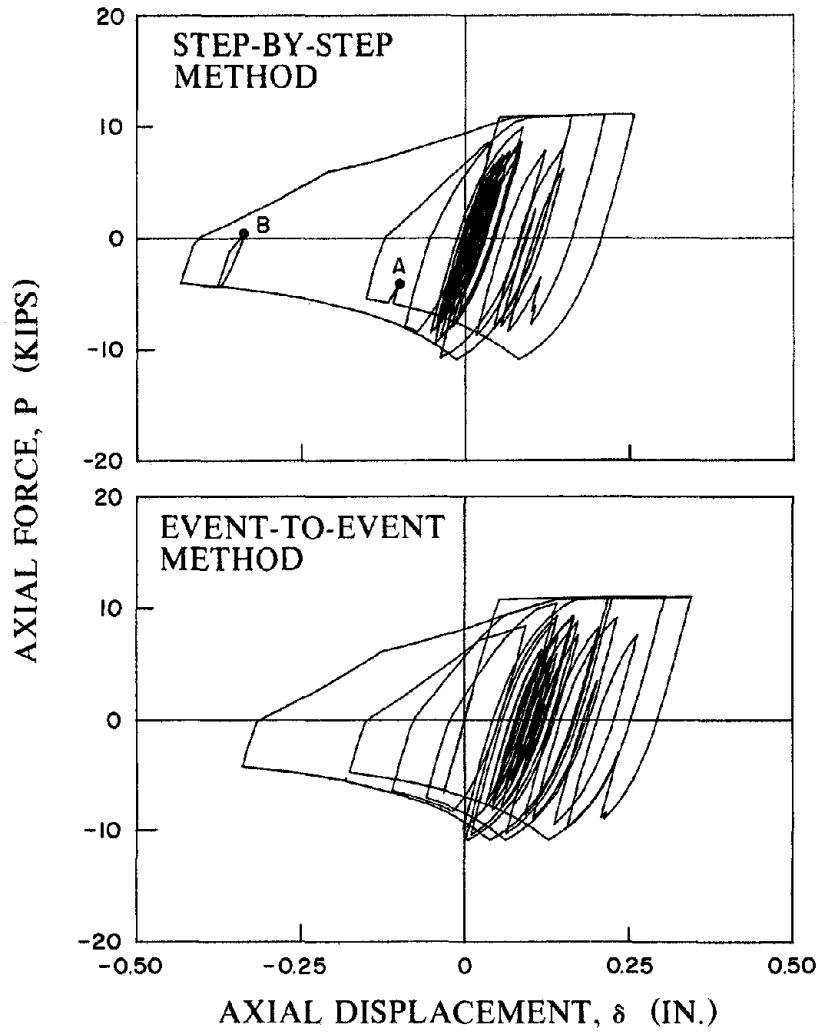


Fig. 5.13 Hysteresis Loops of Brace 4 for Two Numerical Methods ($\Delta t = 0.01$ sec.) (1 kip = 4.45 kN; 1 in. = 25.4 mm)

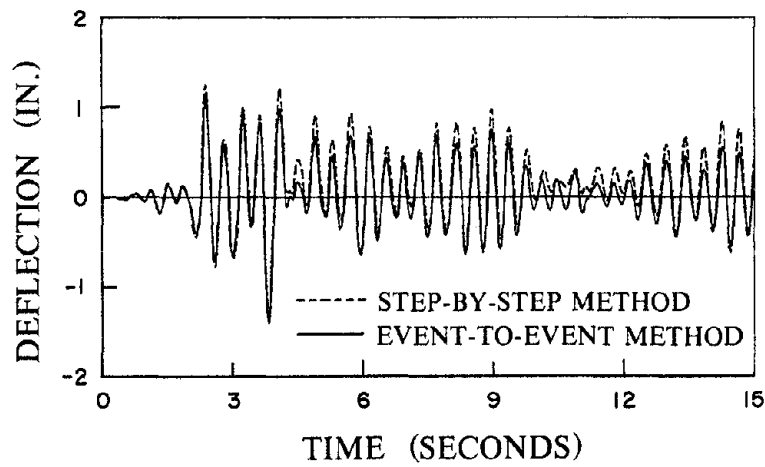


Fig. 5.14 Tip Deflection Histories of the Frame for Two Numerical Methods ($\Delta t = 0.01$ sec.) (1 in. = 25.4 mm)

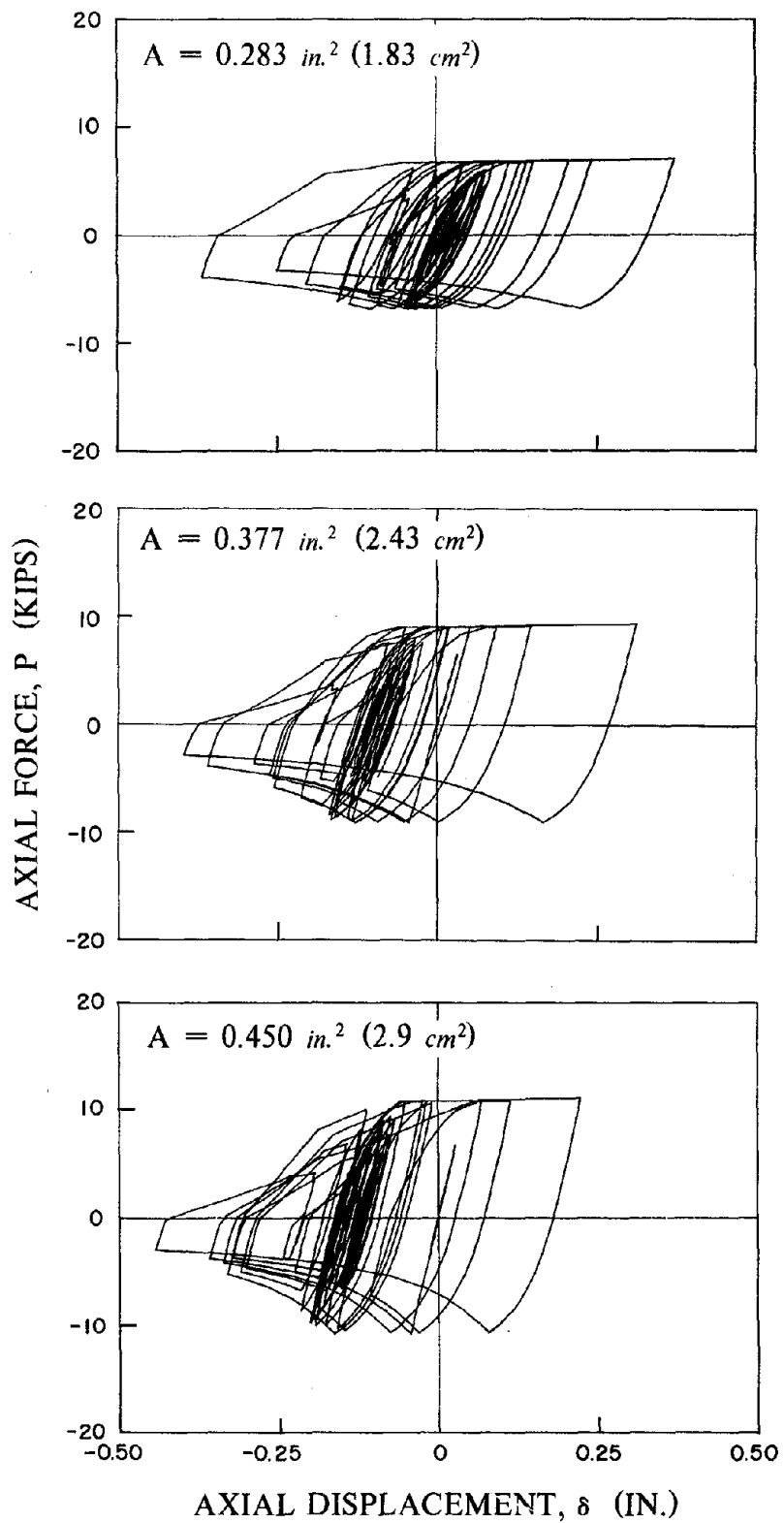


Fig. 5.15 Effects of Cross-Section Areas on Hysteresis Loops of Brace 2 ($\Delta t = 0.01 \text{ sec.}$) (1 kip = 4.45 kN; 1 in. = 25.4 mm)

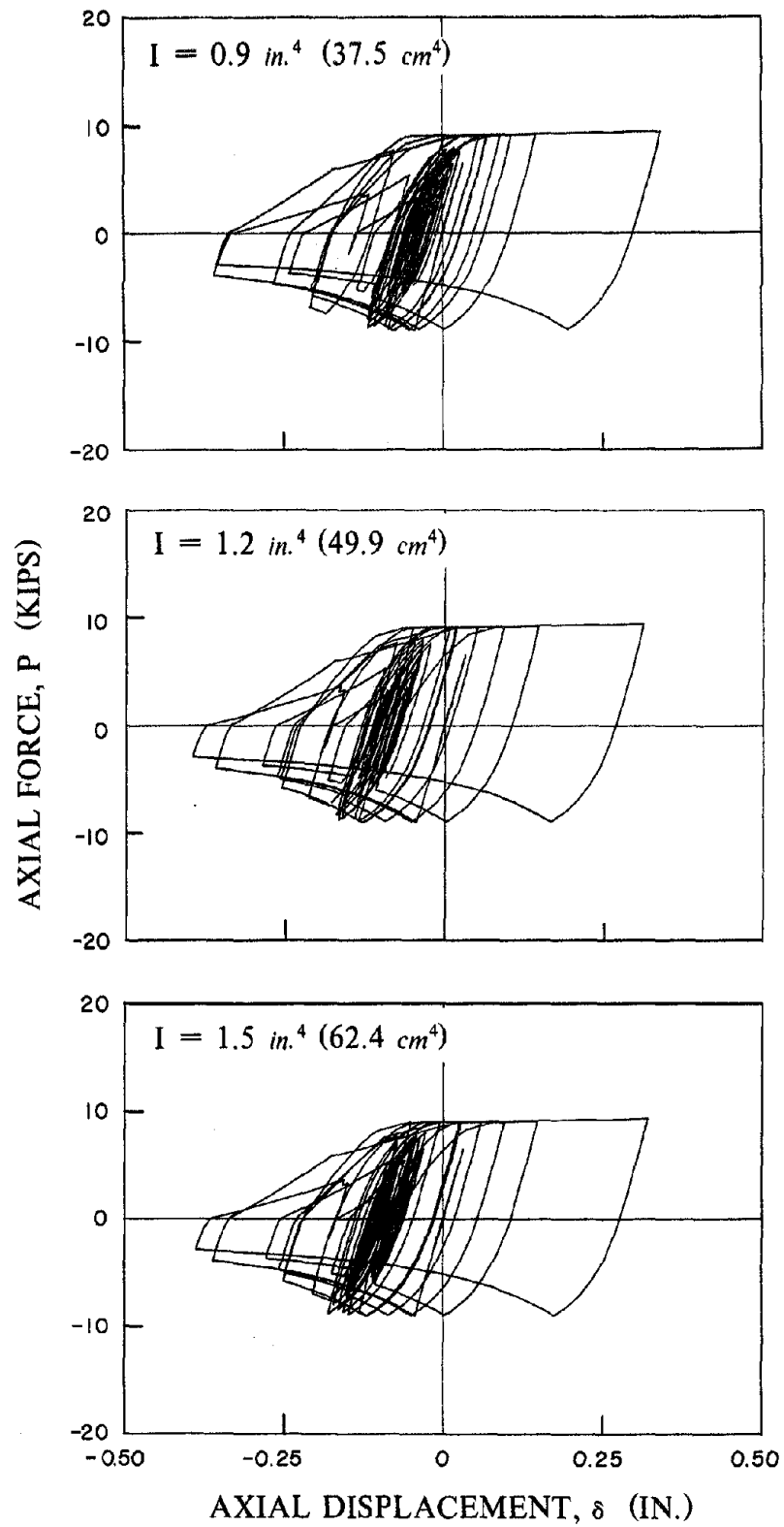


Fig. 5.16 Effects of Cross-Sectional Moments of Inertia on Hysteresis Loops of Brace 2 ($\Delta t = 0.01 \text{ sec.}$) (1 kip = 4.45 kN; 1 in. = 25.4 mm)

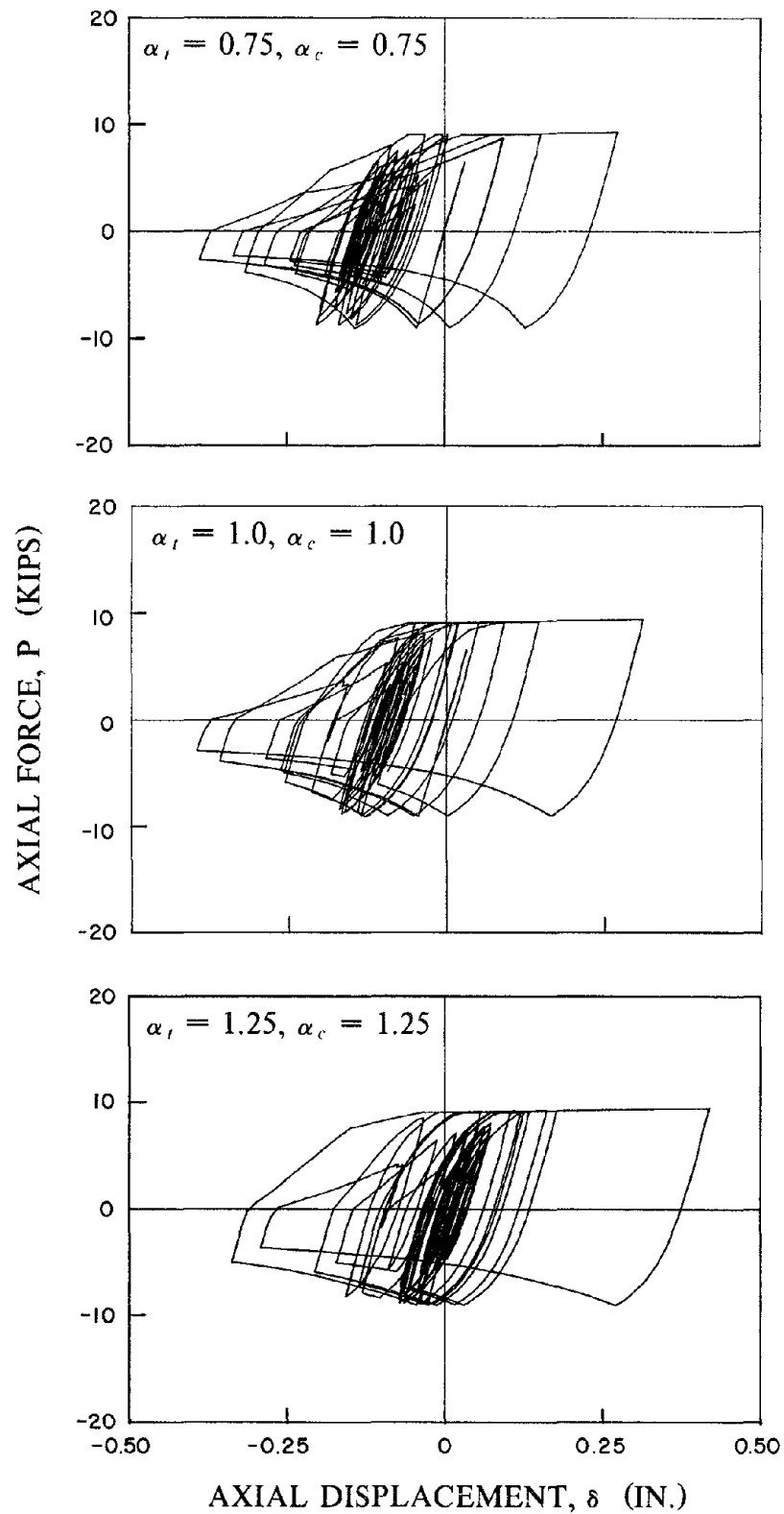


Fig. 5.17 Effects of the Shape of P-M Interaction Curve on Hysteresis Loops of Brace 2 ($\Delta t = 0.01$ sec.) (1 kip = 4.45 kN; 1 in. = 25.4 mm)

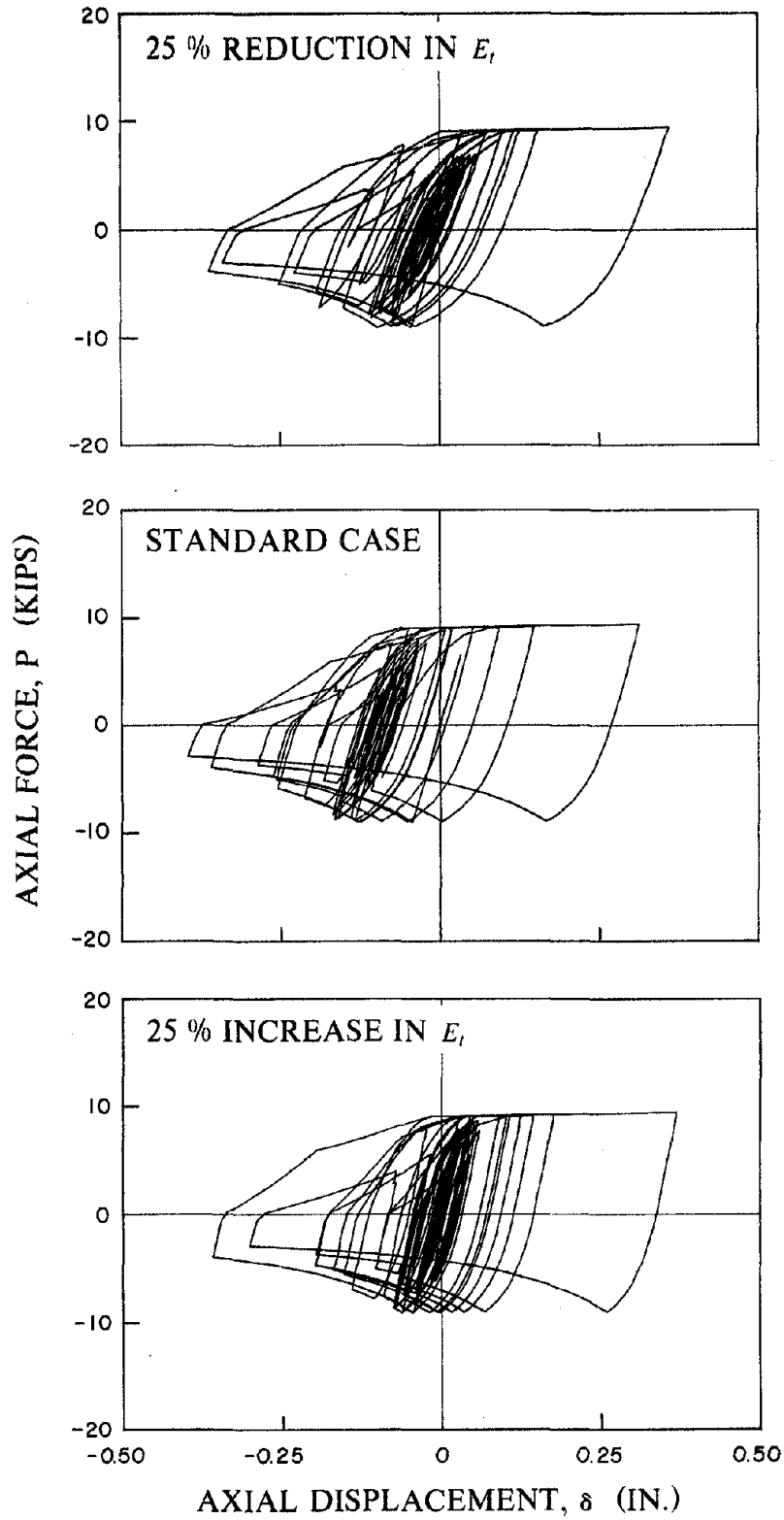


Fig. 5.18 Effects of the Tangent Modulus of Elasticity on Hysteresis Loops of Brace 2 ($\Delta t = 0.01$ sec.) (1 kip = 4.45 kN; 1 in. = 25.4 mm)

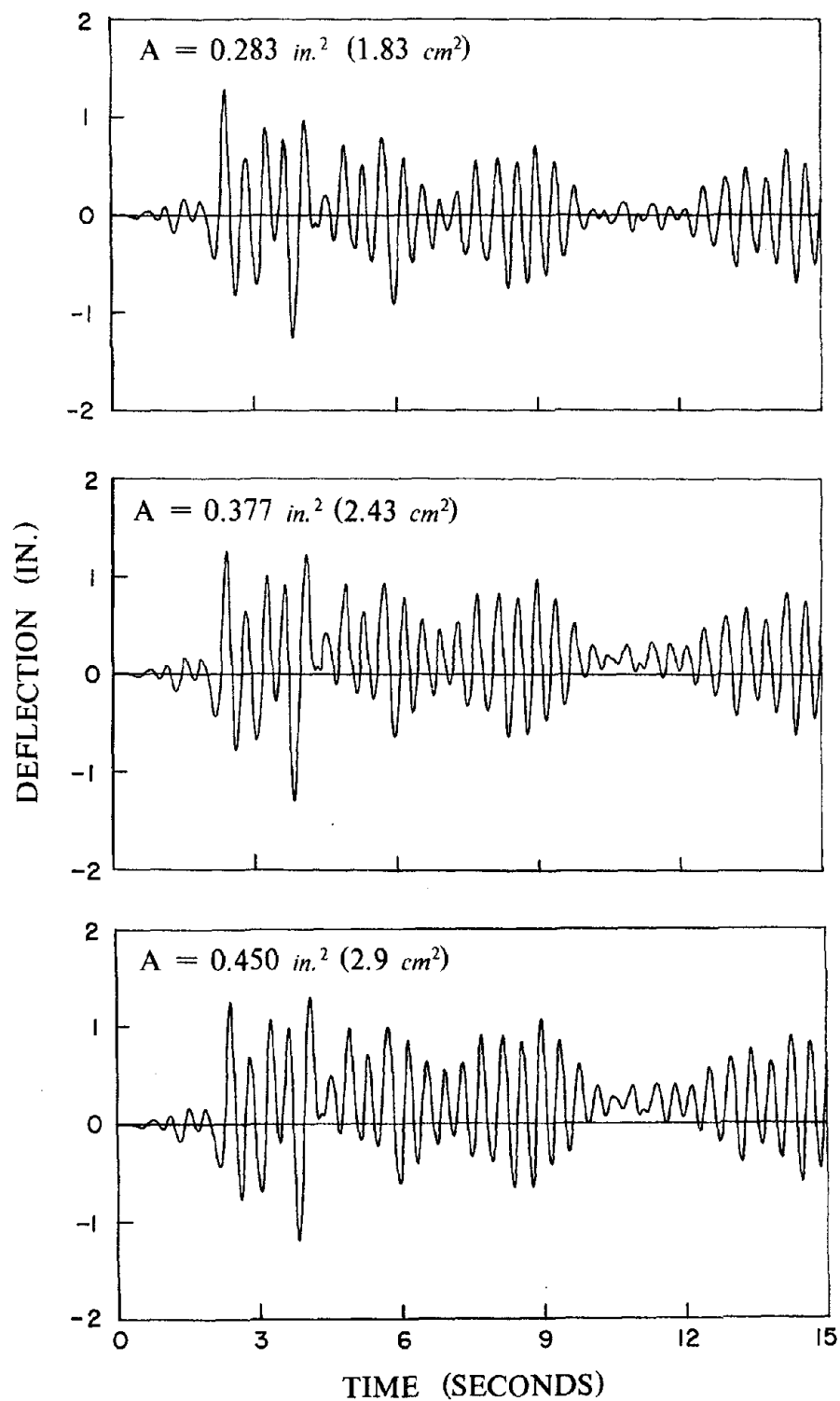


Fig. 5.19 Effects of Cross-Section Areas of Brace 2 on Tip Deflection Histories of the Frame ($\Delta t = 0.01 \text{ sec.}$) (1 kip = 4.45 kN; 1 in. = 25.4 mm)

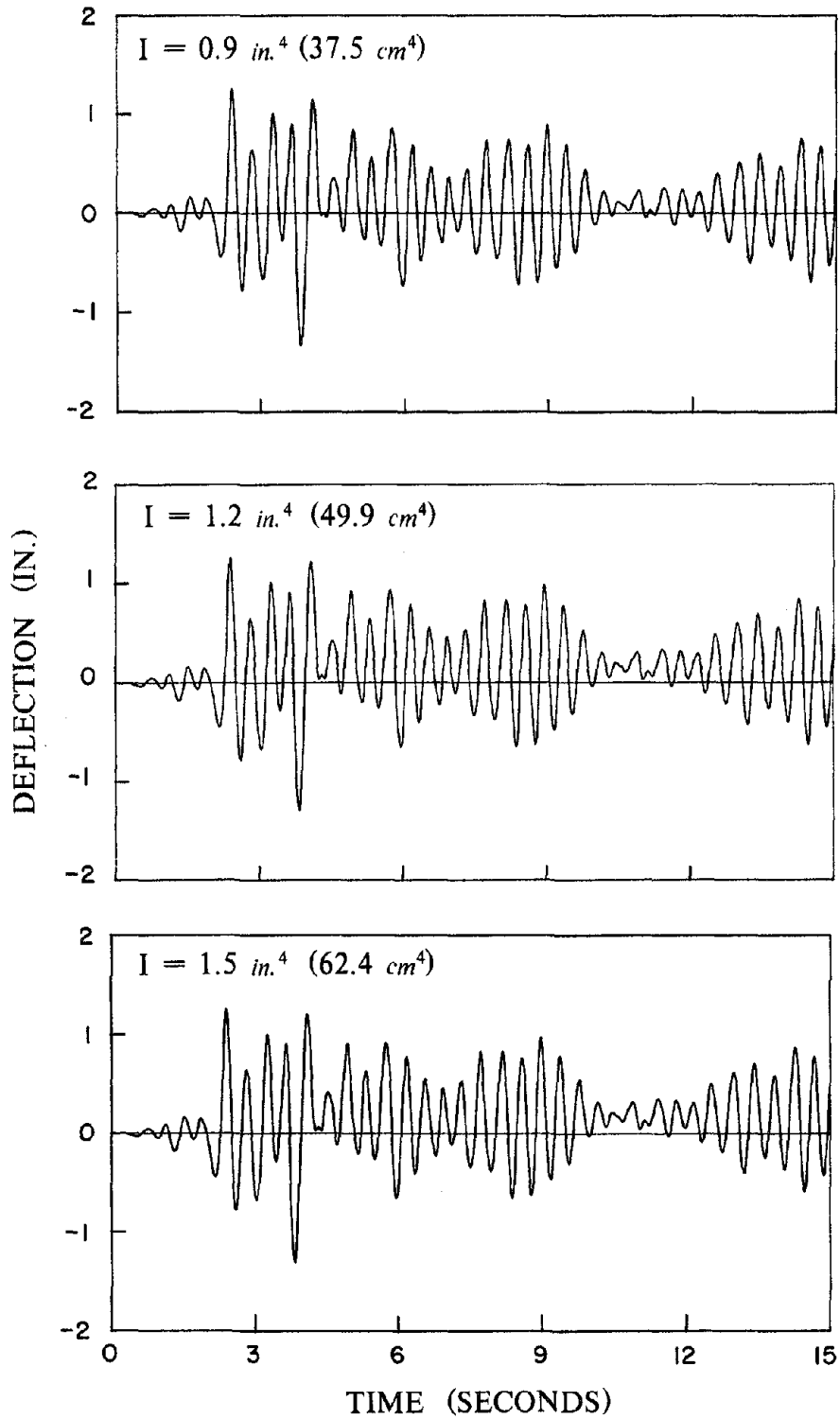


Fig. 5.20 Effects of Cross-Sectional Moments of Inertia of Brace 2 on Tip Deflection Histories of the Frame ($\Delta t = 0.01 \text{ sec.}$) (1 kip = 4.45 kN; 1 in. = 25.4 mm)

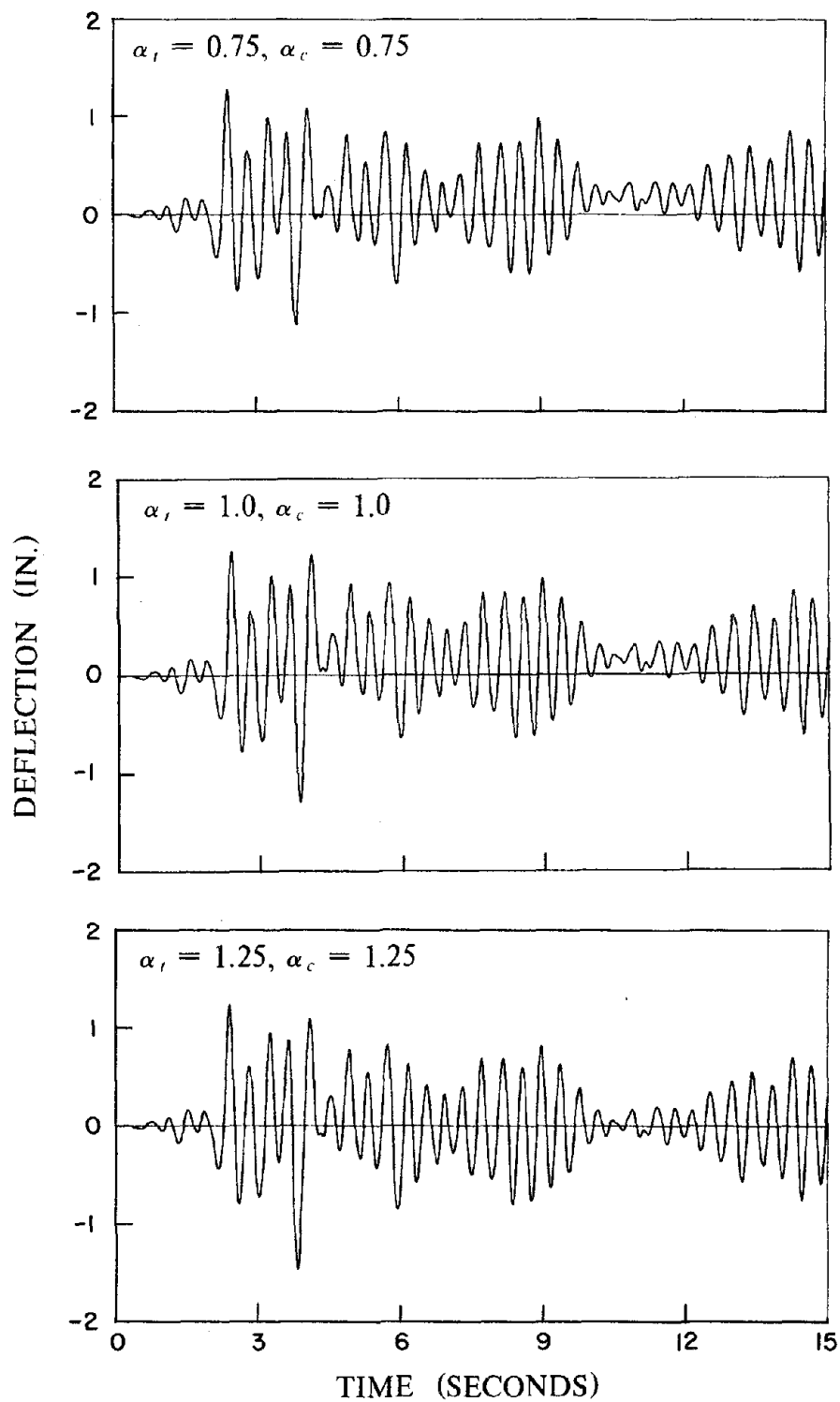


Fig. 5.21 Effects of the Shape of P-M Interaction Curve of Brace 2 on Tip Deflection Histories of the Frame ($\Delta t = 0.01$ sec.) (1 kip = 4.45 kN; 1 in. = 25.4 mm)

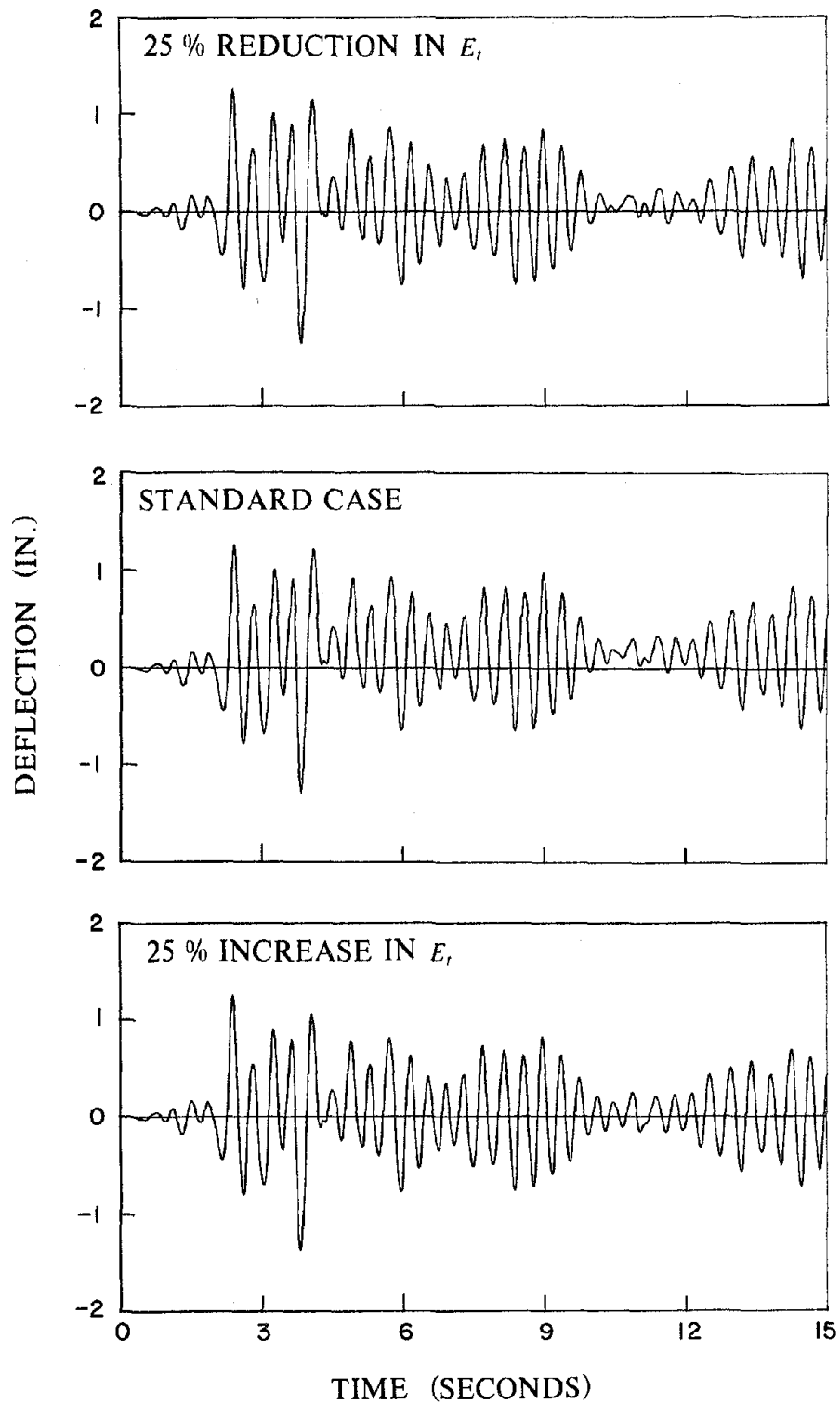


Fig. 5.22 Effects of the Tangent Modulus of Elasticity of Brace 2 on Tip Deflection Histories of the Frame ($\Delta t = 0.01$ sec.) (1 kip = 4.45 kN; 1 in. = 25.4 mm)

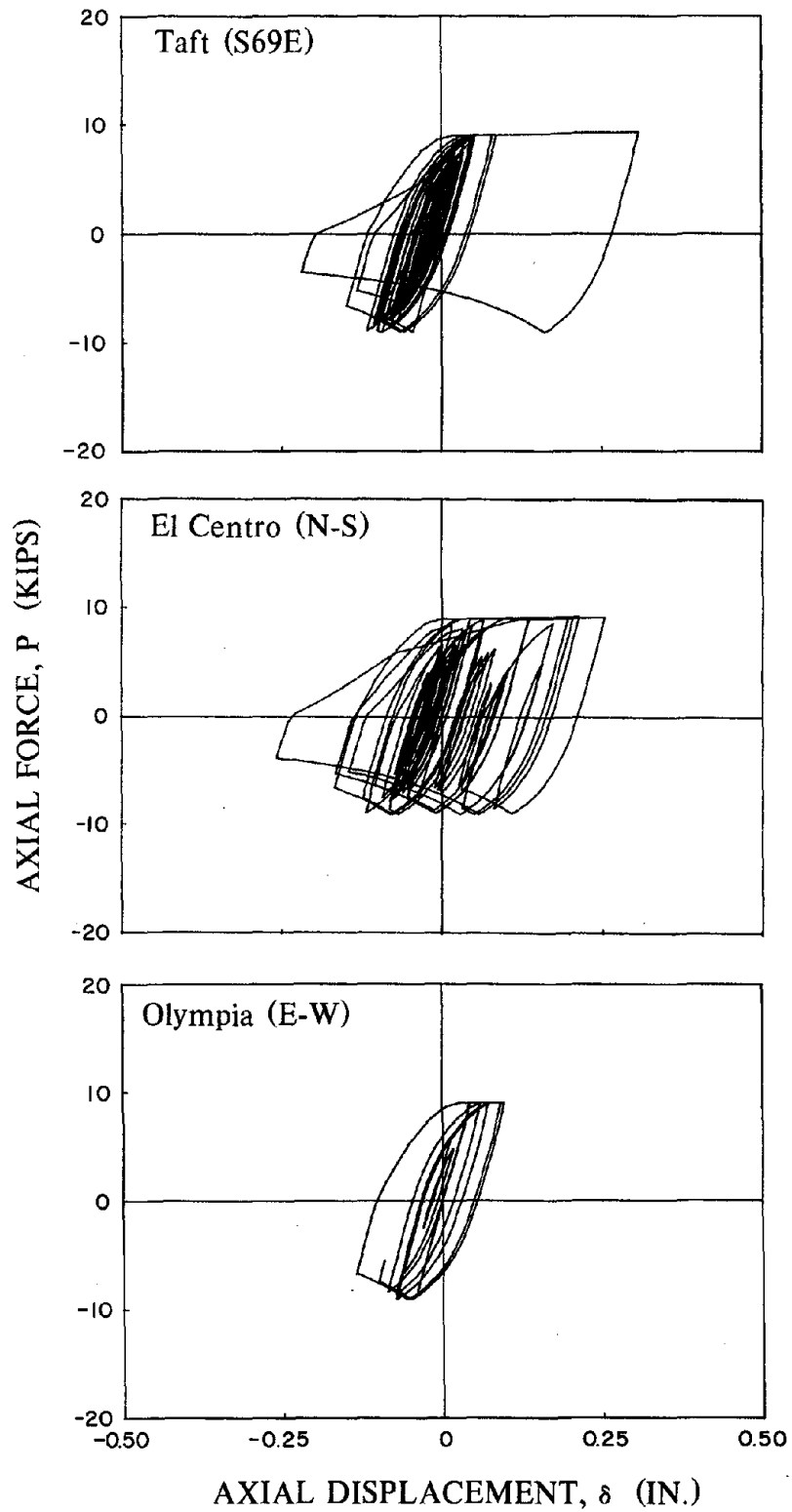


Fig. 5.23 Influence of Earthquake Ground Accelerations on Hysteresis Loops of Brace 2 ($\Delta t = 0.01$ sec.) (1 kip = 4.45 kN; 1 in. = 25.4 mm)

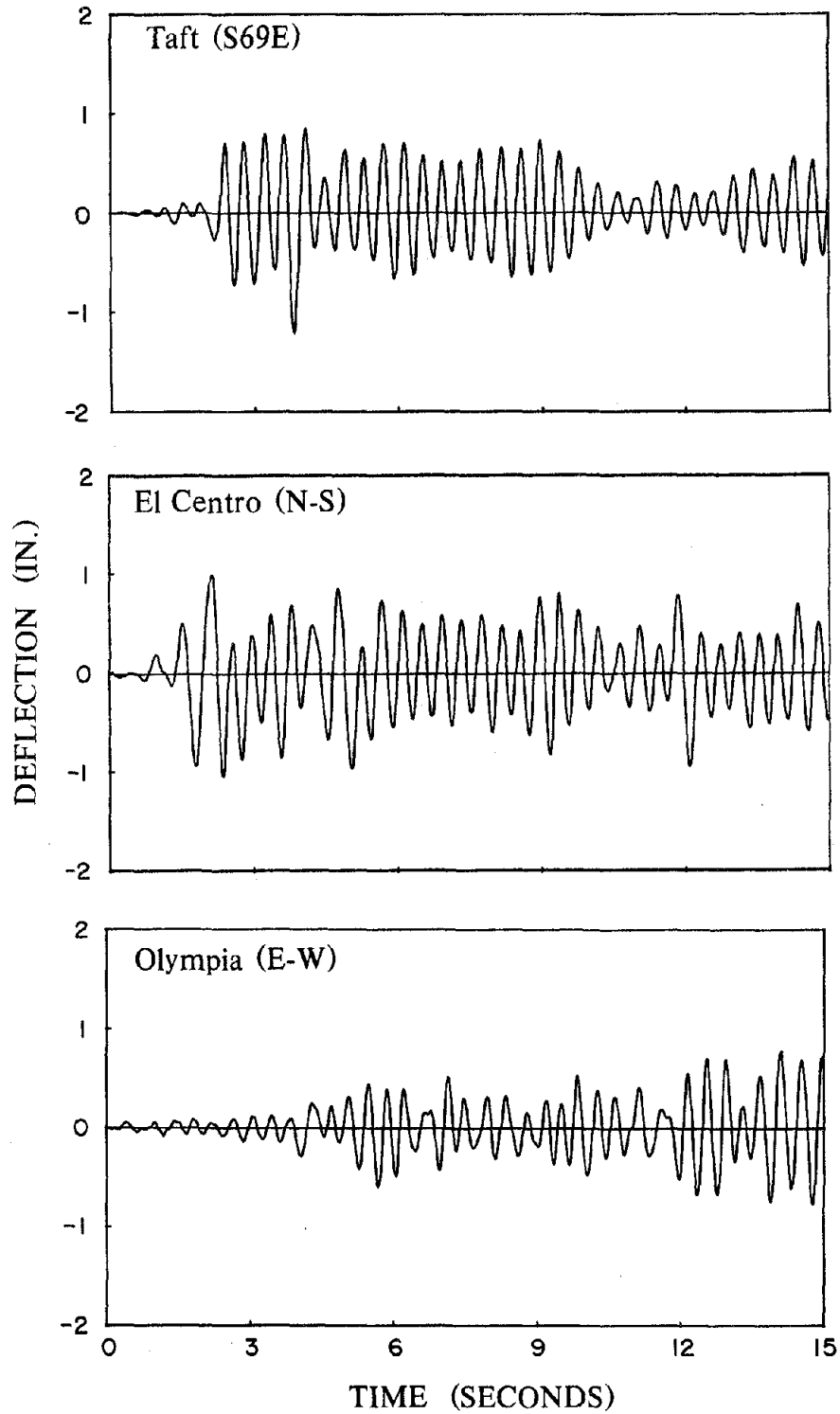


Fig. 5.24 Influence of Earthquake Ground Accelerations on Tip Deflection Histories of the Frame ($\Delta t = 0.01$ sec.) (1 kip = 4.45 kN; 1 in. = 25.4 mm)

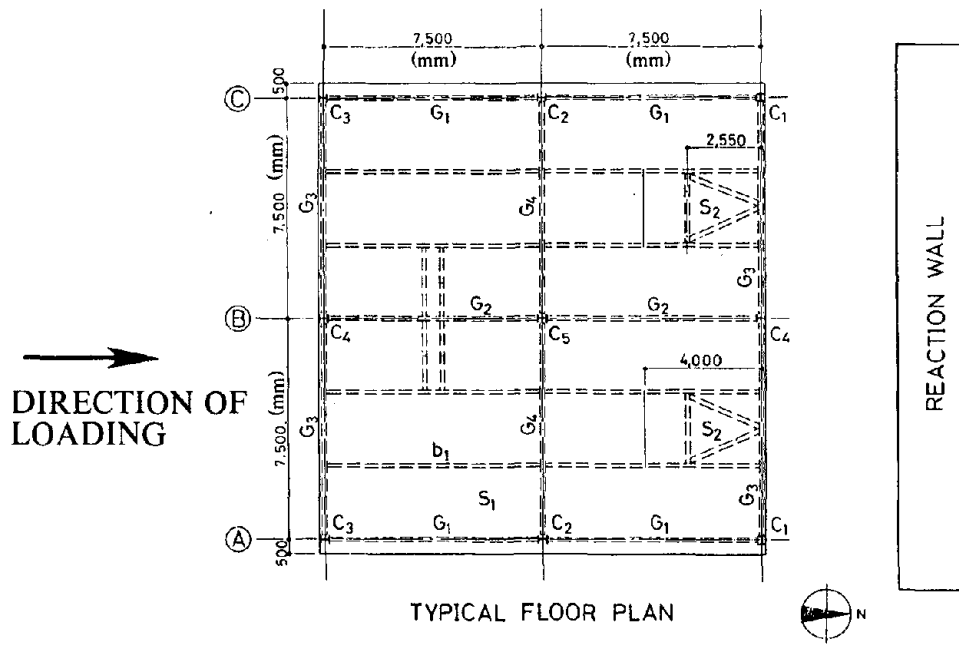


Fig. 6.1 Typical Plan View of the U.S.-Japan Building [34]
(1 in. = 25.4 mm)

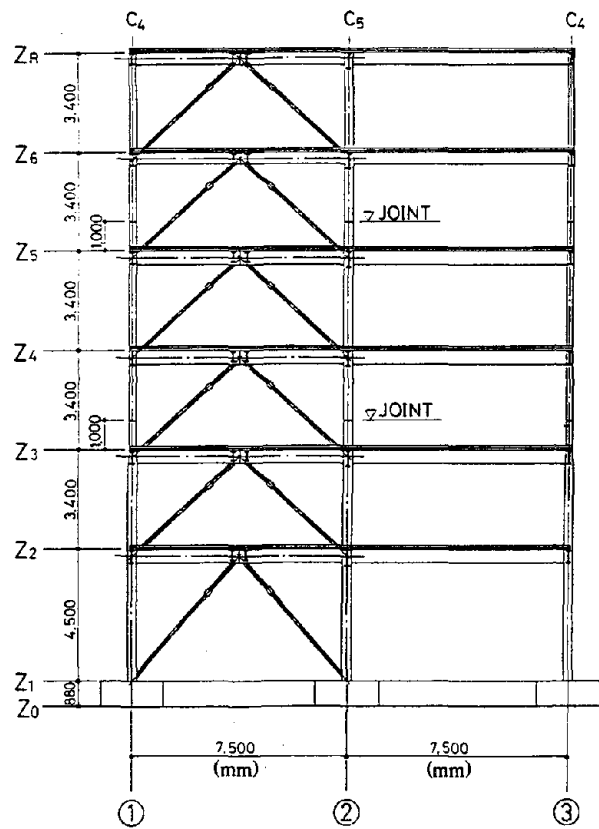


Fig. 6.2 Typical Elevation View of Frame B [34]
(1 in. = 25.4 mm)

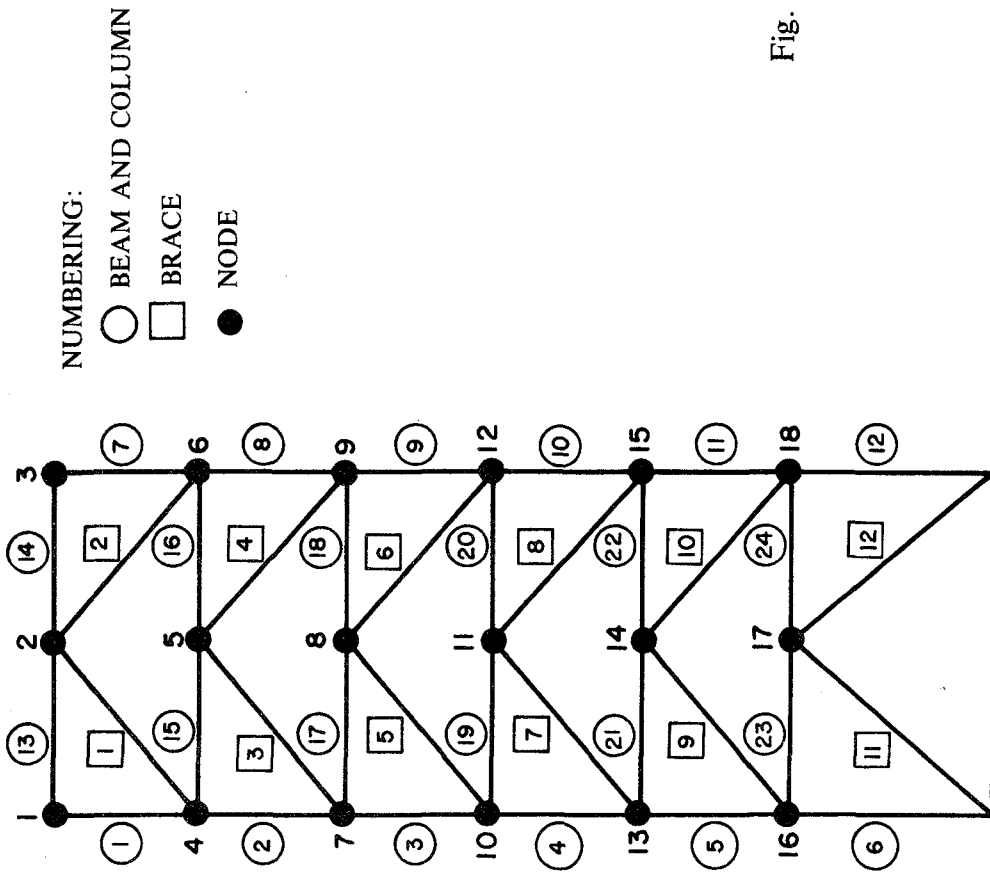


Fig. 6.3 Member Numbering of the K-Braced Frame (the Left Half of Frame B)

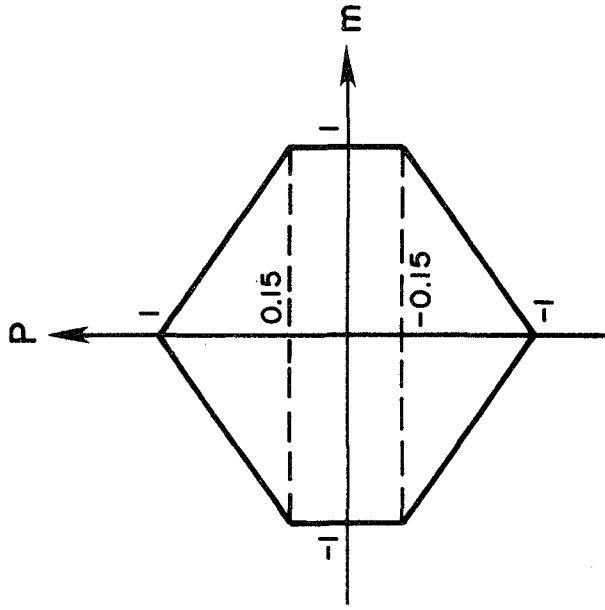


Fig. 6.4 Normalized Interaction Curve used for the Modeling of the Columns and Girders of the K-braced Frame

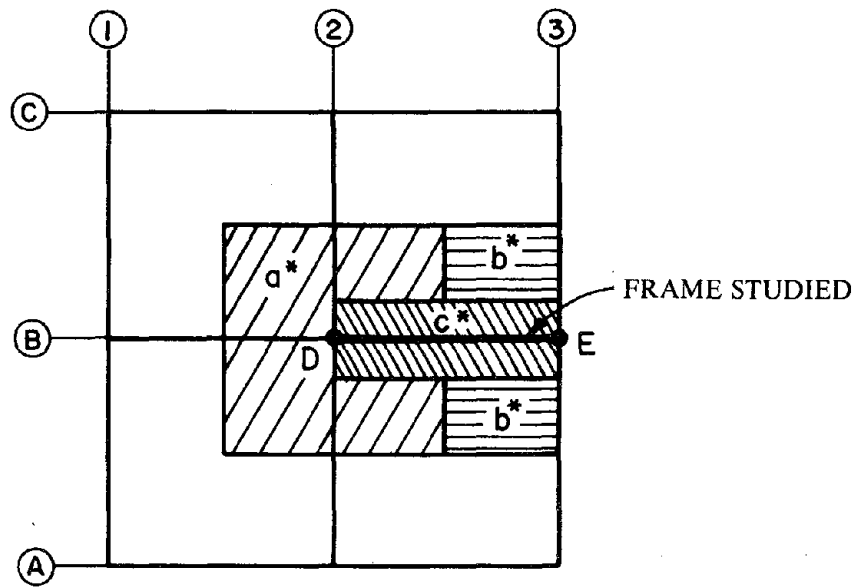


Fig. 6.5 Contributing Areas of the Gravity Loads applied to the K-braced Frame

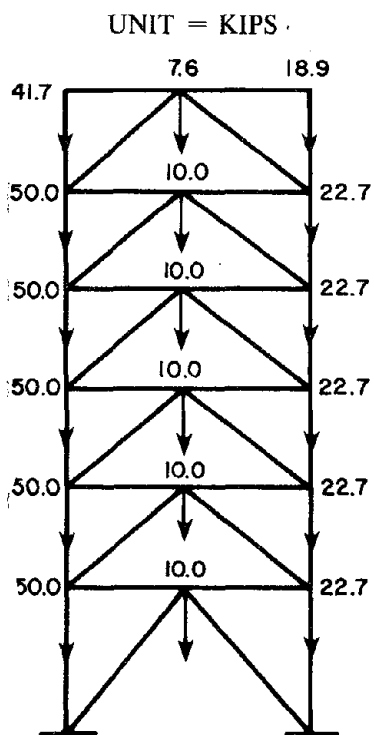


Fig. 6.6 Static Nodal Loads Distribution
(1 kip = 4.45 kN)

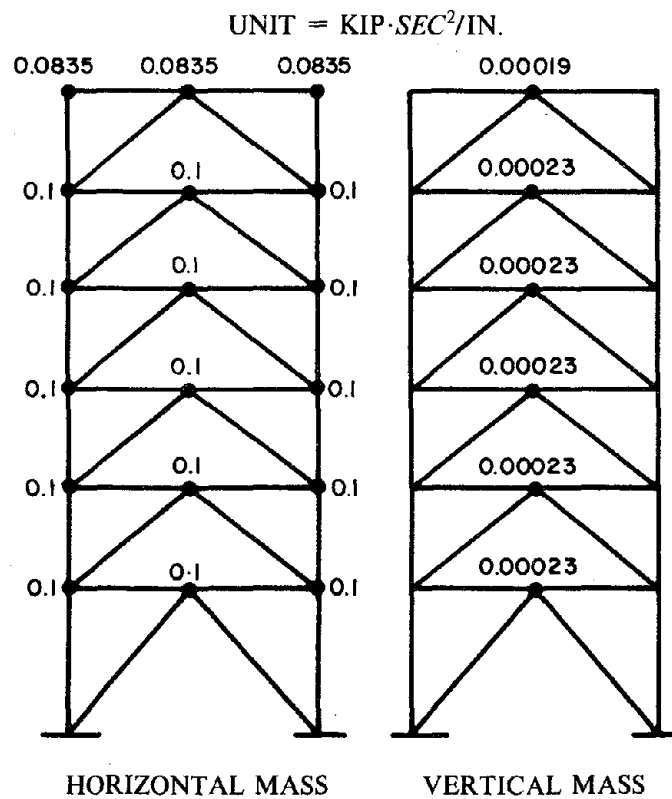


Fig. 6.7 Lumped Mass Distribution
(1 kip·sec²/in. = 174.3 m.t.)

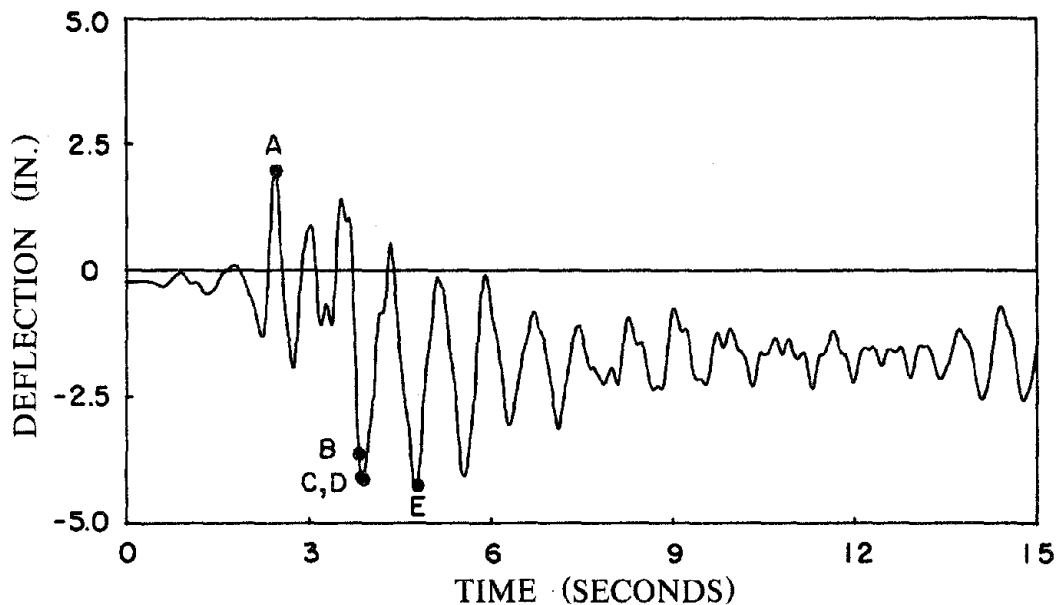


Fig. 6.8 Time History of the Roof Deflection of the K-Braced Frame for the Standard Case (Step-by-Step; $\Delta t = 0.007$ sec.) (1 in. = 25.4 mm)

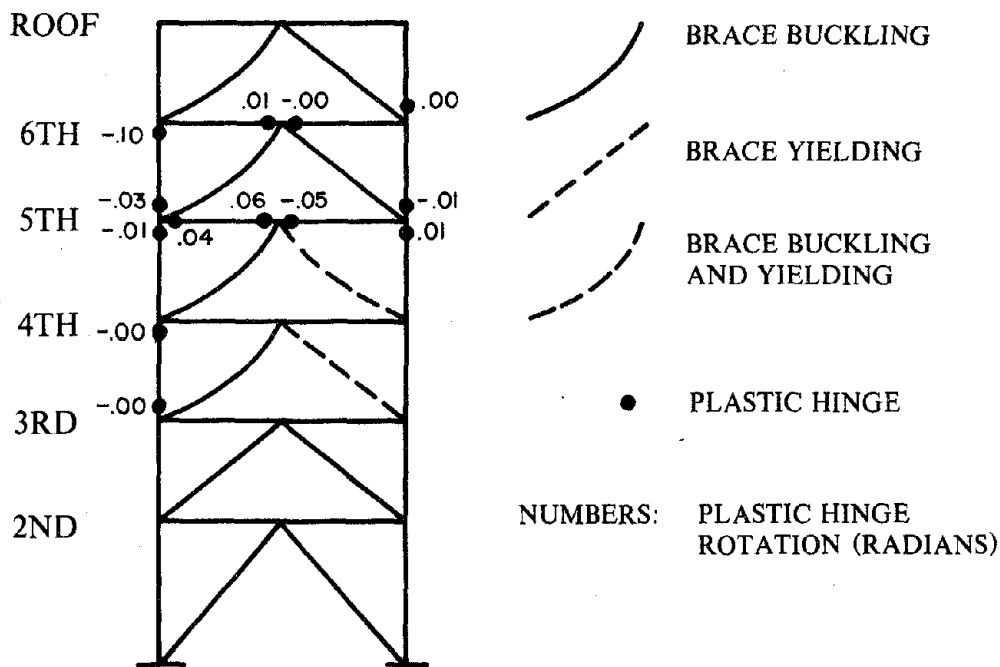


Fig. 6.9 Inelastic Deformations in the Frame for the Standard Case

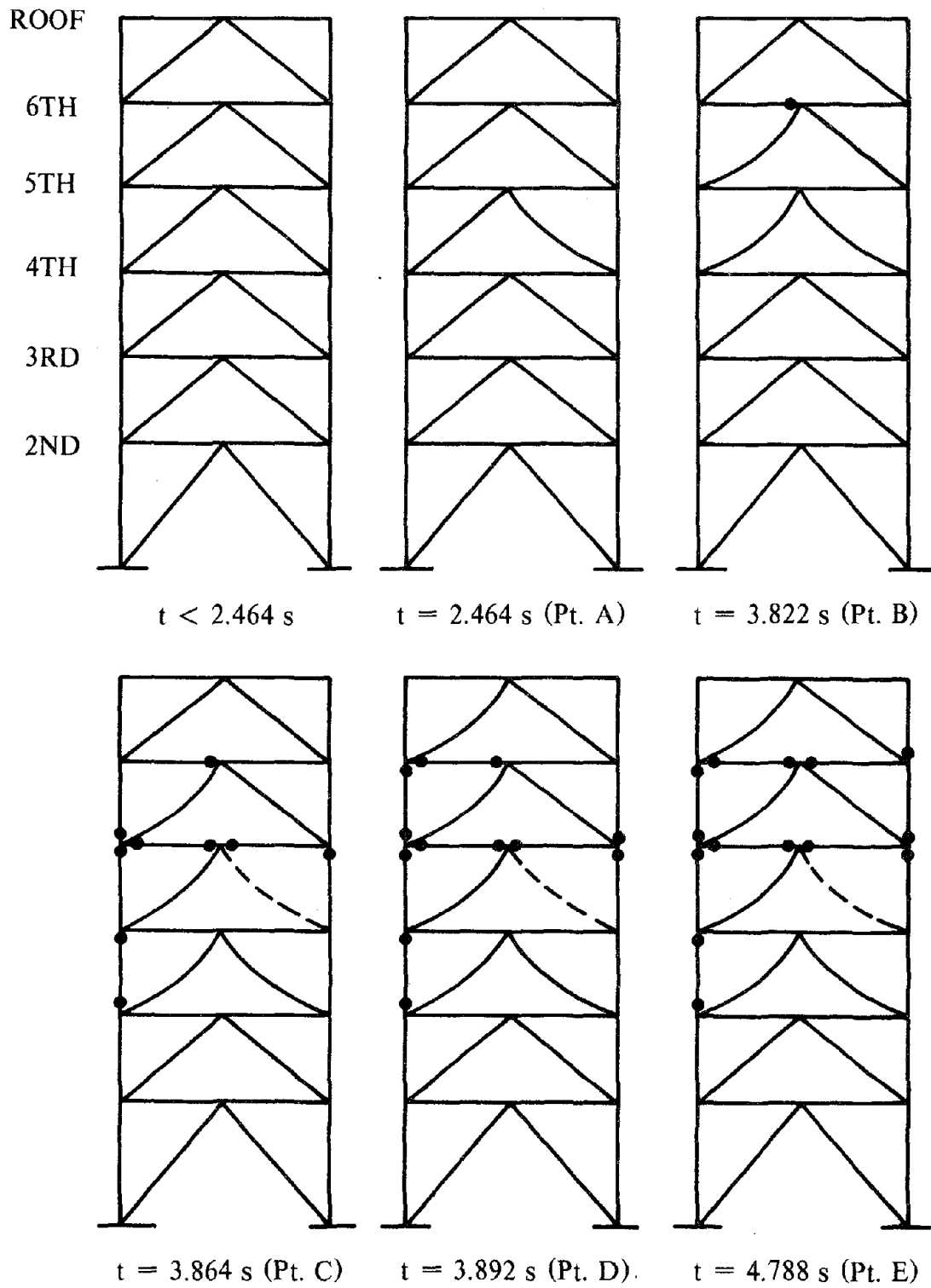


Fig. 6.10 Inelastic Deformations in the Frame at Different Times

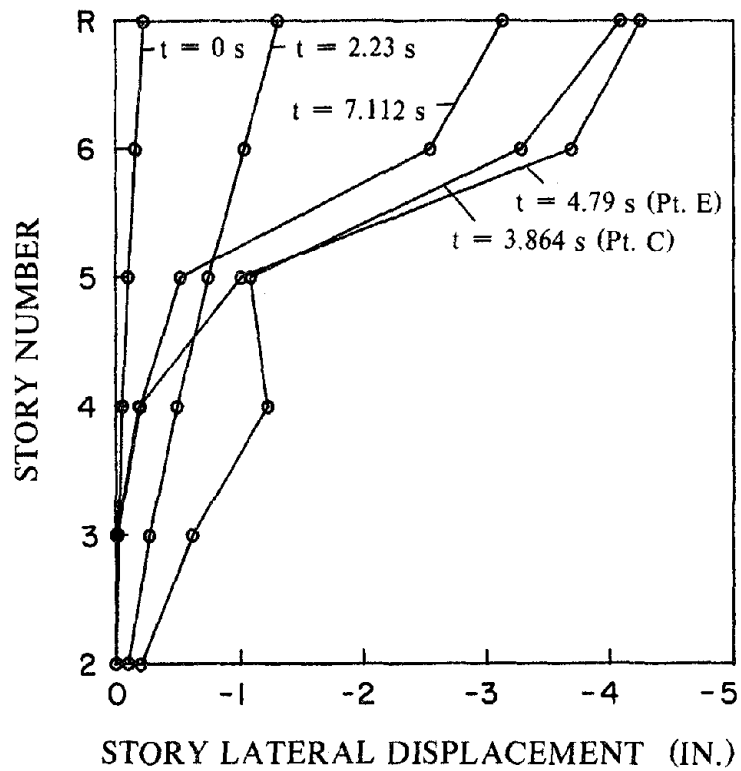


Fig. 6.11 Story Lateral Displacements at Different Times
(1 in. = 25.4 mm)

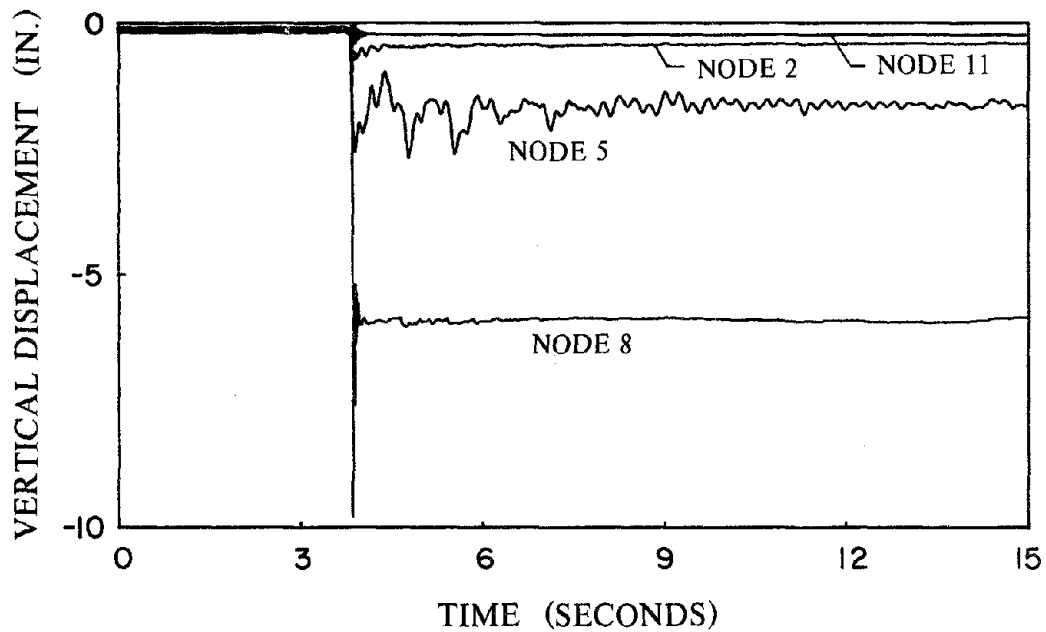


Fig. 6.12 Vertical Displacement Histories of Connection Nodes
between Girders and K-bracings (Nodes 2, 5, 8 and 11)
(1 in. = 25.4 mm)

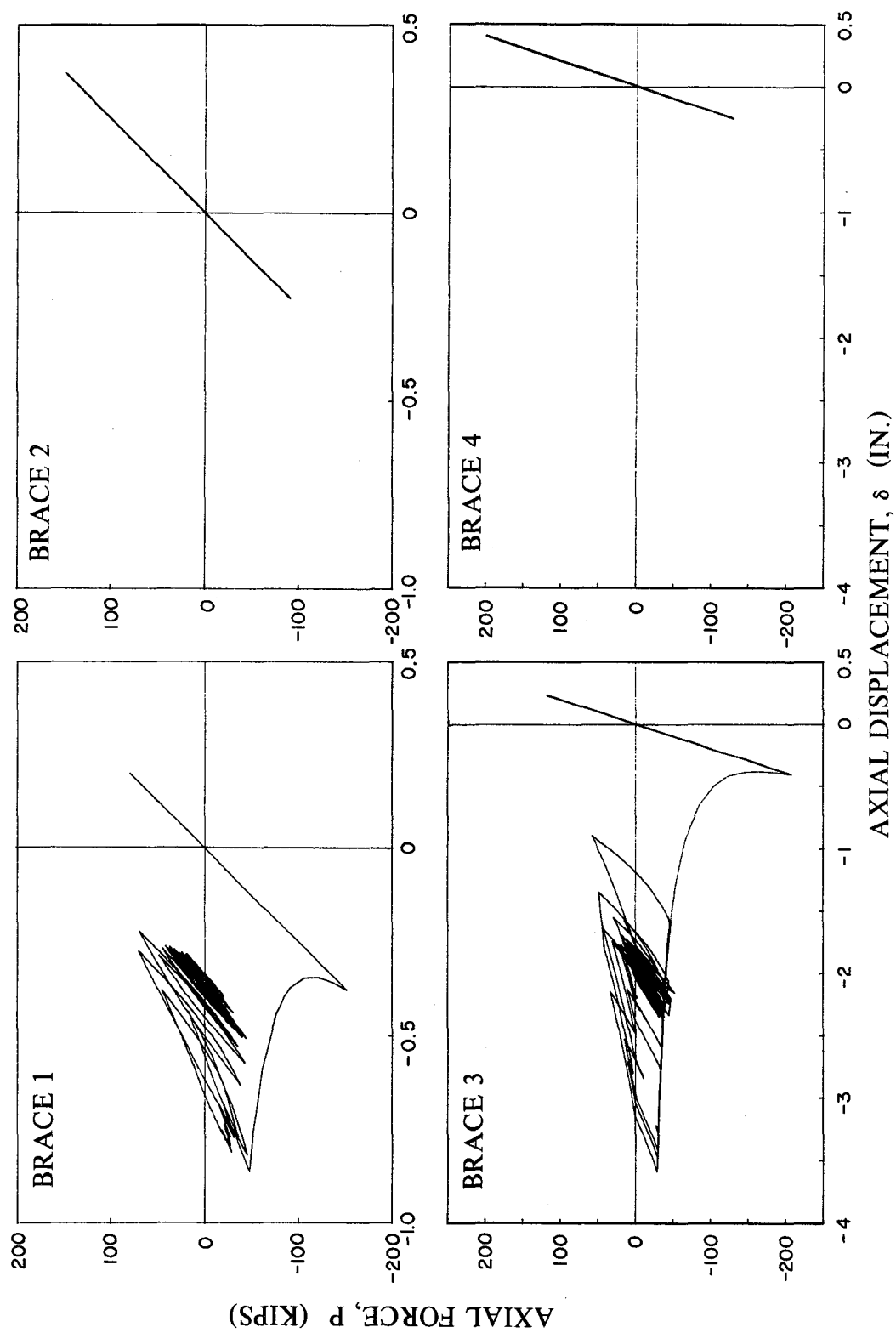


Fig. 6.13 Axial Force - Axial Displacement Curves for Braces 1 through 4
(1 kip = 4.45 kN; 1 in. = 25.4 mm)

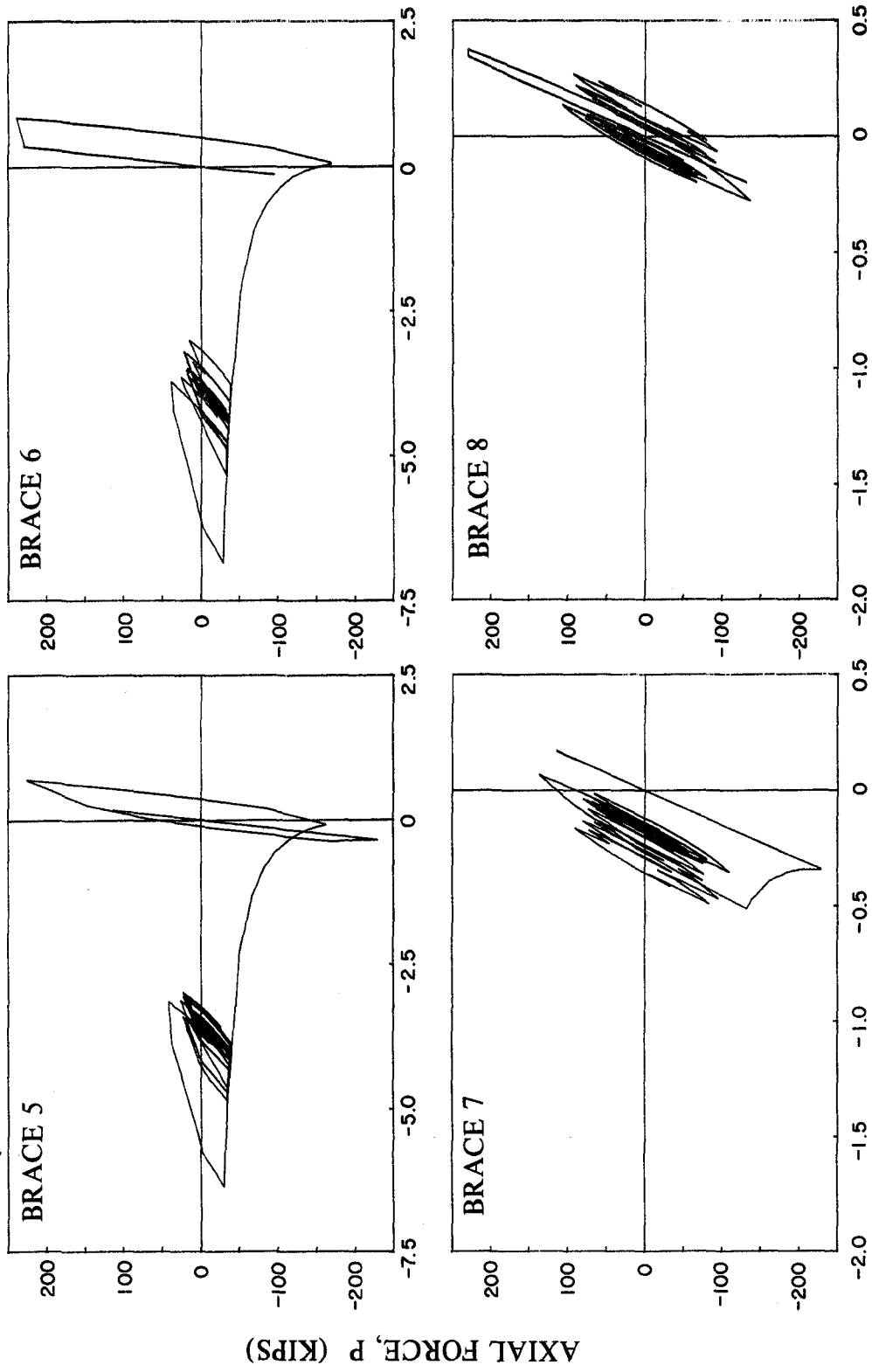


Fig. 6.14 Axial Force - Axial Displacement Curves for Braces 5 through 8
(1 kip = 4.45 kN; 1 in. = 25.4 mm)

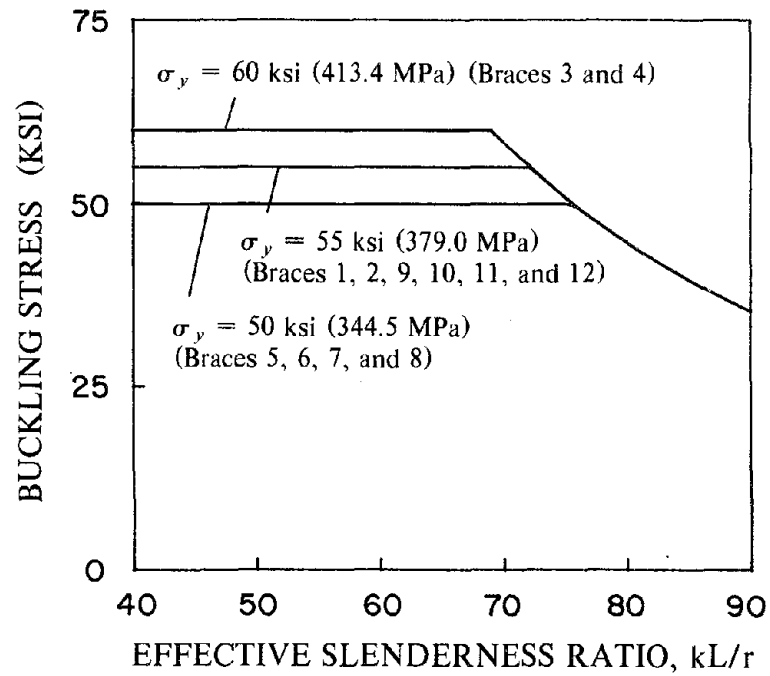


Fig. 6.15 Simplified Buckling Stress versus Effective Slenderness Ratio Relationships (1 ksi = 6.89 MPa)

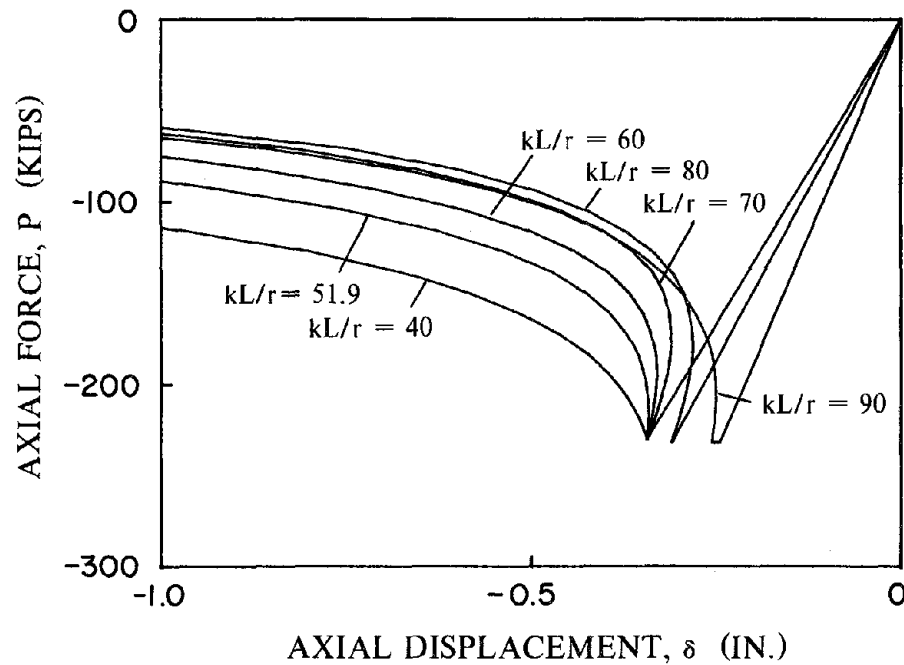


Fig. 6.16 Comparison of the Compressive Side of Axial Force - Axial Displacement Curves of Brace 7 for Different kL/r values (1 kip = 4.45 kN; 1 in. = 25.4 mm)

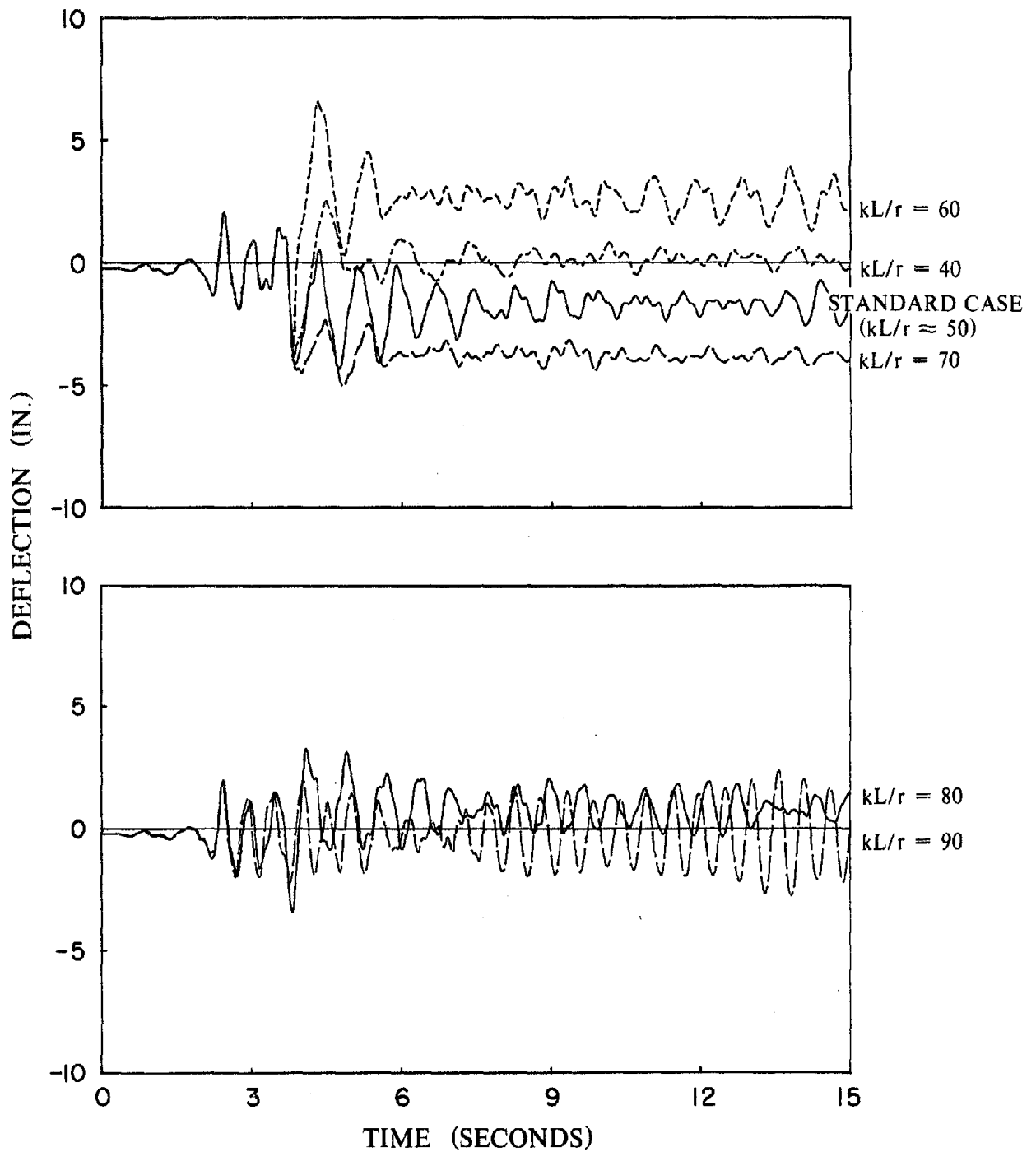


Fig. 6.17 Time Histories of the Roof Deflection of the Frame computed for Different kL/r Values (Step-by-Step; $\Delta t = 0.007$ sec.) (1 in. = 25.4 mm)

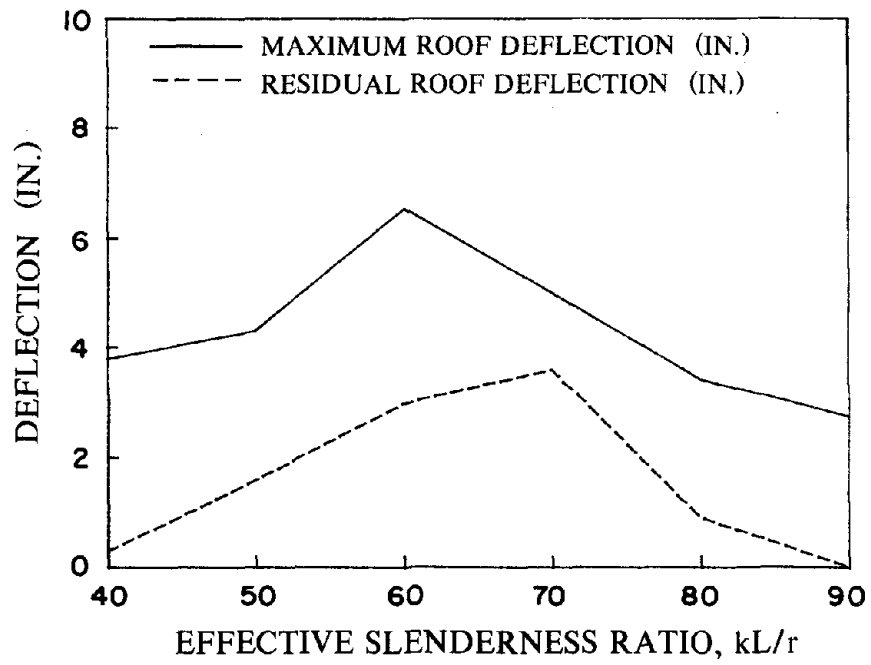


Fig. 6.18 Maximum and Residual Roof Deflections of the Frame as a Function of the kL/r Ratio of the Braces (1 in. = 25.4 mm)

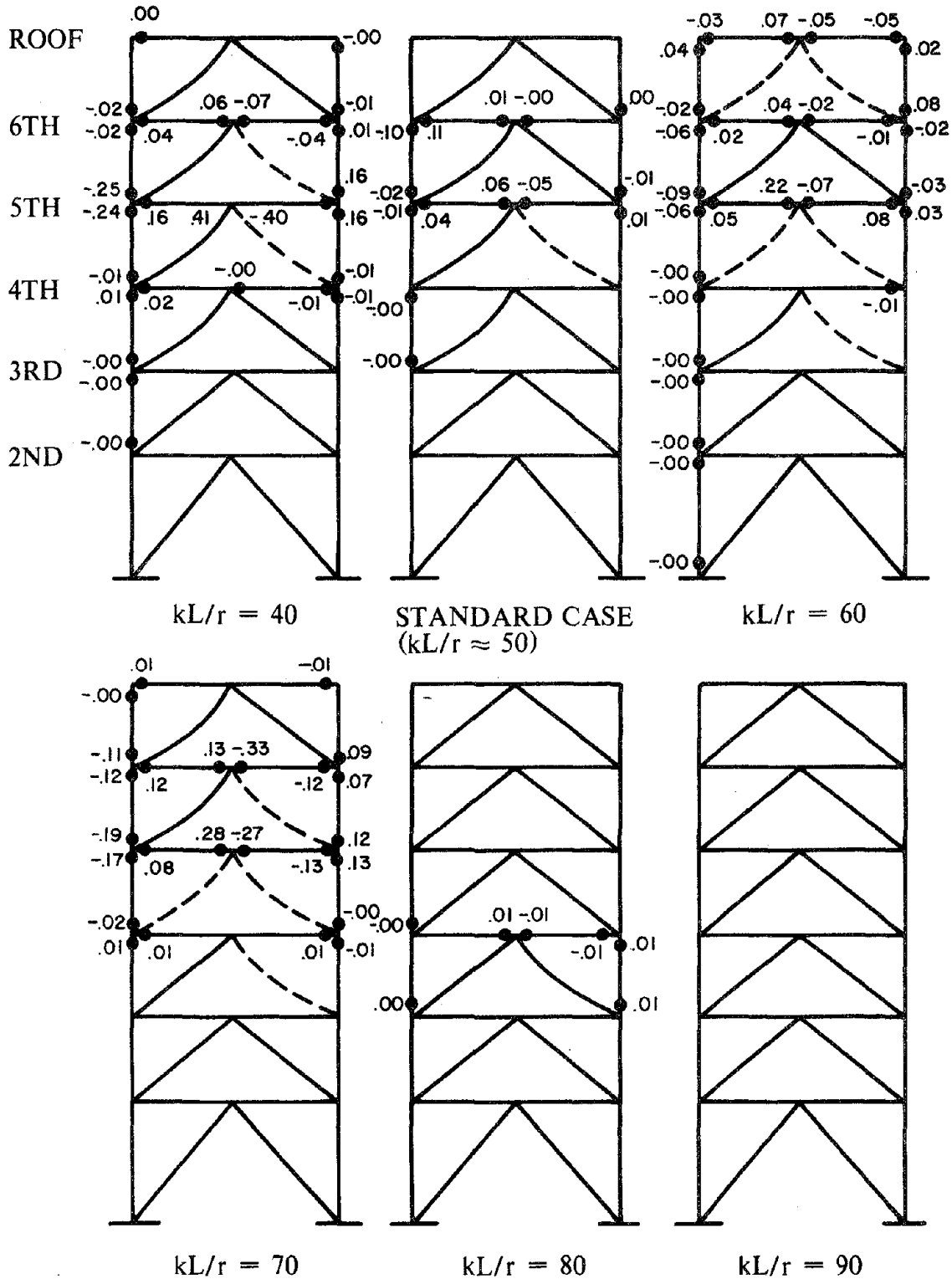


Fig. 6.19 Comparison of Inelastic Deformations in the Frame for Different kL/r Values

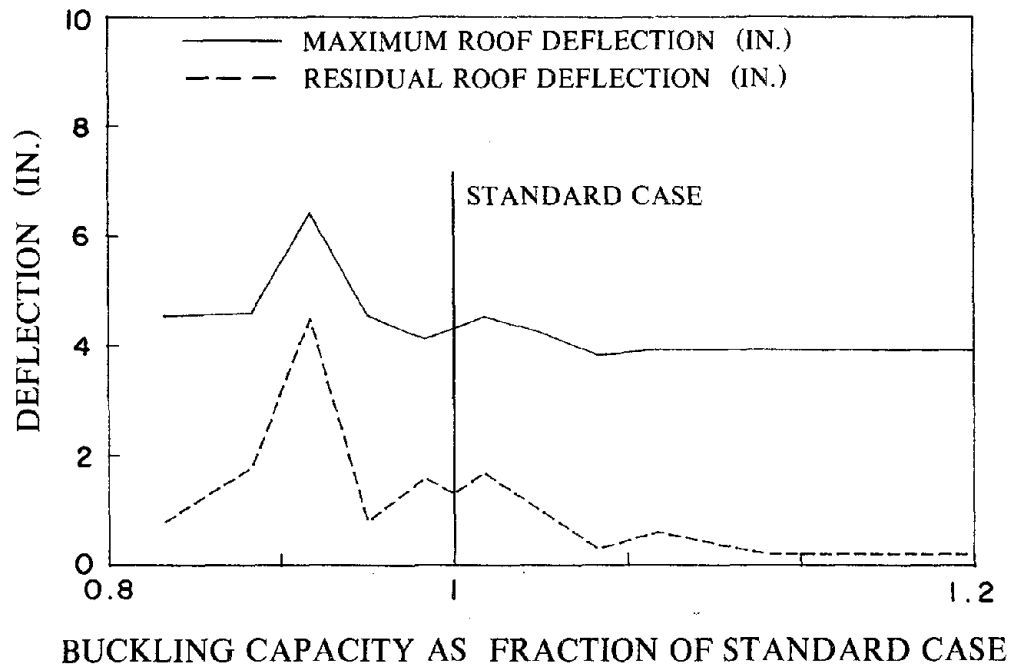


Fig. 6.20 Maximum and Residual Roof Deflections as a Function of Buckling Capacities of Braces 3 and 4 (1 in = 25.4 mm)

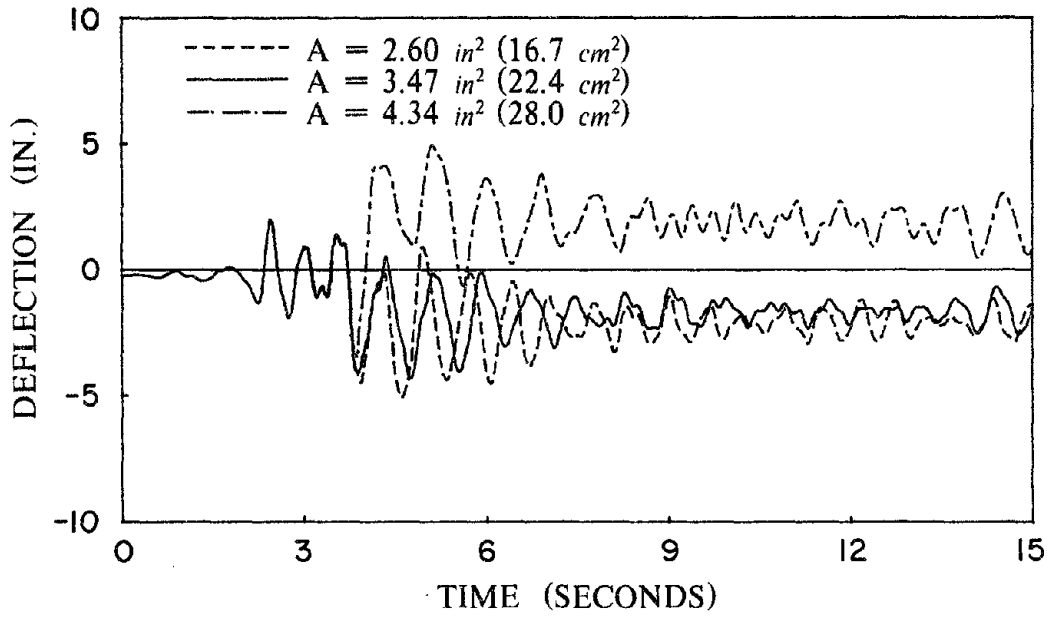


Fig. 6.21 Influence of Cross-Sectional Areas of Brace 3 on the Dynamic Response of the Frame (Step-by-Step; $\Delta t = 0.007 \text{ sec.}$) (1 in. = 25.4 mm)

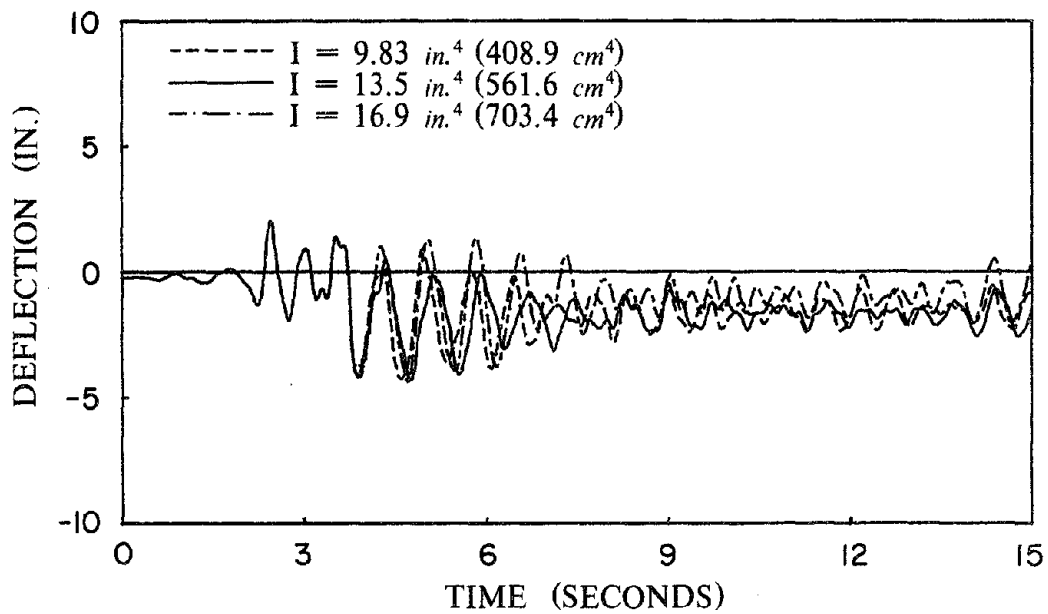


Fig. 6.22 Influence of Cross-Sectional Moments of Inertia of Brace 3 on the Dynamic Response of the Frame (Step-by-Step; $\Delta t = 0.007 \text{ sec.}$) (1 in. = 25.4 mm)

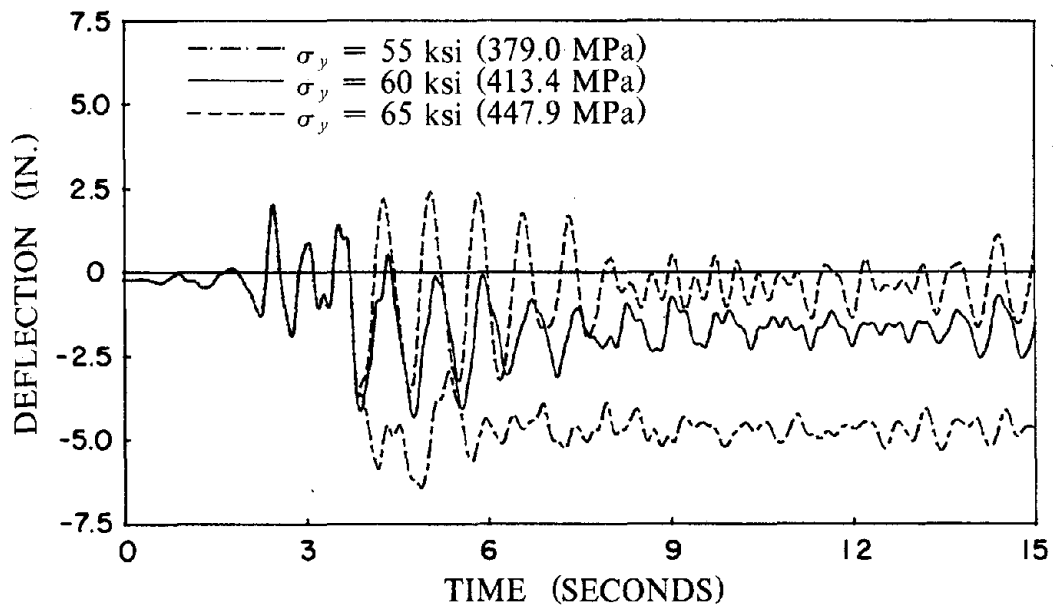


Fig. 6.23 Sensitivity of the Frame Dynamic Response to the Yield Stress of Braces 3 and 4 (1 in. = 25.4 mm; 1 ksi = 6.89 MPa)

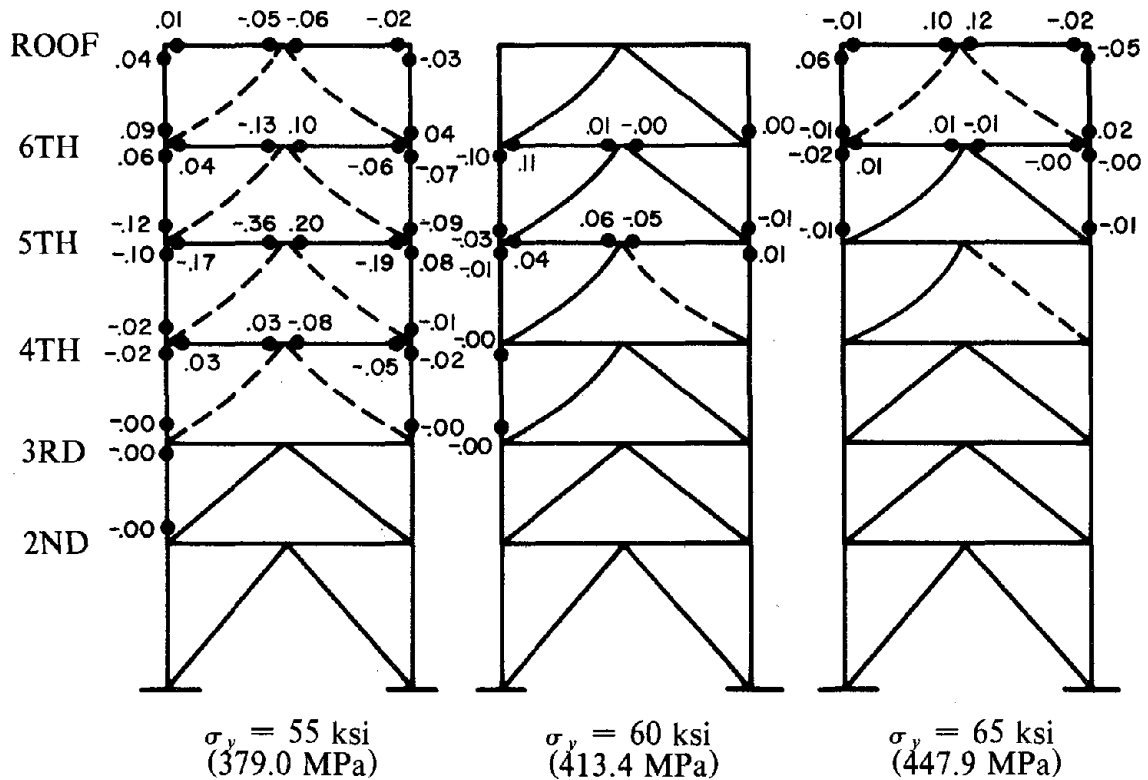


Fig. 6.24 Comparison of Inelastic Deformations in the Frame for Different Yield Stresses of Braces 3 and 4 (1 ksi = 6.89 MPa)

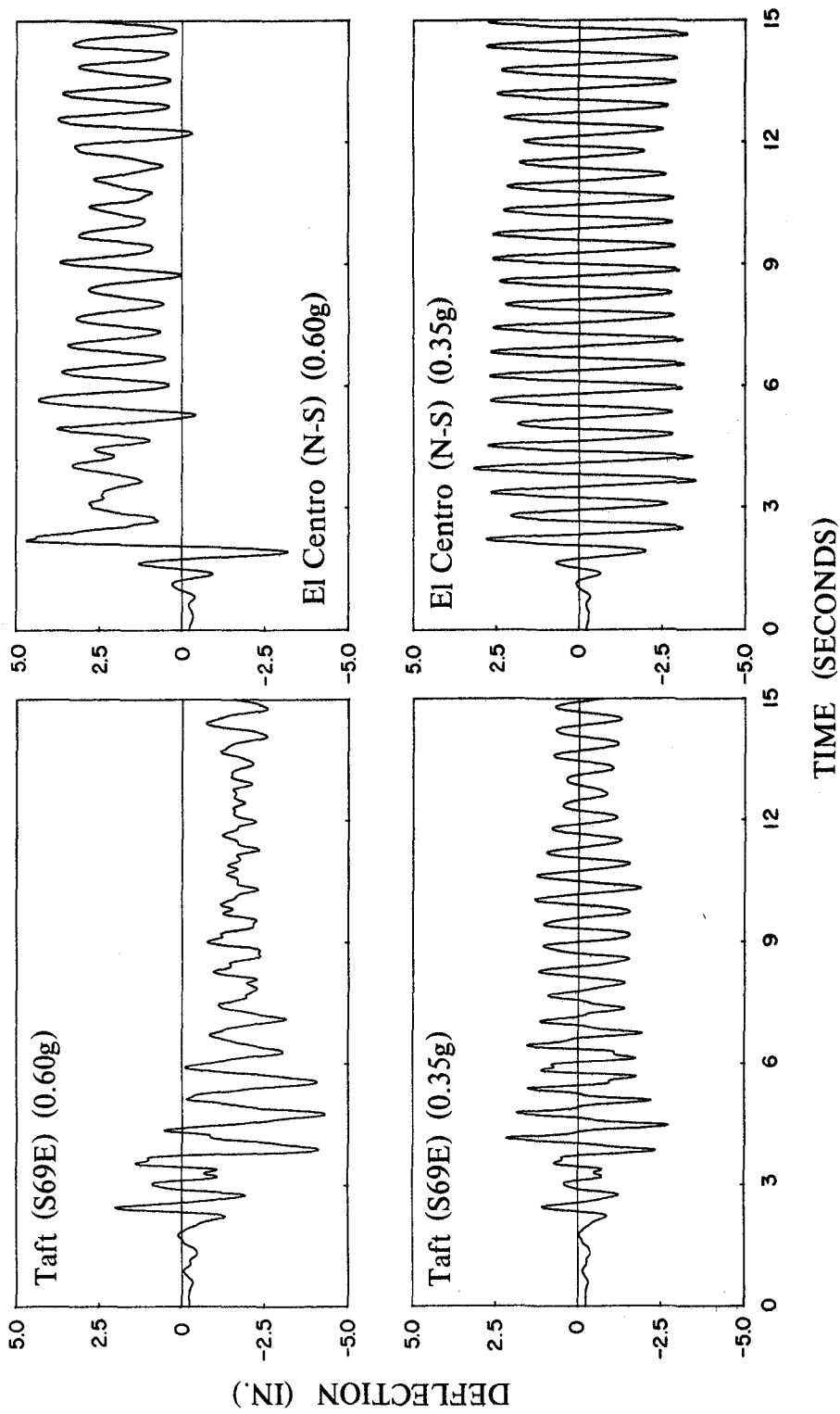


Fig. 6.25 Comparison of Roof Deflection Histories computed using Different Earthquake Ground Accelerations (Step-by-Step; $\Delta t = 0.007$ sec.) (1 in. = 25.4 mm)

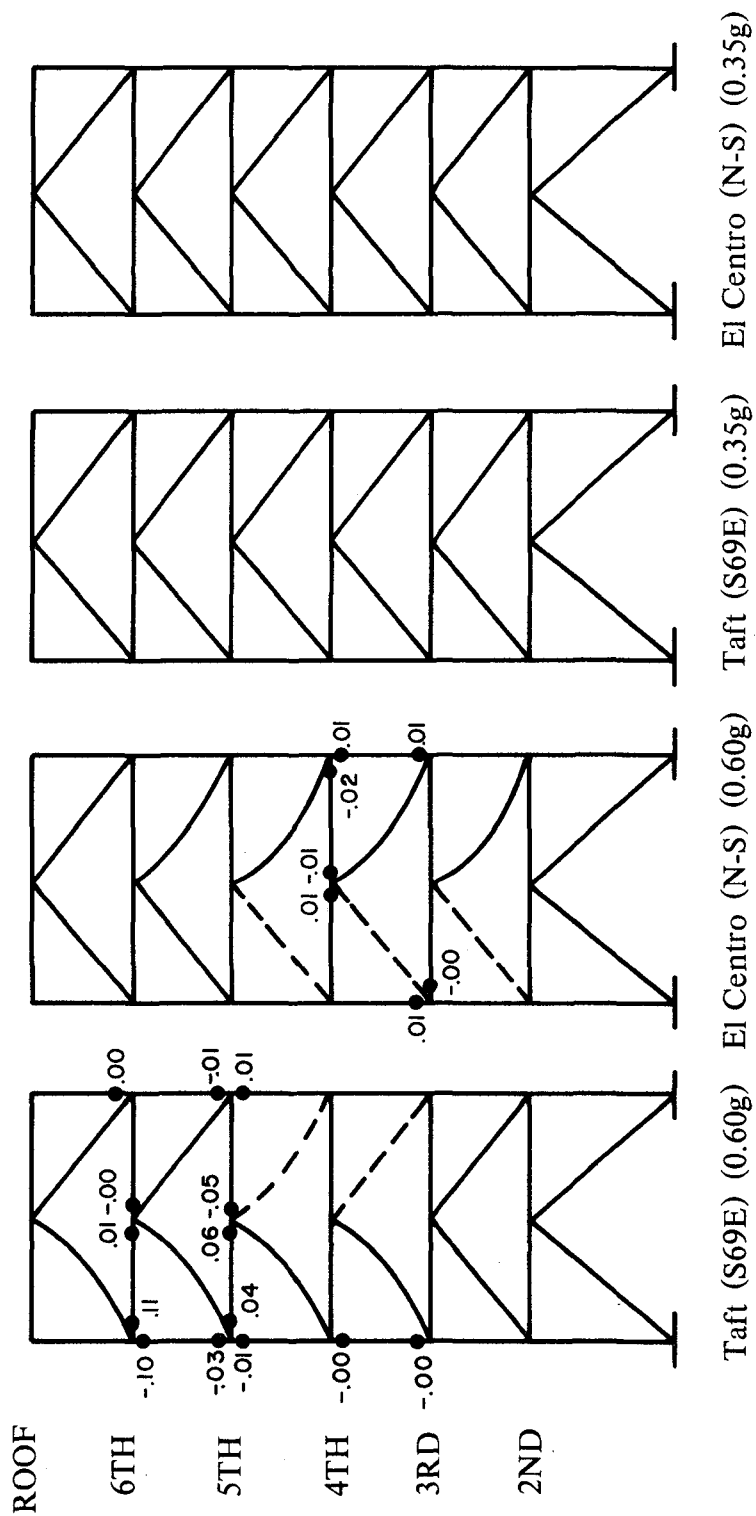


Fig. 6.26 Comparison of Inelastic Deformations in the Frame for Different Earthquake Ground Accelerations

APPENDIX A
DRAIN-2D2 Program

The refined physical theory brace model has been developed as an inelastic truss element for the DRAIN-2D2 program. Detailed information on the assumptions and operating characteristics of this program can be found in Reference 25. The basic characteristics of this program are briefly described below.

This program is a practical and efficient computer program for the inelastic behavior analysis of two-dimensional structures. The structure is idealized as a planer assemblage of discrete elements. The program contains a series of elements in its library; furthermore, new elements may be added without changing the framework of the program. Static loads may be considered in addition to horizontal and vertical components of base ground shaking. In analysis, the direct stiffness method is used with the nodal displacements as unknowns. The dynamic response is determined using step-by-step integration based on the constant average-acceleration method. Each step uses the tangent stiffness of the structure and assumes linear structural behavior during that step. Equilibrium errors (unbalanced forces) resulting from the discrepancies between this linear assumption and actual inelastic member behavior are eliminated by the application of corrective loads in the subsequent time step. The program includes an automatic event-to-event computation option. If this option is specified, the tangent stiffness matrix of the structure is reassembled when the stiffness of a element changes within a step. The use of this option can lessen the unbalanced forces, reducing cumulative errors and increasing the stability of analyses.

APPENDIX B

INPUT DATA FOR THE REFINED PHYSICAL THEORY BRACE MODEL

This appendix presents the input data for the refined model, developed as an element for the DRAIN-2D2 program. See Reference 25 for remainder of input data required.

B.1 Control Information

(a) First Card

COLUMNS	NOTE	NAME	DATA
5(I)			Punch 5 to indicate element group.
6-10(I)		NMEM	Numbers of elements in group.
11-15(I)		KREP	Event-to-event calculation indicator. 0 : use normal step-by-step method. 1 : use event-to-event method.

(b) Second Card

COLUMNS	NOTE	NAME	DATA
1-5(I)	(1)	INTP	Punch 0 if output for mid step events is not desired; Punch 1 if it is desired.
6-10(I)	(2)	ISEC	Numbers of sub-divisions of zones (Doubled for Zone P1).
11-15(I)	(3)	ITEMAX	Maximum number of iterations for regula falsi (must be greater than 1).
16-25(F)	(3)	TOL1	Tolerance for regula falsi. (in.)
26-35(F)	(3)	TOL2	Tolerance for regula falsi. (kips)

(c) **Third Card**

COLUMNS	NOTE	NAME	DATA
5(I)		NSTF	Number of stiffness types.

B.2 **Stiffness Types**(a) **First Card (NSTF x 3 Cards)**

COLUMNS	NOTE	NAME	DATA
1-10(F)		AREA	Cross-sectional area.
11-20(F)		YIESTR	Yield stress.
21-30(F)		RI	Cross-sectional moment of inertia.
31-40(F)		E	Initial modulus of elasticity.
41-50(F)	(4)	e_1	Constants for defining tangent modulus of elasticity.
51-60(F)		e_2	
61-70(F)		e_3	
71-80(F)		e_4	

(b) **Second Card**

COLUMNS	NOTE	NAME	DATA
1-10(F)		PLAMOM	Plastic moment of cross section (M_p).
11-20(F)		THETA	Initial plastic hinge rotation of a strut (radians).
21-30(F)	(5)	RATET	Magnification factor of theoretical $P-M$ interaction curve for $P > 0$.
31-40(F)		RATEC	Magnification factor for $P < 0$.

41-50(F)	(6)	BETA	Constant for defining plastic hinge rotation degradation in Zone EL2.
51-60(F)		HARDEN	Strain hardening modulus, a proportion of the initial modulus of elasticity.
61-70(F)		EFF	Effective length factor.

(c) **Third Card**

COLUMNS	NOTE	NAME	DATA
1-10(F)	(7)	p_{12}	
11-20(F)		b_1	
21-30(F)		c_1	Constants for defining theoretical $P-M$ interaction curve.
31-40(F)		a_2	
41-50(F)		b_2	
51-60(F)		c_2	

B.3 Element Generation Data (NMEM Cards)

COLUMNS	NOTE	NAME	DATA
1-5(I)		IMEM	Element number.
5-10(I)		NODI	Node number at element end I.
11-15(I)		NODJ	Node number at element end J.
16-20(I)		ISTF	Stiffness type number.
21-25(I)	(8)	KOUT	Time History output code. 0 : no print out; 1 : print only; 2 : print and save; 3 : save only;

4 : save and print reorganized time history.

B.4 Notes

- (1) Standard output is presented only at the specified time intervals. By the use of this option, the users are able to receive the information between time intervals.
- (2) Number of subsection of zones used for the computation of the member tangent stiffness (read Section 3.7 of Report for more detail). This variable is also used to define the number of interpolation points between time intervals.
- (3) If the number of iteration exceeds ITEMAX, the program takes the last value and continues the analysis.
- (4) See Subsection 3.4.2 (Fig. 3.8) of Report.
- (5) See Subsection 3.4.1 (Fig. 3.4) of Report.
- (6) See Subsection 3.4.3 (Fig. 3.9) of Report.
- (7) See Subsection 3.4.1 (Fig. 3.5) of Report.
- (8) Standard outputs are not suitable for the plot of the results. By choosing Option 4, users can receive reorganized outputs suitable for the plot.

EARTHQUAKE ENGINEERING RESEARCH CENTER REPORTS

NOTE: Numbers in parentheses are Accession Numbers assigned by the National Technical Information Service; these are followed by a price code. Copies of the reports may be ordered from the National Technical Information Service, 5285 Port Royal Road, Springfield, Virginia, 22161. Accession Numbers should be quoted on orders for reports (PB --- ---) and remittance must accompany each order. Reports without this information were not available at time of printing. The complete list of EERC reports (from EERC 67-1) is available upon request from the Earthquake Engineering Research Center, University of California, Berkeley, 47th Street and Hoffman Boulevard, Richmond, California 94804.

- UCB/EERC-77/01 "PLUSH - A Computer Program for Probabilistic Finite Element Analysis of Seismic Soil-Structure Interaction," by M.P. Romo Organista, J. Lysmer and H.B. Seed - 1977 (PB81 177 651)A05
- UCB/EERC-77/02 "Soil-Structure Interaction Effects at the Humboldt Bay Power Plant in the Ferndale Earthquake of June 7, 1975," by J.E. Valera, H.B. Seed, C.F. Tsai and J. Lysmer - 1977 (PB 265 795)A04
- UCB/EERC-77/03 "Influence of Sample Disturbance on Sand Response to Cyclic Loading," by K. Mori, H.B. Seed and C.K. Chan - 1977 (PB 267 352)A04
- UCB/EERC-77/04 "Seismological Studies of Strong Motion Records," by J. Shoja-Taheri - 1977 (PB 269 655)A10
- UCB/EERC-77/05 Unassigned
- UCB/EERC-77/06 "Developing Methodologies for Evaluating the Earthquake Safety of Existing Buildings," by No. 1 - B. Bresler; No. 2 - B. Bresler, T. Okada and D. Zisling; No. 3 - T. Okada and B. Bresler; No. 4 - V.V. Bertero and B. Bresler - 1977 (PB 267 354)A08
- UCB/EERC-77/07 "A Literature Survey - Transverse Strength of Masonry Walls," by Y. Omote, R.L. Mayes, S.W. Chen and R.W. Clough - 1977 (PB 277 933)A07
- UCB/EERC-77/08 "DRAIN-TABS: A Computer Program for Inelastic Earthquake Response of Three Dimensional Buildings," by R. Guendelman-Israel and G.H. Powell - 1977 (PB 270 693)A07
- UCB/EERC-77/09 "SUBWALL: A Special Purpose Finite Element Computer Program for Practical Elastic Analysis and Design of Structural Walls with Substructure Option," by D.Q. Le, H. Peterson and E.P. Popov - 1977 (PB 270 567)A05
- UCB/EERC-77/10 "Experimental Evaluation of Seismic Design Methods for Broad Cylindrical Tanks," by D.P. Clough (PB 272 280)A13
- UCB/EERC-77/11 "Earthquake Engineering Research at Berkeley - 1976," - 1977 (PB 273 507)A09
- UCB/EERC-77/12 "Automated Design of Earthquake Resistant Multistory Steel Building Frames," by N.D. Walker, Jr. - 1977 (PB 276 526)A09
- UCB/EERC-77/13 "Concrete Confined by Rectangular Hoops Subjected to Axial Loads," by J. Vallenias, V.V. Bertero and E.P. Popov - 1977 (PB 275 165)A06
- UCB/EERC-77/14 "Seismic Strain Induced in the Ground During Earthquakes," by Y. Sugimura - 1977 (PB 284 201)A04
- UCB/EERC-77/15 Unassigned
- UCB/EERC-77/16 "Computer Aided Optimum Design of Ductile Reinforced Concrete Moment Resisting Frames," by S.W. Zagajeski and V.V. Bertero - 1977 (PB 280 137)A07
- UCB/EERC-77/17 "Earthquake Simulation Testing of a Stepping Frame with Energy-Absorbing Devices," by J.M. Kelly and D.F. Tsztoo - 1977 (PB 273 506)A04
- UCB/EERC-77/18 "Inelastic Behavior of Eccentrically Braced Steel Frames under Cyclic Loadings," by C.W. Roeder and E.P. Popov - 1977 (PB 275 526)A15
- UCB/EERC-77/19 "A Simplified Procedure for Estimating Earthquake-Induced Deformations in Dams and Embankments," by F.I. Makdisi and H.B. Seed - 1977 (PB 276 820)A04
- UCB/EERC-77/20 "The Performance of Earth Dams during Earthquakes," by H.B. Seed, F.I. Makdisi and P. de Alba - 1977 (PB 276 821)A04
- UCB/EERC-77/21 "Dynamic Plastic Analysis Using Stress Resultant Finite Element Formulation," by P. Lukkunapvasit and J.M. Kelly - 1977 (PB 275 453)A04
- UCB/EERC-77/22 "Preliminary Experimental Study of Seismic Uplift of a Steel Frame," by R.W. Clough and A.A. Huckelbridge 1977 (PB 278 769)A08
- UCB/EERC-77/23 "Earthquake Simulator Tests of a Nine-Story Steel Frame with Columns Allowed to Uplift," by A.A. Huckelbridge - 1977 (PB 277 944)A09
- UCB/EERC-77/24 "Nonlinear Soil-Structure Interaction of Skew Highway Bridges," by M.-C. Chen and J. Penzien - 1977 (PB 276 176)A07
- UCB/EERC-77/25 "Seismic Analysis of an Offshore Structure Supported on Pile Foundations," by D.D.-N. Liou and J. Penzien 1977 (PB 283 180)A06
- UCB/EERC-77/26 "Dynamic Stiffness Matrices for Homogeneous Viscoelastic Half-Planes," by G. Dasgupta and A.K. Chopra - 1977 (PB 279 654)A06

- UCB/EERC-77/27 "A Practical Soft Story Earthquake Isolation System," by J.M. Kelly, J.M. Eidinge and C.J. Derham - 1977 (PB 276 814)A07
- UCB/EERC-77/28 "Seismic Safety of Existing Buildings and Incentives for Hazard Mitigation in San Francisco: An Exploratory Study," by A.J. Meltsner - 1977 (PB 281 970)A05
- UCB/EERC-77/29 "Dynamic Analysis of Electrohydraulic Shaking Tables," by D. Rea, S. Abedi-Hayati and Y. Takahashi 1977 (PB 282 569)A04
- UCB/EERC-77/30 "An Approach for Improving Seismic - Resistant Behavior of Reinforced Concrete Interior Joints," by B. Galunic, V.V. Bertero and E.P. Popov - 1977 (PB 290 870)A06
- UCB/EERC-78/01 "The Development of Energy-Absorbing Devices for Aseismic Base Isolation Systems," by J.M. Kelly and D.F. Tsztoo - 1978 (PB 284 978)A04
- UCB/EERC-78/02 "Effect of Tensile Prestrain on the Cyclic Response of Structural Steel Connections, by J.G. Bouwkamp and A. Mukhopadhyay - 1978
- UCB/EERC-78/03 "Experimental Results of an Earthquake Isolation System using Natural Rubber Bearings," by J.M. Eidinge and J.M. Kelly - 1978 (PB 281 686)A04
- UCB/EERC-78/04 "Seismic Behavior of Tall Liquid Storage Tanks," by A. Niwa - 1978 (PB 284 017)A14
- UCB/EERC-78/05 "Hysteretic Behavior of Reinforced Concrete Columns Subjected to High Axial and Cyclic Shear Forces," by S.W. Zagajewski, V.V. Bertero and J.G. Bouwkamp - 1978 (PB 283 858)A13
- UCB/EERC-78/06 "Three Dimensional Inelastic Frame Elements for the ANSR-I Program," by A. Riahi, D.G. Row and G.H. Powell - 1978 (PB 295 755)A04
- UCB/EERC-78/07 "Studies of Structural Response to Earthquake Ground Motion," by O.A. Lopez and A.K. Chopra - 1978 (PB 282 790)A05
- UCB/EERC-78/08 "A Laboratory Study of the Fluid-Structure Interaction of Submerged Tanks and Caissons in Earthquakes," by R.C. Byrd - 1978 (PB 284 957)A08
- UCB/EERC-78/09 Unassigned
- UCB/EERC-78/10 "Seismic Performance of Nonstructural and Secondary Structural Elements," by I. Sakamoto - 1978 (PB81 154 593)A05
- UCB/EERC-78/11 "Mathematical Modelling of Hysteresis Loops for Reinforced Concrete Columns," by S. Nakata, T. Sproul and J. Penzien - 1978 (PB 298 274)A05
- UCB/EERC-78/12 "Damageability in Existing Buildings," by T. Blejwas and B. Bresler - 1978 (PB 80 166 978)A05
- UCB/EERC-78/13 "Dynamic Behavior of a Pedestal Base Multistory Building," by R.M. Stephen, E.L. Wilson, J.G. Bouwkamp and M. Button - 1978 (PB 286 650)A08
- UCB/EERC-78/14 "Seismic Response of Bridges - Case Studies," by R.A. Imbsen, V. Nutt and J. Penzien - 1978 (PB 286 503)A10
- UCB/EERC-78/15 "A Substructure Technique for Nonlinear Static and Dynamic Analysis," by D.G. Row and G.H. Powell - 1978 (PB 288 077)A10
- UCB/EERC-78/16 "Seismic Risk Studies for San Francisco and for the Greater San Francisco Bay Area," by C.S. Oliveira - 1978 (PB 81 120 115)A07
- UCB/EERC-78/17 "Strength of Timber Roof Connections Subjected to Cyclic Loads," by P. Gülkan, R.L. Mayes and R.W. Clough - 1978 (HUD-000 1491)A07
- UCB/EERC-78/18 "Response of K-Braced Steel Frame Models to Lateral Loads," by J.G. Bouwkamp, R.M. Stephen and E.P. Popov - 1978
- UCB/EERC-78/19 "Rational Design Methods for Light Equipment in Structures Subjected to Ground Motion," by J.L. Sackman and J.M. Kelly - 1978 (PB 292 357)A04
- UCB/EERC-78/20 "Testing of a Wind Restraint for Aseismic Base Isolation," by J.M. Kelly and D.E. Chitty - 1978 (PB 292 833)A03
- UCB/EERC-78/21 "APOLLO - A Computer Program for the Analysis of Pore Pressure Generation and Dissipation in Horizontal Sand Layers During Cyclic or Earthquake Loading," by P.P. Martin and H.B. Seed - 1978 (PB 292 835)A04
- UCB/EERC-78/22 "Optimal Design of an Earthquake Isolation System," by M.A. Bhatti, K.S. Pister and E. Polak - 1978 (PB 294 735)A06
- UCB/EERC-78/23 "MASH - A Computer Program for the Non-Linear Analysis of Vertically Propagating Shear Waves in Horizontally Layered Deposits," by P.P. Martin and H.B. Seed - 1978 (PB 293 101)A05
- UCB/EERC-78/24 "Investigation of the Elastic Characteristics of a Three Story Steel Frame Using System Identification," by I. Kaya and H.D. McNiven - 1978 (PB 296 225)A06
- UCB/EERC-78/25 "Investigation of the Nonlinear Characteristics of a Three-Story Steel Frame Using System Identification," by I. Kaya and H.D. McNiven - 1978 (PB 301 363)A05

- UCB/EERC-78/26 "Studies of Strong Ground Motion in Taiwan," by Y.M. Hsiung, B.A. Bolt and J. Penzien - 1978 (PB 298 436)A06
- UCB/EERC-78/27 "Cyclic Loading Tests of Masonry Single Piers: Volume 1 - Height to Width Ratio of 2," by P.A. Hidalgo, R.L. Mayes, H.D. McNiven and R.W. Clough - 1978 (PB 296 211)A07
- UCB/EERC-78/28 "Cyclic Loading Tests of Masonry Single Piers: Volume 2 - Height to Width Ratio of 1," by S.-W.J. Chen, P.A. Hidalgo, R.L. Mayes, R.W. Clough and H.D. McNiven - 1978 (PB 296 212)A09
- UCB/EERC-78/29 "Analytical Procedures in Soil Dynamics," by J. Lysmer - 1978 (PB 298 445)A06
- UCB/EERC-79/01 "Hysteretic Behavior of Lightweight Reinforced Concrete Beam-Column Subassemblages," by B. Forzani, E.P. Popov and V.V. Bertero - April 1979 (PB 298 267)A06
- UCB/EERC-79/02 "The Development of a Mathematical Model to Predict the Flexural Response of Reinforced Concrete Beams to Cyclic Loads, Using System Identification," by J. Stanton & H. McNiven - Jan. 1979 (PB 295 875)A10
- UCB/EERC-79/03 "Linear and Nonlinear Earthquake Response of Simple Torsionally Coupled Systems," by C.L. Kan and A.K. Chopra - Feb. 1979 (PB 298 262)A06
- UCB/EERC-79/04 "A Mathematical Model of Masonry for Predicting its Linear Seismic Response Characteristics," by Y. Mengi and H.D. McNiven - Feb. 1979 (PB 298 266)A06
- UCB/EERC-79/05 "Mechanical Behavior of Lightweight Concrete Confined by Different Types of Lateral Reinforcement," by M.A. Manrique, V.V. Bertero and E.P. Popov - May 1979 (PB 301 114)A06
- UCB/EERC-79/06 "Static Tilt Tests of a Tall Cylindrical Liquid Storage Tank," by R.W. Clough and A. Niwa - Feb. 1979 (PB 301 167)A06
- UCB/EERC-79/07 "The Design of Steel Energy Absorbing Restrainers and Their Incorporation into Nuclear Power Plants for Enhanced Safety: Volume 1 - Summary Report," by P.N. Spencer, V.F. Zackay, and E.R. Parker - Feb. 1979 (UCB/EERC-79/07)A09
- UCB/EERC-79/08 "The Design of Steel Energy Absorbing Restrainers and Their Incorporation into Nuclear Power Plants for Enhanced Safety: Volume 2 - The Development of Analyses for Reactor System Piping," "Simple Systems" by M.C. Lee, J. Penzien, A.K. Chopra and K. Suzuki "Complex Systems" by G.H. Powell, E.L. Wilson, R.W. Clough and D.G. Row - Feb. 1979 (UCB/EERC-79/08)A10
- UCB/EERC-79/09 "The Design of Steel Energy Absorbing Restrainers and Their Incorporation into Nuclear Power Plants for Enhanced Safety: Volume 3 - Evaluation of Commercial Steels," by W.S. Owen, R.M.N. Pelloux, R.O. Ritchie, M. Faral, T. Ohhashi, J. Toplosky, S.J. Hartman, V.F. Zackay and E.R. Parker - Feb. 1979 (UCB/EERC-79/09)A04
- UCB/EERC-79/10 "The Design of Steel Energy Absorbing Restrainers and Their Incorporation into Nuclear Power Plants for Enhanced Safety: Volume 4 - A Review of Energy-Absorbing Devices," by J.M. Kelly and M.S. Skinner - Feb. 1979 (UCB/EERC-79/10)A04
- UCB/EERC-79/11 "Conservatism in Summation Rules for Closely Spaced Modes," by J.M. Kelly and J.L. Sackman - May 1979 (PB 301 328)A03
- UCB/EERC-79/12 "Cyclic Loading Tests of Masonry Single Piers: Volume 3 - Height to Width Ratio of 0.5," by P.A. Hidalgo, R.L. Mayes, H.D. McNiven and R.W. Clough - May 1979 (PB 301 321)A08
- UCB/EERC-79/13 "Cyclic Behavior of Dense Course-Grained Materials in Relation to the Seismic Stability of Dams," by N.G. Banerjee, H.B. Seed and C.K. Chan - June 1979 (PB 301 373)A13
- UCB/EERC-79/14 "Seismic Behavior of Reinforced Concrete Interior Beam-Column Subassemblages," by S. Viathanatepa, E.P. Popov and V.V. Bertero - June 1979 (PB 301 326)A10
- UCB/EERC-79/15 "Optimal Design of Localized Nonlinear Systems with Dual Performance Criteria Under Earthquake Excitations," by M.A. Bhatti - July 1979 (PB 80 167 109)A06
- UCB/EERC-79/16 "OPTDYN - A General Purpose Optimization Program for Problems with or without Dynamic Constraints," by M.A. Bhatti, E. Polak and K.S. Pister - July 1979 (PB 80 167 091)A05
- UCB/EERC-79/17 "ANSR-II, Analysis of Nonlinear Structural Response, Users Manual," by D.P. Mondkar and G.H. Powell July 1979 (PB 80 113 301)A05
- UCB/EERC-79/18 "Soil Structure Interaction in Different Seismic Environments," A. Gomez-Masso, J. Lysmer, J.-C. Chen and H.B. Seed - August 1979 (PB 80 101 520)A04
- UCB/EERC-79/19 "ARMA Models for Earthquake Ground Motions," by M.K. Chang, J.W. Kwiatkowski, R.F. Nau, R.M. Oliver and K.S. Pister - July 1979 (PB 301 166)A05
- UCB/EERC-79/20 "Hysteretic Behavior of Reinforced Concrete Structural Walls," by J.M. Vallenat, V.V. Bertero and E.P. Popov - August 1979 (PB 80 165 905)A12
- UCB/EERC-79/21 "Studies on High-Frequency Vibrations of Buildings - 1: The Column Effect," by J. Lubliner - August 1979 (PB 80 158 553)A03
- UCB/EERC-79/22 "Effects of Generalized Loadings on Bond Reinforcing Bars Embedded in Confined Concrete Blocks," by S. Viathanatepa, E.P. Popov and V.V. Bertero - August 1979 (PB 81 124 018)A14
- UCB/EERC-79/23 "Shaking Table Study of Single-Story Masonry Houses, Volume 1: Test Structures 1 and 2," by P. Gülkan, R.L. Mayes and R.W. Clough - Sept. 1979 (HUD-000 1763)A12
- UCB/EERC-79/24 "Shaking Table Study of Single-Story Masonry Houses, Volume 2: Test Structures 3 and 4," by P. Gülkan, R.L. Mayes and R.W. Clough - Sept. 1979 (HUD-000 1836)A12
- UCB/EERC-79/25 "Shaking Table Study of Single-Story Masonry Houses, Volume 3: Summary, Conclusions and Recommendations," by R.W. Clough, R.L. Mayes and P. Gülkan - Sept. 1979 (HUD-000 1837)A06

- UCB/EERC-79/26 "Recommendations for a U.S.-Japan Cooperative Research Program Utilizing Large-Scale Testing Facilities," by U.S.-Japan Planning Group - Sept. 1979(PB 301 407)A06
- UCB/EERC-79/27 "Earthquake-Induced Liquefaction Near Lake Amatitlan, Guatemala," by H.B. Seed, I. Arango, C.K. Chan, A. Gomez-Masso and R. Grant de Ascoli - Sept. 1979(NUREG-CRL341)A03
- UCB/EERC-79/28 "Infill Panels: Their Influence on Seismic Response of Buildings," by J.W. Axley and V.V. Bertero Sept. 1979(PB 80 163 371)A10
- UCB/EERC-79/29 "3D Truss Bar Element (Type 1) for the ANSR-II Program," by D.P. Mondkar and G.H. Powell - Nov. 1979 (PB 80 169 709)A02
- UCB/EERC-79/30 "2D Beam-Column Element (Type 5 - Parallel Element Theory) for the ANSR-II Program," by D.G. Row, G.H. Powell and D.P. Mondkar - Dec. 1979(PB 80 167 224)A03
- UCB/EERC-79/31 "3D Beam-Column Element (Type 2 - Parallel Element Theory) for the ANSR-II Program," by A. Riahi, G.H. Powell and D.P. Mondkar - Dec. 1979(PB 80 167 216)A03
- UCB/EERC-79/32 "On Response of Structures to Stationary Excitation," by A. Der Kiureghian - Dec. 1979(PB 80166 929)A03
- UCB/EERC-79/33 "Undisturbed Sampling and Cyclic Load Testing of Sands," by S. Singh, H.B. Seed and C.K. Chan Dec. 1979(ADA 087 298)A07
- UCB/EERC-79/34 "Interaction Effects of Simultaneous Torsional and Compressional Cyclic Loading of Sand," by P.M. Griffin and W.N. Houston - Dec. 1979(ADA 092 352)A15
- UCB/EERC-80/01 "Earthquake Response of Concrete Gravity Dams Including Hydrodynamic and Foundation Interaction Effects," by A.K. Chopra, P. Chakrabarti and S. Gupta - Jan. 1980(AD-A087297)A10
- UCB/EERC-80/02 "Rocking Response of Rigid Blocks to Earthquakes," by C.S. Yim, A.K. Chopra and J. Penzien - Jan. 1980 (PB80 166 002)A04
- UCB/EERC-80/03 "Optimum Inelastic Design of Seismic-Resistant Reinforced Concrete Frame Structures," by S.W. Zagajeski and V.V. Bertero - Jan. 1980(PB80 164 635)A06
- UCB/EERC-80/04 "Effects of Amount and Arrangement of Wall-Panel Reinforcement on Hysteretic Behavior of Reinforced Concrete Walls," by R. Iliya and V.V. Bertero - Feb. 1980(PB81 122 525)A09
- UCB/EERC-80/05 "Shaking Table Research on Concrete Dam Models," by A. Niwa and R.W. Clough - Sept. 1980(PB81 122 368)A06
- UCB/EERC-80/06 "The Design of Steel Energy-Absorbing Restrainers and their Incorporation into Nuclear Power Plants for Enhanced Safety (Vol 1A): Piping with Energy Absorbing Restrainers: Parameter Study on Small Systems," by G.H. Powell, C. Oughourlian and J. Simons - June 1980
- UCB/EERC-80/07 "Inelastic Torsional Response of Structures Subjected to Earthquake Ground Motions," by Y. Yamazaki April 1980(PB81 122 327)A08
- UCB/EERC-80/08 "Study of X-Braced Steel Frame Structures Under Earthquake Simulation," by Y. Ghanaat - April 1980 (PB81 122 335)A11
- UCB/EERC-80/09 "Hybrid Modelling of Soil-Structure Interaction," by S. Gupta, T.W. Lin, J. Penzien and C.S. Yeh May 1980(PB81 122 319)A07
- UCB/EERC-80/10 "General Applicability of a Nonlinear Model of a One Story Steel Frame," by B.I. Sveinsson and H.D. McNiven - May 1980(PB81 124 877)A06
- UCB/EERC-80/11 "A Green-Function Method for Wave Interaction with a Submerged Body," by W. Kioka - April 1980 (PB81 122 269)A07
- UCB/EERC-80/12 "Hydrodynamic Pressure and Added Mass for Axisymmetric Bodies," by F. Nilrat - May 1980(PB81 122 343)A08
- UCB/EERC-80/13 "Treatment of Non-Linear Drag Forces Acting on Offshore Platforms," by B.V. Dao and J. Penzien May 1980(PB81 153 413)A07
- UCB/EERC-80/14 "2D Plane/Axisymmetric Solid Element (Type 3 - Elastic or Elastic-Perfectly Plastic) for the ANSR-II Program," by D.P. Mondkar and G.H. Powell - July 1980(PB81 122 350)A03
- UCB/EERC-80/15 "A Response Spectrum Method for Random Vibrations," by A. Der Kiureghian - June 1980(PB81 122 301)A03
- UCB/EERC-80/16 "Cyclic Inelastic Buckling of Tubular Steel Braces," by V.A. Zayas, E.P. Popov and S.A. Mahin June 1980(PB81 124 885)A10
- UCB/EERC-80/17 "Dynamic Response of Simple Arch Dams Including Hydrodynamic Interaction," by C.S. Porter and A.K. Chopra - July 1980(PB81 124 000)A13
- UCB/EERC-80/18 "Experimental Testing of a Friction Damped Aseismic Base Isolation System with Fail-Safe Characteristics," by J.M. Kelly, K.E. Beucke and M.S. Skinner - July 1980(PB81 148 595)A04
- UCB/EERC-80/19 "The Design of Steel Energy-Absorbing Restrainers and their Incorporation into Nuclear Power Plants for Enhanced Safety (Vol 1B): Stochastic Seismic Analyses of Nuclear Power Plant Structures and Piping Systems Subjected to Multiple Support Excitations," by M.C. Lee and J. Penzien - June 1980
- UCB/EERC-80/20 "The Design of Steel Energy-Absorbing Restrainers and their Incorporation into Nuclear Power Plants for Enhanced Safety (Vol 1C): Numerical Method for Dynamic Substructure Analysis," by J.M. Dickens and E.L. Wilson - June 1980
- UCB/EERC-80/21 "The Design of Steel Energy-Absorbing Restrainers and their Incorporation into Nuclear Power Plants for Enhanced Safety (Vol 2): Development and Testing of Restraints for Nuclear Piping Systems," by J.M. Kelly and M.S. Skinner - June 1980
- UCB/EERC-80/22 "3D Solid Element (Type 4-Elastic or Elastic-Perfectly-Plastic) for the ANSR-II Program," by D.P. Mondkar and G.H. Powell - July 1980(PB81 123 242)A03
- UCB/EERC-80/23 "Gap-Friction Element (Type 5) for the ANSR-II Program," by D.P. Mondkar and G.H. Powell - July 1980 (PB81 122 285)A03

- UCB/EERC-80/24 "U-Bar Restraint Element (Type 11) for the ANSR-II Program," by C. Oughourlian and G.H. Powell July 1980(PB81 122 293)A03
- UCB/EERC-80/25 "Testing of a Natural Rubber Base Isolation System by an Explosively Simulated Earthquake," by J.M. Kelly - August 1980(PB81 201 360)A04
- UCB/EERC-80/26 "Input Identification from Structural Vibrational Response," by Y. Hu - August 1980(PB81 152 308)A05
- UCB/EERC-80/27 "Cyclic Inelastic Behavior of Steel Offshore Structures," by V.A. Zayas, S.A. Mahin and E.P. Popov August 1980(PB81 196 180)A15
- UCB/EERC-80/28 "Shaking Table Testing of a Reinforced Concrete Frame with Biaxial Response," by M.G. Oliva October 1980(PB81 154 304)A10
- UCB/EERC-80/29 "Dynamic Properties of a Twelve-Story Prefabricated Panel Building," by J.G. Bouwkamp, J.P. Kollegger and R.M. Stephen - October 1980(PB82 117 128)A06
- UCB/EERC-80/30 "Dynamic Properties of an Eight-Story Prefabricated Panel Building," by J.G. Bouwkamp, J.P. Kollegger and R.M. Stephen - October 1980(PB81 200 313)A05
- UCB/EERC-80/31 "Predictive Dynamic Response of Panel Type Structures Under Earthquakes," by J.P. Kollegger and J.G. Bouwkamp - October 1980(PB81 152 316)A04
- UCB/EERC-80/32 "The Design of Steel Energy-Absorbing Restraints and their Incorporation into Nuclear Power Plants for Enhanced Safety (Vol 3): Testing of Commercial Steels in Low-Cycle Torsional Fatigue," by P. Spencer, E.R. Parker, E. Jongewaard and M. Drory
- UCB/EERC-80/33 "The Design of Steel Energy-Absorbing Restraints and their Incorporation into Nuclear Power Plants for Enhanced Safety (Vol 4): Shaking Table Tests of Piping Systems with Energy-Absorbing Restraints," by S.F. Stiemer and W.G. Godden - Sept. 1980
- UCB/EERC-80/34 "The Design of Steel Energy-Absorbing Restraints and their Incorporation into Nuclear Power Plants for Enhanced Safety (Vol 5): Summary Report," by P. Spencer
- UCB/EERC-80/35 "Experimental Testing of an Energy-Absorbing Base Isolation System," by J.M. Kelly, M.S. Skinner and K.E. Beucke - October 1980(PB81 154 072)A04
- UCB/EERC-80/36 "Simulating and Analyzing Artificial Non-Stationary Earthquake Ground Motions," by R.F. Nau, R.M. Oliver and K.S. Pister - October 1980(PB81 153 397)A04
- UCB/EERC-80/37 "Earthquake Engineering at Berkeley - 1980," - Sept. 1980(PB81 205 874)A09
- UCB/EERC-80/38 "Inelastic Seismic Analysis of Large Panel Buildings," by V. Schrieker and G.H. Powell - Sept. 1980 (PB81 154 338)A13
- UCB/EERC-80/39 "Dynamic Response of Embankment, Concrete-Gravity and Arch Dams Including Hydrodynamic Interaction," by J.F. Hall and A.K. Chopra - October 1980(PB81 152 324)A11
- UCB/EERC-80/40 "Inelastic Buckling of Steel Struts Under Cyclic Load Reversal," by R.G. Black, W.A. Wenger and E.P. Popov - October 1980(PB81 154 312)A08
- UCB/EERC-80/41 "Influence of Site Characteristics on Building Damage During the October 3, 1974 Lima Earthquake," by P. Repetto, I. Arango and H.B. Seed - Sept. 1980(PB81 161 739)A05
- UCB/EERC-80/42 "Evaluation of a Shaking Table Test Program on Response Behavior of a Two Story Reinforced Concrete Frame," by J.M. Blondet, R.W. Clough and S.A. Mahin
- UCB/EERC-80/43 "Modelling of Soil-Structure Interaction by Finite and Infinite Elements," by F. Medina - December 1980(PB81 229 270)A04
- UCB/EERC-81/01 "Control of Seismic Response of Piping Systems and Other Structures by Base Isolation," edited by J.M. Kelly - January 1981 (PB81 200 735)A05
- UCB/EERC-81/02 "OPTNSR - An Interactive Software System for Optimal Design of Statically and Dynamically Loaded Structures with Nonlinear Response," by M.A. Bhatti, V. Ciampi and K.S. Pister - January 1981 (PB81 218 851)A09
- UCB/EERC-81/03 "Analysis of Local Variations in Free Field Seismic Ground Motions," by J.-C. Chen, J. Lysmer and H.B. Seed - January 1981 (AD-A099508)A13
- UCB/EERC-81/04 "Inelastic Structural Modeling of Braced Offshore Platforms for Seismic Loading," by V.A. Zayas, P.-S.B. Shing, S.A. Mahin and E.P. Popov - January 1981(PB82 138 777)A07
- UCB/EERC-81/05 "Dynamic Response of Light Equipment in Structures," by A. Der Kiureghian, J.L. Sackman and B. Nour-Omid - April 1981 (PB81 218 497)A04
- UCB/EERC-81/06 "Preliminary Experimental Investigation of a Broad Base Liquid Storage Tank," by J.G. Bouwkamp, J.P. Kollegger and R.M. Stephen - May 1981(PB82 140 385)A03
- UCB/EERC-81/07 "The Seismic Resistant Design of Reinforced Concrete Coupled Structural Walls," by A.E. Aktan and V.V. Bertero - June 1981(PB82 113 358)A11
- UCB/EERC-81/08 "The Undrained Shearing Resistance of Cohesive Soils at Large Deformations," by M.R. Pyles and H.B. Seed - August 1981
- UCB/EERC-81/09 "Experimental Behavior of a Spatial Piping System with Steel Energy Absorbers Subjected to a Simulated Differential Seismic Input," by S.F. Stiemer, W.G. Godden and J.M. Kelly - July 1981

- UCB/EERC-81/10 "Evaluation of Seismic Design Provisions for Masonry in the United States," by B.I. Sveinsson, R.L. Mayes and H.D. McNiven - August 1981 (PB82 166 075)A08
- UCB/EERC-81/11 "Two-Dimensional Hybrid Modelling of Soil-Structure Interaction," by T.-J. Tzong, S. Gupta and J. Penzien - August 1981 (PB82 142 118)A04
- UCB/EERC-81/12 "Studies on Effects of Infills in Seismic Resistant R/C Construction," by S. Brokken and V.V. Bertero - September 1981 (PB82 166 190)A09
- UCB/EERC-81/13 "Linear Models to Predict the Nonlinear Seismic Behavior of a One-Story Steel Frame," by H. Valdimarsson, A.H. Shah and H.D. McNiven - September 1981 (PB82 138 793)A07
- UCB/EERC-81/14 "TLUSH: A Computer Program for the Three-Dimensional Dynamic Analysis of Earth Dams," by T. Kagawa, L.H. Mejia, H.B. Seed and J. Lysmer - September 1981 (PB82 139 940)A06
- UCB/EERC-81/15 "Three Dimensional Dynamic Response Analysis of Earth Dams," by L.H. Mejia and H.B. Seed - September 1981 (PB82 137 274)A12
- UCB/EERC-81/16 "Experimental Study of Lead and Elastomeric Dampers for Base Isolation Systems," by J.M. Kelly and S.B. Hodder - October 1981 (PB82 166 182)A05
- UCB/EERC-81/17 "The Influence of Base Isolation on the Seismic Response of Light Secondary Equipment," by J.M. Kelly - April 1981 (PB82 255 266)A04
- UCB/EERC-81/18 "Studies on Evaluation of Shaking Table Response Analysis Procedures," by J. Marcial Blondet - November 1981 (PB82 197 278)A10
- UCB/EERC-81/19 "DELIGHT.STRUCT: A Computer-Aided Design Environment for Structural Engineering," by R.J. Balling, K.S. Pister and E. Polak - December 1981 (PB82 218 496)A07
- UCB/EERC-81/20 "Optimal Design of Seismic-Resistant Planar Steel Frames," by R.J. Balling, V. Ciampi, K.S. Pister and E. Polak - December 1981 (PB82 220 179)A07
- UCB/EERC-82/01 "Dynamic Behavior of Ground for Seismic Analysis of Lifeline Systems," by T. Sato and A. Der Kiureghian - January 1982 (PB82 218 926)A05
- UCB/EERC-82/02 "Shaking Table Tests of a Tubular Steel Frame Model," by Y. Ghanaat and R. W. Clough - January 1982 (PB82 220 161)A07
- UCB/EERC-82/03 "Behavior of a Piping System under Seismic Excitation: Experimental Investigations of a Spatial Piping System supported by Mechanical Shock Arrestors and Steel Energy Absorbing Devices under Seismic Excitation," by S. Schneider, H.-M. Lee and W. G. Godden - May 1982 (PB83 172 544)A09
- UCB/EERC-82/04 "New Approaches for the Dynamic Analysis of Large Structural Systems," by E. L. Wilson - June 1982 (PB83 148 080)A05
- UCB/EERC-82/05 "Model Study of Effects of Damage on the Vibration Properties of Steel Offshore Platforms," by F. Shahriyar and J. G. Bouwkamp - June 1982 (PB83 148 742)A10
- UCB/EERC-82/06 "States of the Art and Practice in the Optimum Seismic Design and Analytical Response Prediction of R/C Frame-Wall Structures," by A. E. Aktan and V. V. Bertero - July 1982 (PB83 147 736)A05
- UCB/EERC-82/07 "Further Study of the Earthquake Response of a Broad Cylindrical Liquid-Storage Tank Model," by G. C. Manos and R. W. Clough - July 1982 (PB83 147 744)A11
- UCB/EERC-82/08 "An Evaluation of the Design and Analytical Seismic Response of a Seven Story Reinforced Concrete Frame - Wall Structure," by F. A. Charney and V. V. Bertero - July 1982 (PB83 157 628)A09
- UCB/EERC-82/09 "Fluid-Structure Interactions: Added Mass Computations for Incompressible Fluid," by J. S.-H. Kuo - August 1982 (PB83 156 281)A07
- UCB/EERC-82/10 "Joint-Opening Nonlinear Mechanism: Interface Smeared Crack Model," by J. S.-H. Kuo - August 1982 (PB83 149 195)A05
- UCB/EERC-82/11 "Dynamic Response Analysis of Teché Dam," by R. W. Clough, R. M. Stephen and J. S.-H. Kuo - August 1982 (PB83 147 496)A06
- UCB/EERC-82/12 "Prediction of the Seismic Responses of R/C Frame-Coupled Wall Structures," by A. E. Aktan, V. V. Bertero and M. Piazza - August 1982 (PB83 149 203)A09
- UCB/EERC-82/13 "Preliminary Report on the SMART 1 Strong Motion Array in Taiwan," by B. A. Bolt, C. H. Loh, J. Penzien, Y. B. Tsai and Y. T. Yeh - August 1982 (PB83 159 400)A10
- UCB/EERC-82/14 "Shaking-Table Studies of an Eccentrically X-Braced Steel Structure," by M. S. Yang - September 1982 (PB83 260 778)A12
- UCB/EERC-82/15 "The Performance of Stairways in Earthquakes," by C. Rocha, J. W. Axley and V. V. Bertero - September 1982 (PB83 157 693)A07
- UCB/EERC-82/16 "The Behavior of Submerged Multiple Bodies in Earthquakes," by W.-G. Liao - Sept. 1982 (PB83 158 709)A07
- UCB/EERC-82/17 "Effects of Concrete Types and Loading Conditions on Local Bond-Slip Relationships," by A. D. Cowell, E. P. Popov and V. V. Bertero - September 1982 (PB83 153 577)A04

- UCB/EERC-82/18 "Mechanical Behavior of Shear Wall Vertical Boundary Members: An Experimental Investigation," by M. T. Wagner and V. V. Bertero - October 1982 (PB83 159 764)A05
- UCB/EERC-82/19 "Experimental Studies of Multi-support Seismic Loading on Piping Systems," by J. M. Kelly and A. D. Cowell - November 1982
- UCB/EERC-82/20 "Generalized Plastic Hinge Concepts for 3D Beam-Column Elements," by P. F.-S. Chen and G. H. Powell - November 1982 (PB83 247 981)A13
- UCB/EERC-82/21 "ANSR-III: General Purpose Computer Program for Nonlinear Structural Analysis," by C. V. Oughourlian and G. H. Powell - November 1982 (PB83 251 330)A12
- UCB/EERC-82/22 "Solution Strategies for Statically Loaded Nonlinear Structures," by J. W. Simons and G. H. Powell - November 1982 (PB83 197 970)A06
- UCB/EERC-82/23 "Analytical Model of Deformed Bar Anchorages under Generalized Excitations," by V. Ciampi, R. Elieghausen, V. V. Bertero and E. P. Popov - November 1982 (PB83 159 532)A06
- UCB/EERC-82/24 "A Mathematical Model for the Response of Masonry Walls to Dynamic Excitations," by H. Sucuoğlu, Y. Mengi and H. D. McNiven - November 1982 (PB83 169 011)A07
- UCB/EERC-82/25 "Earthquake Response Considerations of Broad Liquid Storage Tanks," by F. J. Cambra - November 1982 (PB83 251 215)A09
- UCB/EERC-82/26 "Computational Models for Cyclic Plasticity, Rate Dependence and Creep," by B. Mosaddad and G. H. Powell - November 1982 (PB83 245 829)A08
- UCB/EERC-82/27 "Inelastic Analysis of Piping and Tubular Structures," by M. Mahasuverachai and G. H. Powell - November 1982 (PB83 249 987)A07
- UCB/EERC-83/01 "The Economic Feasibility of Seismic Rehabilitation of Buildings by Base Isolation," by J. M. Kelly - January 1983 (PB83 197 988)A05
- UCB/EERC-83/02 "Seismic Moment Connections for Moment-Resisting Steel Frames," by E. P. Popov - January 1983 (PB83 195 412)A04
- UCB/EERC-83/03 "Design of Links and Beam-to-Column Connections for Eccentrically Braced Steel Frames," by E. P. Popov and J. O. Malley - January 1983 (PB83 194 811)A04
- UCB/EERC-83/04 "Numerical Techniques for the Evaluation of Soil-Structure Interaction Effects in the Time Domain," by E. Bayo and E. L. Wilson - February 1983 (PB83 245 605)A09
- UCB/EERC-83/05 "A Transducer for Measuring the Internal Forces in the Columns of a Frame-Wall Reinforced Concrete Structure," by R. Sause and V. V. Bertero - May 1983 (PB84 119 494)A06
- UCB/EERC-83/06 "Dynamic Interactions between Floating Ice and Offshore Structures," by P. Croteau - May 1983 (PB84 119 486)A16
- UCB/EERC-83/07 "Dynamic Analysis of Multiply Tuned and Arbitrarily Supported Secondary Systems," by T. Igusa and A. Der Kiureghian - June 1983 (PB84 118 272)A11
- UCB/EERC-83/08 "A Laboratory Study of Submerged Multi-body Systems in Earthquakes," by G. R. Ansari - June 1983 (PB83 261 842)A17
- UCB/EERC-83/09 "Effects of Transient Foundation Uplift on Earthquake Response of Structures," by C.-S. Yim and A. K. Chopra - June 1983 (PB83 261 396)A07
- UCB/EERC-83/10 "Optimal Design of Friction-Braced Frames under Seismic Loading," by M. A. Austin and K. S. Pister - June 1983 (PB84 119 288)A06
- UCB/EERC-83/11 "Shaking Table Study of Single-Story Masonry Houses: Dynamic Performance under Three Component Seismic Input and Recommendations," by G. C. Manos, R. W. Clough and R. L. Mayes - June 1983
- UCB/EERC-83/12 "Experimental Error Propagation in Pseudodynamic Testing," by P. B. Shing and S. A. Mahin - June 1983 (PB84 119 270)A09
- UCB/EERC-83/13 "Experimental and Analytical Predictions of the Mechanical Characteristics of a 1/5-scale Model of a 7-story R/C Frame-Wall Building Structure," by A. E. Aktan, V. V. Bertero, A. A. Chowdhury and T. Nagashima - August 1983 (PB84 119 213)A07
- UCB/EERC-83/14 "Shaking Table Tests of Large-Panel Precast Concrete Building System Assemblages," by M. G. Oliva and R. W. Clough - August 1983
- UCB/EERC-83/15 "Seismic Behavior of Active Beam Links in Eccentrically Braced Frames," by K. D. Hjelmstad and E. P. Popov - July 1983 (PB84 119 676)A09
- UCB/EERC-83/16 "System Identification of Structures with Joint Rotation," by J. S. Dimsdale and H. D. McNiven - July 1983
- UCB/EERC-83/17 "Construction of Inelastic Response Spectra for Single-Degree-of-Freedom Systems," by S. Mahin and J. Lin - July 1983

- UCB/EERC-83/18 "Interactive Computer Analysis Methods for Predicting the Inelastic Cyclic Behaviour of Structural Sections," by S. Kaba and S. Mahin - July 1983 (PB84 192 012) A06
- UCB/EERC-83/19 "Effects of Bond Deterioration on Hysteretic Behavior of Reinforced Concrete Joints," by F.C. Filippou, E.P. Popov and V.V. Bertero - August 1983 (PB84 192 020) A10
- UCB/EERC-83/20 "Analytical and Experimental Correlation of Large-Panel Precast Building System Performance," by M.G. Oliva, R.W. Clough, M. Velkov, P. Gavrilovic and J. Petrovski - November 1983
- UCB/EERC-83/21 "Mechanical Characteristics of Materials Used in a 1/5 Scale Model of a 7-Story Reinforced Concrete Test Structure," by V.V. Bertero, A.E. Aktan, H.G. Harris and A.A. Chowdhury - September 1983 (PB84 193 697) A05
- UCB/EERC-83/22 "Hybrid Modelling of Soil-Structure Interaction in Layered Media," by T.-J. Tzong and J. Penzien - October 1983 (PB84 192 178) A08
- UCB/EERC-83/23 "Local Bond Stress-Slip Relationships of Deformed Bars under Generalized Excitations," by R. Eligehausen, E.P. Popov and V.V. Bertero - October 1983 (PB84 192 848) A09
- UCB/EERC-83/24 "Design Considerations for Shear Links in Eccentrically Braced Frames," by J.O. Malley and E.P. Popov - November 1983 (PB84 192 186) A07
- UCB/EERC-84/01 "Pseudodynamic Test Method for Seismic Performance Evaluation: Theory and Implementation," by P.-S. B. Shing and S. A. Mahin - January 1984 (PB84 190 644) A08
- UCB/EERC-84/02 "Dynamic Response Behavior of Xiang Hong Dian Dam," by R.W. Clough, K.-T. Chang, H.-Q. Chen, R.M. Stephen, G.-L. Wang, and Y. Ghanaat - April 1984
- UCB/EERC-84/03 "Refined Modelling of Reinforced Concrete Columns for Seismic Analysis," by S.A. Kaba and S.A. Mahin - April, 1984
- UCB/EERC-84/04 "A New Floor Response Spectrum Method for Seismic Analysis of Multiply Supported Secondary Systems," by A. Asfura and A. Der Kiureghian - June 1984
- UCB/EERC-84/05 "Earthquake Simulation Tests and Associated Studies of a 1/5th-scale Model of a 7-Story R/C Frame-Wall Test Structure," by V.V. Bertero, A.E. Aktan, F.A. Charney and R. Sause - June 1984
- UCB/EERC-84/06 "R/C Structural Walls: Seismic Design for Shear," by A.E. Aktan and V.V. Bertero
- UCB/EERC-84/07 "Behavior of Interior and Exterior Flat-Plate Connections subjected to Inelastic Load Reversals," by H.L. Zee and J.P. Moehle
- UCB/EERC-84/08 "Experimental Study of the Seismic Behavior of a two-story Flat-Plate Structure," by J.W. Diebold and J.P. Moehle
- UCB/EERC-84/09 "Phenomenological Modeling of Steel Braces under Cyclic Loading," by K. Ikeda, S.A. Mahin and S.N. Dermitzakis - May 1984
- UCB/EERC-84/10 "Earthquake Analysis and Response of Concrete Gravity Dams," by G. Fenves and A.K. Chopra - August 1984
- UCB/EERC-84/11 "EAGD-84: A Computer Program for Earthquake Analysis of Concrete Gravity Dams," by G. Fenves and A.K. Chopra - August 1984
- UCB/EERC-84/12 "A Refined Physical Theory Model for Predicting the Seismic Behavior of Braced Steel Frames," by K. Ikeda and S.A. Mahin - July 1984